Centre Armand-Frappier Santé Biotechnologie

Insights into the molecular mechanism modulating the proapoptotic activity of human galectin-7

Par

Ngoc Thu Hang Pham

Thèse présenté(e) pour l'obtention du grade de
Philosophiae Doctor (Ph.D.)
en Biologie

Jury d'évaluation

Président du jury et examinateur interne	Jonathan Perreault Centre Armand-Frappier Santé-Biotechnologie Institut national de la recherche scientifique (INRS)
Examinateur externe	Guillaume Lamoureux Department of Chemistry and Center for Computational and Integrative Biology Rutgers University-Camden
Examinateur externe	Denis Giguère Département de chimie Université Laval
Directeur de recherche	Nicolas Doucet Centre Armand-Frappier Santé-Biotechnologie Institut national de la recherche scientifique (INRS)
Codirecteur de recherche	Charles Calmettes Centre Armand-Frappier Santé-Biotechnologie Institut national de la recherche scientifique (INRS)

“The real act of discovery is not in finding new lands, but in seeing with new eyes.”

- Marcel Proust

“Go confidently in the direction of your dreams! Live the life you’ve imagined!”

- Henry David Thoreau

ACKNOWLEDGEMENTS

As Minions say in the computer-animated film: “I always wanted to win the lottery. But tonight, I look around at my beautiful family and realize I already have!” I am blessed to have had such wonderful people with me on this unforgettable PhD journey. Without their help and support, this “Minion” of the lab could not have successfully completed this adventure.

Before anyone else, I am grateful to my director, Pr. Nicolas Doucet, not only for welcoming me in his lab, but also for giving me freedom to exploiting all possible options to drive this project forward, and for patiently directing me throughout this process. He has played multiple roles in the accomplishment of this thesis: researcher, critic, editor, mentor, artist, psychologist. I have been affected by his contagious passion in science, his kindness, his magical writing, and his incredible gift for science popularization. He had an artistic power to transform my jumble first drafts into a nice story and deliverable manuscript. He was always ready to explain anything that I do not understand. He gave me relevant feedbacks so that I could better improve my work. He showed me how to make stunning figures. He encouraged me to go explore protein science in different national and international conferences. He also helped me during difficult moments, especially during the COVID-19 pandemic period. Just by sending him an email, a Slack message, or knocking on his office door, he was always there for his students. It is no exaggeration to say that he is the father of the lab.

Second, I’d like to thank our research assistant known as “the saviour of the lab”, Myriam Létourneau. She was the person that you always wanted to track with a GPS because everybody needed her anywhere and anytime. Positively energized and enthusiastic, she unconditionally helped me, not only for all experimental troubleshooting, but also for my writing revisions. I always enjoyed having many discussions with her on science and life inside and outside the lab. She was always ready to listen to me and give me good advice when I shared my challenges. She also reminded me how important it is to keep a good mental health. She introduced me to the Capoeira gang, with whom I nourished my positive mind and re-energized myself after work and for going through the PhD process. No words can describe all the support that Myriam gave me for this accomplishment.

Third, I benefited from the guidance of many professors in this highly collaborative project. Thanks to my co-director, Pr. Charles Calmettes, for walking me through the X-ray crystallography experiments and for supporting me psychologically. He showed me how to mount crystals, perform data collection, and solve protein structures. He accompanied me to the structural biology

center at McGill for the first screening experiments. He counted on me to perform synchrotron data collection remotely overnight in his office. If I have the right to have too many fathers, then he would be the second father of the lab. I am also indebted to Pr. Yves St-Pierre for transferring me his wonderful knowledge of the galectin world, for giving me relevant writing feedback, and for boosting me with sweet caramel candies. I am thankful to Pr. Patrick Lagüe for patiently explaining molecular dynamics simulations and network analysis, and especially for taking his time to help me speed up the analysis so that I can finish this project on time. I also acknowledge Pr. David Chatenet for giving me relevant feedback during interlab meetings and for reviewing my article manuscripts. Finally, I owe a lot to Pr. Philippe Constant for helping me with statistical analyses.

At various stages of this project, some experiments were performed with help from warm and enthusiastic people. I would like to thank Marlène for helping me carry out all apoptosis tests in this project. Marlène and I got along well and coordinated our timed experiments perfectly. She is adorable, friendly, cheerful, kind, and shining like her bright blond hair! She always helped me when I needed something. I cannot wait to offer her the promised Indian butter chicken dishes once I complete my thesis. I am grateful to Alex Paré for patiently helping me to analyze all results of molecular dynamics simulations. I appreciate all the efforts and valuable hours he dedicated to this project, allowing me to quickly acquire MD results to complete my research on time. I also enjoyed discussing with him and learning how to run code for the analysis. He is a charming, social guy who is always in harmony with everyone. Thanks Alex for installing the LED lights so that I can transform the lab office into a catwalk light show! I would also like to thank Gabriel Bégin, who was involved in the development of the network analysis method.

I was lucky to have the support of top-notch teams of researchers in the Doucet Lab, Calmettes Lab, St-Pierre Lab, Chatenet Lab, and other labs. I enjoyed discussing science and gadgets with my best brother Yossef López de los Santos and learned from his braveness, kindness, and great dedication to work. I shared many fun moments with him and his family: Brenda, Killian, and Lucian. I was affected by the strong positive attitude of Chitra Narayanan, who can be described by this Minion quote: “Let your smile change the world! Don’t let the world change your smile!”. I had so much fun hiking with her and her partner, Yevgen Nazarenko. We had interesting discussions about PhD life, society, and many other things, which gave me new perspectives to look at the world differently. I would like to thank to Ying Lian Chew Fajardo, who always motivated me to work out and share positive things about life; to Andrés Mauricio Rueda Rueda for his humorous criticism on anything about the world and his tasty empanadas; to David Bernard for his funny signature laugh, to Carlos Eduardo Dulcey Jordan for mentoring me during

my first days in the lab; to Jacinthe Gagnon for showing me crystallization techniques and structural resolution; to Philippe Egesborg for starting preliminary work on the GAL-7 project; to Louise Roux for the traditional birthday cake idea; to Mariem Chalbi for being the fantastic DJ of the lab; to Quynh Tran for her support and her super delicious shared food; to Hieu Bui for helping me to extract raw data in important moments and for repairing my bike several times; to Imene Kouidmi, Jihen Ati, Livie Lestin, Rose Ragot, and Thibault Bourdin for boosting my positive attitude and supporting me psychologically. Finally, I appreciated Mirana Rakotoarivony, Sammy Nyongessa, Mustapha Iddir, Cyrielle Martini, Philippine Granger, Camille Fuselier, Juan Francisco Guerra Maldonado, Cecilia Nieves, Abdelkader Mellouk, Michel Lê, Dazhong Zheng, Quentin Fort, Carolina Perusquía Hernández, Marie-Aude Pinoteau, Pablo Raúl Armoa Ortiz, Samy Ajarrag, Judith Monguong, Narin Srei, Hoang-Van Tran, Mohammad Mehdi Haghdoost Manjili, Golara Golbaghi, and Hala El-Asmy for sharing memorable moments with me at the institute.

I would like to acknowledge my scientific friend Leidy Diana Caraballo Galva for accompanying me in my research career. I was inspired by her overwhelming dedication to research, her critical thinking and problem-solving skills, and her persistence in work. We have known each other for ten years now, from the days at our engineering school (INSA) in Toulouse. We did an internship together at Boston University, then graduated together. After graduation, we continued working together as research assistants at Boston University. Later, we pursued our PhD dreams. Even if we did not perform our PhD at the same place, we always called each other and shared our research stories, supported and encouraged each other through every challenges during our PhD journeys. I would like to thank the universe or my destiny to have offered me this wonderful opportunity to meet a wonderful person like her. I still learn from her on how to become a better scientist. She already got her Ph.D. degree in early 2022. Now is my turn to complete mine in the middle of 2022. I cannot wait to call her: “Hey, mira mamá, lo hice!” (I always called her “mom” as a nickname).

As Minions say: “If you have crazy friends, you have everything!” I am blessed to have been in contact with so many friends, roommates, and pets (!) to support me. I would like to thank my 238 Avenue Brien gang: Isabelle Thouin, Philippe Latour, Jean-Christophe Ngando Moukala, Juan Manuel Pardo, Nicolas Simoneau, Marie-Ève Thuot, Rose Ragot; my Vietnamese friends: Tam, Trang, Minh, Van, Quynh, Tuyen, Cedric, Tho, Thao, Diep, Hai, and Tan, and my friend Claudèle Lemay-St-Denis for their support and encouragement. I am grateful to my Capoeira gang: Perninha, Astral, Urso, Boa Gente, Zangada, Pikachu, Camaleão, Turista, Malandro and Palhaço for helping me to keep a positive attitude. I would like to acknowledge my Cambly

teachers Joyce Siders and Robert Micheal for helping me improve my English conversation. As Minions say: “The best therapist has fur and four legs.” Consequently, I would like to thank all the cats that I met, lived with, or played with: Timothé, Flacko, Cooki, Xam, Vang, Tom, and random cats in my neighborhood. These hilarious and funny cats helped me lower my stress levels and overcome the boredom of COVID-19 periods. I owe a lot to Isabelle Queval and Elizabeth-Doiron, who supported me psychologically at the end of my journey.

“Do you ever write a really long message and about halfway through you’re like “you know what, they don’t even care” and delete it”, a Minion said. Writing is a long process requiring a lot of persistence that would be challenging to do alone. I am grateful to have access to the Thèsez-vous organization, which accompanied me for almost half a year of thesis writing. I would like to thank all animators and other members of Thèsez-vous: Raphaëlle Côté-Parent, Julie Lauzier, David Azoulay, Geneviève Brodeur, Julie Bernard, Audrey Bélanger, Félix L. Delauriers, Vanessa Blanchette-Luong, Ledy Rivas, Cynthia Vincent, Anne Iavaronne-Turcotte, Brintha Koneshachandra, Marion Gringras-Gagné, Arianne Gauthier, Mathilde Tiède, Sèverine Lanoue, Yan St-Onge, with whom I spent almost a “thousand tomatoes.” Thanks to their support and contagious energetic animation, I can now absorb more Pomodoro vitamins to accomplish my writing! I also acknowledge INRS for the financial aid that helped me access all the services of Thèsez-vous.

“Family is not about blood. It’s about who is willing to hold your hand when you need it the most”, a Minion believes. My deepest gratitude goes to my family, who patiently supported me for this long PhD journey. Even with the distance of half the circumference of the Earth between my parents and I, they always answered my calls, day or night. They knew that I needed them for these moments, and they tried their best to console me during tough moments. I was lucky to have my sister joining me in Québec and supporting me for this long adventure.

RESUME

La galectine humaine 7 (GAL-7) est à la fois une protéine protumorale (sein, ovaires, etc.) et antitumorale (côlon, prostate, etc.) prototypique caractérisée par une architecture moléculaire homodimérique et un site de liaison pour les β-galactosides (GBS). En formant un réseau extracellulaire de galectines-glycoprotéines via le GBS ou en établissant des interactions indépendantes du GBS avec d'autres protéines intracellulaires, GAL-7 régule l'apoptose, l'adhésion et la migration cellulaire, la différenciation cellulaire et la prolifération. Depuis plusieurs années, de nombreux efforts ont été consacrés à la conception d'inhibiteurs de galectines se liant au GBS en utilisant des molécules à base de glycanes, afin de perturber l'interaction entre GAL-7 et les récepteurs glycosylés dans le traitement de cancers associés à son rôle protumoral. Cependant, cette stratégie s'est avérée inefficace pour cibler les fonctions indépendantes du GBS de GAL-7, en plus de comporter un risque élevé d'effets hors cible en raison de la grande homologie entre les GBS de différentes galectines homologues. Ainsi, de nouvelles approches visant le développement d'inhibiteurs sélectifs de GAL-7 sont souhaitables. La modulation allostérique étant reconnue comme étant plus sélective et parfois plus efficace que l'inhibition orthostérique traditionnelle, elle s'avère une approche prometteuse dans l'optique d'une modulation fonctionnelle des galectines. Or, la conception d'inhibiteurs allostériques rationnelle requiert le développement et l'application de méthodes permettant la caractérisation de sites allostériques potentiels. Une étude précédente a révélé l'existence d'une coopérativité positive à longue distance entre chaque GBS des deux protomères de GAL-7, maintenue par des interactions électrostatiques entre les résidus opposés de l'interface homodimérique. Nous avons ainsi soulevé l'hypothèse que l'activité protumorale de GAL-7 puisse être allostériquement modulée par des résidus de l'interface dimérique. Ainsi, l'objectif de la présente recherche vise à prédire et à caractériser les potentiels sites de modulation allostérique situés à l'interface dimérique de GAL-7 en lien avec son activité apoptotique. Pour ce faire, des tests d'apoptose cellulaire, de résolution de structure par cristallographie aux rayons X, de caractérisation biophysique et de prédictions bioinformatiques ont été effectués. En étudiant trois régions physicochimiques différentes de l'interface homodimérique de GAL-7, nous avons démontré que différentes positions de l'interface dimérique peuvent être ciblées pour moduler négativement ou positivement l'activité pro-apoptotique de GAL-7. La déstabilisation de l'interface homodimérique, la perturbation de la communication inter-protomérique et la régulation dynamique sont autant de mécanismes moléculaires distincts qui modulent la structure et la fonction de cette protéine

tumorale. À la lumière de ces connaissances, des pistes pertinentes pourront être établies dans le but d'améliorer la conception de modulateurs allostériques négatifs ou positifs visant le traitement personnalisé de pathologies selon l'effet souhaité.

Mots-clés: galectine-7 humaine, modulation allostérique, site de liaison des β-galactosides (GBS), activité pro-tumorale, activité anti-tumorale, interface dimérique, apoptose, caractérisation biophysique, modélisation moléculaire, cristallographie aux rayons X, dynamique des protéines.

ABSTRACT

Human galectin 7 (GAL-7) is both a prototypical protumoral (breast, ovarian, etc.) and antitumoral (colon, prostate, etc.) protein characterized by a homodimeric molecular architecture and a binding site for β-galactosides (GBS). By forming an extracellular galectin-glycoprotein network via its GBS or by establishing GBS-independent interactions with other intracellular proteins, GAL-7 regulates apoptosis, cell adhesion and migration, cell differentiation, and proliferation. For several years, numerous efforts have been devoted to the design of GBS-binding galectin inhibitors using glycan-based molecules to disrupt the interaction between GAL-7 and glycosylated receptors in the treatment of cancers associated with its protumoral function. However, this strategy has proven ineffective for targeting GBS-independent functions of GAL-7, in addition to carrying a high risk of off-target effects due to the high homology between GBSs of different homologous galectins. Thus, new approaches aimed at the development of selective GAL-7 inhibitors are desirable. As allosteric modulation is known to be more selective and sometimes more efficient than traditional orthosteric inhibition, it is a promising approach for functional modulation of galectins. However, the design of rational allosteric inhibitors requires the development and application of methods to characterize potential allosteric sites. A previous study revealed the existence of positive long-range cooperativity between each GBS of the two GAL-7 protomers, maintained by electrostatic interactions between opposite residues at the homodimeric interface. We thus hypothesized that the protumoral activity of GAL-7 may be allosterically modulated by residues of the dimer interface. Therefore, the objective of the present research is to predict and characterize potential allosteric modulation sites located at the dimer interface of GAL-7 in relation to its apoptotic activity. To this end, cellular apoptosis, structure resolution by X-ray crystallography, biophysical characterization, and bioinformatics predictions were performed. By studying three different physicochemical regions of the GAL-7 homodimeric interface, we demonstrated that different positions of the dimer interface can be targeted to negatively or positively modulate the pro-apoptotic activity of GAL-7. Destabilization of the homodimeric interface, disruption of inter-protomeric communication, and dynamic regulation are distinct molecular mechanisms that modulate the structure and function of this tumor protein. In light of this knowledge, relevant avenues can be established to improve the design of negative or positive allosteric modulators for the development of personalized treatment of pathologies with desired effects.

Keywords: human galectin-7, allosteric modulation, galactoside glycan binding site (GBS), pro-tumorigenic activity, anti-tumorigenic activity, dimer interface, apoptosis, biophysical characterization, molecular simulation, X-ray crystallography, protein dynamics.

SOMMAIRE RECAPITULATIF

Puisque les galectines jouent un rôle critique dans le cancer (Chou et al., 2018; Dubé-Delarosbil et al., 2018; Girotti et al., 2019; Labrie et al., 2014; Liu et al., 2005; Wdowiak et al., 2018) de nombreuses études se sont concentrées sur la synthèse d'inhibiteurs de galectines pour le traitement du cancer (Chou et al., 2018; Girard et al., 2018; Sörme et al., 2003). Malgré plus de deux décennies consacrées à ce domaine, la lente progression n'a permis le développement que de six composés ciblant les GAL-1, -3 ou -9, qui sont soumis à des essais cliniques (Chou et al., 2018; Girard et al., 2018). Par conséquent, peu de types de cancers associés aux galectines pourraient actuellement être traités sur la base de leur inhibition. Il est donc essentiel de consacrer des efforts à la synthèse d'inhibiteurs d'autres galectines. Dans le présent travail, nous nous sommes concentrés sur l'étude de GAL-7, car cette galectine représente une nouvelle cible potentielle pour le traitement du cancer du sein triple négatif (TNBC), qui est difficile à reconnaître et à éradiquer en raison de l'absence de trois récepteurs spécifiques : ER-, PR-, HER2- (Demers et al., 2010; Grosset et al., 2014, 2016; Wu et al., 2021). GAL-7 est une galectine prototypique caractérisée par un site de liaison aux β-galactosides (GBS) (Leonidas et al., 1998). En effet, la surexpression de GAL-7 chez les cellules cancéreuses du sein favorise non seulement la résistance de ces cellules à l'apoptose, mais également l'apoptose des cellules T activées, en formant une matrice galectine-glycoprotéine extracellulaire à la surface des cellules T (Demers et al., 2010; Grosset et al., 2014, 2016; St-Pierre, 2012). Depuis les premières tentatives d'inhibition il y a désormais 16 ans, le développement d'un inhibiteur de GAL-7 est principalement axé sur des composés à base de sucre et de petites molécules visant à perturber les interactions des glycorécepteurs (Cumpstey et al., 2005; Masuyer et al., 2012; Salameh et al., 2006). Étant donné la grande similarité entre les GBS de différents homologues de galectines, cette stratégie est confrontée à des effets non ciblés, incluant des effets d'inhibition non-spécifiques ciblant d'autres galectines ayant une activité antitumorale bénéfique, notamment GAL-4 et GAL-9 (Morishita et al., 2021; Satelli et al., 2011; Tadokoro et al., 2016). De plus, ces inhibiteurs sont inefficaces pour perturber les interactions indépendantes du GBS, telle que l'interaction intracellulaire entre GAL-7 et BCL-2, qui semble moduler l'apoptose cellulaire (Villeneuve et al., 2011). Une approche alternative doit donc être élaborée pour développer de nouveaux inhibiteurs efficaces et spécifiques à GAL-7.

Il a été démontré que les modulateurs allostériques sont plus sélectifs et efficaces que les inhibiteurs ciblant le site actif (Wenthur et al., 2014). Ainsi, cibler les régions non-GBS de GAL-7

permettrait de moduler spécifiquement des activités dépendantes et indépendantes du GBS de GAL-7. En appui à cette direction, malgré une structure tertiaire globalement similaire, l'architecture oligomérique des galectines humaines est différente entre elles (Kamitori, 2018). Ceci suggère donc que cibler l'interface homodimérique améliorerait la spécificité d'un inhibiteur de GAL-7. De plus, l'oligomérisation est importante pour la formation d'un réseau galectine-glycoprotéine qui lui permet de contrôler de multiples processus cellulaires associés à la progression du cancer (Boscher et al., 2011; Brewer, 2002; Sacchettini et al., 2001). En outre, Ermakova et al. ont montré que la liaison au lactose induit une coopérativité positive à longue distance en traversant l'interface du dimère entre les deux GBS sur les protomères opposés de GAL-7 (Ermakova et al., 2013). Pour toutes ces raisons, des peptides interférant avec le dimère de GAL-7 (dimer interfering peptides, ou DIPs) ont été récemment développés pour modifier la stabilité du dimère ainsi (Boscher et al., 2011; Brewer, 2002; Sacchettini et al., 2001) que la fonction de la protéine (Vladoiu et al., 2015). Parmi les DIPs conçus, il a été démontré que le peptide hGAL-7(129-135) diminue avec succès l'activité proapoptotique dépendante du GBS de GAL-7 sur les cellules T Jurkat en perturbant l'équilibre d'interaction monomère-monomère en solution. Cependant, la majorité des DIPs possèdent une faible affinité pour GAL-7 (mM) et une faible solubilité, ce qui limite significativement leur application thérapeutique. Dans le but d'améliorer la conception des DIPs, il est donc nécessaire de mieux comprendre le rôle de chaque résidu appartenant à l'interaction homodimérique dans la régulation de l'activité de GAL-7. Tous ces résidus de l'interface de l'homodimère sont-ils impliqués dans le contrôle de l'activité de GAL-7 ? Contrôlent-ils de manière allostérique l'activité dépendante du GBS ? Quelles positions doivent être ciblées ou évitées pour moduler l'activité de GAL-7 de manière négative ou positive ? Pour répondre à toutes ces questions, nous avons caractérisé le mécanisme moléculaire de l'interaction de l'homodimère modulant l'activité proapoptotique dépendante du GBS chez GAL-7.

En partant de l'hypothèse que **la force d'interaction du dimère pourrait moduler l'activité proapoptotique de GAL-7 (*hypothèse 1*)**, l'article "**Perturbing dimer interactions and allosteric communication modulates the immunosuppressive activity of human galectin-7**" (Pham et al., 2021) a présenté une analyse *in silico* en utilisant les algorithmes PoPMuSiC et BeAtMuSiC dans le but de prédire la formation d'un pont disulfure covalent (G16C) et une mutation déstabilisante (G16S) pour contrôler la force de l'interaction protomère-protomère. Afin d'évaluer l'impact de ces mutations sur l'activité de GAL-7, nous avons effectué un test d'apoptose sur des cellules T Jurkat en collaboration avec le laboratoire du Prof. Yves St-Pierre. Parallèlement, des techniques biophysiques de thermophorèse (MST), de dichroïsme circulaire

(CD) et de titrage calorimétrique isotherme (ITC) ont été utilisées pour évaluer la force de l'interaction homodimérique, la stabilité et l'affinité des mutants de GAL-7 envers lactose. La cristallographie aux rayons X et des simulations de dynamique moléculaire ont également été effectuées en collaboration avec le laboratoire du Prof. Patrick Lagüe afin d'évaluer l'effet perturbateur de ces mutations sur le changement structural et la transmission allostérique entre les protomères de GAL-7 et ses deux sites GBSs. À partir des résultats de simulations, nous avons établi le premier réseau allostérique de GAL-7, permettant d'identifier les voies allostériques potentielles qui relient les GBS au sein de chaque protomère. La reconnaissance de ces voies allostériques a illustré la coopérativité positive entre les deux GBSs précédemment suggérée (Ermakova et al., 2013). En général, nos résultats ont démontré que malgré la conservation de la structure globale, de l'affinité de liaison au lactose pour les mutants G16X, et même des voies allostériques reliant les deux GBS chez GAL-7, l'activité proapoptotique de la protéine pouvait être modulée positivement ou négativement via le renforcement ou l'affaiblissement de la force de l'homodimérisation.

Dans le manuscrit "**Allosteric network analysis in galectin-7 uncovers key residues controlling communication between two opposite glycan binding sites ",** nous avons étudié l'impact de la perturbation de la communication interprotomère mise en évidence dans l'analyse de réseau de l'étude précédente (Pham et al., 2021) sur la fonction de GAL-7. L'analyse des réseaux allostériques de GAL-7 avait précédemment suggéré que **R20, R22 et D103 étaient importants pour maintenir la communication entre les deux protomères de GAL-7 (*hypothèse 2*)** (Ermakova et al., 2013). Par conséquent, nous avons caractérisé les conséquences de trois mutations simples R20A, R22A, D103A et d'une double mutation R20A-R22A sur l'activité de GAL-7 et ses propriétés biophysiques, structurales et allostériques. Nos résultats ont démontré que malgré la préservation des structures globales de GAL-7 et de l'affinité de liaison au lactose, la réduction de la communication inter-protomérique et l'altération de la voie allostérique, ainsi que la déstabilisation de l'interaction homodimérique et de l'intégrité de la protéine causée par ces mutations ont empêché GAL-7 d'induire l'apoptose dans les cellules T Jurkat. Dans cette étude, nous avons également apporté une nouvelle approche pour évaluer le flux de la communication globale entre les deux GBS, en démontrant la diminution de la communication globale entre deux GBS chez tous les mutants.

Dans les deux études précédentes, nous avons étudié l'impact de la perturbation de l'interaction des homodimères dans la région supérieure (R20, R22, D103) et centrale (F135, G16) (Pham et al., 2021) de l'interface homodimérique (Figure 5.1) de GAL-7. Pour obtenir une

image complète de la modulation de l'activité proapoptotique de GAL-7 à l'interface de l'homodimère, nous avons étudié les effets de la perturbation de l'interaction électrostatique de R14 et de D94/D95 (région inférieure de l'interface du dimère) sur l'activité proapoptotique de GAL-7. De plus, une étude précédente (Ermakova et al., 2013) a suggéré que le résidu R14 était possiblement impliqué dans le changement dynamique du GBS à l'interface du dimère. Cette observation suggère **que la perturbation de l'interaction électrostatique entre R14 et les résidus D94 ou D95 peut modifier l'activité proapoptotique de GAL-7 (*hypothèse 3*)**. Afin de répondre à cette hypothèse, nous avons utilisé le test d'apoptose des cellules T Jurkat, la résolution de structure par cristallographie aux rayons X et la caractérisation biophysique des mutants. Nos résultats ont indiqué que la mutation D94A avait augmenté la capacité de GAL-7 à induire l'apoptose dans les cellules T Jurkat, alors qu'aucune altération de l'apoptose ne semble être causée par la mutation R14A. Cependant, nous avons observé un effet synergique des mutations R14A-R22A sur la modulation négative de l'activité proapoptotique de GAL-7. Cet effet pourrait s'expliquer par une déstabilisation de l'interaction homodimérique, une altération de la stabilité de la protéine, et/ou encore par la réduction de l'affinité de liaison du ligand pour R14A-R22A. Néanmoins, l'augmentation de l'activité proapoptotique causée par D94A demeure inexplicable puisqu'aucune corrélation directe n'est observable entre cette activité et l'affinité de liaison au ligand, ou encore entre l'intégrité de l'homodimère et la stabilité de la protéine. Comme D94 et R14 sont situés sur des régions en boucle, leur mécanisme de modulation pourrait possiblement être impliqué dans la modulation de la dynamique liant les GBSs à l'interface du dimère (Ermakova et al., 2013). Pour confirmer cette hypothèse, des expériences de caractérisation biophysique et de dynamique moléculaire *in silico* pourraient être entreprises.

En conclusion, nous avons démontré que les interactions des résidus au niveau de l'interaction du dimère jouent un rôle critique dans la modulation de l'activité proapoptotique de GAL-7. De manière intéressante, selon l'interaction de la paire de résidus ciblée, l'activité proapoptotique de GAL-7 peut être régulée négativement ou positivement en altérant différents mécanismes moléculaires. En effet, la perturbation de la région centrale de l'interface du dimère permet d'augmenter ou de diminuer l'activité proapoptotique de GAL-7 via le contrôle de la force d'interaction entre les protomères (Pham et al., 2021). L'altération de la région électrostatique supérieure de l'interface homodimérique permet de moduler négativement l'activité proapoptotique de GAL-7 en interrompant la communication allostérique entre protomères, ainsi qu'en réduisant l'affinité de l'interaction homodimérique. La perturbation de la région inférieure de l'interface du dimère semble quant à elle permettre l'amélioration ou l'altération de l'activité proapoptotique de GAL-7, probablement via la régulation dynamique de GAL-7 (Ermakova et al.,

2013). Cependant, comme nous n'avons pas pu tester le remplacement de ces résidues par autre type d'acide amines, nous ne pourrions pas conclure que la perturbation à ces positions permet uniquement une modulation exclusivement positive ou négative de l'activité proapoptotique de GAL-7. Il est possible qu'un autre type de perturbation introduite à la même position puisse donner un effet complètement différent que la mutation vers alanine. En général, cibler les positions 20, 22, 103, 16, 94, 14 pourrait permettre de moduler le GAL-7 proapoptotique. Le type de perturbation qui favorise la déstabilisation de l'intéraction homodimérique sur ces positions, à l'exception de la 94, pourrait réduire l'activité proapoptotique de GAL-7. Ces connaissances mettent en évidence de nouvelles voies pour la conception de modulateurs fonctionnels ciblant l'interface dimérique de GAL-7.

TABLE OF CONTENTS

LIST OF FIGURES

LIST OF TABLES

LIST OF ACRONYMS

3D	three dimensions
AML	Acute Myeloid Leukemia
aa	amino acids
AMP	Adenosine monophosphate
AMPK	AMP-activated protein Kinase
ASD	AlloSteric Database
ATP	Adenosine triphosphate
BPP-LED	Bipolar Pulse Pair – Longitudinal-Eddy-current Delay
CD	Circular Dichroism
C/EBP-β	CCAAT/enhancer binding protein beta
CI	Confindential Interval
ConA	Concanavalin A
CRD	Carbohydrate Recognition Domains
D	Dimer
$\Delta\Delta G_B$	Folding free energy
$\Delta\Delta G_F$	Protein-protein binding free energy
ΔH	Enthalpy
ΔS	Entropy
DCs	Dendritic cell
DIP	Dimer Interfering Peptide
DISC	Death Inducing Signaling Complex
DNA	Deoxyribonucleic acid
E	Extended β-strand
EBV	Epstein-Barr Virus
EC50	Half maximal effective concentration
E.coli	*Escherichia coli*
EGF	Epidermal Growth Factor
EGFR	EGF Receptor
ER	Estrogen Receptor
ERK	Extracellular signal-regulated kinases
ESCRT	Endosomal Complexes Required For Transport
EV71	Entero Virus 71
F-face	The opposing face of sugar-binding S-face in CRD structure of galectin
FDA	Food and Drug Administration
F.R.S-FNRS	Fonds de la Recherche Scientifique
FRQNT	Fonds de Recherche du Québec–Nature et technologies
FRQS	Fonds de Recherche du Québec–Santé

GAL	Galectin
GAL-7	Galectin-7, la galectine-7
GAS	Group A Streptococcus
GBS	β-galactoside glycan binding site, sites de liaison des glycanes
Gli	Glioma-associated oncogene protein
HEK	Human Embryonic Kidney
HER2	Human Epidermal growth factor Receptor 2
HFCs	High Fatality Cancers
hGALs	Human galectins
HGF	Hepatocyte growth factor
Hh	Hedgehog
HIV-1	Human Immunodeficiency Virus type 1
HSV-1	Herpes Simplex Virus
HTLV-1	Human T Cell Leukemia Virus type 1
HTS	High-Throughput Screening
IDH	Isocitrate dehydrogenase
INRS	Institut National De La Recherche Scientifique
IL	Interleukin
IPTG	Isopropyl-β-D-1-Thiogalactopyranoside
IR-laser	Infrared Laser
ITC	Isothermal Titration Calorimetry
JNK	c-Jun N-Terminal Kinase
K_a	Association Constants
K_D	Dissociation Constant
LacNAc	*N*-acetyl-lactosamine
LB	Lysogeny Broth
LPS	Lipopolysaccharides
M	Monomer
MAPK	Mitogen-activated protein kinase
MD	Molecular Dynamics
MEI	Ministère de l'Économie et de l'Innovation du Québec
MEK	Mitogen-activated protein kinase
MMP-9	Matrix Metalloproteinase-9
MDS	Myelodysplastic Syndrome
mRNA	messenger ribonucleic acid
MST	Microscale Thermophoresis
mTOR	mammalian Target Of Rapamycin
NASH	Non-alcoholic steatohepatitis
NF-κB	Nuclear factor-kappa B
NG2	Neural/Glial antigen 2

NIGMS	National Institute of General Medical Sciences
NK	Natural killer cells
NKT	Natural killer T cells
NPT	Isothermal isobaric
NRC	National Research Council
NSERC	Natural Sciences and Engineering Research Council of Canada
PCA	Principal Component Analysis
PCDH-24	Protocadherin-24
PDB	Protein Data Bank
PDE4	Phosphodiesterase isozyme 4
PI	Propidium Iodide
PI3K	Phosphoinositide 3-Kinases
PIC	Protein Interaction Calculator
PME	Particle Mesh Ewald
PR	Progesterone Receptor
Raf	Ras effector
RMSD	Root Mean Square Deviation
RMSF	Root Mean Square Fluctuation
RSA	Relative accessible Surface Area
sasa	solvent-accessible surface area
SEM	Standard Error of Mean
S-face	The sugar-binding face in CRD structure of galectin
SMN	Survival Of Motor Neuron
snRNPs	Small Nuclear Ribonucleoproteins
Sufu	Suppressor of fused homolog
T	Elements turn
TCF	Transcription Factor
TGF-β	Transforming Growth Factor Beta
T_m	Melting Temperature
TNBC	Triple-Negative Breast Cancer, cancer du sein triple négatif
tol-DCs	tolerogenic phenotype of Dendritic Cells
TRIMs	Tripartite Motif Containing Proteins
TTF	Thyroid Transcription Factor
UV	Ultraviolet
VEGFR	Vascular Endothelial Growth Factor
WT	Wild Type

1 INTRODUCTION

1.1 Context

In 2020, female breast cancer led the worldwide cancer incidence and mortality in women, with 2,261,419 cases and 684,996 deaths, respectively. It was also the most widespread cancer in women, occurring in 159 out of 185 countries and causing deaths in 110 countries (Sung et al., 2021). Based on the presence or absence of different molecular markers [i.e. estrogen receptor (ER), progesterone receptor (PR), human epidermal growth factor receptor 2 (HER2)], along with the expression level of cellular proliferation marker KI-67, five breast cancer subtypes have been characterized: luminal A (ER+ or/and PR+, HER2-, low level of KI-67), luminal B (ER+ and/or PR+, high level of KI-67), triple-negative/basal-like (ER-, PR-, HER2-), HER2-enriched (ER-, PR-, HER2+), and normal-like (similar to luminal A but with different expression profile). Among these subtypes, triple-negative breast cancer (TNBC), accounting for 10–20 % of all breast cancers (*Triple-Negative Breast Cancer*, 2021), is the hardest subtype to treat due to the lack of molecular targets (Wu et al., 2021). TNBC cells were found to overexpress galectin-7 (GAL-7), which not only helps these cells acquire resistance to apoptosis, but also leads to metastasis (Demers et al., 2010; Grosset et al., 2014, 2016; St-Pierre, 2012). It was shown that GAL-7 promotes cancer by inducing the expression of matrix metalloproteinase-9 (MMP-9), which plays a critical role in tumor growth and metastasis. GAL-7 is also known to trigger the transforming growth factor beta (TGF-β) signaling pathway and, like many other galectins, to induce killing of activated immune cells (Demers et al., 2005; Salatino et al., 2013; Sturm et al., 2004). Therefore, the development of specific inhibitors targeting GAL-7 potentially represents a promising target for the treatment of many cancers, particularly TNBC.

GAL-7 is a prototypical galectin characterized by a β-galactoside glycan binding site (GBS) and a homodimeric molecular architecture. At the cell surface, GAL-7 homodimers crosslink to various glycoconjugated receptors via their GBS and form a dynamic extracellular lattice that can modulate different cellular functions, including cell apoptosis, adhesion, differentiation, proliferation, and migration (Advedissian et al., 2017a; Nabi et al., 2015). Furthermore, GAL-7 cellular modulation is also GBS-independent through interaction with the anti-apoptotic BCL-2 regulator, or through binding with E-cadherin on epithelial cells (Advedissian et al., 2017b; Villeneuve et al., 2011).

To this day, the development of GAL-7 modulators has almost exclusively favored GBS inhibition to perturb the interaction between GAL-7 and glycoreceptors (Cumpstey et al., 2005;

Denavit et al., 2018; Salameh et al., 2006). However, considering the high degree of homology among GBS residues in different galectin homologs, this glycan-based strategy to modulate galectin function generates off-target inhibitory effects, including on beneficial anti-tumorigenic galectins, e.g. GAL-4 and GAL-9 (Morishita et al., 2021; Satelli et al., 2011; Tadokoro et al., 2016). Moreover, GBS inhibitors cannot disrupt glycan-independent functions also promoted by GAL-7 (Kuwabara et al., 2002; Labrie et al., 2015; Truong et al., 2007; Villeneuve et al., 2011). New approaches are thus required to develop effective and highly specific GAL-7 inhibitors. Among such strategies, targeting allosteric sites in proteins has been shown to offer better efficiency and selectivity than the design of orthosteric ligands (Wenthur et al., 2014). Interestingly, it has been proposed that evolution has favored stabilization of the oligomeric galectin architecture to improve ligand affinity and biological function (Konno et al., 2011; St-Pierre et al., 2018; Vasta, 2016). Accordingly, positive cooperativity between two GBSs on opposite protomers has been suggested to be functionally maintained via long-range allosteric communication through the dimer interface (Ermakova et al., 2013). This potential allosteric network remains largely uncharacterized but opens the possibility of allosterically modulating the activity of selected members of the galectin family. The present study aims to uncover the mechanistic details governing the link between allosteric communication and biological function in human GAL-7.

1.2 Overview of Galectins

1.2.1 Galectin family and overall structure

Galectins belong to a subfamily of animal lectins characterized by their conserved β-galactoside binding site (GBS) within a carbohydrate recognition domain (CRD) of ~ 130-140 amino acids (aa). The first vertebrate galectin was discovered in 1975 (Teichberg et al., 1975) and 19 mammal galectins have been identified to date. Among of them, 13 galectins were found in humans (galectin-1, -2, -3, -4, -7, -8, -9, -10, -12, -13, -14, -16, -17). Galectins are subdivided into three groups according to their quaternary structure: tandem repeat (galectin-4, -6, -8, -9, -12), chimera (galectin-3), and prototype (galectin-1, -2, -5, -7, -10, -11, -13, -14, -15, -16, -17, -19, -20) (Varki et al., 2015). Tandem repeat galectins have two different carbohydrate recognition domains (CRDs) covalently joined by a short peptide chain linker. The chimera galectin-3, existing as a monomer or as oligomeric state, has a CRD and a collagen-like N-terminus. Prototype galectins have two identical CRDs forming a non-covalent homodimer, with the exception of GAL-13, which links its two protomers with disulfide bridges (Kamitori, 2018; Su et al., 2018) (Figure 1.1A).

Despite high variation in primary sequence identity among human galectin members, ranging from 6 % to 75 % (Figure 1.1B), these lectin-like proteins share high homology of their overall tertiary CRD structure (Figure 1.1D). The backbone root mean square deviation (RMSD) between representative galectin members is lower than 2Å, which indicates low dissimilarity (Figure 1.1C). The CRD is composed of antiparallel β-strands folded in a “jelly roll” motif. This protein fold consists of a concave sugar-binding face (S-face) and an opposing convex F-face. The GBS, which is located in the S-face cavity, is highly conserved among human galectins (Figure 1.1D). The minimum binding glycan unit of this GBS is usually a disaccharide unit of lactose or *N*-acetyl-lactosamine (LacNAc). This binding is primarily maintained by interactions with His, Asn, and Arg residues on strand S4, Arg on strand S5, and Trp, Glu, and Arg on strand S6 (Figure 1.2A). While polar residues on strands S4 and S5 form hydrogen-bonding interactions with the galactose moiety and Trp makes CH-π interactions with the opposite face of the same monosaccharide (Diehl, 2021; Kiessling et al., 2021; Modenutti et al., 2019), Glu and Arg residues on strand S6 make electrostatic interactions with the glucose moiety (Figure 1.2B).

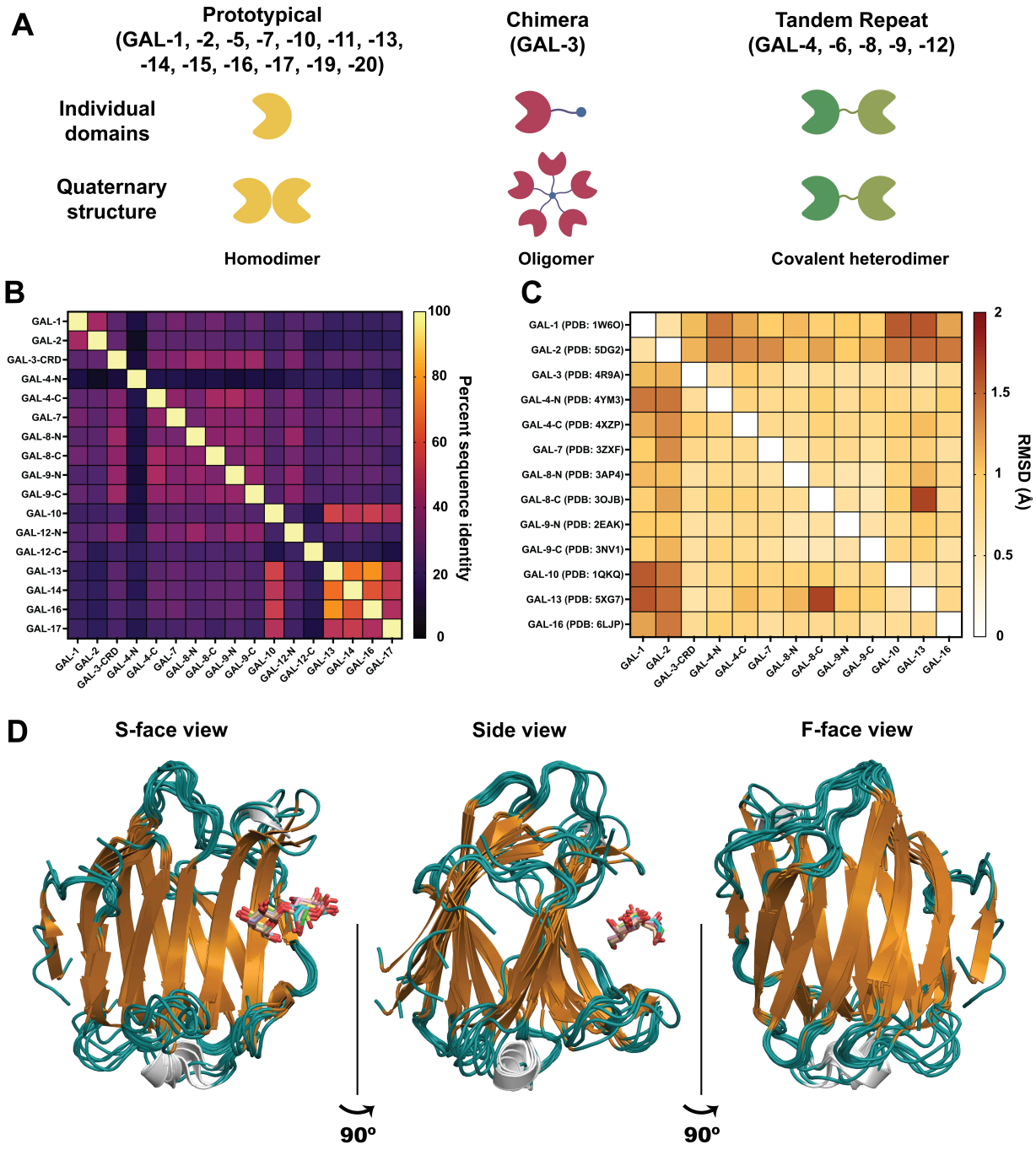

Figure 1.1 Galectin family members.

A. Galectins are subdivided into three groups according to their quaternary structure: prototypical (galectin-1, -2, -5, -7, -10, -11, -13, -14, -15, -16, -17, -19, -20) (*left*), chimera (galectin-3) (*middle*), and tandem repeat (galectin-4, -6, -8, -9, -12) (*right*) (image created with BioRender.com). B. Multiple sequence alignment of galectin CRDs using Clustal Omega shows high variation in sequence identity between human galectin members, ranging from 6 % to 75 %. Sequence identity is color-ramped from black (low) to yellow (high). N and C indicate CRD position located on N- or C-terminal within a tandem repeat galectin. C. RMSD matrix obtained by superimposition of all structural single human CRDs from GAL-1, -2, -3, -4, -7, -8, -9, -10, -13, -16 (PDBs 1W6O, 5DG2, 4R9A, 4YM3, 4ZXP, 3ZXF, 3AP4, 3OJB, 2EAK, 3NV1, 1QKQ, 5XG7, and 6LJP). D. Superimposition of human galectin CRDs in presence of lactose from GAL-1, -2, -3, -4, -7, -8, -9 (PDBs 2EAK, 4GAL, 3AP4,1W6O, 4R9A, 4YM3, and 5DG2). The lactose bound ligands of GAL-1, -2, -3, -4, -7, -8, -9 are shown as sticks in carbon, cyan, salmon, light blue, pale yellow, light pink, and wheat color, respectively. Despite high variations in sequence identity, the overall CRD structure as well as the GBS and lactose position are highly conserved among galectin members.

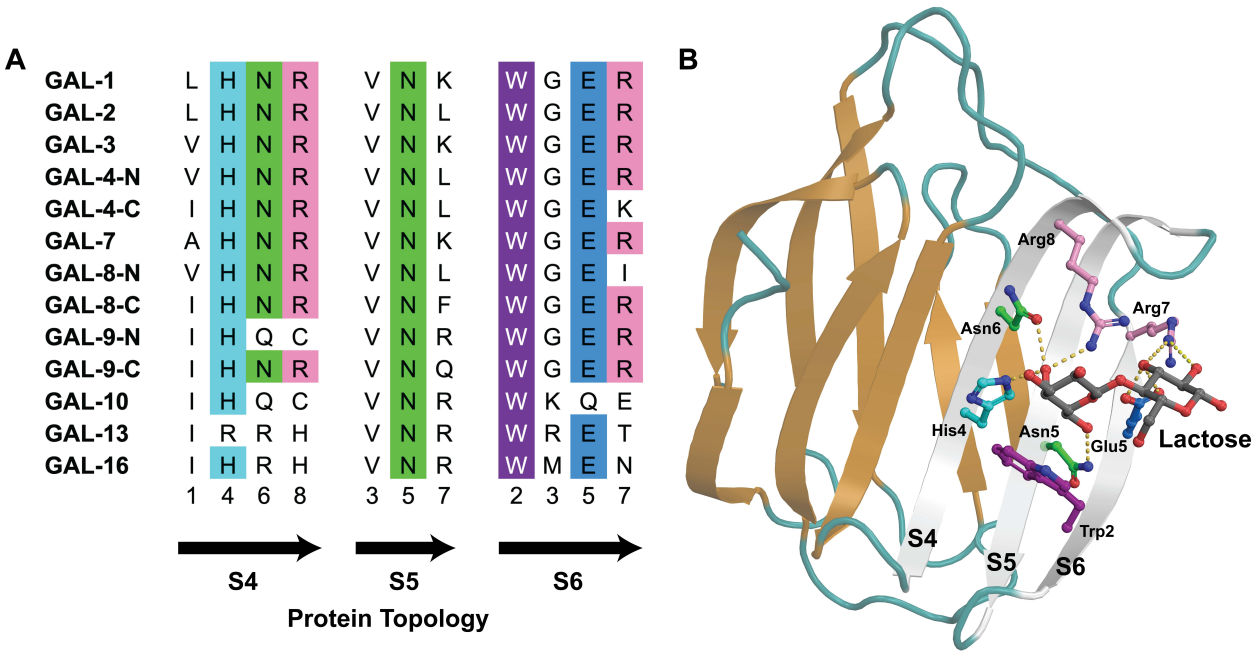

Figure 1.2 GBS conservation among human galectins.

A. Highly conserved GBS residues along the S4-S6 β-strands of the protein topology are highlighted in different colors: cyan, green, pink, purple, and marine for histidine, asparagine, arginine, tryptophan, and glutamate, respectively. The number indicates the relative position of each residue within its strand. B. Three-dimensional illustration of highly conserved residues in the GBS of GAL-1 (PDB 1W6O). These residues and the lactose bound ligand are shown as ball and sticks. Residues are shown using with the same color code used in panel A. Lactose carbons are colored grey, with red and blue spheres representing oxygen and nitrogen atoms, respectively. Polar interactions between GBS residues and lactose are shown as yellow dashes.

Galectins are widely distributed in various species, including vertebrates (human, bird, amphibian, fish) and non-vertebrates (*Drosophila melanogaster*, *Caenorhabditis elegans*, plants) (Cooper, 2002). The conservation of primary structures and domain organization between species suggests that oligomerization of this lectin family plays a fundamental role in their biological functions (Vasta, 2016) (Figure 1.3). Indeed, a study has shown that evolutionary pressure has favored dimer stabilization of the fish galectin congerin in such a way that offspring members ConI and ConII exhibit enhanced biological activity relative to their ancestral protein. Moreover, this evolutionary pressure promoted carbohydrate specificity with carbohydrate association constants (K_a) showing high correlation with dimer interface enhancement (area and H-bonding interactions) (Konno et al., 2011). In another study performed on the plant lectin concanavalin A (ConA), which exhibits the same primary fold as galectins, it was demonstrated that the switch between tetramer to dimer state implied a change in oligosaccharide binding specificity (Mandal et al., 1993). As for human galectins, their multimerization allows them to form extracellular lattices by crosslinking to multivalent glycosylated ligands, which ultimately gives rise to distinct cellular functions (Nabi et al., 2015) (Figure 1.4). Interestingly, the glycan-independent multimerization of GAL-10, which

forms crystals in the mucus, stimulated innate and adaptative immunity in asthma (Persson et al., 2019). Overall, such evidence supports the importance of oligomerization in the cellular activities promoted by galectins.

Even though galectins exhibit high 3D structure homology in their protomeric CRDs, dimer organization differs significantly between family members and may not even exist in GAL-16 (Si et al., 2021). Based on spatial organization, three homodimeric prototype galectin sub-groups have been observed to date: side-to-side (GAL-1, GAL-2, GAL-13), back-to-back (GAL-7), and face-to-face (GAL-10, GAL-14) (Figure 1.3B). As for heterodimers of tandem-repeat human galectins, they also exhibit distinct quaternary structures. In fact, recent X-ray crystallization studies revealed a back-to-side architecture in GAL-8, while GAL-9 forms a back-to-back complex (Kamitori, 2018). In addition to their distinct oligomerization patterns, the Mayo group recently suggested that prototype GAL-1, -7, and chimera-type GAL-3 could form hetero-oligomers to synergetically modulate cellular function. For example, GAL-1 and -7 could synergetically attenuate the endothlial cell migration and proliferation (Dings et al., 2021). However, these observations remain *in vitro* preliminary results with no evidence for the existence of these hetero-oligomer galectin complexes *in vivo.* Overall, the unique spatial arrangements of each human galectin family member implies formation of a particular glycan-galectin cross-linking lattice architecture, giving rise to distinctive biological functions.

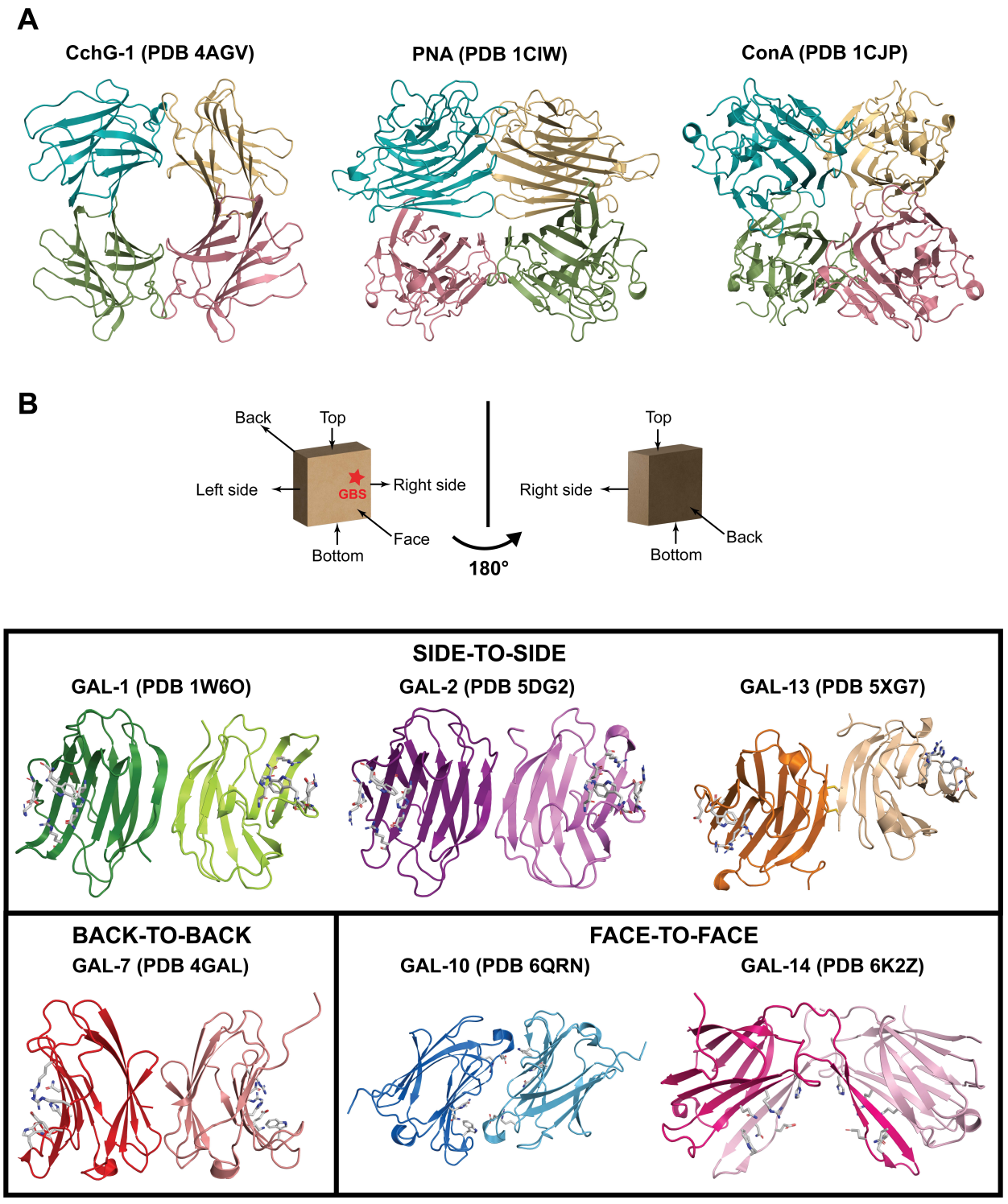

Figure 1.3 Structural conservation and oligomeric organization of galectin and lectin CRDs

A. Homologous plant and ancestral lectins display distinct tetrameric architectures, as illustrated with CchG-1 galectin (Ball sponge, PDB 4AGV), PNA lectin (Peanut lectin, PDB 1CIW), and ConA (Jack bean lectin, PDB 1CJP). B. Despite conserving similar 3D CRD structures, prototypic human galectins form distinct quaternary structural homodimers: side-to-side (GAL-1, GAL-2, and GAL 13, PDBs 1W6O, 5DG2, and 5XG7), back-to-back (GAL-7, PDB 4GAL), face-to-face (GAL-10 and GAL-14, PDBs 6QRN and 6K2Z). Highly conserved GBS residues are shown as sticks with the following coloring scheme: white for carbon, red for oxygen, and blue for nitrogen.

1.2.2 Human galectin functions

Galectins are cytosolic proteins which are exported out of the cell by a non-classical secretion process and/or translocated into the nucleus (Johannes et al., 2018; Nabi et al., 2015). Residing in all three main cellular compartments (extracellular, cytoplasm, and nucleus), galectins modulate various cellular events, including growth, adhesion, migration, differentiation, cell death (apoptosis), intracellular trafficking, innate immune response, and pre-mRNA splicing (Arthur et al., 2015; Johannes et al., 2018; Liu et al., 2005; Nabi et al., 2015).

- *Extracellular functions*
    - *Endocytosis*

Extracellular galectins crosslink cell-surface glycoconjugates or glycoproteins (integrins, laminin, fibronectin, hensin, and elastin) via their GBS to form an extracellular lattice (Liu et al., 2005) (Figure 1.4). Since interactions between galectins and glyco-partners are multivalent and glycosidic bonds of glycan complexes are free to rotate, this lattice behaves like a dynamic planar gel polymer (Nabi et al., 2015). Through this lattice, galectins can modulate the endocytosis of different glycoproteins and amino acids. For example, GAL-3 modulates the internalization of CD44, CD59, and MHC1, GAL-8 favors the uptake of CD166 in lymphocytes, GAL-12 decreases glutamine cellular penetration, while E-cadherin internalization depends on GAL-7 levels (Johannes et al, 2020; Katzenmaier et al., 2019; Lakshminarayan et al., 2014; Mathew 2018; Renard et al., 2020). In contrast, GAL-7 blocks E-cadherin internalization in keratinocytes via a glycan-independent interaction (Advedissian et al., 2017b).

    - *Cell adhesion and migration*

Extracellular galectins also play an important role in cell adhesion. For instance, GAL-3 aids with the adhesion of T cells to dendritic cells and macrophages, and the adhesion of human neutrophils to endothelial cells, possibly through interactions with laminin (Kuwabara et al., 1996; Sato et al., 2002; Swarte et al., 1998). GAL-8 regulates the integrin-based interaction between the human carcinoma 1299 cells and the extracellular matrix (Hadari et al., 2000). Furthermore, exogenous galectins also promote cell migration. Indeed, GAL-3, -7, and -8 enhance migration of HTR-8/SVneo human trophoblast cells, endometrial cancer cells, and U87 glioblastoma cells, respectively (Bojić-Trbojević et al., 2019; Menkhorst et al., 2018; Metz et al., 2016). Conversely, GAL-4 inhibits migration of pancreatic cancer cells (Belo et al., 2013).

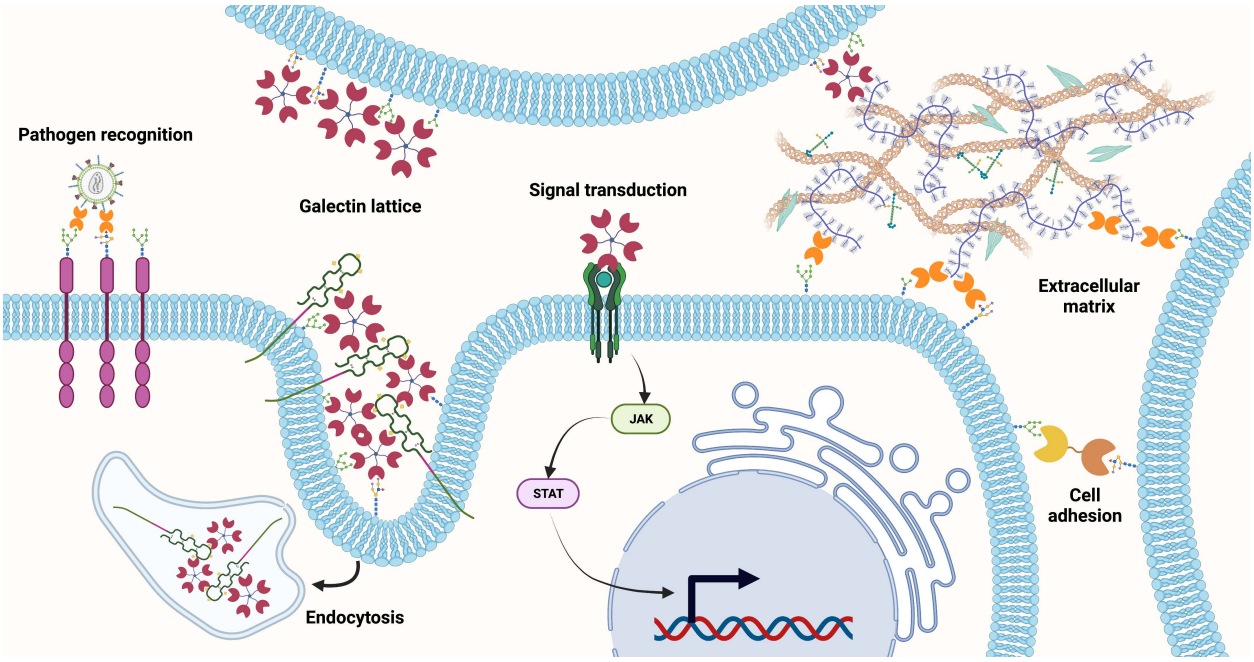

Figure 1.4 Extracellular functions of human galectins.

Extracellular galectins bind to glycolysated receptors to form galectin lattices, which are involved in multiple cellular functions. These include endocytosis (illustrated by the internalization of CD44 by GAL-3), cell adhesion and cell-extracellular matrix interaction, pathogen recognition and response, as well as signal transduction (illustrated by the regulation of JAK-STAT pathway of GAL-3 in immune cells). Galectins are shown as Pac-Man forms in red, orange, and yellow colors representing chimera, prototypic, and tandem-repeat galectins, respectively. Image created with BioRender.com.

- *Hemostasis, Tissue Repair and Angiogenesis*

Besides the above mentioned functions, exogenous galectins modulate hemostasis, tissue repair and wound (Arthur et al., 2015; Cao et al., 2002). For example, GAL-1 promotes muscle formation and regeneration angiogenesis (Ahmed et al., 2009; Georgiadis et al., 2007; Thijssen et al., 2006). GAL-1, -3, and -8 regulate activation of platelets using different pathways. GAL-8 tunes Factor V levels, while GAL-1 and -3 block the interaction between platelets and the von Willebrand factor by binding its *N*-glycan moiety (Pacienza et al., 2008; Romaniuk et al., 2010; Saint-Lu et al., 2012). In tissue repair, GAL-3 and -7 induce cell migration and proliferation after an epithelial wound by enhancing fusion of myoblasts with myotubes (Cao et al., 2002). Moreover, GAL-7 can modulate apoptosis, proliferation, and migration of kerinocyte during skin repair or stimulate the healing of corneal epithelial wound (Advedissian et al., 2017a; Cao et al., 2003; Gendronneau et al., 2008). In addition to their role in hemostasis and tissue repair, GAL-1, -3, and -8 also facilitate angiogenesis through interactions with vascular endothelial growth factor 1 (VEGFR1) and VEGFR2, neural/glial antigen 2 (NG2), and α3β1 integrins, and CD166,

respectively (Delgado et al., 2011; D'Haene et al., 2013; Fukushi et al., 2004; Nangia-Makker et al., 2000).

- *Immune system regulation*

Extracellular galectins recognize leucocyte glycoreceptors from both adaptive and innate immune systems, playing important roles in immunomodulatory processes (Arthur et al., 2015; Compagno et al., 2020; Giovannone et al., 2018b; Pereira et al., 2018; Rabinovich et al., 2002, 2012; Sun et al., 2021; Xu et al., 2021) (Figure 1.5). Indeed, distinct galectins modulate T cell viability and activation as well as cytokine production. For example, human GAL-1, -2, -3, -4, -7, -8, and -9 induce apoptosis of T cells (Kovács-Sólyom et al., 2010; Labrie et al., 2014; Lhuillier et al., 2015; Norambuena et al., 2009; Pace et al., 2000; Paclik et al., 2008a, 2008b; Perillo et al., 1995; Sebban et al., 2007; Stillman et al., 2006; Sturm et al., 2004). However, GAL-1 and -8 also facilitate T-cell activation, while GAL-3 inihibits this process (Chen et al., 2009; Demetriou et al., 2001; Tribulatti et al., 2012). GAL-1, -2, and -3 reduce IFNγ production whereas GAL-9 reduces this production (Cedeno-Laurent et al., 2012; Chen et al., 2009; Lhuillier et al., 2015; Sturm et al., 2004). GAL-1 and -4 increase production of interleurkins IL-10 and IL-6, respectively (Chen et al., 2009; Hokama et al., 2004). Noteworthy, IFNγ, IL-10 and IL-6 induce autocrine/paracrine signaling on immune cells to regulate the JAK-STAT pathway, which plays an important role in immune cell responses (Seif et al., 2017). Moreover, IFNγ and IL-6 are generally associated to pro-inflammatory responses, while IL-10 can inhibit this cytokine-induced inflammatory stimulus (Chen et al., 2017). Additionally, GAL-3 can indirectly reduce chemokine production by restricting the diffusion of their inducer IFNγ through the GAL-3 tumor extracellular matrix, allowing tumor cells to escape from T-cell chemotaxis, and therefore T-cell infiltration (Gordon-Alonso et al., 2017).

In addition to T cell regulation, galectins also regulate B cell immunity (Giovannone et al., 2018). For instance, during B cell development in bone marrow, the extracellular GBS-independent interaction of GAL-1 with pre-B-cell receptor triggers pre-BII cell proliferation and differentiation (Elantak et al., 2012; Espeli et al., 2009; Gauthier et al., 2002). Galectins also control the differentiation of naïve B cells after their maturation along with translocation to the splenic environment. Indeed, binding of extracellular GAL-1 and -8 on matured B cells enhances their differentiation into antibody secreting plasma cells (Tsai et al., 2011). GAL-1,-3, and -9 can positively and/or negatively regulate B cell activation and signaling (Arthur et al., 2015; Cao et al., 2018; Clark et al., 2012; Fouillit et al., 2000; Giovannone, 2018a, 2018b; Tsai et al., 2014). For example, GAL-1, -3 or -9 binding to CD45 located on the cell surface of BL36 Burkitt lymphoma

cells, geminal center B cells, or naïve B cells, respectively, inhibits the CD45 phosphatase activity of these cells, reducing B cell proliferation. However, GAL-1 binding to the B-cell receptor stimulates B-cell activity in chronic lymphocytic leukemia.

In regards to the innate immune system, extracellular galectins have a wide range of effects on multiple cell types (Arthur et al., 2015; Liu et al., 2010). For example, GAL-1 expressed by glioma cells helps these cells to escape eradication by NK cells (Baker et al., 2014). GAL-3 binds to NKp30 on the surface of NK cells and blocks their cytolysis (Wang et al., 2014). GAL-9 regulates NKT cells homeostasis by interacting with TIM-3 expressed in different cell types. Indeed, the interaction of GAL-9 with TIM-3 on NKT cells induces apoptosis of these cells, while interaction with TIM-3 on Kuffer cells enhances the secretion of IL-15, which is a crucial factor inducing NKT cell proliferation (Tang et al., 2013).

Concerning monocytes, GAL-1 and -3 regulate the activation of macrophages (Barrionuevo et al., 2007; MacKinnon et al., 2008). GAL-3 also enhances the respiratory burst and impedes cytokine response in macrophages induced by lipopolysaccharides (LPS) (Li et al., 2008; Liu et al., 1995) . GAL-1 induces the tolerogenic phenotype of dendritic cells (tol-DCs) (Blois et al., 2007). In fact, tol-DCs are semi-mature dendritic cells with immunosupressive properties playing a crucial role in balancing immune homeostasis (Domogalla et al., 2017). In contrast, exposition of DCs to GAL-9 enhances immune response by stimulating production of IL-12, which ultimately promotes IFNγ production as well as cytolytic activity and proliferation of NK and T cells (Dai et al., 2005; Vecchio et al., 2007). In addition, GAL-1, -2, -3, -4, -8 sensitize neutrophils to phagolytic removal by inducing preaparesis, a process known as the exposure of phosphotidylserine in neutrophiles without causing their apoptosis (Nishi et al., 2003; Stowell et al., 2006, 2008, 2009). GAL-1 and -3 also control extravasation, the oxidative burst and chemotaxis of neutrophils, regulating their inflammatory activity (Almkvist et al., 2001, 2002; Bhaumik et al., 2013; Cooper et al., 2008; Karlsson et al., 1998; La et al., 2003; Sato et al., 2002; Yamaoka et al., 1995). GAL-1 disfavors the degranulation of mast cells whereas GAL-3 favors this cellular process and induces mast cell apoptosis (Rabinovich et al., 2000; Suzuki et al., 2008). GAL-9 regulates chemotaxis and viability of eosinophils and GAL-3 prohibits the production of IL-5 in these cells (Cortegano et al., 1998; Matsumoto et al., 1998, 2002) .

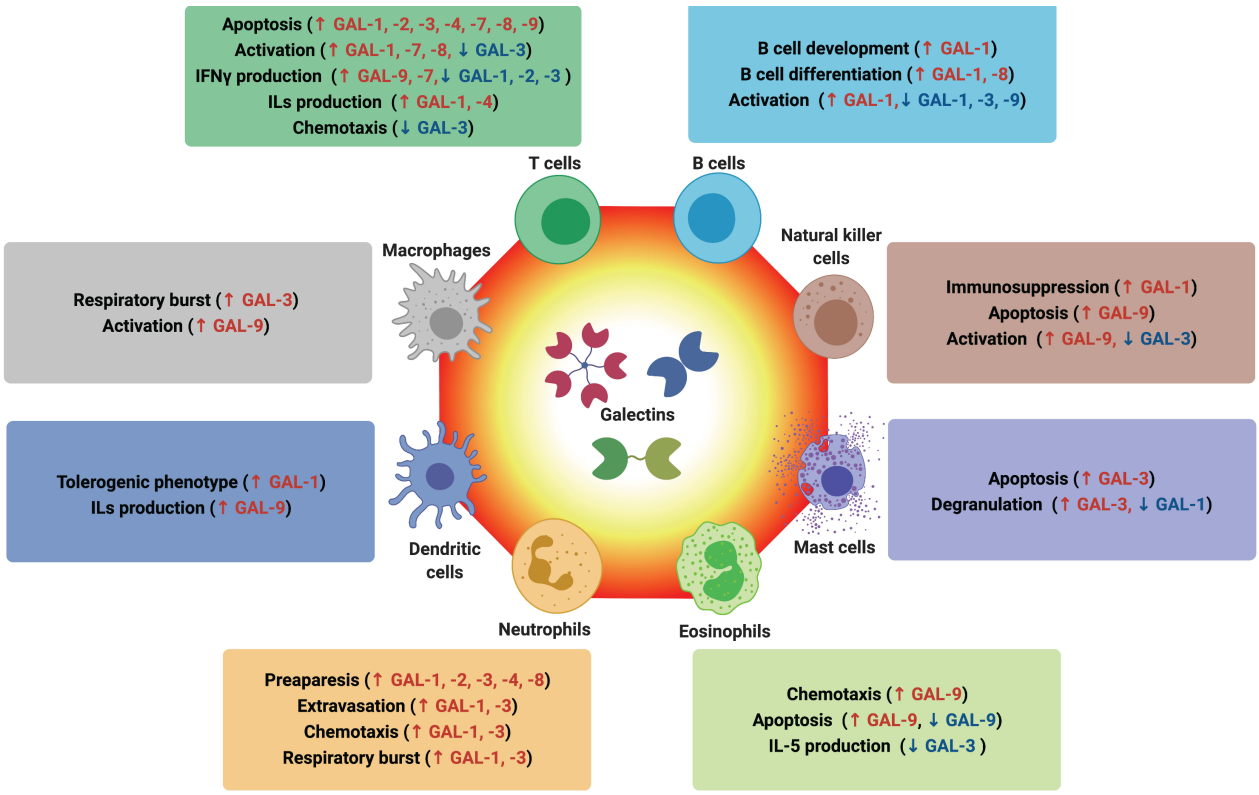

Figure 1.5 Role of human galectins in immune system regulation.

Human galectins control multiple cellular processes in different immune cells. Within the adaptative immune system, galectins regulate apoptosis, immune cell activation, IFNγ and ILs production, chemotoaxis of T cells, and the development, differentiation, and activation of B cells. Within the innate immune system, galectins modulate the immunosuppression, apoptosis, and activation of natural killer cells; apoptosis and degranulation of mast cells; chemotaxis, apoptosis, and IL-5 production of eosinophils; preaparesis, extravasation, chemotaxis, and respiratory burst of neutrophils; tolerogenic phenotype and ILs production of dendritic cells; and the respiratory burst and activation of macrophages. Red and blue labeling colors/arrows denote an increase or decrease in galectin function, respectively. Image created with BioRender.com.

- *Pathogenic responses*

Due to their broad glycan recognition range, human galectins can bridge host cell glycans with pathogenic glycans, playing a crucial role in host defense (Arthur et al., 2015; Ayona et al., 2020) (Figure 1.4). For example, GAL-1 inhibits the internalization of Nipah, Influenza, and Dengue viruses, while GAL-3 facilitates the killing of *Candida* spp, *Candida albicans, Toxoplasma gondii,* and restrains the growth of *Streptococus* (Chen et al., 2015; Debierre-Grockiego et al., 2010; Farnworth et al., 2008; Garner et al., 2014; Kohatsu et al., 2006; Toledo et al., 2014). In addition, GAL-4 and GAL-8 can kill bacteria expressing blood group antigen B (Stowell et al., 2010). However, pathogens including viruses, bacteria, parasites, and fungus can also exploit extracellular galectins to infect the host cell (Arthur et al., 2015; Ayona et al., 2020). For instance, GAL-1 facilitates the viral infection by Human Immunodeficiency Virus Type 1 (HIV-1), Human T

Cell Leukemia Virus Type 1 (HTLV-1), Herpes Simplex Virus (HSV-1), Epstein-Barr Virus (EBV), and Enterovirus 71 (EV71) (Gauthier et al., 2008; Gonzalez et al., 2005; Lee et al., 2015; Mercier et al., 2008; Ouyang et al., 2011). GAL-3 is frequently involved in fungal (*Histoplasma capsulatum*), parasitic (*Trypanosoma cruzi, Plasmodium* spp.*),* and bacterial (*Salmonella* spp., *Listeria monocytogenes, Neisseria meningitidis,* Group A Streptococcus (GAS)*, Helicobacter pylori, Pseudomonas aeruginosa, Proteus mirabilis)* infections (Altman et al., 2001; Farnworth et al., 2008; Fowler et al., 2006; Gupta et al., 1997; Kleshchenko et al., 2004; Li et al., 2008; Quattroni et al., 2012; Toscano et al., 2012; Weng et al., 2009; Wu et al., 2013). Besides, GAL-7, GAL-8, and GAL-9 also favor other pathogenic infections. Hence, human galectins are a double-edged sword for pathogen eradication and invasion (Ayona et al., 2020; Chernyy et al., 2011; Klibi et al., 2009; Li et al., 2019; Pineda et al., 2015; Wang et al., 2011).

- *Intracellular functions*

Although extracellular galectin functions are generally related to their glycan-binding ability occurring at the GBS, a large number of *in vivo* and *in vitro* studies have demonstrated that intracellular galectins can modulate various intracellular signaling pathways via both GBS-dependent and GBS-independent interactions with an intracellular partner. Indeed, intracellular galectins have been shown to regulate apoptosis, cell cycle, cell proliferation, intracellular trafficking, as well as mediate the response to damaged endocytosis vesicles and control the transcriptional activity of transcription factors (Figure 1.6) (Arthur et al., 2015; Johannes et al., 2018; Liu et al., 2002; Vladoiu et al., 2014).

  - *Apoptosis*

In SKW6.4 cells, cytoplasmic GAL-3 interacts with CD95 to form the death inducing signaling complex (DISC), which stimulates caspase-8 activation to induce cell apoptosis (Fukumori et al., 2004). However, GAL-3 also inhibits apoptosis by interacting with the proapoptotic Bax protein, which prevents its oligomerization (Harazono et al., 2014). Moreover, GAL-3 partners with the anti-apoptotic protein BCL-2 in mitochondria, preventing mitochondrial damage and cytochrome c release (Akahani et al., 1997; Harazono et al., 2014; Yang et al., 1996). In addition, GAL-3 possesses a NWGR motif, an amino acid sequence conserved in the BH1 domain of BCL-2 family members including Bax, Bak, and BCL-XL, protein partners that interact together to control cellular apoptosis. This anti-apoptotic effect of GAL-3 probably relies on its interaction with synexin to mediate its translocation from cytoplasm to mitochondria (Yu et al., 2002). On the contrary, mitochondrial GAL-7 makes a GBS-independent interaction with BCL-2 to sensitize mitochondria to the apoptotic signal (Villeneuve et al., 2011). In the cytoplasm, GAL-

7 also induces the apoptosis of colorectal DLD-1, keratinocyte HaCaT, and HeLa cell lines through the c-Jun N-terminal kinase (JNK) pathway and mitochondrial cytochrome *c* release (Chen et al., 2016; Kuwabara et al., 2002). Besides GAL-3 and GAL-7, intracellular GAL-12 promotes the apoptosis of adipocytes and cervical cancer cells, in a GBS-independent manner (Wan et al., 2018).

- *Cell cycle*

In mitochondria, GAL-3 interacts with the F_0 subunit of ATP synthase and inhibits its activity, which may affect the interphase cell cycle in human colon cancer cells in presence of anti-cancer drugs (doxorubicin, nocodazole) (Kim et al., 2008). In addition, intracellular GAL-3 was shown to induce G1 arrest of epithelial breast BT549 cells by down-regulating cyclin E and A levels, and up-regulating expression of their inhibitory p21 and p27 proteins (Kim et al., 1999) . GAL-12 initiates G1 cell cycle arrest in adipose tissue (Wan et al., 2018).

- *Cell proliferation*

Intracellular galectins can modulate cell proliferation through Wnt and Ras-GTPase signaling pathways. Under Wnt stimulation, cytoplasmic GAL-3 forms a complex with Axin, ß-catenin, and GSK-3ß which induces GAL-3 phosphorylation. ß-catenin is then imported into the nucleus by phosphorylated GAL-3 to promote cell proliferation (Shimura et al., 2004, 2005). Inversely, interaction between GAL-4 and these proteins reduces nuclear import of ß-catenin, preventing cell proliferation (Maftouh et al., 2014). Regarding Ras-GTPase signaling pathway, cytoplasmic GAL-1 interacts with the Ras binding domain of Raf (Ras effector) to form H-Ras-GTP nanoclusters through GAL-1 dimerization (Blaževitš et al., 2016), inducing an increased MAPK signaling pathway output which enhances cell proliferation (Pudewell et al., 2021). On the other hand, cytosolic GAL-3 interacts with the farnesyl group of K-Ras-GTP to increase nanocluster formations at the plasma membrane (Shalom-Feuerstein et al., 2008b), resulting in different output signals depending on tissue type. For example, GAL-3-K-Ras-GTP clusters exclusively activate Phosphoinositide 3-kinases (PI3K) pathway in HEK-293 cells while MAPK is activated in BT549 cells (Elad-Sfadia et al., 2004; Shalom-Feuerstein et al., 2008b). In addition, the anchorage of GAL-1 and GAL-3 by Protocadherin-24 (PCDH-24) in cytosol was suggested to impede activation of PI3K pathway in HCT116 colon cancer cells (Ose et al., 2012).

- *Cellular responses to damaged endocytic vesicles*

Cytoplasmic galectins can also bind to glycans exposed at the lumen side of disrupted endocytic vesicles resulting from a pathogenic infection, virulence factors, mineral crystals or

chemical reagents (Figure 1.6) (Hong et al., 2021). This accumulation around impaired vesicles has been shown to be spatiotemporally distinct among diverse galectins. Galectins further activate autophagy of these damaged vesicles by linking them to autophagy adapter proteins (NDP52, p62), AMP-activated protein kinase (AMPK), mammalian target of rapamycin (mTOR) complex, or tripartite motif containing proteins (TRIMs) (Chauhan et al., 2016; Hong et al., 2019; Jia et al., 2018; Thurston et al., 2012). Moreover, galectins can also recruit antimicrobial proteins (e.g., antimicrobial interferon-inducible guanylate binding proteins) into the vesicle to act against bacteria (Feeley et al., 2017). Noteworthy, GAL-3 can either trigger or obstruct autophagy. Indeed, GAL-3 accumulation inhibits autophagy in *Listeria* infection but promotes autophagy of endocytic vesicles damaged by red laser light (Hong et al., 2019, 2021)

- *Intracellular trafficking*

Under epidermal growth factor (EGF) stimulation, GAL-3 can regulate the interaction between the EGF receptor (EGFR) and Alix, a component of ESCRT (endosomal complexes required for transport), therefore modulating intracellular trafficking of EFGR (Liu et al., 2012). GAL-3 may also regulate cell differentiation through the Hedgehog (Hh) pathway by monitoring the distribution of Sufu (suppressor of fused) between nucleus and cytoplasm (Haudek et al., 2010). Indeed, translocation of Sufu from cytoplasm to nucleus is linked to modulation of Gli transcriptional activities within Hh pathway (Paces-Fessy et al., 2004). Moreover, GAL-3 is involved in the non-raft-associated sorting of apical cargo. In contrast, GAL-4 influences protein trafficking at the apical membrane by clustering lipid rafts through interaction with sulfatides and galactosylceramides (Delacour et al., 2005).

- *Nuclear galectin functions*

In the nucleus, GAL-1 and GAL-3 are classified as mRNA splicing factors (Dagher et al., 1995; Vyakarnam et al., 1997). They are associated with Gemin 4 within the Survival of Motor Neuron (SMN) complex involved in the recycling of small nuclear ribonucleoproteins (snRNPs) for the splicing pathway (Charroux et al., 2000; Park et al., 2001; Pellizzoni et al., 1998). Nuclear GAL-3 also forms a complex with β-catenin and TCF-4 to promote the transcriptional activity of TCF-4 in breast cancer cells (Shimura et al., 2004). Since TCF-4 is known to induce epithelial-mesenchymal transition (Forrest et al., 2014), GAL-3 might promote metastasis of breast cancer cells through the TCF-4/β-catenin pathway. Moreover, GAL-3 directly interacts with the homeodomain of TTF-1 and stimulates its transcriptional activity by enhancing its DNA binding activity. High transcriptional activity of TTF-1 therefore promotes proliferation of thyroid cells (Paron et al., 2003). GAL-7 has also been shown to act within cell nuclei. It promotes nuclear

export of Smad3 in response to Hepatocyte Growth Factor (HGF). Since HGF inhibits the transforming growth factor β (TGF-β) pathway, hepatic anti-fibrosis is induced (Inagaki et al., 2008).

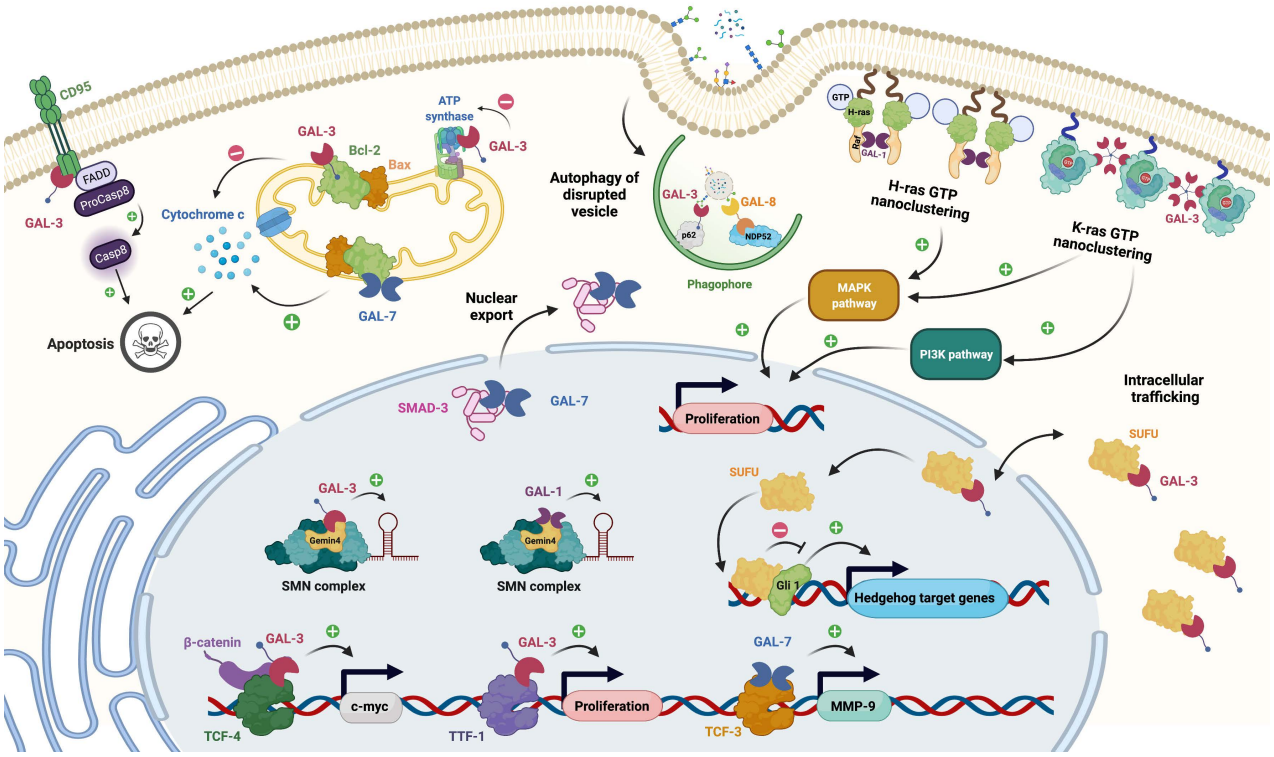

Figure 1.6 Intracellular functions of human galectins.

Galectins modulate apoptosis by activating caspase 8 (GAL-3, red Pac-Man) or regulate cytochrome *c* release via interaction with the anti-apoptotic BCL-2 protein (GAL-3, -7, blue Pac-Man). GAL-3 and -8 (orange-yellow Pac-Man) activate autophagy of damaged vesicles by linking them to the autophagy adapter protein p62 and NDP52, respectively. GAL-1(purple Pac-Man) and -3 enhance cellular proliferation through activation of Ras-GTPase pathway. GAL-3 also controls the hedgehog pathway by regulating the distribution of SUFU between the nucleus and cytoplasm. In the nucleus, GAL-7 is involved in nuclear export of SMAD-3. GAL-7 also induces the expression of MMP-9 in tumor cells (breast, ovarian, head and neck, cervix, gastric cells, and carcinoma) to promote tumor progression. GAL-1 and -3 regulate the mRNA splicing activity of SMN complex by binding to Germin4 proteins. GAL-3 promotes metastasis of breast cancer cells by inducing the expression of c-myc via interaction with theTCF-4/β-catenin complex. GAL-3 also enhances cellular proliferation by interacting with TTF-1. Image created with BioRender.com.

1.2.3 Galectins in cancer

With the involvement of diverse galectin members in numerous cellular functions, it is not surprising that these proteins significantly contribute to tumor progression (Chou et al., 2018; Dubé-Delarosbil et al., 2018; Girotti et al., 2019; Liu et al., 2005; Vladoiu et al., 2014; Wdowiak et al., 2018). In fact, galectins have been shown to contribute to all 10 tumor hallmarks: enhanced cell proliferation signal, tumor suppressors inactivation, sustained immune escape, promotion of limitless replicative potential, stimulation of tumor-associated inflammation response, invasion and metastasis, angiogenesis, chromosomal alterations, resistance to apoptosis, and altered energy metabolism (Girotti et al., 2019; Gordon-Weeks, 2020; Huang et al., 2021; Martínez-Bosch, 2020; St-Pierre, 2021) (Figure 1.7B). For example, GAL-7 and -8 promote migration of endometrial cancer cells and U87 glioblastoma cells, respectively (Menkhorst et al., 2018; Metz et al., 2016). Reduced IFNγ production, induced tol-DCs phenotype, and neutrophil preaparesis, as well as T cell apoptosis caused by diverse galectins promote an immunosuppressive/immunoescaping environment (Cedeno-Laurent et al., 2012; Chen et al., 2009; Nishi et al., 2003; Stowell et al., 2006, 2008, 2009; Sturm et al., 2004). Moreover, tumor cell proliferation can be stimulated by GAL-1 and-3 through Wnt, Ras signaling pathways, and regulation of TCF-4 and TTF-1 transcriptional activity (Blaževitš et al., 2016; Charroux et al., 2000; Elad-Sfadia et al., 2004; Forrest et al., 2014; Paron et al., 2003; Pudewell et al., 2021; Shalom-Feuerstein et al., 2005; Shalom-Feuerstein et al., 2008a, 2008b; Shimura et al., 2004, 2005). Finally, inhibition of apoptosis caused by galectins helps cancer cells to be more resistant to cell death (Aboulhagag et al., 2018; Fukumori et al., 2004).

Depending on cancer types, each galectin can either be pro- or anti-tumorigenic (Figure 1.7A) (Ajarrag et al., 2021; Dubé-Delarosbil et al., 2018; Pergialiotis et al., 2021; Sewgobind et al., 2021). For example, GAL-1, -3, -4 promote the progression of liver cancer, while GAL-9 inhibits it (Bacigalupo et al., 2015; Cai et al., 2014; Fang et al., 2011; Inufusa et al., 2001; Li et al., 2012; Liang et al., 2015; Manzi et al., 2016; Serizawa et al., 2015; Spano et al., 2010; Zhang et al., 2016; Zhang et al., 2012; Zheng et al., 2014). GAL-4 is pro-tumorigenic for lung cancer but anti-tumorigenic for pancreatic cancer (Belo et al., 2013; Hayashi et al., 2013; Maftouh et al., 2014). Although GAL-7 promotes breast cancer, this protein also reduces tumor progression of stomach cancer (Grosset et al., 2016; Kim et al., 2013). The ability of galectins to facilitate cancer progression can be induced by both GBS-dependent or -independent interactions with their various partners. For instance, extracellular galectins have been previously shown to induce T cell apoptosis by binding to surface glycoproteins through their GBS, allowing tumors to escape

from immune destruction (Kovács-Sólyom et al., 2010; Labrie et al., 2014; Lhuillier et al., 2015; Norambuena et al., 2009; Pace et al., 2000; Paclik et al., 2008a, 2008b; Perillo et al., 1995; Sebban et al., 2007; Stillman et al., 2006; Sturm et al., 2004). The immunosuppressive activity of galectins can be mediated by GBS-independent interactions between intracellular galectins and the anti-apoptotic protein BCL-2 (Akahani et al., 1997; Harazono et al., 2014; Villeneuve et al., 2011; Yang et al., 1996). In addition, non-GBS interactions involving GAL-3 and K-Ras-GTP intensify the downstream signaling of KRAS pathway, resulting in continuous tumor proliferation. Hence, galectins are potential targets for cancer therapeutics (Seguin et al., 2017).

To this day in the United States, six compounds (GCS-100, Davanat, GR-MD-02, OTX008, GB0139 and LYT-200) targeting galectins, and three compounds (TSR-002, LY3321367, and Sabatolimab) targeting TIM-3, a galectin-9 binding partner, were submitted to clinical trials for various cancer treatments in combination with chemotherapy (5-fluorouracil) or immunotherapy (ipilimumab, pembrolizumab) (Chou et al., 2018; Girard et al., 2018) (Table 1.1). Among the 24 clinical trials reported to use a galectin inhibitor, 25% were withdrawn, terminated or unknown status, and only three compounds advanced to phase II (GR-MD-2, GCS-100, and GB0139). In contrast, clinical trials targeting TIM-3 appear to be more efficient since a candidate (Sabatolimab) advanced to phase III. Despite more than two decades dedicated to this research, these observations demonstrate that significant challenges still hamper the design of effective and specific galectin inhibitors (Dubé-Delarosbil et al., 2018; Sörme et al., 2003). Indeed, the development of functional modulators has exclusively favored inhibition of galectins at their glycan binding sites, aiming to perturb the interactions between galectins and their glycoprotein partners (Denavit et al., 2018). However, considering high GBS similarity among different galectin homologs (Figure 1.1D), this is a risky strategy due to significant off-target effects observed on other important galectins such as anti-pancreatic-tumor GAL-4. As stated previously, GBS inhibitors are ineffective for targeting glycan-independent functions of galectins. Therefore, it is crucial to establish a new approach to develop effective and specific galectin inhibitors that rely on distinct molecular mechanisms and strategies (St-Pierre et al., 2018)

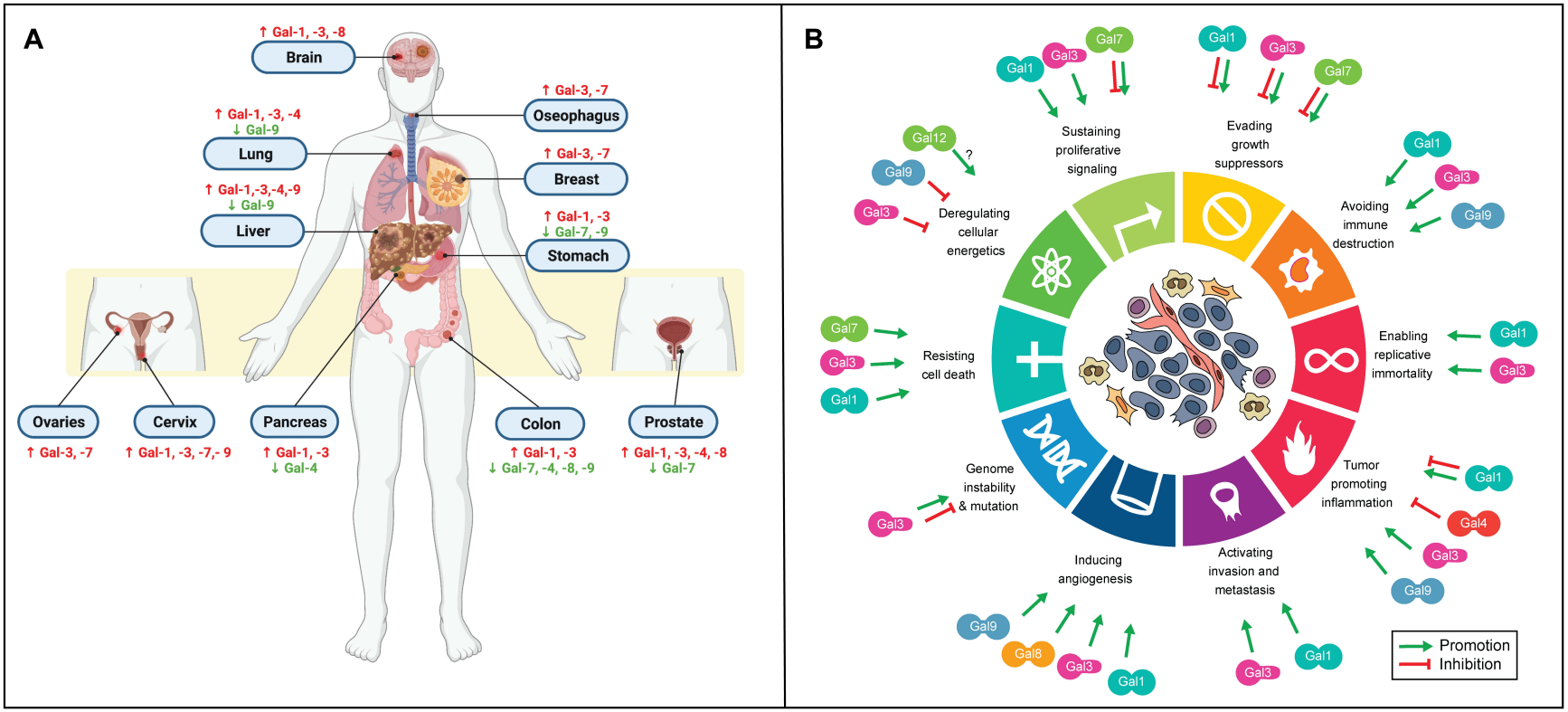

Figure 1.7 Galectins in cancer.

A. Pro- and anti-tumor functions of galectins in different types of cancers are highlighted in red and green, respectively (Barrow et al., 2011; Dubé-Delarosbil et al., 2018; Martínez-Bosch et al., 2019; Wang et al., 2013). Image created with BioRender.com. B. Role of human galectins on hallmarks of cancer (figure from (Girotti et al., 2019)). Galectins can either promote (green) or inhibit (red) the various cellular and molecular processes involved in tumor growth and progression. Studies have mainly focused on the role of galectins on selected cancer hallmarks such as the ones listed in this figure, but their influence could include other cancer-related phenomena not yet fully investigated.

Table 1.1 List of compounds targeting galectins or galectin partners submitted to clinical trials for cancer therapy

Sponsor	Compound	Proposed Target	Indication	Intervention	Phase	NCT number	Status
Galectin Therapeutics	DAVANAT (GM-CT-01)	GAL-1 and -3	Colorectal, lung, breast, prostate, head and neck cancer	In combination with 5-fluorouracil	1	NCT00054977	Completed (n=40)
			Gallbladder cancer Cancer of the bile duct	In combination with 5-fluorouracil	2	NCT00386516	Withdrawn
			Colorectal cancer	In combination with 5-fluorouracil, leukovorin, bevacizumab	2	NCT00388700	Withdrawn
				In combination with 5-fluorouracil	2	NCT00110721	Terminated (n=20)
			Metastatic melanoma	In combination with tumor specific peptides: MAGE-3.A1 and / or NA17.A2	2	NCT01723813	Terminated (n=6)
	Belapectin (GR-MD-02)	GAL-3	Melanoma, lung cancer, head and neck cancer	In combination with pembrolizumab	1	NCT02575404	Active, not recruiting
			Metastatic Melanoma	In combination with Ipilimumab	1	NCT02117362	Completed (n=8)
			Non-alcoholic steatohepatitis (NASH), liver fibrosis	Only belapectin	1	NCT01899859	Completed (n=31)
					2	NCT02421094	Completed (n=30)
			Hypertension, protal, liver fibrosis, nash cirrhosis		2	NCT02462967	Completed (n=162)
			Psoriosis		2	NCT02407041	Completed (n=5)
			Hepatic impairment		1	NCT04332432	Completed (n=38)
			NASH, cirrhosis, esophageal varices		2	NCT04365868	Recruiting

Oncoethix GmBH	OTX008	GAL-1	Solid Tumors	Only OTX008	1	NCT01724320	Unknown
Pure Tech	LYT-200	GAL-9	Metastatic cancer, solid tumor, cholangiocarcinoma, colorectal and pancreatic cancer	In combination with Anti-PD-1, gemcitabine/nab-paclitaxel	1	NCT04666688	Recruiting
La Jolla Pharmaceuticals	GCS-100	GAL-3	Chronic kidney disease	Only GCS-100	1	NCT01717248	Completed (n=29)
					2	NCT01843790	Completed (n=120)
					2	NCT02155673	Completed (n=92)
					2	NCT02333955	Withdrawn
			Chronic lymphocytic leukemia		2	NCT00514696	Completed (n=12)
			Diabetic chronic kidney disease		2	NCT02312050	Unknown
Eli Lilly and Co.	LY3321367	TIM-3	Solid Tumors	In combination with LY3300054	1	NCT03099109	Active, not recruiting
			Solid Tumors, cutaneous melanoma, pancreatic cancer, breast cancer (HR+HER2-)	In combination with LY3300054, ramucirumab, abemaciclib, merestinib, LY3321367	1	NCT02791334	Active, not recruiting
Tesaro, Inc.	TSR-022	TIM-3	Liver cancer	Only TSR-022	2	NCT03680508	Recruiting
			Neoplasms	In combination with nivolumab, TSR-042, TSR-033, docetaxel, pemetrexed, cisplatin, carboplatin	1	NCT02817633	Active (n=58)
			Neoplasms, Metastatic, Solid Tumor, Lung cancer	In combination with niraparib, carboplatin-paclitaxel, bevacizumab, carboplatin-pemetrexed, carboplatin-nab-paclitaxel, TSR-042	1	NCT03307785	Recruiting
			Melanoma Stage III and IV	In combination with dostarlimab (TSR-042)	2	NCT04139902	Recruiting

Novartis	Sabatolimab (MBG453)	TIM-3	Advanced malignancies	In combination with PDR001, decitabine	1	NCT02608268	Active (n=252)
			Acute myeloid leukemia (AML)	In combination with venetoclax, azacitidine	2	NCT04150029	Recruiting
				In combination with azacitidine	1	NCT04623216	Recruiting
			Myelodysplastic syndrome (MDS)	In combination with venetoclax, azacitidine	2	NCT04812548	Recruiting
				In combination with NIS793, canakinumab	1	NCT04810611	Recruiting
				In combination with hypomethylating agents	2	NCT03946670	Active (n=127)
				In combination with azacytidine, decitabine	2	NCT04878432	Recruiting
			AML, MDS	In combination with HMD201	1	NCT03940352	Recruiting
			Glioblastoma multiforme	Only MBG453	1	NCT03961971	Recruiting
			MDS, leukemia, myelomonocytic, chronic	In combination with azacitidine	3	NCT04266301	Active (n=530)
			Leukemia, MDS	In combination with azacytidine, decitabine, PDR001	1	NCT03066648	Active (n=243)
			Myelofribosis	In combination with ruxolitinib, siremadlin, crizanlinumab, LTT462, NIS793	1	NCT04097821	Recruiting
Galecto Biotech AB	GB0139 (TD139)	GAL-3	Idiopathic Pulmonary Fibrosis (IPF)	Only TD139	1 & 2	NCT02257177	Completed (n=60)
					2	NCT0383294	Active, not recruiting
			COVID-19	In combination with Nafamostat Mesilate	1 & 2	NCT04473053	Active, not recruiting

*Source: (*Home - ClinicalTrials.Gov*, n.d.) (accessed on May, 30th, 2022)

1.3 Galectin-7 (GAL-7)

1.3.1 Expression

Human GAL-7 was first reported in two independent studies published in 1995. One study originally identified GAL-7 under the name IEF17 from the search of a keratinocyte protein marker responsible for this phenotype (Madsen et al., 1995). The other study identified GAL-7 from the isolation of an epidermal-specific cDNA clone 1A12 responsible for keratinocyte differentiation (Magnaldo et al., 1995). Based on sequence analysis and confirmation of lactose binding ability, both studies used the name "galectin-7" according to the nomenclature proposed by galectin researchers (Barondes et al., 1994).

GAL-7 is encoded by the LGALS7 gene mapped to chromosome 9. Its expression is tissue specific to a high degree and especially marked in epithelial cells (Magnaldo et al., 1998; Saussez et al., 2006; St-Pierre, 2012). GAL-7 expression can be induced via different transcription factors, including wild-type and mutant p53, and CCAAT/enhancer-binding protein beta (C/EBPb) 2 transcription factor (Campion et al., 2014; St-Pierre, 2021). In the case of mutant p53, its expression can also involve a gain-of-function mechanism via Nf-kB, depending on the cancer cell type (Campion et al., 2013, 2014). GAL-7 is frequently located in the nucleus and cytoplasm, but can also be secreted through a non-classical secretory pathway like other galectins (St-Pierre, 2012).

1.3.2 Structure

GAL-7 is a prototype galectin characterized by a homodimeric molecular architecture. Each protomer is composed of 11 antiparallel β-strands folded into a “jelly roll”-type motif. This fold consists of a sugar-binding face (S-face) defined by β-1, -10, -3, -4, -5, -6 strands and an opposing F-face defined by β-11, -2, -7, -8, -9 strands. GAL-7 homodimerization is organized in a “back-to-back” orientation of 1494 $Å^2$ surface area with central hydrophobic interactions (leucine, isoleucine, valine, phenylalanine) stabilized by terminal polar interactions (arginine, lysine, aspartate, and glutamate) between the F-faces of two protomers (Leonidas et al., 1998; Masuyer et al., 2012) (Figure 1.8). Polar interactions involving side-chain and backbone atoms on the two opposite protomers are formed between residues Arg14, Pro15, Gly16, Val18, Arg20, Ile91, Ala92, Ser93, Lys98, Val100, Asp103, and Phe135. Salt bridges are formed between residue pairs Arg14-Asp95, Arg14-Asp94, Arg20-Glu87, Arg20-Asp103, Arg22-Asp103, Lys98-Phe135, and Asp103-Arg133 across the homodimer interface (Table 1.2 and Figure 1.8). Inter-

protomer hydrophobic interactions are primarily maintained by Val18, Leu89, Ile91, Val100, and Phe135 (Figure 1.8).

The glycan binding pocket of GAL-7, located on the S-face, is formed by an ionic network involving Arg31, His33, His49, Asn51, Arg53, Glu58, Val60, Arg62, Ser63, Lys64, Trp69, Arg71, Glu72, Glu73, and Arg74 (Leonidas et al., 1998). Among these residues, seven (His49, Asn51, Arg53, Arg62, Trp69, Glu72, and Arg74) are highly conserved among galectin family members and are essential for direct interactions with β-galactoside ligands (Figure 1.2) (Leonidas et al., 1998; Modenutti et al., 2019). Indeed, O4, O5, and O6 of the galactose moiety make hydrogen bonding interactions with residues His49, Asn51, and Arg53, while the oxygen atom of the glycosilic bond and O3 of glucose moiety form hydrogen bonds with Arg53 and Glu72 (Table 1.3 and Figure 1.8) (Leonidas et al., 1998). Finally, Trp69 makes a CH-π interaction with the glucose moiety (Diehl, 2021; Kiessling et al., 2021; Modenutti et al., 2019).

Table 1.2 Intermolecular Contacts at the Dimer Interface

(PDB 1BKZ) (adapted from (Leonidas et al., 1998))

Polar (distance < 3.3 Å)			**van der Waals interactions** (the maximum distances allowed values of C-C, 4.1 Å; C-N, 3.8 Å; C-O, 3.7 Å; O-O, 3.3 Å; O-N, 3.4 Å; and N-N,3.4 Å)		
Molecule A	Molecule B	Distance (Å)	Molecule A	Molecule B	No. of contacts
Arg 14 N*h*2	Asp 94 O*d*1	2.5	Arg14	Asp 94, Asp 95	7
Arg 14 N*h*2	Asp 95O*d*1	3.1	Pro 15	Pro 15, Ser 93, Asp 94	4
Gly 16 O	Lys 98 N*z*	2.8	Gly 16	Gly 16, Ile 91, Ala 92, Lys 98	6
Arg 20 N*h1*	Asp 103 O*d*1	3.0	Val 18	Val 18	1
Lys 98 N*z*	Gly 16 O	3.0	Arg 20	Asp 103	4
Lys 98 N*z*	Phe 135 OT	2.9	Ile 91	Gly 16	1
Asp 103 O*d*1	Arg 20 N*h1*	2.6	Ala 92	Gly 16	1
Asp 103 O*d*2	Arg 20 N*h2*	2.6	Ser 93	Pro 15	1
Asp 103 O	Arg 133 N*h1*	3.2	Lys 98	Gly 16, Phe 135	5
Asp 103 O	Arg 133 N*h2*	3.0	Val 100	Phe 135	2
			Asp 103	Arg 20, Arg 133, Phe 135	8
			Phe 135	Ile 91, Lys 98, Val 100, Asp 103	10

Table 1.3 Hydrogen bonding interactions between GAL-7 and lactose

(PDB 4GAL) (adapted from (Leonidas et al., 1998))

Donor	Acceptor	Distance (Å)
His 49 N*e*2	O4	2.8
O4	Asn 51 O*d*1	2.9
Arg 53 N*h*2	O4	2.6
Arg 53 N*h*2	O5	2.9
Asn 62 N*d*2	O6	3.4
O6	Glu 72 O*e*1	3.1
O3'	Glu 72 O*e*1	2.5

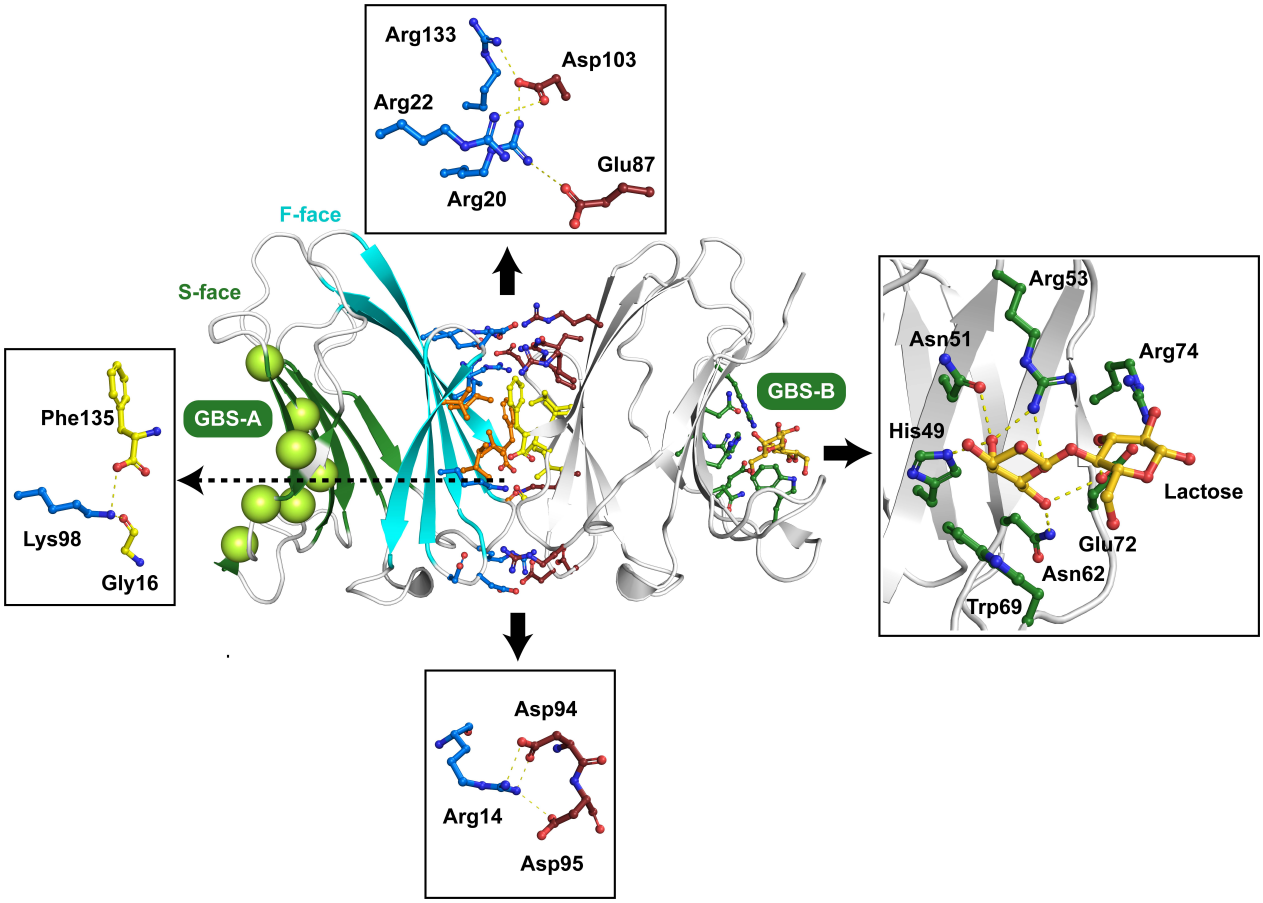

Figure 1.8 Overall structure of GAL-7

GAL-7 folds as "jelly roll" protein fold consisting of a S-face (green) and a F-face (cyan) (PDB 4GAL). Back-to-back homodimeric interactions within GAL-7 are formed by outer edge electrostatic interactions shielding a central hydrophobic core. Dimer interface residues between protomer A (left) and B (right) are shown as ball-and-stick representation using marine (protomer A) and brown (protomer B) coloring for polar residues, and orange (protomer A) and yellow (protomer B) for hydrophobic residues. Interprotomer electrostatic interactions are shown in the top, bottom, and left inset boxes. Salt bridges between residues are represented as a yellow dashed lines (distance cut-off value of 4 Å). GBS residues are shown as green spheres and as ball-all-stick representation in protomers A and B, respectively. Conserved residues (green) involved in direct binding with lactose (gold) are shown in the right inset box.

1.3.3 Long-range positive cooperativity between the two GBSs on opposite GAL-7 protomers

In 2013, Ermakova and coworkers used nuclear magnetic resonance (NMR) titration experiments to determine that lactose affinity is characterized by two different association constants when binding to the GAL-7 homodimer complex (K_{a1} = 0.9 ± 0.6 x 10^3 M^{-1} and K_{a2} = 3.4 ± 0.8 x 10^3 M^{-1}). They hypothesized that GAL-7 could be subjected to cooperative binding (Palmer et al., 2011; Stefan et al., 2013), whereby lactose binding to the first protomer would induce long-range conformational changes that would increase binding affinity on the opposite protomer (Ermakova et al., 2013). Using molecular dynamics simulations and energy calculations, they suggested that binding of the first lactose moiety would induce internal motions within loop 3 and restrict motions of loops 1 and 5, which would further increase dimer stability. The authors suggested that induced positive ligand binding cooperativity between the two opposite GBSs was stabilized by electrostatic interactions between residues of the GAL-7 dimer interface. Despite not having demonstrated this fact, their overall results suggest the existence of an allosteric network of cross talking residues governing communication between the GBS of each GAL-7 protomer, with dimer interface residues potentially controlling communication.

1.3.4 Glycan-dependent and -independent functions of GAL-7

Like other galectin members, GAL-7 regulates diverse cellular functions such as apoptosis, cell proliferation, cell differentiation, cell adhesion, cell migration, pathogen binding, and nuclear export (Figure 1.9) (Advedissian et al., 2017a; Saussez et al., 2006; St-Pierre, 2012). These functions can be driven with or without GBS activity. Indeed, exogenous GAL-7 induces apoptosis of Jurkat T cells through interactions with glycoproteins located at the T cell membrane (Labrie et al., 2014). GAL-7 facilitates trophoblast-endometrial epithelial intercellular adhesion, potentially by crosslinking with extracellular matrix glycoproteins (integrins, laminin, fibronectin, etc.) via its GBS (Menkhorst et al., 2014). Furthermore, through this galectin-glycan matrix lattice, GAL-7 also promotes cell migration during epithelial wound healing (Cao et al., 2002, 2003; Gendronneau et al., 2008, 2015).

On the other hand, GAL-7 has been shown to induce apoptosis of cervical cancer HeLa cells, of colorectal adenocarcinoma DLD-1 cells, and of prostate cancer DU-145 cells via the JNK pathway in a GBS-independent fashion (Kuwabara et al., 2002; Labrie et al., 2015). Through the same pathway, GAL-7 also regulates cell differentiation of keratinocytes (Truong et al., 2007). Besides its proapoptotic activity, GAL-7 exhibits a glycan-independent anti-apoptotic effect on

breast cancer MCF-7 cells and on B16F1 melanoma cells (Grosset et al., 2014). Moreover, GAL-7 is suggested to regulate cell apoptosis through a glycan-independent interaction with the anti-apoptotic protein BCL-2 (Villeneuve et al., 2011). Finally, the GBS-independent binding of GAL-7 on E-cadherin immobilizes this protein on cell membranes, preventing its endocytosis in keratinocytes (Advedissian et al., 2017b).

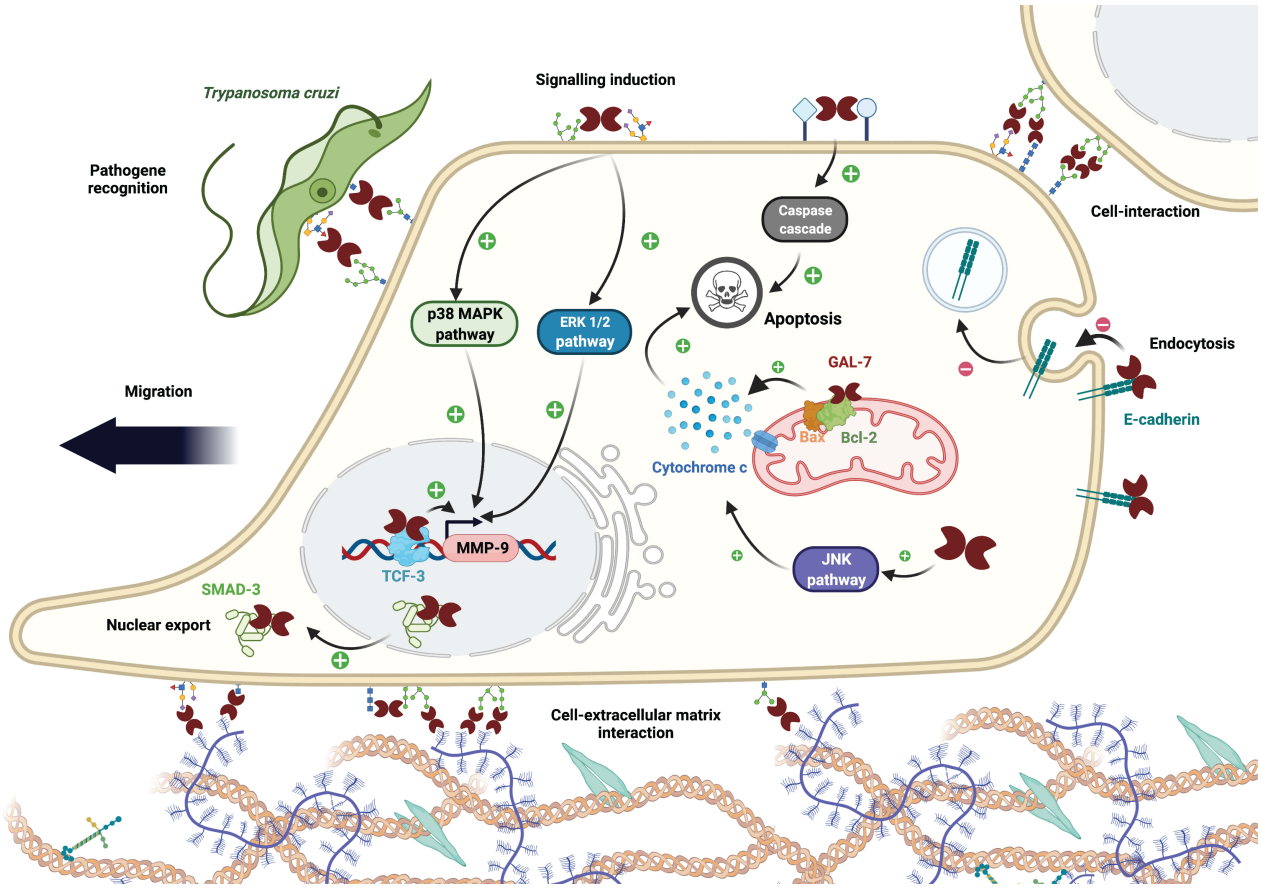

Figure 1.9 Biological functions of GAL-7.

Extracellular GAL-7 binds to glyco receptors to facilitate cell migration, cell adhesion, and *Trypanosoma cruzi* infection. GBS-dependent binding of GAL-7 to cell membranes also promotes the expression of MMP-9 in cancer cells through p38 MAPK and ERK 1/2 pathways for cell migration and induces the apoptosis of T cells. GAL-7 also binds to E-cadherin to prevent its endocytosis, a mechanism that is glycan-independent. In the cytoplasm, GAL-7 induces cellular apoptosis by upregulating the release of cytochrome *c* via interaction with BCL-2 or through the JNK pathway. In the nucleus, GAL-7 is involved in nuclear export of SMAD-3. Image created with BioRender.com.

1.3.5 GAL-7 in cancer

GAL-7 plays a dual role in cancer. Depending on cancer types, this protein can be pro-tumorigenic (oral skin, thyroid, esophagus, breast, gastric, ovaries, cervix, lymphs) or be more anti-tumorigenic (colon, prostate) (Figure 1.10) (Campion et al., 2013; Demers et al., 2007, 2009, 2010; Grosset et al., 2016; Guo et al., 2017; Higareda-Almaraz et al., 2016; Kim et al., 2013; Kuwabara et al., 2002; Labrie et al., 2014; Moisan et al., 2003; Park et al., 2009; Rorive et al., 2002; Schulz et al., 2017; Wang et al., 2020; Zhu et al., 2013; Zhu et al., 2010). The pro-tumorigenic function of GAL-7 is thought to be linked with p53, MMP-9, and Smad 2/3 proteins. Indeed, mutation of p53, which is well known as a major cause of aggressive cancer, induces high expression of GAL-7 through the NF-κB pathway in cancer cells. Then, secreted GAL-7 undergoes autocrine signaling to induce over-expression of MMP-9 via the p38 MAPK, ERK1/2 and JNK pathways, resulting in cancer cell invasion (St-Pierre, 2021). On the other hand, GAL-7 is also supposed to modulate the nuclear export of Smad2/3, interfering with the TGF-β pathway, therefore promoting tumorigenesis (Inagaki et al., 2008; St-Pierre, 2021).

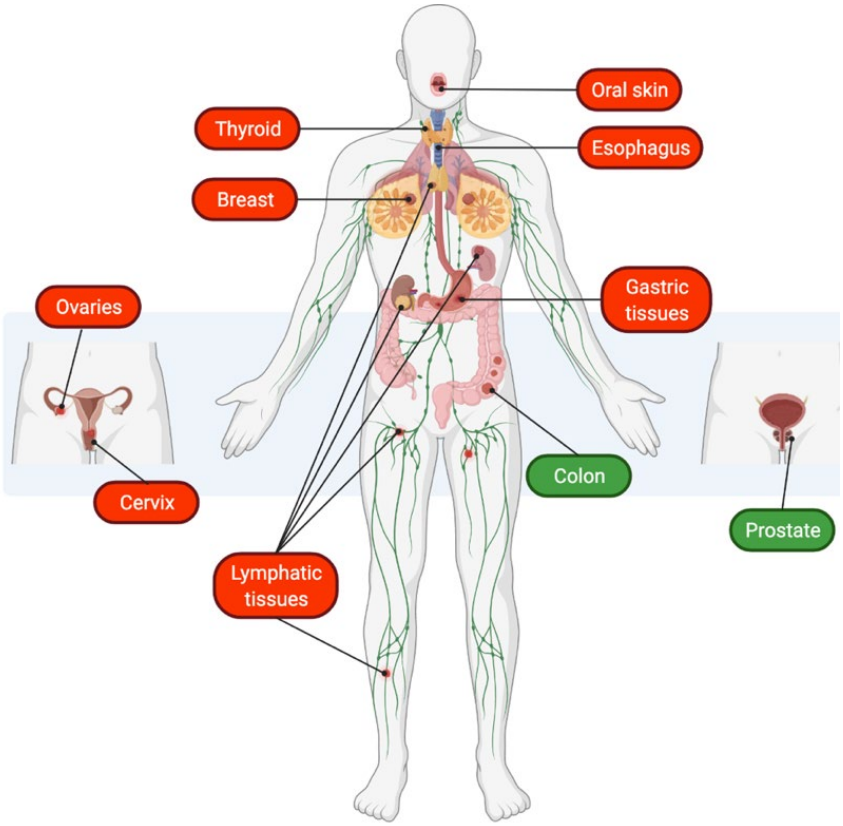

Figure 1.10 Role of GAL-7 in cancers.

GAL-7 is pro-tumorigenic (red boxes - oral skin, thyroid, esophagus, breast, gastric tissues, ovaries, cervix, lymphatic tissues) or anti-tumorigenic (green boxes - colon, prostate). Image created with BioRender.com.

1.4 GAL-7 inhibitor design trends

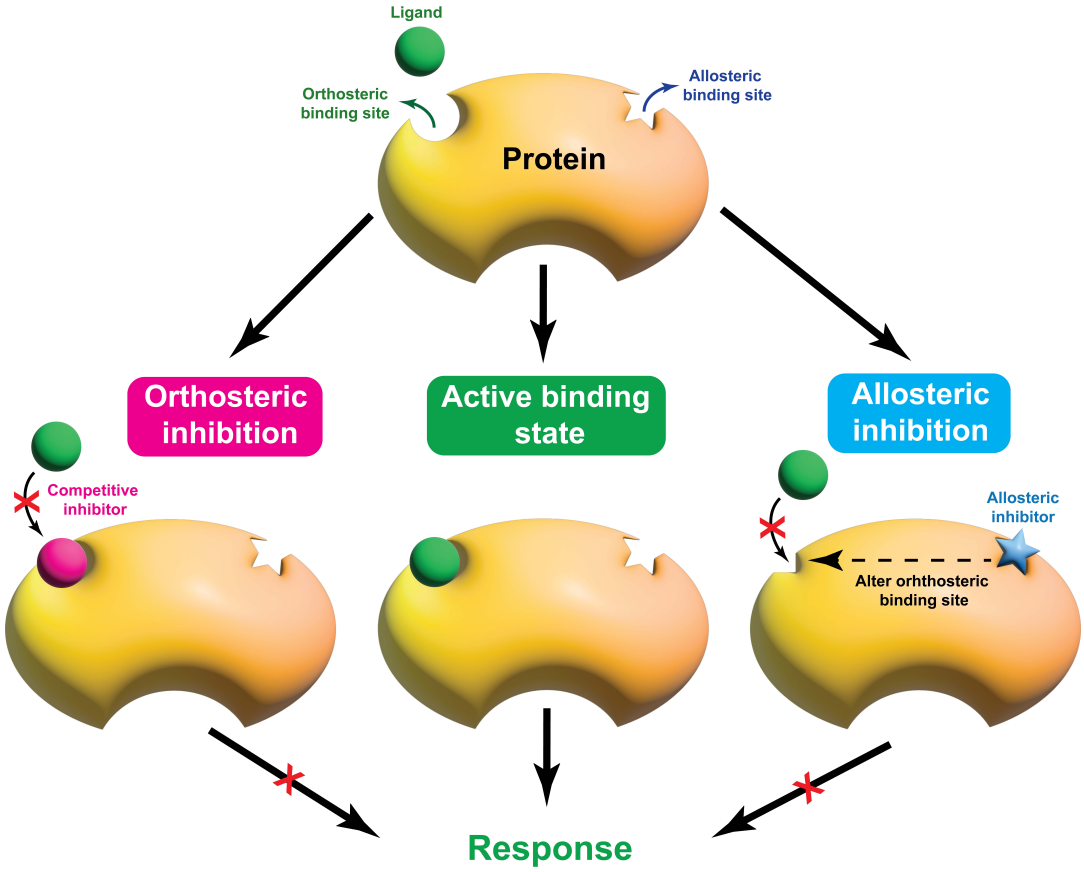

Figure 1.11 Approaches for the design of a protein inhibitor

Two primary approaches govern inhibitor design of a protein activity. The first approach is orthosteric inhibition, whereby an inhibitor molecule directly targets the active site (or orthosteric site) of a protein. This inhibitor molecule (pink sphere) directly competes with active-site binding of a natural protein ligand (green sphere) to alter protein function. The second approach is allosteric inhibition, whereby an inhibitor molecule targets a different site than the orthosteric site. This distant site is called an allosteric site. Once the inhibitor binds to the allosteric site (blue star), a cascade of dynamics and/or conformational changes are induced in the protein structure, which remotely prevents the binding of a natural ligand to the orthosteric site. This also results in modulation of protein activity, with added benefit of positive or negative regulation (Wodak et al., 2019; Xie & Lai, 2020).

1.4.1 Orthosteric inhibition approach - GBS inhibitors of GAL-7

The first attempt to design a GAL-7 inhibitor was performed in 2005 by the Nilsson group (Cumpstey et al., 2005), using mouse GAL-7 as template. By replacement of the *N*-acetyl glucosamine moiety of LacNAc by a non-carbohydrate aglycon, the authors synthesized three specific analogs that bind the mouse GAL-7 GBS with a dissociation constant (K_D) in the 100 nM range, which is 10-fold higher in affinity than with other galectins (Molecules 1, 2 and 3) (Figure

1.12, Table 1.4). Later in the same year, Salameh and his colleagues synthetized a thioureido *N*-acetyllactosamine derivative binding to GAL-7 with a better K_D (around 23 nM) (Molecule 4) (Figure 1.12, Table 1.4). (Salameh et al., 2006), but showed low specificity for GAL-7 in comparison with other galectins. In 2011, the Nilsson and Acharya groups reported the crystal structure of human GAL-7 bound to the novel 2-*O*-benzylphosphate-galactoside inhibitor with a K_D of 450 nM (Molecule 5) (Figure 1.12, Table 1.4). (Masuyer et al., 2012). Still, it is unclear whether this new inhibitor is specific for GAL-7. Despite 16 years since the first attempt, the development of GBS inhibitor specifically targeting GAL-7 has yet to reach a turning point. The high GBS similarity among different galectin homologs makes small-molecule GAL-7 GBS inhibitor design challenging. Noteworthy, targeting the GBS using small-molecule compounds does not inhibit glycan-independent activities of GAL-7, preventing full control over its diverse biological functions.

Table 1.4 List of GAL-7 inhibitors synthesized up to date.

		K_D (nM)					
Molecules	**Name**	**Human GAL-1**	**Human GAL-3**	**Human GAL-7**	**Mouse GAL-7**	**Human GAL-8N**	**Human GAL-9N**
1	1,5-Bis(β-D-galactopyranosylthio)-2,4-dinitrobenzene	1900	n.b	na	**170**	n.b	n.b
2	5-Benzylsulfanyl-2,4-dinitrophenyl 1-thio-β-D-galactopyranoside	n.b	n.b	na	**180**	2200	n.b
3	2,4-Diacetamido-5-benzylsulfanyl-phenyl-1-thio-β-D-galactopyranoside	n.b	1800	na	**140**	n.b	n.b
4	Methyl-3-deoxy-3-(*N*'-(3-pyridylmethylthioureido))-β-D-galactopyranosyl-(1-4)-2-acetamido-2-deoxy-β-D-glucopyranoside	43	35	**23**	na	na	47
5	2-O-benzylphosphate-galactoside	na	na	**450**	na	na	na

n.b : no binding, na : not applicable/not tested

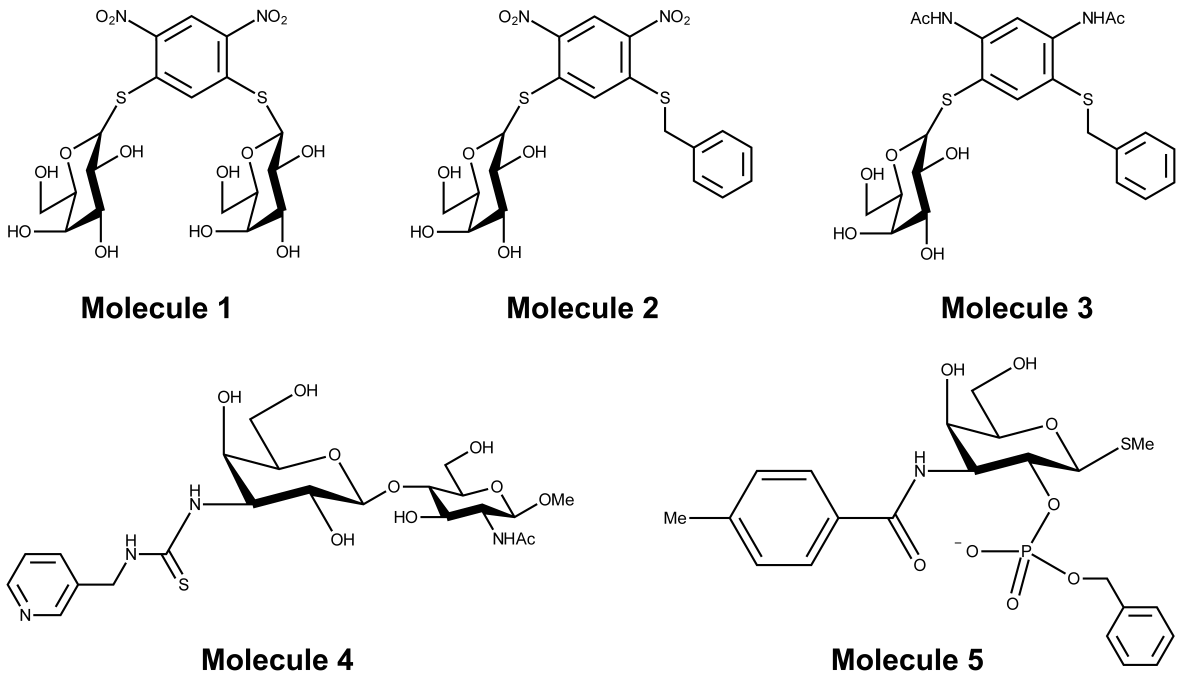

Figure 1.12 Structure of GAL-7 GBS inhibitors

Molecule 1: 1,5-Bis(β-D-galactopyranosylthio)-2,4-dinitrobenzene. Molecule 2: 5-Benzylsulfanyl-2,4-dinitrophenyl 1-thio-β-D-galactopyranoside. Molecule 3: 2,4-Diacetamido-5-benzylsulfanyl-phenyl-1-thio-β-D-galactopyranoside. Molecule 4: Methyl-3-deoxy-3-(*N*'-(3-pyridylmethylthioureido))-β-D-galactopyranosyl-(1-4)-2-acetamido-2-deoxy-β-D-glucopyranoside. Molecule 5: 2-O-benzylphosphate-galactoside.

1.4.2 Allosteric inhibition approach - Dimer interface inhibitors of GAL-7

The first allosteric mechanism was described in 1965 by Monod, Wyman, and Changeux (Monod et al., 1965). It is defined by a conformational or dynamic change at a position on a protein induced by perturbation of an another distal site on the same protein (Guo et al., 2016; Motlagh et al., 2014; Nussinov et al., 2015) (Figure 1.11). Since the allosteric binding sites are less evolutionary conserved than the orthosteric binding sites (Panjkovich et al, 2010; Wei et al., 2016), allosteric inhibition is more selective and efficient than orthosteric inhibition (Lu et al., 2017; Nussinov et al., 2011; Nussinov et al., 2012; Wootten et al., 2013). For this reason, drug discovery and design have shifted focus toward allosteric inhibition to improve compound selectivity and efficiency (Wenthur et al., 2014). To this day, the AlloSteric Database (ASD) 2019 holds over 1949 protein targets and 82,070 allosteric modulators (Huang et al., 2011, 2014; Liu et al., 2020; Shen et al., 2016). Based on DrugBank database information accessed on March, 27th 2022, 25 allosteric drugs were already approved by the FDA for maket use (Wishart et al., 2006). For example, Drotaverine inhibits phosphodiesterase-4 (PDE4) and is used for treatment of gastrointestinal diseases and smooth muscle spasms (Mk, 2020). Enasidenib, an allosteric

inhibitor of isocitrate dehydrogenase-2 (IDH2), is applied for the treatment of myeloid leukemia. Trametinib is an allosteric kinase inhibitor of Mitogen-activated protein kinase (MEK) 1 and MEK2 for melanoma treatment (Stein et al., 2017). Although no galectin allosteric modulator has yet been approved in the market, antitumor calixarene 0118 (OXT008) was found to allosterically inhibit the GBS activity of GAL-1 (Dings et al., 2012), and was then advanced to phase 1 clinical trial for solid tumor treatment (Table 1.1). In 2021, OXT008 was shown to prevent proliferation, migration, and invasion of six thyroid cancer cell lines overexpressing GAL-1 (Gheysen et al., 2021). Based on the progress of this GAL-1 allosteric inhibitor study, the same strategy could be applied for the functional modulation of GAL-7.

To overcome the limitations of designing GBS inhibitors, our group targeted the functionally relevant dimer interface of GAL-7. This approach is based on three main considerations. First, the oligomeric structure of prototypic galectins is the result of selective pressure and is strictly conserved among diverse human proteins of this family. Based on this evidence, it can be presumed that the GAL-7 homodimer architecture is functionally important, especially for the formation of glycan-galectin matrix lattices that confer the extracellular function of GAL-7. Second, the “back-to-back” quaternary architecture of the GAL-7 homodimer is unique among human galectins. Therefore, targeting this dimer interface would significantly improve inhibitor specificity for GAL-7. Third, Ermakova and colleagues previously illustrated the existence of long-range positive binding cooperativity between the two GBSs located on opposite GAL-7 protomers, suggesting functional communication occurring through the dimer interface (Ermakova et al., 2013). Thus, destabilization of the dimer interface could inhibit both GBS-dependent and oligomerization-dependent functions of GAL-7. As a result, our group previously designed peptides mimicking a portion of the dimer interface (St-Pierre et al., 2018; Vladoiu et al., 2015). These Dimer Interfering Peptides (DIPs) were designed to disrupt β-strands 13-25 and 129-135, which are directly involved in protomer-protomer interactions. Among the synthesized peptides, $DIP_{129\text{-}135}$ specifically inhibited GAL-7 dimer formation and reduced the proapoptotic activity of GAL-7 on Jurkat T cells, but did not alter GAL-7 binding at the surface of T cells (St-Pierre et al., 2018; Vladoiu et al., 2015). This achievement is a proof-of-concept demonstrating that GAL-7 activity is tunable through the modulation of its oligomerization architecture (St-Pierre et al., 2018).

1.5 Thesis

1.5.1 Problem Statement

As detailed above, GAL-7 plays a pro-tumorigenic role in many epithelial cancers, making it a promising target for cancer therapy, especially for TNBC treatment. Currently, the development of inhibitors targeting the GAL-7 GBS has not yet reached a milestone. The novel approach encompassing the design of an inhibitor targeting the dimer interface appears to be a promising strategy to specifically and efficiently modulate GAL-7 activity (St-Pierre et al., 2018; Vladoiu et al., 2015). In fact, the dimer interface has been suggested to play an important role for remote positive ligand binding cooperativity between GBSs located on opposite protomers (Ermakova et al., 2013). However, due to the lack of information on key residues involved in stabilizing this protomer-protomer interaction, it is challenging to identify potential regions of the dimer interface that should be targeted for modulation. Although the DIP alternative shows interesting modulating properties, their affinity is low (mM range) and initial attempts to optimize DIP affinity towards GAL-7 did not result in tangible improvements. Thus, a better understanding of the residue network controlling the allosteric communication between GAL-7 protomers is mandatory to lay down the fundamental knowledge that could lead to the design of improved GAL-7 modulators, either as activators or inhibitors of GAL-7 depending on the targeted cellular activity and cancer tissue type.

1.5.2 Hypothesis and Objectives

Since destabilization of the dimer interface by a DIP showed inhibition of the GAL-7 immunosuppressive activity, we hypothesized that **GAL-7 activity is at least partly modulated by dimer interaction strength *(Hypothesis 1)***. To validate this hypothesis, an *in-silico* analysis of GAL-7 dynamics was performed to provide insights on putative strengthening and weakening mutations located at the dimer interface. **Two single GAL-7 variants, G16C and G16S, were prepared as improved and weakened GAL-7 homodimer affinity, respectively, to investigate their impact on the immunosuppressive activity of GAL-7 *(Objective 1).*** Multiple methods combining biological assays, X-ray crystallography, biophysical, and computational characterization were carried out to accomplish this objective. The details of this work are described in the article presented in chapter 2: **“Perturbing dimer interactions and allosteric communication modulates the immunosuppressive activity of human galectin-7” (Pham et al., 2021)**. This study was published in the *Journal of Biological Chemistry* in 2021.

This initial work presented the establishment of a residue network governing the molecular function of GAL-7 and highlighted the fact that residues involved in protomer-protomer communication at the interface are crucial to maintain allosteric communication. We then further hypothesized that **perturbing this inter-protomer communication would weaken the communication network between protomers, as well as affect GAL-7 function in the cell *(Hypothesis 2)***. Our second objective **investigated the consequences of disrupting inter-protomer communication on GAL-7 function *(Objective 2).*** The results of this objective are detailed in the manuscript presented in chapter 3, which will shortly be submitted for publication.

We functionally sectioned and studied the dimer interface of GAL-7 into three distinct regions: a central section primarily consisting of hydrophobic interactions involving residues Phe135, Arg98, and Gly16, complemented by two primarily electrostatic regions located on top (Arg20, Arg22, Asp103, Arg133, and Glu87) and bottom (Arg14, Asp94, and Asp95) of the dimer interface. Results from objectives 1 and 2 of this thesis investigated interactions located in the central and top sections of the GAL-7 interface. Moreover, the bottom section residue Arg14 was previously suggested to be involved in a dynamical alteration linking the distant GBS to the dimer interface (Ermakova et al., 2013). This observation suggests that **perturbing the interaction between R14 and D94 (or D95) may alter the GBS-dependent proapoptotic activity of GAL-7 *(Hypothesis 3)***. Therefore, the last objective of this study **investigated the effects of perturbing electrostatic interactions between Arg14, Asp94, and Asp95 on the proapoptotic activity of GAL-7 *(Objective 3)*.** The results of this objective are detailed in chapter 4 and paint a complete picture of the modulation of GAL-7 activity through homodimer interactions.

2 FIRST ARTICLE: "PERTURBING DIMER INTERACTIONS AND ALLOSTERIC COMMUNICATION MODULATES THE IMMUNOSUPPRESSIVE ACTIVITY OF HUMAN GALECTIN-7"

La perturbation des interactions dimériques et de la communication allostérique module l'activité immunosuppressive de la galectine-7 humaine

N. T. Hang Pham[1], Myriam Létourneau[1], Marlène Fortier[1], Gabriel Bégin[2,3], M. Sameer Al-Abdul-Wahid[4] , Fabrizio Pucci[5], Benjamin Folch[1], Marianne Rooman[5], David Chatenet[1], Yves St-Pierre[1], Patrick Lagüe[2,3], Charles Calmettes[1,3] , and Nicolas Doucet[1,3]

[1]Centre Armand-Frappier Santé Biotechnologie, Institut National de la Recherche Scientifique (INRS), Université du Québec, Laval, Quebec, Canada

[2]Département de Biochimie, de Microbiologie et de Bio-informatique and Institut de Biologie Intégrative et des Systèmes (IBIS)

[3]PROTEO, the Québec Network for Research on Protein Function, Engineering, and Applications, Université Laval, Québec, Quebec, Canada

[4]Nuclear Magnetic Resonance Centre, University of Guelph, Guelph, Ontario, Canada

[5]Computational Biology and Bioinformatics, Université Libre de Bruxelles, Brussels, Belgium

Received for publication, July 22, 2021, and in revised form, October 10, 2021 ; Published online, October 18, 2021, https://doi.org/10.1016/j.jbc.2021.101308

Journal of Biological Chemistry, Research article, Volume 297, issue 5,101308, November 2021.

Author contributions: I am the main author of this article, with help from Myriam Létourneau, Patrick Lagüe, and Nicolas Doucet for manuscript writing. It was also reviewed by all authors. In this study, I performed all protein expressions, biophysical characterization, X-ray crystallography experiments, as well as data analysis of all results. Myriam Létourneau was involved in data analysis of biophysical experiments and biological assays. Apoptosis assays were carried out by Marlène Fortier. NMR experiments were completed by M. Sameer Al-Abdul-Wahid. *In silico* predictions of interface mutants were performed by Fabrizio Pucci, Benjamin Folch, and Marianne Rooman. Molecular dynamics simulations were executed by Gabriel Bégin and Patrick Lagüe. I also performed allosteric network analyses, with help and guidance from Patrick Lagüe. The overall study was supervised by David Chatenet, Yves St-Pierre, Patrick Lagüe, Charles Calmettes, and Nicolas Doucet.

2.1 Résumé

La conception de modulateurs allostériques pour contrôler la fonction des protéines est un aspect important de la découverte de médicaments. L'altération de la fonction de résidus essentiels d'un réseau allostérique permet de cibler spécifiquement des protéines venant d'une même sous famille et de minimiser les effets hors cible non désirés, tout en évitant l'acquisition d'une résistance au médicament, un problème généralement associé aux composés qui ciblent les sites orthostériques. Dans cette étude, nous avons utilisé l'ingénierie des protéines et des mutations de l'interface du dimère pour moduler positivement et négativement l'activité immunosuppressive de la protéine pro-apoptotique galectine-7 humaine (GAL-7). Les algorithmes PoPMuSiC et BeAtMuSiC ont servi à prédire les positions et l'identité des résidus à muter qui pourraient soit altérer, soit stabiliser l'interface dimérique de GAL-7. En introduisant un lien covalent via un pont disulfure entre les deux protomères pour contrôler la force de l'interaction et la stabilité de l'homodimère, nous démontrons l'importance des perturbations de l'interface dimérique sur le réseau allostérique qui relie les deux sites de liaison aux glycanes (GBS) de GAL-7, ce qui contrôle l'apoptose des cellules T Jurkat induite par GAL-7. L'étude moléculaire des variants G16X de GAL-7 par la cristallographie aux rayons X ainsi que les caractérisations biophysiques et computationnelles dévoilent les résidus impliqués dans la stabilité du dimère, la communication allostérique et les effets dynamiques à longue portée impliquant les boucles 1, 2 et 3. Ainsi, nous montrons que la perturbation de l'interface homodimérique entre les protomères de GAL-7 peut moduler sa fonction biologique même si la structure globale et l'affinité de liaison du ligand demeurent inchangées. Cette étude met donc en évidence de nouvelles avenues pour la conception de modulateurs spécifiques de galectines pouvant influencer les interactions dépendantes et indépendantes de glycanes par les protéines de cette famille.

2.2 Abstract

The design of allosteric modulators to control protein function is a key objective in drug discovery programs. Altering functionally essential allosteric residue networks provides unique protein family subtype specificity, minimizes unwanted off-target effects, and helps avert resistance acquisition typically plaguing drugs that target orthosteric sites. In this work, we used protein engineering and dimer interface mutations to positively and negatively modulate the immunosuppressive activity of the proapoptotic human galectin-7 (GAL-7). Using the PoPMuSiC and BeAtMuSiC algorithms, mutational sites and residue identity were computationally probed and predicted to either alter or stabilize the GAL-7 dimer interface. By designing a covalent

disulfide bridge between protomers to control homodimer strength and stability, we demonstrate the importance of dimer interface perturbations on the allosteric network bridging the two opposite glycan-binding sites on GAL-7, resulting in control of induced apoptosis in Jurkat T cells. Molecular investigation of G16X GAL-7 variants using X-ray crystallography, biophysical, and computational characterization illuminates residues involved in dimer stability and allosteric communication, along with discrete long-range dynamic behaviors involving loops 1, 3, and 5. We show that perturbing the protein–protein interface between GAL-7 protomers can modulate its biological function, even when the overall structure and ligand-binding affinity remains unaltered. This study highlights new avenues for the design of galectin-specific modulators influencing both glycan-dependent and glycan-independent interactions.

2.3 Introduction

Human galectins (GAL) are oligomeric β-galactoside binding lectins assembled from small (~15 kDa) protomeric carbohydrate recognition domains (CRD). In mammals, they are categorized by their CRD architecture and form three broadly defined structural groups: prototype (GAL-1, -2, -5, -7, -10, -11, -13, -14, -15, -16), tandem repeat (GAL-4, -6, -8, -9, -12), and chimera-type (GAL-3) (Cummings et al., 2015). While prototype galectins exist as noncovalent or disulfide-bridged homodimers, tandem repeat galectins are built from heterodimeric CRDs covalently linked by short peptide linkers. In contrast, the monomeric chimera-type GAL-3 is unique in its ability to oligomerize through its collagen-like N-terminal tail (Ahmad et al., 2004). Galectins are known to bind cell surface glycoconjugates via their glycan-binding sites (GBS), initiating the formation of an extracellular lattice through divalent and multivalent cross-linking of glycosylated receptors (Kamitori, 2018). This dynamic lattice imparts galectins with the ability to regulate multiple cellular functions, including cell adhesion, cell signaling, and intracellular trafficking (Nabi et al., 2015). This is particularly true when galectins bind to glycoreceptors on activated immune cells to induce apoptosis (Perillo et al., 1995). As a result, galectins act as key apoptotic regulators and potential disease targets in multiple disorders, including cancer tumor progression and metastasis (Dubé-Delarosbil et al., 2018)

Among prototype galectins, galectin-7 (GAL-7) is recognized for its preferential expression profiles in normal epithelial cells (St-Pierre, 2021). When overexpressed in many tissues, it can accelerate cancer progression. This is particularly true for lymphoma (Demers et al., 2005, 2007), triple-negative breast cancer (Demers et al., 2010; Grosset et al., 2014), endometrial cancer (Menkhorst et al., 2018), and other subtypes of cancer (Advedissian et al., 2017a). GAL-7 also

plays important cellular functions in cell adhesion, migration, differentiation, proliferation, and apoptosis (Advedissian et al., 2017a) via glycan-dependent or glycan-independent protein–protein interactions with other cellular partners. For example, while extracellular GAL-7 can trigger apoptosis of activated T cells following binding to glycoreceptors via its GBS (Labrie et al., 2014), it can also bind E-cadherin on epithelial cells independently of its GBS. Glycan-independent interactions implicating GAL-7 have also been reported inside the cells, most notably with the anti-apoptotic BCL-2 regulator (Villeneuve et al., 2011). Overexpression of GAL-7 has also been implicated in other pathologies, including preeclampsia (Menkhorst et al., 2020) and abnormal wound healing of the skin and cornea (Cao et al., 2003; Gendronneau et al., 2015).

For more than a decade, the development of galectin modulators has almost exclusively focused on sugar-based, small-molecule compounds aimed at perturbing glyco-receptor interactions (Denavit et al., 2018). However, the high degree of GBS homology among family members renders highly specific, high-affinity galectin modulators extremely difficult to synthesize. As a result, GBS inhibition remains a high-risk strategy because of unwanted off-target effects involving binding to other highly homologous and often beneficial anti-tumorigenic galectin members, e.g., GAL-4 (Belo et al., 2013; Satelli et al., 2011). To further complicate matters, an increasing number of studies have now confirmed the importance of GBS-independent activities modulated by galectins (Advedissian et al., 2017b; Chun, 2020; Meinohl et al., 2020), including potentially relevant hetero-oligomeric galectin architectures, modular designs, and valence variability (Ludwig et al., 2021; Ludwig et al., 2019a, 2019b; Miller et al., 2018). This should come as no surprise, as it has been known for a while that lectin can bind non-carbohydrate compounds, often exhibiting higher affinities than their “natural” saccharide ligands (Komath et al., 2006). GBS inhibitors are ineffective at targeting glycan-independent galectin function, further exemplifying the need to establish new approaches for targeting unique galectin members in highly specific therapeutic circumstances.

These observations have awakened interest in targeting and modulating galectin function using newly developed allosteric effectors. In many instances, allosteric modulation of protein function was shown to be more selective and effective than traditional orthosteric inhibition (Wenthur et al., 2014). Furthermore, such strategy has proven effective in finding compounds inhibiting mammalian C-type lectins, a protein family initially deemed undruggable (Aretz et al., 2018; Borrok et al., 2007). Targeting non-GBS regions in galectins would also offer means to develop new generations of galectin inhibitors that specifically modulate glycan-independent functions in the cell, a therapeutic strategy that remains marginally represented. In support of this

avenue, galectins have been shown to undergo evolutionary pressure that stabilizes their quaternary oligomeric architecture to improve ligand affinity and biological function (St-Pierre et al., 2018). The relatively low sequence identity and unique dimer architecture among members of the prototypic galectin family (Kamitori, 2018) offer means to specifically target their dimer interface to improve inhibitor specificity.

We recently developed GAL-7 dimer interfering peptides (DIPs) to alter dimer stability in this functionally important protein (Vladoiu et al., 2015). Among selected designer sequences, peptide hGAL-7(129–135) was shown to effectively reduce the pro- apoptotic activity of GAL-7 on Jurkat T cells by disrupting the monomer–dimer equilibrium in solution. This sequence was also shown to promote accumulation of GAL-7 on the surface of T cells. These results suggest that dimer interface perturbation might alter the specificity and affinity of the GAL-7 GBS against distinct glycosylated receptors, potentially acting via an allosteric mechanism involving homodimer interface communication. This hypothesis is further strengthened by prior work suggesting the existence of lactose-induced, long-range positive cooperativity between the two GBSs on opposite GAL-7 protomers (Ermakova et al., 2013). Despite being largely uncharacterized, positive cooperativity behavior suggests the involvement of long-range, organized residue networks relaying dynamic information between GAL-7 protomers. Further, characterizing the relationship between the biological function of GAL-7 and allosteric communication would significantly improve our ability to design GAL-7-specific allosteric inhibitors.

In this work, we studied the impact of homodimer interface mutations on the induction of Jurkat T cell apoptosis, allowing us to positively and negatively modulate the biological activity of GAL-7 by designing a covalent disulfide bridge (G16C) and destabilizing mutation (G16S) to control homodimer strength, stability, and biological activity. Biophysical, structural, and computational characterization of G16X variants provides a clearer view of the allosteric network governing molecular function in GAL-7.

2.4 Results and discussion

2.4.1 Prediction and design of GAL-7 variants that destabilize homodimer integrity

A number of structural studies have previously highlighted the unique “back-to-back” homodimer architecture adopted by GAL-7 in solution (Brinda et al., 2005; Kamitori, 2018; Leonidas et al., 1998; St-Pierre et al., 2018). Some reports have also alluded to the potential

importance of interface residues involved in dimer formation and stability, in addition to proposing the existence of allosteric networks connecting the two distant GBS sites on opposite GAL-7 protomers (Ermakova et al., 2013). To confirm complex formation and stability in apo and holo forms, we tested the integrity of the GAL-7 homodimer in solution. NMR translational diffusion measurements were performed on free and lactose-bound WT GAL-7 complexes of increasing protein–ligand molar ratios. Our results not only confirm the existence of a stable WT GAL-7 homodimer in solution, but further demonstrate that diffusion coefficients are not significantly altered upon addition of increasing lactose concentrations to GAL-7 (Figure 2.4). This supports structural integrity, stability, and biological relevance of a stable WT GAL-7 homodimer in its apo and holo forms.

The propensity of GAL-7 to maintain homodimer integrity upon interface perturbation was thus interrogated by performing computational mutational predictions at the interface using the algorithms PoPMuSiC (Gilis et al., 2000) and BeAtMuSiC (Dehouck et al., 2013). These tools provide computer-aided design of all possible single-site mutational replacements in proteins. PoPMuSiC evaluates the folding free energy changes ($\Delta\Delta G_F$) resulting from each mutated site, while BeAtMuSiC evaluates protein– protein binding free energy alterations upon mutation ($\Delta\Delta G_B$). Both algorithms were used in complementary fashion to help with prediction and design of experimental point mutations that effectively promote stabilization or destabilization of the GAL-7 monomer–dimer equilibrium.

We first searched for GAL-7 protomer interface mutations that favored stabilization of the monomer over that of the dimer. Using PoPMuSiC, we computationally introduced and evaluated all possible single-site mutations in GAL-7. Residues located at the dimer interface and exhibiting solvent accessibility differences greater than 10% between monomer and dimer states were prioritized. Mutations with significant monomer–dimer stability differences were selected, as defined by $\Delta\Delta G_F$ (dimer) - $\Delta\Delta G_F$ (monomer) ≥ 2 kcal/mol (Table 2.1). Amino acid replacements satisfying these criteria were found at positions Gly16, Val18, Ile91, and Phe135 (Table 2.1). Mutations at positions Gly16/Phe135 were prioritized over Val18/ Ile91 since they exerted a greater number of dimer destabilizing effects in addition to displaying an extended dimer interface, as exemplified by greater solvent accessibility changes upon binding. We applied further restrictions on the variants to prevent detrimental secondary structure perturbations or disulfide bridge formation (i.e., no Gly, Pro, Cys replacements) (Table 2.1). We also avoided variants that altered the overall charge of the protein. BeATMuSiC calculations predicted significant dimer affinity alterations for all remaining variants, with $\Delta\Delta GB \geq 4$ kcal/mol (Table 2.1). We finally

prioritized individual substitutions G16S and F135S, as they caused the largest $\Delta\Delta G_B$ among all remaining variants. These two variants were thus experimentally tested in the context of GAL-7 dimer stability and function. Interestingly, the main chain oxygen atoms of Gly16 and Phe135 both make inter-protein H-bonding interactions with the Nζ atom of Lys98, according to the Protein Interaction Calculator (PIC) (Tina et al., 2007). Phe135 is also involved in hydrophobic contacts with Leu89, Ile91, and Val100 on the opposite chain. We expected that mutation to serine would break these interactions.

As a counterpart to destabilizing mutations, we also searched for mutational predictions that favored stabilization of the GAL-7 homodimer rather than its monomeric form. Analysis of the WT homodimer structure (PDB entry 4GAL) highlighted ideal distance between Gly16-Cα atoms in each protomer (4 Å), suggesting that introduction of a cysteine at this site could favor formation of a covalently linked GAL-7 homodimer through formation of a disulfide bridge, with only slight structural reorganization. As a result, we also designed a G16C variant for further functional and structural investigation.

Based on our computational predictions, mutations G16S and F135S should weaken GAL-7 homodimer interactions, while formation of a disulfide bridge in G16C could strengthen protomer interactions and favor GAL-7 homodimer stability. Recombinant expression of mutational constructs yielded soluble proteins for the G16X variants, but F135S was found to be systematically expressed as inclusion bodies, despite several trials to improve its solubility. These results suggest irreversible structural alterations and/or limited stability upon introduction of a polar residue at position 135. Interestingly, Phe135 is the terminal residue within the primary structure of GAL-7, forming van der Waals interactions with neighboring residues Ile91, Lys98, and Asp103 on β-strand 7. A ConSurf analysis (Ashkenazy et al., 2010) illustrates that this position is the terminal amino acid residue for only 12/81 nonredundant galectin homologs, exhibiting limited sequence variability and strict hydrophobic conservation (Phe, Val, Leu, and Ile). This observation suggests that replacing the benzyl moiety with a polar hydroxyl group at position 135 impedes essential hydrophobic interactions involved in preserving monomer–dimer stability in GAL-7.

2.4.2 Perturbing homodimer stability alters the proapoptotic activity of GAL-7

Galectins are known to induce apoptosis of human T cells by binding to their glycosylated receptors, thereby modulating cell fate in diseases such as cancer (Girotti et al., 2019). For a number of years, our group has extensively used GAL-7 as a relevant model for studying Jurkat

T cell induced apoptosis, providing additional information on molecular and cellular mechanisms governing GAL-7 function in the cell (Grosset et al., 2014; Labrie et al., 2014; López de los Santos et al., 2020; Vladoiu et al., 2015). Despite several studies detailing the existence of a homodimeric structure in GAL-7, few reports have thus far interrogated the importance of maintaining the integrity and stability of this dimer for preservation of function. To investigate the computational predictions of G16X replacements, we performed Jurkat T cell apoptosis experiments with variants G16S and G16C. Our results show that the G16S mutation decreases the proapoptotic activity of GAL-7, yielding an EC50 of 13.7 μM (95% confidence interval [CI95%] between 10.2 and 18.3 μM) relative to 8.4 μM (CI95% 7.6–9.1 μM) for WT GAL-7 (Figure 2.1A). Conversely, the G16C variant has a greater capacity to induce apoptosis of Jurkat T cells than WT (Figure 2.1A), yielding an EC50 of 5.9 μM (CI95% 5.2–6.7 μM). These results suggest that residue Gly16 is directly involved in monomer–dimer stabilization and/or allosteric communication between protomers in GAL-7.

2.4.3 Perturbing dimer interface alters GAL-7 stability but does not affect glycan-binding affinity

The overall fold and stability of the GAL-7 variants were assessed by performing CD spectropolarimetry in the presence and absence of α-lactose. Under these conditions, the far UV molar ellipticity spectra (200–260 nm) of all proteins is virtually indistinguishable, further illustrating that Gly16 mutations do not perturb the overall fold of free or lactose-bound GAL-7 (Figure 2.5). Thermal denaturation experiments were also carried out to examine the effects of mutations on GAL-7 stability. CD melting curves show that G16C is the most stable variant (T_m = 70.0 ± 0.1 ºC), followed by WT (T_m = 67.8 ± 0.2 ºC) and G16S (T_m = 58.7 ± 0.2 ºC) (Figure 2.1B). These results confirm the thermal stability advantage conferred by the G16C mutation, which provides a 2.2 ºC increase in Tm relative to WT. Conversely, the G16S mutation weakens GAL-7 stability, inducing a 9.1 ºC decrease in melting temperature. By incubating protein with saturating concentrations of α-lactose, we observe an overall thermal stability increase of 2.7 for WT (T_m = 70.5 ± 0.1 ºC), 1.9 ºC for G16C (T_m = 71.9 ± 0.2 ºC), and 2.9 ºC for G16S (T_m = 61.6 ± 0.1 ºC). These results confirm the previously observed thermal stability advantage conferred by lactose binding to GAL-7 (Ermakova et al., 2013). This effect is more prominent in WT GAL-7 and variant G16S than in G16C, further suggesting the existence of a covalent link in the latter variant.

We also used microscale thermophoresis (MST) to investigate the strength of dimer association and equilibrium induced by Gly16 replacements. In this experiment, the fluorophore-labeled GAL-7 dimer is incubated at higher temperature with unlabeled GAL-7, resulting in

weakening of noncovalent dimer interactions and induction of equilibrium exchange between labeled and unlabeled complexes to form mixed heterodimers. This allows extraction of the GAL-7 equilibrium dimer dissociation constant (K_D) under specific experimental conditions and protein concentration range. It also further provides an estimate of dimer affinity perturbations induced upon mutation at the protomer interface. GAL-7 was previously shown to be predominantly dimeric at concentrations around 1.6 μM and above (Ermakova et al., 2013). Consistent with these observations, our MST results show that WT GAL-7 adopts a dimeric form in similar experimental conditions, exhibiting a dimer equilibrium dissociation constant (K_D) of 0.06 μM (Figure 2.1C). In contrast, the G16S variant displays 32-fold lower dimer affinity relative to WT GAL-7 (K_D = 1.88 μM), indicative of significant homodimer destabilization induced by the mutation. As hypothesized, no binding-associated MST signal was observed for G16C, lending support to stabilization by formation of a disulfide bridge between the two G16C GAL-7 protomers. The dimer interaction energies between the apo WT, G16C, and G16S were also evaluated using FoldX (Schymkowitz et al., 2005) and protein structures from MD simulations (see below). Results were averaged over 5000 dimer structures from the respective trajectories of WT and G16X variants. Consistent with our MST results, G16S was found to be the least stable homodimer, with a dimer interaction energy of -11.6 ± 0.1 kcal/mol. Interaction energies of −13.1 ± 0.2 kcal/mol and −14.8 ± 0.1 kcal/mol were also calculated for WT and G16C, respectively. As expected, the disulfide bridge between the G16C homodimers was found to be a significant contributor to dimer stability.

In addition to testing dimer stability, we also performed ITC experiments to investigate whether mutations at the dimer interface affect long-range glycan-binding affinity in the GAL-7 GBS. Our results show that α-lactose-binding affinities (K_D) were found to be similar for WT GAL-7 and G16X variants (Figure 2.1D and Table 2.2). Closer thermodynamic investigation illustrates that although WT and G16C exhibit very similar entropic (ΔS) and enthalpic (ΔH) contributions to ligand binding, variant G16S shows significantly altered ΔH and ΔS contributions relative to the two more stable WT and G16C forms of the protein, in line with the lower stability observed in variant G16S.

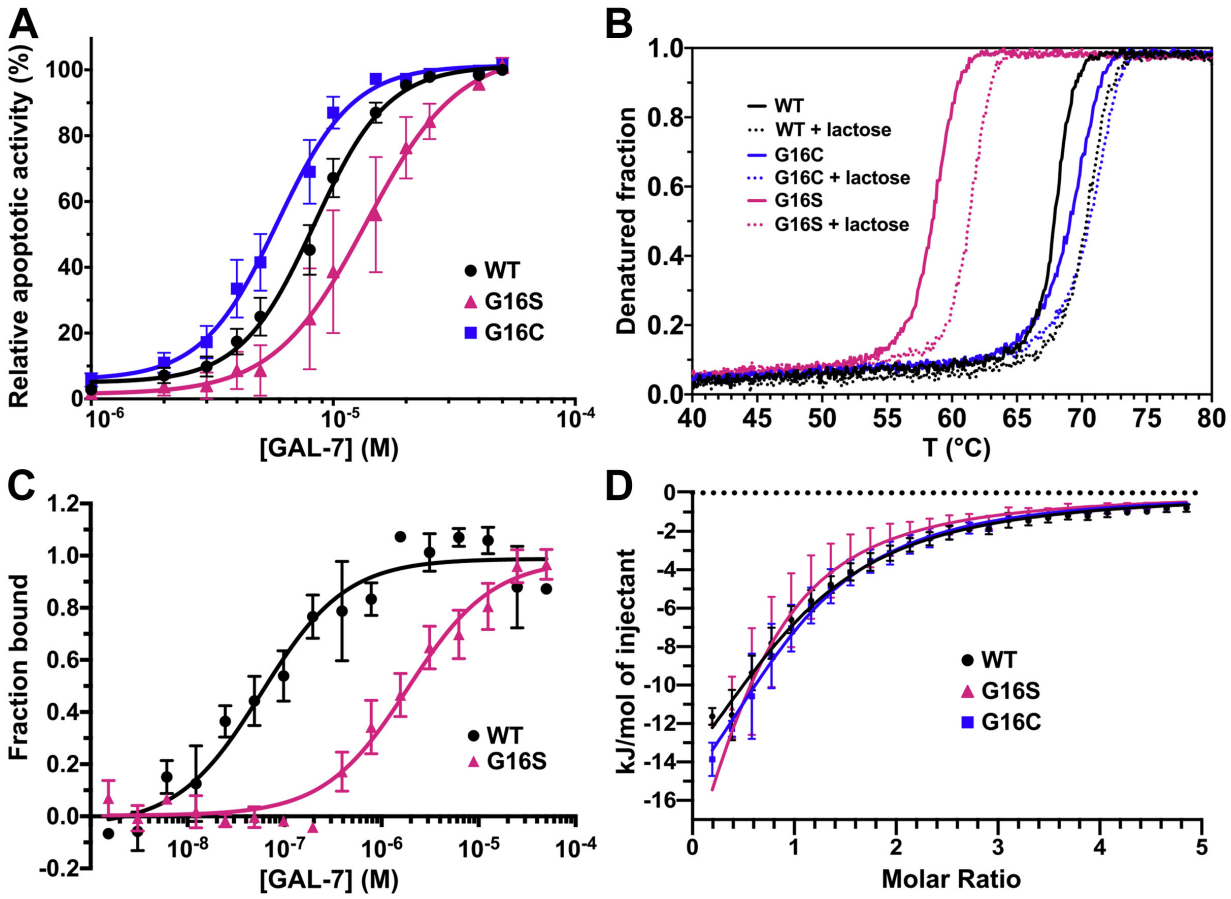

Figure 2.1 Single-site dimer-interfering mutations G16C and G16S act as positive and negative functional regulators of the proapoptotic activity of GAL-7.

A, GAL-7-induced apoptosis of human Jurkat T cells for WT GAL-7 (black circles), G16S (pink triangles), and G16C (blue squares), as evaluated by positive Annexin V staining using flow cytometry analysis. B, thermal stability of WT GAL-7 and variants G16S and G16C in the absence and presence of lactose, as measured by CD-induced thermal denaturation. C, dimer equilibrium affinity of WT GAL-7 and the G16S variant, as measured by MST. D, α-lactose-binding isotherm of WT GAL-7 and variants G16S and G16C, as measured by ITC.

2.4.4 G16C and G16S variants maintain dimer architecture in free and lactose-bound states

Since the proapoptotic activity of GAL-7 on Jurkat T cells involves glycosylated receptors and since no significant change in lactose-binding affinity was observed in variants G16C and G16S, it is unclear how homodimer formation and stability modulate GAL-7 activity in the cell. To examine whether these functional changes are rooted in structural perturbations at the molecular level, we solved the X-ray structures of lactose-bound WT GAL-7 and that of variants G16C and G16S in their apo and holo states (Table 2.3). We found that both G16C and G16S variants maintain GAL-7 dimer architecture in solution (Figure 2.2A), unlike other protomer interface mutations that likely perturb the hydrophobic core of the dimer interface, resulting in insoluble constructs (e.g., F135S). Apo structures of G16C (PDB 6VTP) and G16S (PDB 6VTR) were

crystallized as dimers in the $P2_12_12_1$ space group at 2.3 Å resolution (Table 2.3). As predicted from our calculations and in support of our MST results, the apo G16C omit map revealed the formation of a Cys16-Cys16 disulfide bridge at the dimer interface (Figure 2.2B). Overall, GAL-7 dimer architecture is minimally perturbed, as illustrated by Cα structural alignments between apo WT GAL-7 (PDB 3ZXF) and apo G16C (RMSD 6VTP versus 3ZXF = 0.686 Å) or between apo WT and apo G16S (RMSD 6VTR versus 3ZXF = 0.629 Å). The lactose-bound holo crystal structures of WT (PDB 6VTO), G16C (PDB 6VTQ), and G16S (PDB 6VTS) were resolved at 1.69 Å, 1.95 Å, and 1.9 Å, respectively. These structures also appear as dimers in the $P2_12_12_1$ space group (Table 2.3 and Figure 2.2A). Similar to the apo forms, no major change in the overall structure was observed between WT GAL-7 and G16C (RMSD 6VTQ versus 6VTO =0.477 Å) or between WT and G16S (RMSD 6VTS versus 6VTO = 0.357 Å). Much like its apo counterpart, a Cys16-Cys16 disulfide bridge between each protomer was also confirmed by the presence of a clear electron density map in the G16C holo structure (PDB 6VTQ). In contrast to the apo G16C structure, two disulfide bridge conformers are observed in the electron density of the Cys16-Cys16 covalent bond at the dimer interface of holo G16C (Figure 2.2B)

2.4.5 Glycan-binding site organization and ligand positioning

In accordance with the overall structural similarity, overall GBS organization and residue positioning remain largely unchanged between WT and G16X variants. This was expected since Gly16 mutations are located at the homodimer interface, more than 20 Å away from the GBS. Except for Arg71, side chain conformations for all GBS residues were found to adopt similar orientations in all GAL-7 holo structures (Figure 2.2C). However, since Arg71 is located at the crystal contact surface, this dissimilarity could easily be an artifact of crystal packing. Lactose positioning within the GBS also remains analogous for WT GAL-7 and G16X variants, preserving the vast majority of the previously described polar interactions (Leonidas et al., 1998). These results are supported by the largely unaffected α-lactose-binding affinities (K_D) calculated for WT GAL-7 and G16X variants (see above). The previously published lactose-bound WT GAL-7 structure of Leonidas et al. (PDB 4GAL) was shown to limit lactose access to the binding site of one GAL-7 protomer due to crystal packing. In contrast, our omit maps clearly show the presence of a bound lactose molecule in the GBS of both protomers within the WT, G16C, and G16S complexes (Figure 2.2A). This is likely explained by the use of different crystallization techniques, i.e., soaking of WT GAL-7 crystals in lactose solution (Leonidas et al., 1998) versus cocrystallization with lactose (present study). Interestingly, the D-glucose moiety of lactose was found to adopt an open linear chain configuration in our WT GAL-7 structure (PDB 6VTO),

contrary to its typical closed pyranose ring. This could result from X-ray irradiation during crystal shooting (Dizdaroglu et al., 1977) or protonation of the ring oxygen atom of the glucose moiety by the nearby terminal guanidinium group of Arg74. In a similar fashion, the ring opening of glucose was previously shown to be catalyzed by the amine group of a nearby lysine in the binding site of human serum albumin (Wang et al., 2013).

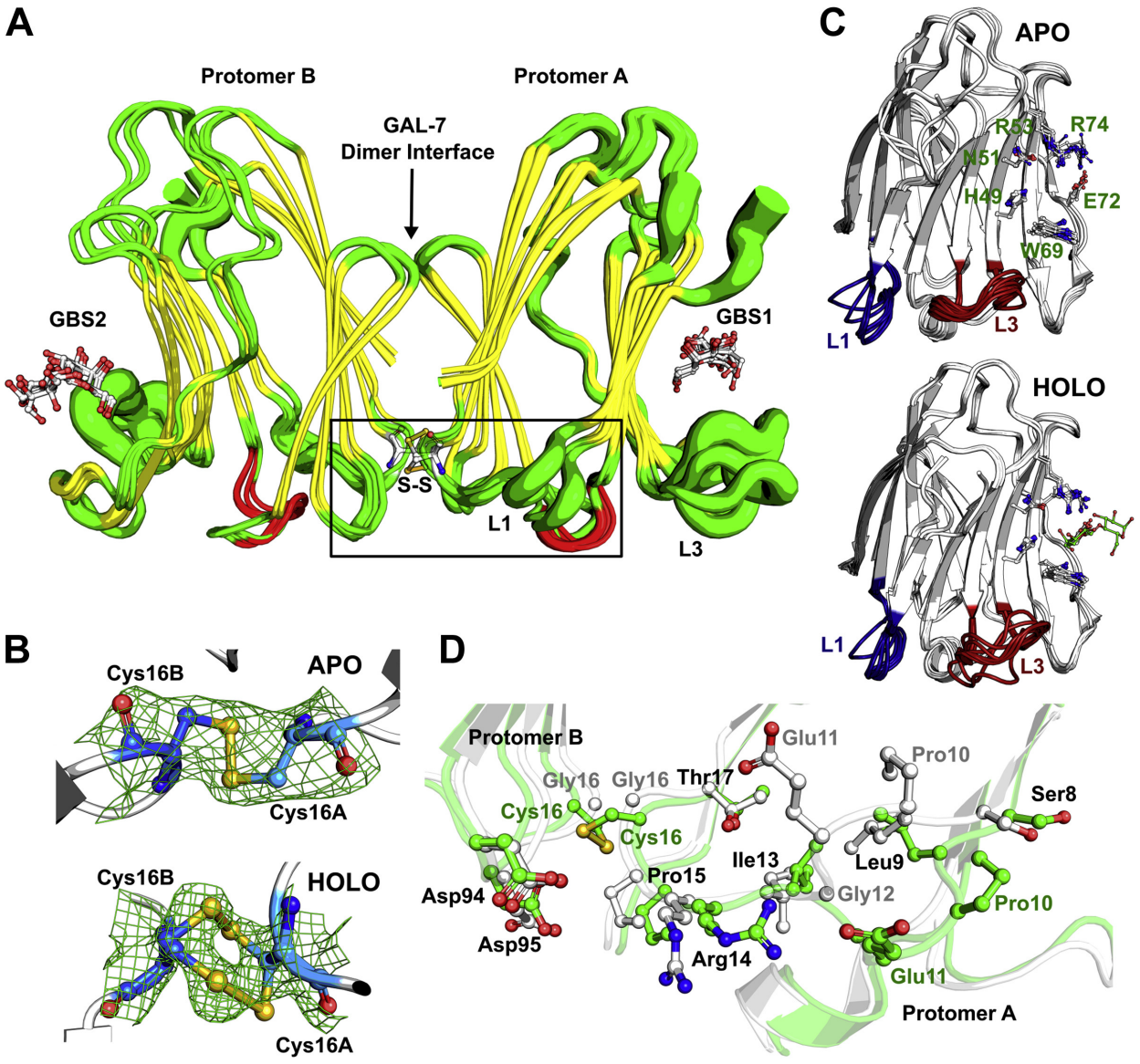

Figure 2.2 Crystal structures of WT, G16S, and G16C variants of GAL-7.

A, structural overlay of ligand-bound forms of WT GAL-7 (PDB 4GAL and 6VTO), G16S (PDB 6VTS), and G16C (PDB 6VTQ). Width of putty cartoon representation illustrates B-factor values, highlighting conformational variations observed in loop 1 (L1) and loop 3 (L3). The engineered disulfide bridge between protomers A (right) and B (left) in variant G16C is labeled S-S and shown in ball-and-stick representation. The two opposite glycan-binding sites are labeled GBS1 (protomer A) and GBS2 (protomer B). Bound ligands are shown in red and white atomic representation. Local environment perturbations resulting from G16X mutations in L1 are shown in panel D (black rectangle). B, electron density map surrounding the Cys16A-Cys16B disulfide bridge at the dimer interface of apo (top) and holo (bottom)

GAL-7 variant G16C. C, overlay of CRD protomers A and B in apo (top) and holo (bottom) structures of WT GAL-7 and variants G16S and G16C. L1 (blue) and L3 (red) are highlighted in apo (PDB 1BKZ, 3ZXF, 6VTP, and 6VTR) and holo (PDB 4GAL, 6VTO, 6VTQ, and 6VTS) GAL-7 structures. Main GBS residues are labeled and shown in ball-and-stick representation on apo panel. D, atomic view of the overlay between WT (white) and G16C variant (green) showing the local environment surrounding the Gly16 site of mutation and neighboring conformational change experienced by selected residues in loop 1.

2.4.6 Apo and holo GAL-7 structures suggest distinct dynamic behavior for loops 1, 3, and 5 in G16X variants

Previous simulations suggested the existence of positive binding cooperativity in GAL-7, whereby entropic penalty at a ligand-free binding site (i.e., increased dynamics in GBS residues) may facilitate induced fit and binding of a second ligand to the GBS in the opposite protomer (Ermakova et al., 2013). It has been proposed that these effects would be compensated by rigidification of other internal motions observed elsewhere in the protein. In line with this observation and despite overall structural similarity to WT GAL-7, apo versus holo G16X structures suggest distinct long-range conformational alterations triggered by interface mutation and ligand binding. One of the most significant structural rearrangements between WT and G16X apo structures occurs in the local environment of residues 8–17 (loop 1), which exhibit significant atomic-scale deviations in the variants (Figure 2.2A-C). This local rearrangement of loop 1 involves Gly16 and its neighboring residues, particularly residues Pro10, Glu11, Gly12, and Arg14 (Figure 2.2D). Contrary to apo structures, the conformation of loop 1 in both chains is not as significantly perturbed in ligand-bound WT and G16X variants (Figure 2.2C).

To evaluate conformational changes observed between apo and holo structures independent of X-ray artifacts and crystal variability, Z-scores of the atomic B-factors were calculated and used for comparative assessment (Broom et al., 2020). Cα B'-factors between apo and holo WT structures show that chain B is less flexible, while chain A is more flexible in the presence of lactose (Figure 2.6). This indicates that loop 1 experiences distinct dynamic behavior in each GAL-7 chain upon ligand binding, an observation that was not immediately obvious from a previous GAL-7 dynamic investigation (Ermakova et al., 2013). Similarly, although both chains in G16X structures exhibit increased Cα B'-factor values for residues 10–15 (loop 1), the mobility gain in one chain was found to be significantly higher than that observed in the opposite chain (Figure 2.6, B and C). In addition to the previously highlighted holo loop 1 rigidification in WT (Ermakova et al., 2013), these results suggest that GAL-7 may rely on an asymmetric allosteric network involving distinct loop 1 rigidification (or flexibility) in chains A and B to facilitate cooperativity between the two protomers. Even when similar loop 1 conformations are observed in each chain between holo WT and G16X structures (Figure 2.6, D and E), Cα B'-factor analysis

shows an increase in loop 1 mobility for the mutationally induced G16X structures upon ligand binding. These observations further suggest the importance of loop 1 dynamics in interface communication between protomers, in line with the proapoptotic functional effects we illustrated above.

In comparison with holo WT, holo G16X structures also exhibit higher Cα B'-factor values in loop 1, especially for residues Ile13, Arg14, and Pro15, which are located near the site of mutation. In some protomer–protomer interactions, a shift in the side chain of Arg14 leads to the loss of a salt bridge between its terminal guanidinium moiety and residue Asp94 on the opposite protomer. Neighboring residues Asp94 and Asp95 on the opposite protomer also exhibit altered conformational states relative to WT. This leads to the loss of a salt bridge between Arg14 and Asp95 in the G16X variants, a result supported by reduced population of this electrostatic interaction in our MD simulations (see below). These results suggest that homodimer destabilization in variant G16S is partly attributed to changes inside chain conformation and dynamics involving residues Arg14, Asp94, and Asp95, which also neighbor the site of mutation (Figure 2.6, D and E). This structural reorganization also results in the overall reduction of the surface area defining the dimer interface in G16C and G16S variants (Table 2.4).

Besides loop 1, holo structures of G16S and G16C exhibit increased conformational variations in residues 37–46 (loop 3) relative to WT, a structural element neighboring the GBS (Figure 2.2C). The Cα B'-factor of these residues increases in the presence of lactose for WT and G16X variants (Figure 2.6, A-C). However, except for Glu41, G16X variants exhibit higher loop 3 Cα B'-factor values than WT (Figure 2.6, D and E). Moreover, holo structures of WT and G16X variants display distinct rigidity behaviors in residues 64–74 (loop 5), a structural element encompassing several GBS residues. In the presence of lactose, loop 5 Cα B'-factor values decrease in WT, while conversely increasing in G16X variants (Figure 2.6, A-C). Increased loop 3 dynamics upon ligand binding supports the importance of long-range allosteric communication between the dimer interface, the GBS, and neighboring structural elements. Furthermore, although gain of loop 5 dynamics for G16X variants does not significantly contribute to the affinity of small glycan compounds such as lactose, it might still affect GAL-7 binding to more complex glycoreceptors.

2.4.7 G16X variants experience similar residue fluctuations but altered interprotomer dynamics relative to WT

To further investigate the role of interface mutation on potential allosteric communication in GAL-7, we performed principal component analysis (PCA) to allow visualization of the overall protein dynamics. The Cα backbone root mean square fluctuations (RMSFs) for each residue within apo WT, G16C, and G16S are presented in Figure 2.7, while the first five PCA normal modes are presented in Figure 2.8. Movies WT-PCA.mov, G16C-PCA.mov, and G16S-PCA.mov are also presented in supplementary information for the first ten PCA normal modes of WT, G16C, and G16S, respectively. For all GAL-7 variants, most residues display RMSF values below 1.5 Å, suggesting overall protein rigidity, except for specific segments. In addition to the N-terminus, protein segments exhibiting significant mobility (i.e., higher RMSF values) are located in residues 8–12 (located in loop 1), 39–43 (in loop 3), and 64–68 (in loop 5). For both protomers and for all three protein systems, the highest mobility observed lies within residues 64–68 (loop 5). Noteworthy, the C-termini of GAL-7 displayed low RMSF values because of its location at the homodimer interface. Overall, we observe no significant difference in RMSF values between WT and G16X variants. However, comparison of apo WT with apo G16X normal modes supports the involvement of long-range, global alterations to the rocking movement between protomers triggered by the mutations at the interface (Figure 2.8).

2.4.8 GAL-7 dynamical network analysis uncovers critical edges that define interprotomer communication between the two glycan-binding sites

A previous study observed positive cooperativity in ligand binding to GAL-7 (Ermakova et al., 2013), suggesting that one or more long-range allosteric residue networks can modulate binding properties between the two opposite glycan-binding sites in the GAL-7 homodimer. As described previously (Barbeau et al., 2017), we used a dynamical network analysis approach similar to the dynamical network of residue–residue contact to calculate allosteric effects in a protein (Doshi et al., 2016). This network analysis was performed on WT GAL-7 and variants G16X to identify potential allosteric pathways that connect the GBS within each protomer and to estimate the effect of mutation on network pathways. Details of network construction and allosteric pathway identification are described in the Experimental procedures.

Our results illuminate critical edges within WT GAL-7 and G16X mutants that support the importance of the dimer interface in allosteric communication. Indeed, the highest prevalent edges of the network are located at the dimer interface (Figure 2.3). Interprotomer communication in WT GAL-7 is primarily formed by seven critical edges between protomers A and B: R20(A)-D103(B),

R20(B)-D103(A), V18(A)-I91(B), V18(B)-I91(A), V18(A)-V18(B), F135(A)- V100(B), and F135(B)-V100(A). Except for the F135(A)-V100(B) and F135(B)-V100(A) pairs, these critical edges are conserved in the G16C and G16S network (Figure 2.3B). These results indicate that only the F135(A)-V100(B) and F135(B)-V100(A) interactions are significantly weakened by the G16X mutations, and that the contact interactions involving other residues between protomers are similar or only slightly affected.

We further investigated the allosteric pathway between the two opposite GBSs within each protomer using the shortest path method, i.e., the path for which the sum of its constituent edges is minimized. The shortest pathway connecting both opposite GBSs exhibits an identical pathway weight value of 0.27 and is identical for both WT and G16C: N62(A)-F61(A)-Y106(A)-A104(A)-D103(A)-R20(B)-V88(B)-F50(B)-H49(B) (Figure 2.3A). The shortest pathway between the two G16S opposite GBSs also exhibits a similar weight value of 0.27 and involves the same sequence of residues but transposed to the other protomer: N62(B)-F61(B)-Y106(B)-A104(B)-D103(B)-R20(A)-V88(A)-F50(A)-H49(A) (Figure 2.3A). The shortest pathway between the two G16S opposite GBSs also exhibits a similar weight value of 0.27 and involves the same sequence of residues but transposed to the other protomer: N62(B)-F61(B)-Y106(B)-A104(B)-D103(B)-R20(A)-V88(A)-F50(A)-H49(A) (Figure 2.3A). These results suggest that the primary interaction network connecting the GBS of each protomer is conserved in G16X mutants, although transposed between the A and B protomers in G16S.

2.5 Conclusion

In this work, we used protein engineering to illuminate the importance of long-range interprotomer communication involving the homodimer interface in GAL-7. Our mutational results show that subtle interface perturbations can be exploited to alter residue communication between protomers, further supporting the previously observed positive cooperativity in GAL-7 (Ermakova et al., 2013). Subtle engineering changes that perturb dimer stability at the interface can be positively or negatively exploited to control the proapoptotic activity of GAL-7 at the cellular level. This functional modulation further demonstrates the relevance of this protein–protein interaction as an efficient interface for future rational drug discovery programs targeting GAL-7. Indeed, many structurally homologous galectins are involved in mediating subtle yet critical glycan-dependent and -independent interactions between pro- and antiapoptotic molecular partners in the cell (Borrok et al., 2007; López de los Santos et al., 2020; Villeneuve et al., 2011). As a result of their highly homologous GBS interactions, the specific targeting of selected galectin members remains

one of the most promising avenues for future disease treatments. Our results identified residues involved in dimer stability and allosteric communication between protomers, along with altered dynamic behaviors involving loops 1, 3, and 5, which could also potentially be used to modulate GAL-7 function. Overall, these observations highlight new avenues for the design of galectin-specific modulators to alter GAL-7-mediated functions in cancer and other diseases.

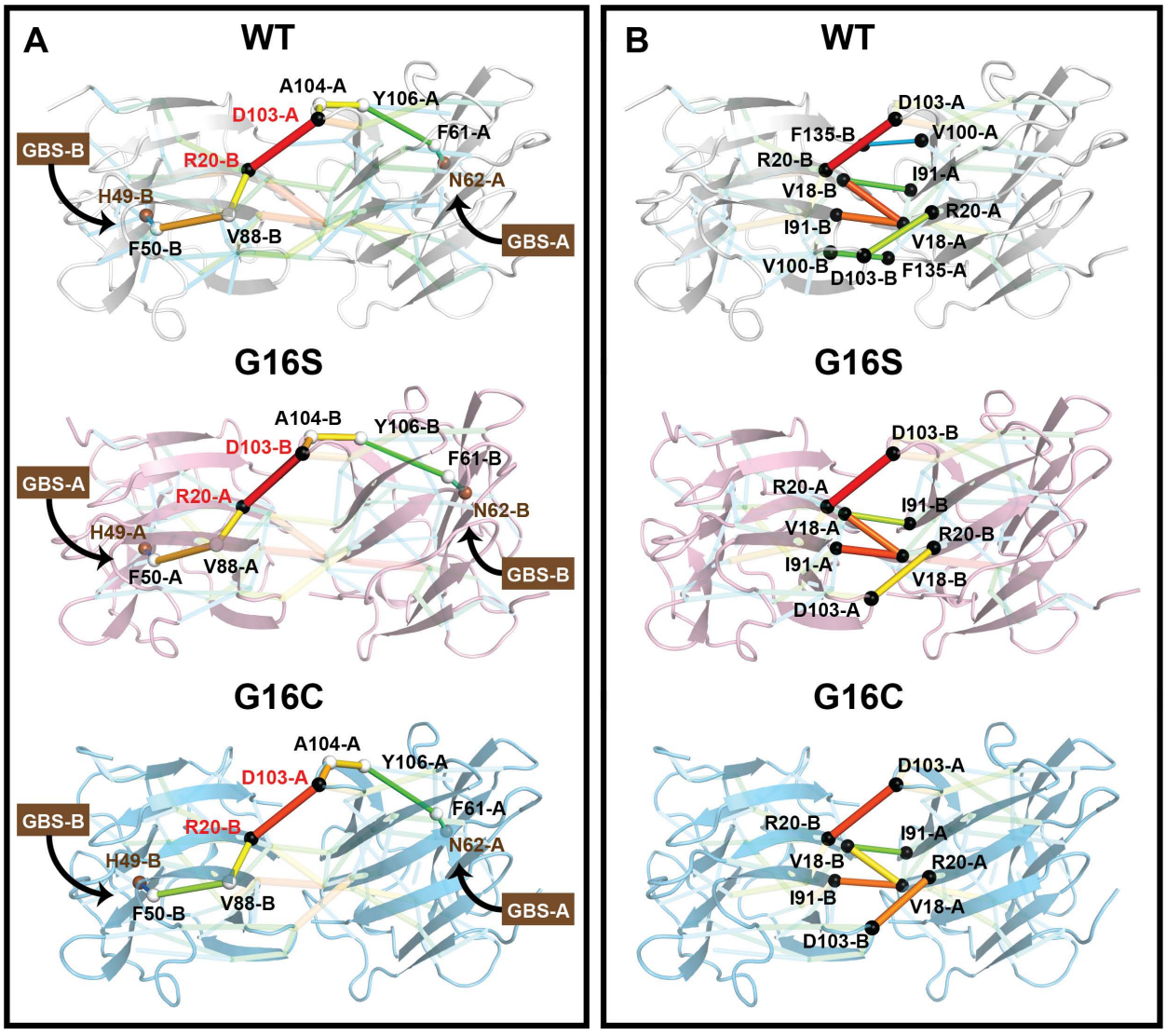

Figure 2.3 Dynamical network analysis of WT GAL-7, G16S, and G16C variants.

A, the shortest pathway between two opposite GBSs (N62-H49) is highlighted on WT GAL-7 (white, top), G16S (pink, middle), and G16C (blue, bottom). Residues involved in interprotomer communication at the dimer interface are represented by black spheres. Communication between residues is represented by sticks. The critical edge of communication is color scaled from blue-to-red and is proportional to stick thickness. Selected GBS residues are labeled and colored brown. B, residues involved in interprotomer communication at the dimer interface are represented by black spheres, with similar critical edge color scale and thickness to represent importance. For clarity and better visual comparison, note that protomers A and B are swapped in variant G16S.

2.6 Experimental procedures

2.6.1 GAL-7 dimer stability assessment

The PoPMuSiC algorithm was used to estimate the impact of amino acid substitutions on protein stability (Gilis et al., 2000). PoPMuSiC predicts changes in folding free energy ($\Delta\Delta G_F$) upon single-site mutation using solvent-accessibility-dependent combinations of statistical potentials. GAL-7 PDB entry 1BKZ was used as input for the algorithm, which requires the experimental or modeled 3D structure of the target protein. Analyses were also performed with the BeAtMuSiC algorithm (Dehouck et al., 2013), which uses similar potential combinations to predict changes in binding affinity ($\Delta\Delta G_B$) of protein–protein complexes upon mutation.

2.6.2 DNA constructs and site-directed mutagenesis

The recombinant human gene encoding for galectin-7 (GAL-7) was subcloned into vector pET-22b(+) using NdeI and HindIII restriction enzymes and propagated as previously described (Grosset et al., 2014). G16C and G16S mutants were generated with the Q5 Site-Directed Mutagenesis Kit (NEB) using the forward (G16Cf: 5'-atccgcccttgcacggtgctg-3'; G16Sf: 5' atccgcccttccacggtgctg-3') and reverse (G16Xr: 5'-gccctcgggcagtgaggacttg-3') primers. The F135S mutant was generated by the QuikChange site-directed mutagenesis method with PfU DNA polymerase (Bio Basic) using forward (F135f: 5'-gactccgtgaggatctcctgaaacgttgcgg-3') and reverse (F135r: 5'-ccgcaacgtttcaggagatcctcacggagtc-3') primers. All gene sequences were confirmed by DNA sequencing. Plasmid constructs were further employed for all protein expressions.

2.6.3 Recombinant expression and purification of WT GAL-7 and variants

All pET-22b(+) constructs were transformed into *E. coli* BL21(DE3) for recombinant protein overexpression under control of the T7 promoter. A volume of 500 ml of lysogeny broth (LB) medium was inoculated with a 5-mL overnight preculture of *E. coli* BL21(DE3) carrying WT recombinant human GAL-7 or G16X mutant plasmids. Culture growth was carried out at 37 ºC until OD600 nm = 0.6 – 0.7, after which protein expression was induced with 0.5 mM isopropyl-β-D-1-thiogalactopyranoside (IPTG) at 16 ºC overnight. Bacterial cells were harvested by centrifugation for 30 min at 3800g (4 ºC). Pellets were resuspended in 80 ml of buffer A (50 mM Tris pH 8.0, 150 mM NaCl) and lysed by sonication using a 1/200 wave horn connected to a 450 Sonifier (Branson). Sonication was performed at power output level 7 with 70% pulse rate for 2-min cycles and 1 min cooling between each cycle. Cells were completely lysed after four cycles.

The sonicated lysate was centrifuged for 30 min at 17,600g (4 ºC). The supernatant was filtered and the protein was purified by lactose affinity gravity-flow purification at 4 ºC. A 2-ml volume of α- lactose-agarose matrix (Sigma-Aldrich, Oakville, ON) was added into a 24 ml gravity column and then equilibrated with 50 ml buffer A. Filtered supernatant was applied to the column, which was then washed extensively with 50 ml buffer A. The pure protein was eluted with 15 ml buffer B (50 mM Tris pH 8.0, 150 mM NaCl, 150 mM α-lactose) and 1.5 ml fractions were collected. α-lactose was removed from the eluted protein by dilution in buffer C (20 mM Tris pH 8.0, 150 mM NaCl) for protein crystallization, buffer D (20 mM potassium phosphate, pH 7.2) for circular dichroism (CD) and isothermal titration calorimetry (ITC), or PBS (0.144 g/L KH_2PO_4, 0.795 g/l NaH_2PO_4, 9 g/l NaCl, pH 7.4) for microscale thermophoresis (MST) and cell assays. Dilution factors were set at 160,000-fold or higher to remove all α-lactose traces. Protein solutions were further concentrated using 3-kDa Amicon Ultra 15 ml Filters (EMD Millipore) at 3800g (4 ºC).

2.6.4 Translational diffusion analysis of free and lactose-bound WT GAL-7

Diffusion measurements were conducted using the BPP-LED (bipolar pulse pair–longitudinal-eddy-current delay) sequence (Wu et al., 1995), modified to include continuous wave water saturation during the relaxation delay, diffusion period, and LED period (i.e., the ledbpgppr2s sequence as provided by the spectrometer vendor). In the BPP-LED experiment, the NMR signal intensity (I) is dependent on the molecular diffusion coefficient (D) and may be expressed as a function of the strength of the gradients used to probe the diffusion coefficient (g):

$$I(g) = I(0)\, exp\left[-D(\gamma g \delta)^2 \left(\Delta - \frac{\delta}{3} - \frac{\tau}{2}\right)\right]$$

where γ is the 1H gyromagnetic ratio, δ/2 is the duration of each gradient pulse, Δ is the delay between the so-called “encoding” and “decoding” gradients, and τ is the gradient stabilization delay. In this work, δ/2 was fixed at 4.3 ms, Δ was held at 70 ms, and τ was maintained at 0.226 ms, while g was varied linearly in 40 steps from 3.6 to 32.5 G/cm (accounting for the sine-bell amplitude profile of the gradient pulses). The LED time was set to 5 ms. Sixteen transients were collected at each gradient strength, with a 5-s relaxation delay between scans, for a total experiment time of roughly 1 h. The sample temperature was regulated at 25 ± 1 ºC, using a high gas flow of 1070 L/h to minimize convection-related artifacts in the diffusion measurement (Swan et al., 2015). Spectra were processed using a 20 Hz line-broadening window function along with polynomial baseline correction. Signal intensity of the protein in the methyl region (0.8 ppm) was integrated to provide 40 values of I(g). The methyl region was selected because it is far away

from peaks associated with water or buffer, is less likely to be affected by solvent exchange, and is intense. A nonlinear-least-squares fit of the I(g) values against g provided the reported diffusion coefficients. The error in the diffusion measurement was calculated as 0.14×10^{-11} m^2/s, as determined from the spread of fitted diffusion coefficients from five technical replicates of the diffusion measurement of the final titration point.

2.6.5 Apoptosis assays with Annexin V/PI staining

Apoptosis was measured by flow cytometry using FITC-labeled Annexin V (Biolegend, San Diego, CA) and propidium iodide (PI) (Vladoiu et al., 2015). Increasing concentrations of WT and GAL-7 variants (1–50 μM) were incubated with 2.5×10^5 Jurkat T cells maintained in RPMI 1640 medium (Life Technologies, Burlington, ON) at 37 ºC for 4 h. After incubation, cells were centrifuged for 8 min at 900g at 4 ºC. Cell pellets were then resuspended in 100 μl of a solution containing Annexin V-FITC buffer (0.01 M HEPES pH 7.4, 0.14 M NaCl, 2.5 mM $CaCl_2$, 0.63 μg/ml Annexin V) (Biolegend, San Diego, CA) and incubated for 15 min at room temperature in the dark. Four-hundred microliters of propidium iodide (PI) buffer (0.01 M HEPES pH 7.4, 0.14 M NaCl, 2.5 mM $CaCl_2$, 0.25 μg/ml PI) was added to cells prior to flow cytometry analysis. In total, 5000 events were recorded and analyzed using a BD FACS Calibur flow cytometer. Controls included unstained cells to set positivity and a no-GAL-7 untreated control, value of which was subtracted for each data point. Results were based on three independent assays performed in duplicate. Proapoptotic activity was normalized to activity of 50 μM WT GAL-7 and evaluated the day of the assay, and the resulting percentages were plotted as a function of variant concentration using GraphPad Prism 9.0 (GraphPad Software). EC50 values were determined by nonlinear least squares regression fitting. Fitted concentration curves and best-fit values were compared using the extra sum-of-squares F-test method. The comparison analysis concluded that the preferred model was each dataset representing a different curve ($a = 0.05$, $p \leq 0.0003$).

2.6.6 Circular dichroism and thermal unfolding

Thermal unfolding of WT and GAL-7 variants was monitored by circular dichroism (CD) using a Jasco J-815 spectropolarimeter equipped with Peltier Jasco CDF-426S/15 thermostatic system. All thermal scanning experiments were acquired with 50 μM apo or holo protein (in presence of 6 mM α-lactose) in 200 μl buffer D (20 mM potassium phosphate, pH 7.2). Initial spectra were acquired at 20 ºC from 250 nm to 200 nm in a 1 mm pathlength quartz cuvette. Thermal denaturation experiments were performed by monitoring changes in ellipticity at 220 nm

between 20 ºC and 80 ºC with a heating rate of 1 ºC /min. T_m values were determined using the first order derivatives and polynomial functions of the Jasco Spectra Manager software with the Savitzky–Golay algorithm.

2.6.7 Microscale thermophoresis (MST)

GAL-7 dimer equilibrium affinity was measured by MST using the Monolith NT.115 Pico instrument (NanoTemper Technologies GmbH) at 25 ºC. In accordance with the manufacturer's protocol, WT GAL-7 and G16S variants were labeled with RED-NHS second generation using a Monolith NT.115 Protein Labeling Kit (Nanotemper Technologies) in PBS buffer. The excessive dye was separated by the provided column and protein was eluted in 20 mM Tris-HCl pH 8, 150 mM NaCl, supplemented with 0.05 % (v/v) Tween 20. Each binding assay experiment consisted of 16 2-fold serial dilutions of 50 µM (starting concentration) unlabeled GAL-7 prepared in 5 nM labeled GAL-7. All samples were incubated at 40 ºC in a water bath for 45 min prior to loading into a NT.115 MST premium coated capillary. MST was induced by a 21s infrared laser (IR-laser) activation at 25 ºC. All experiments were performed in triplicate. Raw data were preanalyzed and extracted using MO.Affinity software, version 2.3 (Nanotemper Technologies). Thermophoresis-induced changes in fluorescence were plotted as a function of unlabeled GAL-7 concentration using GraphPad Prism 9.0 (GraphPad Software). Dimer equilibrium dissociation constants (K_D) were determined using the least squares regression fitting method. The G16S homodimer K_D was determined with the initial fluorescent signal while the WT homodimer K_D was calculated using the MST on-time signal between 4 and 5 s.

2.6.8 Isothermal titration calorimetry (ITC)

All ITC experiments were carried out in triplicate at 25 ºC using a Nano ITC microcalorimeter (TA Instruments). In total, 300 µl of 200 µM WT GAL-7 and G16X variants were prepared in 20 mM potassium phosphate (pH 7.2) and injected in the Nano ITC cell. 6 mM α-lactose was dissolved in the same buffer and filled in the syringe. Titration was performed with 25 injections of 2 µl ligand into protein with a stirring rate of 150 rpm and a 150-s interval between each injection. A blank experiment was carried out by titrating each ligand in a protein-free buffer. Data was analyzed and fitted using the NanoAnalyze software v2.3.6 (TA Instruments).

2.6.9 Protein crystallization

- *Lactose-bound WT GAL-7*

Cocrystallization of WT GAL-7 with α-lactose was performed using the sitting-drop vapor diffusion technique. Crystals were obtained by incubating a drop consisting of a 1:1 mixture of 1 µl of 7.5 mg/ml WT GAL-7 solution (50 mM Tris pH 8.0, 150 mM NaCl, 7.5 mM α-lactose) with 0.1 M NaCl, 0.1 M Tris pH 8.0, 20 % PEG 3350, 15% glycerol at room temperature after 1 week. Crystals were cryo-protected by soaking in a solution of 0.1 M NaCl, 0.1 M Tris pH 8.0, 20 % PEG 3350, 30% glycerol.

- *Apo GAL-7 (G16C)*

One microliter of 7.5 mg/ml GAL-7 (G16C) solution (in buffer C) was mixed at 1:1 ratio with 0.1 M NaCl, 0.1 M Tris pH 8.0, 20 % PEG 3350, 15% glycerol. Crystals were obtained by the sitting-drop vapor diffusion technique at room temperature after 1 week. Crystals were cryo-protected by soaking in a solution of 0.1 M NaCl, 0.1 M Tris pH 8.0, 20 % PEG 3350, 30% glycerol.

- *Lactose-bound GAL-7 (G16C)*

Cocrystallization of GAL-7 (G16C) with α-lactose was performed by the hanging-drop vapor diffusion technique. Crystals were obtained by incubating a drop consisting of a 1:1 mixture of 1 µl of 7.5 mg/ml GAL-7 (G16C) solution (50 mM Tris pH 8.0, 150 mM NaCl, 7.5 mM α-lactose) with 0.1 M NaCl, 0.1 M Tris pH 8.0, 25 % PEG 3350 at room temperature after 1 week. Crystals were cryo-protected by soaking in a solution of 0.1 M NaCl, 0.1 M Tris pH 8.0, 25 % PEG 3350, 30% glycerol.

- *Apo GAL-7 (G16S)*

One microliter of 7.5 mg/ml GAL-7 (G16S) solution (in buffer C) was mixed at ratio 1:1 with 0.1 M NaCl, 0.1 M Tris pH 8.0, 20 % PEG 3350, 17.5% glycerol. Crystals were obtained by the sitting-drop vapor diffusion technique at room temperature after 1 week.

- *Lactose-bound GAL-7 (G16S)*

Cocrystallization of GAL-7 (G16S) with α-lactose was performed by the hanging-drop vapor diffusion technique. Crystals were obtained by incubating a drop consisting of a 1:1 mixture of 1 µl of 7.5 mg/ml GAL-7 (G16S) solution (50 mM Tris pH 8.0, 150 mM NaCl, 150 mM α-lactose) with 0.1 M NaCl, 0.1 M Tris pH 8.0, 16 % PEG 3350 at room temperature after 1 week. Crystals were cryo-protected by soaking in a solution of 0.1 M NaCl, 0.1 M Tris pH 8.0, 15 % PEG 3350, 20% glycerol.

2.6.10 Data collection, structure resolution, and refinement

All diffraction data of crystals in the presence and absence of α-lactose were collected at the Canadian Macromolecular Crystallography Facility Beamline 08B1-1 and 08ID-1 of the Canadian Light Source Synchrotron (Fodje et al., 2014; Grochulski et al., 2011). Raw data was immediately processed on the MxLIVE platform after collection. Structure resolution and refinement were carried out using the PHENIX software suite. Phase was calculated using the molecular replacement method using 1BKZ and 4GAL PDB structures as models for apo and holo structures, respectively. All structural

Ccomparisons and visualizations were performed with the Open-Source PyMOL Molecular Graphics System, Version 2.4 (Schrödinger, LLC). The Cα B-factor profiles were normalized and compared using the BANΔIT server using IBM z-Score (MADE) and MMLigner methods (Barthels et al., 2021).

2.6.11 Statistical analysis

Results represent at least three independent experiments and are plotted as mean with standard error of the mean (SEM) using GraphPad Prism 9.0 (GraphPad Software). Statistical significance was evaluated with F-test (cell assays, ITC and MST experiments) or one-way ANOVA with Tukey post-hoc tests (CD experiments). Two data sets were considered significantly different if p-value ≤ 0.05.

2.6.12 Molecular dynamics simulations

Structural coordinates from PDB 4GAL (Leonidas et al., 1998) were used to build the WT GAL-7, G16C, and G16S apo systems. Ionizable residues were considered in their standard protonation state at pH 7.0 with neutral histidine protons placed at ND1 or NE2 positions, according to the interactions with their respective neighbors within the structure. Systems were built using the CHARMM-GUI (Brooks et al., 2009; Jo et al., 2008; Lee et al., 2016) and the G16C and G16S mutations were introduced using the CHARMM-GUI tools. Structures were immersed in neutrally charged orthogonal boxes of water with a 10 Å distance from the protein to the edges of each box. Na^+ and Cl^- ions were added at a concentration of 150 mM. MD simulations were performed with NAMD 2.13b1 (Phillips et al., 2020) using the CHARMM36m force field parameters for proteins and carbohydrates (Huang et al., 2017) and TIP3P waters (Price et al., 2004). Simulations were carried out at 303.15 K under isothermal-isobaric (NPT) ensemble conditions with a 2-fs time step and periodic boundary conditions. Langevin damping with a

coefficient of 1 ps−1 was used to maintain constant temperature, while pressure was controlled by a Nosé–Hoover Langevin piston at 1 atm. Bond length between hydrogen and heavy atoms was constrained using SETTLE (Miyamoto et al., 1992) for water molecules and SHAKE (Ryckaert et al., 1977) for all other molecules. Cutoffs for the short-range electrostatics and the Lennard–Jones interactions were set at 12 Å, with the latter smoothed via a switching function over the range of 10–12 Å. Long-range electrostatic interactions were calculated with the Particle Mesh Ewald (PME) method (Darden et al., 1993; Essmann et al., 1995) using a sixth-order interpolation and a grid spacing of ≈1 Å at every integration step. Nonbonded pair lists were updated at every ten steps, and coordinates were saved every 10 ps for analysis. For each system (WT, G16C and G16S), three 1000-ns trajectories were recorded.

2.6.13 Trajectory analysis

The first 500 ns of all trajectories was considered as equilibration time and was not included in the analyses. The last 500 ns of each of the trajectories was concatenated into three trajectories (one for each system) at a rate of ten frames every ns, for a total of 15,000 frames per trajectory. Only the proteins were included in the concatenated trajectories, which were aligned on the initial structure. The interface binding energies of WT, G16C, and G16S dimers were evaluated using the *AnalyseComplex* command from FoldX (Schymkowitz et al., 2005). This analysis was conducted on 5000 frames from the respective concatenated trajectories. For surface areas, final values were calculated using ten block averages over the trajectories and errors were calculated as standard deviations.

2.6.14 Allosteric analysis

The protein dynamical network analysis was realized following the methodology exposed in a previous work (Barbeau et al., 2017). In short, the nodes of the network were represented by the residue heavy atom center of mass. Edges that transfer allosteric information between the nodes were drawn between the nodes for which the respective residue maintains any of its heavy atoms within a distance of 4.5 Å for at least 75% of the time in the trajectories. The weight of the edges between the nodes i and j was defined as the coefficient of variation of the distance between the nodes:

$$C_{ij} = \frac{\sqrt{\langle \left(r_{ij} - \langle r_{ij} \rangle\right)^2 \rangle}}{\langle r_{ij} \rangle}$$

where $r_{ij} = |r_{ij}| = |r_i - r_j|$ is the distance between the center of mass of residues i and j. In contrast to the calculation of the positional fluctuation correlations, the separation distance approach does not require prior removal of the global motions. NetworkX (Hagberg et al., 2008) was used to calculate the edge betweenness centralities using the Ulrik-Brandes algorithm (Brandes, 2001). All edges were ranked based on their betweenness centrality, the critical edges identified as edges with a prevalence of being part of an optimal path between any two nodes of at least three standard deviations (3σ) from the edge prevalence distribution.

2.7 Data availability

X-ray coordinates for human GAL-7 in complex with 4-O-beta-D-galactopyranosyl-D-glucose, apo GAL-7 variant G16C, holo GAL-7 variant G16C in complex with lactose, apo GAL-7 variant G16S, and holo GAL-7 variant G16S in complex with lactose have been deposited in the RCSB PDB under accession codes 6VTO, 6VTP, 6VTQ, 6VTR, and 6VTS, respectively.

2.8 Acknowledgments

The authors thank Carolina Perusquía Hernández and Stéphane Beauchamp (INRS) for technical assistance. Part of this research was also performed using beamlines CMCF-ID and CMCF-BM at the Canadian Light Source, a national research facility of the University of Saskatchewan, which is supported by NSERC, the Canada Foundation for Innovation (CFI), the National Research Council (NRC), the Canadian Institutes of Health Research (CIHR), the Government of Saskatchewan, and the University of Saskatchewan. All computations were performed on the Helios supercomputer at Université Laval, which is managed by Calcul Québec and Compute Canada. Operation of this supercomputer is funded by the CFI, the ministère de l'Économie et de l'Innovation du Québec (MEI), and the Fonds de recherche du Québec–Nature et technologies (FRQNT).

2.9 Author contributions

N. T. H. P., M. L., P. L. and N. D. conceptualization; N. T. H. P., M. L., M. F., P. L., Y. S.-P., and N. D. data curation; F. P., B. F., M. R., N. T. H. P., C. C., P. L., N. D., and M. L. formal analysis; C. C., Y. S.-P., P. L., D. C., and N. D. funding acquisition; N. T. H. P., M. L., M. S. A.-A.-W., P. L., Y. S.-P., and N.D. investigation; N. T. H. P., M. L., G. B., P. L., C. C., Y. S.-P., and N.D. methodology; C. C., Y. S.-P., P. L., D. C., N. D. supervision; N. T.H. P., M. L., P. L., and N. D.

writing–original draft; N. T. H. P., M. L., M. F., G. B., M. S. A.-A.-W., F. P., B. F., M. R., D. C., Y. S.-P., P. L., C. C., and N. D. writing–review and editing.

2.10 Funding and additional information

This work was supported in part by the National Institute of General Medical Sciences (NIGMS) of the NIH (under Award R01GM105978, to N. D.) and the Natural Sciences and Engineering Research Council of Canada (NSERC) (Discovery Grants RGPIN 2016-05557 to N. D. and RGPIN-2017-06091 to C. C.). N. T. H. P is the recipient of a Doctoral Training scholarship from the Fonds de Recherche du Québec–Santé (FRQS) (287239), and G. B. is the recipient of a PROTEO undergraduate scholarship. F. P. and M. R. are Postdoctoral Researcher and Research Director, respectively, at and funded by the Fonds de la Recherche Scientifique (F.R.S-FNRS) (Belgium). C. C. holds an FRQS Research Scholar Junior 1 Career Award (251848), and N. D.holds an FRQ-S Research Scholar Senior Career Award (281993).The content is solely the responsibility of the authors and does not necessarily represent the official views of the National Institutes of Health.Conflict of interest—The authors declare that they have no conflicts of interest with the contents of this article.

2.11 Abbreviations

The abbreviations used are: CRD, carbohydrate recognition domain; GAL-7, galectin-7; GBS, glycan-binding site; DIP, dimer interfering peptide.

2.12 Supplementary data

Table 2.1 List of mutations exhibiting the largest folding free energy difference ($\Delta\Delta G_F$) between dimer (D) and monomer (M) forms of GAL-7.

The prediction was performed by PoPMuSiC (Gilis et al., 2000). The change in binding affinity upon mutation ($\Delta\Delta G_B$) was predicted by BeATMuSiC (Dehouck et al., 2013). Secondary structure elements turn (T), coil (C), and extended β-strand (E) were computed by an in-house program. The two mutations predicted to destabilize the dimer state relative to the monomeric state are shown in dark red and have been selected for further experimental characterization.

Position	Wild-type	Mutant	Secondary Structure	RSA(M) %	$\Delta\Delta G_F$(M) (kcal/mol)	RSA(D) (%)	$\Delta\Delta G_F$(D) (kcal/mol)	$\Delta\Delta G_F$(D)-$\Delta\Delta G_F$(M)	$\Delta\Delta G_B$ (kcal/mol)
16	GLY	GLU	T	67	0.79	0	3.71	2.92	6.47
16	GLY	ASP	T	67	0.44	0	3.18	2.74	5.91
16	GLY	LYS	T	67	0.90	0	3.36	2.46	5.43
16	**GLY**	**SER**	**T**	**67**	**0.50**	**0**	**2.64**	**2.14**	**4.36**
16	GLY	ASN	T	67	0.29	0	2.37	2.08	4.06
16	GLY	THR	T	67	0.88	0	2.90	2.02	4.29
18	VAL	GLU	E	23	0.93	0	3.47	2.54	5.95
18	VAL	LYS	E	23	1.03	0	3.30	2.27	5.52
18	VAL	ASP	E	23	1.58	0	3.71	2.13	5.44
91	ILE	GLU	E	19	2.05	0	4.46	2.41	6.83
91	ILE	LYS	E	19	2.04	0	4.23	2.19	6.36
91	ILE	ASP	E	19	2.56	0	4.74	2.18	6.42
91	ILE	PRO	E	19	2.76	0	4.79	2.03	6.21
135	PHE	GLY	C	68	0.36	10	3.33	2.97	6.60
135	PHE	ASP	C	68	0.13	10	2.80	2.67	5.78
135	**PHE**	**SER**	**C**	**68**	**0.20**	**10**	**2.84**	**2.64**	**5.66**
135	PHE	ALA	C	68	0.28	10	2.91	2.63	5.60
135	PHE	GLU	C	68	0.07	10	2.51	2.44	5.08
135	PHE	PRO	C	68	0.25	10	2.64	2.39	5.13
135	PHE	LYS	C	68	0.16	10	2.50	2.34	4.98
135	PHE	ASN	C	68	0.16	10	2.49	2.33	4.93
135	PHE	GLN	C	68	0.12	10	2.38	2.26	4.70
135	PHE	THR	C	68	0.08	10	2.17	2.09	4.18
135	PHE	CYS	C	68	0.07	10	2.09	2.02	3.98

Table 2.2 ITC binding properties of α-lactose to WT GAL-7 and G16X variants

	α-lactose		
	WT	**G16C**	**G16S**
K_D (μM)	135.3 ± 1.2	109.0 ± 1.0	122.7 ± 10.8
N	0.93 ± 0.03	0.93 ± 0.03	0.50 ± 0.01
Δ*H* (kJ/mol)	-22.8 ± 0.1	-22.4 ± 1.3	-38.5 ± 6.9
Δ*S* (J/mol·K)	-0.7 ± 3.2	-0.5 ± 4.3	-54.3 ± 23.9

Table 2.3 Crystallography data collection and refinement statistics.

	GAL-7 WT – 4-*O*-β-D-Galactopyranosyl-D-glucose	Apo GAL-7 G16C	GAL-7 G16C - Lactose	Apo GAL-7 G16S	GAL-7 G16S - Lactose
PDB ID	6VTO	6VTP	6VTQ	6VTR	6VTS
Data collection[a]					
Space group	$P\,2_12_12_1$	$P\,2_12_12_1$	$P\,2_12_12_1$	$P\,2_12_12_1$	$P\,2_12_12_1$
			Cell dimensions		
a, b, c (Å)	30.52, 77.24, 111.44	53.60, 67.15, 71.92	30.37, 66.21, 111.56	54.01, 66.70, 71.43	30.30, 76.87, 113.77
α, β, γ (°)	90, 90, 90	90, 90, 90	90, 90, 90	90, 90, 90	90, 90, 90
Resolution (Å)	45.19 - 1.69 (1.75 - 1.69)	42.98 - 2.3 (2.382 - 2.3)	42.66 - 1.95 (2.02 - 1.95)	48.75 - 2.3 (2.382 - 2.3)	45.73 - 1.9 (1.968 - 1.9)
R_{merge}	0.08592 (0.8361)	0.1506 (2.416)	0.1069 (1.037)	0.04706 (0.4427)	0.06688 (1.224)
I/σI	15.71 (2.99)	14.49 (1.21)	16.73 (3.09)	31.65 (5.86)	23.53 (2.44)
$CC_{1/2}$	0.999 (0.839)	0.999 (0.569)	0.999 (0.865)	1 (0.964)	1 (0.843)
*CC**	1 (0.955)	1 (0.852)	1 (0.963)	1 (0.991)	1 (0.957)
Completeness (%)	99.09 (99.22)	98.78 (97.62)	99.86 (99.88)	98.45 (97.48)	99.84 (99.72)
Redundancy	6.9 (7.2)	9.7 (10.0)	12.6 (12.7)	9.8 (10.0)	12.6 (12.4)
Refinement					
Resolution (Å)	1.69	2.3	1.95	2.3	1.9
No. reflections	30152 (2929)	11899 (1148)	17137 (1701)	11780 (1161)	21749 (2113)
R_{work} / R_{free}	0.183/0.215	0.214/0.261	0.188/0.243	0.204/0.256	0.192/0.231
No. of (non-hydrogen) atoms	2502	2179	2250	2184	2266
Protein	2143	2123	2105	2115	2098
Ligand/ion	46	12	58	14	64
Water	313	44	87	55	104
B factors	19.73	65.11	33.28	60.72	38.32
Protein	18.2	65.53	33.15	61.11	37.81
Ligand/ion	24.17	48.07	34.46	53.9	45.53
Water	29.58	49.48	35.59	47.4	44.2
r.m.s. deviations					
Bond lengths (Å)	0.012	0.005	0.013	0.004	0.011
Bond angles (°)	1.43	1.13	1.61	1.01	1.51

Table 2.4 Dimer interface surface area in apo WT and variants G16C and G16S.

	Surface area exposed to dimer interface (Å^2)[a]		
Subunit	**WT**	**G16C**	**G16S**
A	715 (8)	661 (7)	650 (5)
B	613 (6)	565 (6)	558 (5)

[a]The protein surface area exposed to the dimer interface was calculated using the *measure sasa* function of the VMD program (Humphrey et al., 1996) in WT, G16C and G16S, respectively. For each system, the surface of each residue exposed to the dimer interface was obtained from the difference in their solvent-accessible surface area (sasa) calculated from the dimer and their corresponding monomers. The total surface exposed to the interface from each monomer was obtained from the sum of the values from each residue composing each respective monomer. Final values were calculated using 10 block averages over the trajectories and errors (in parentheses) were calculated as standard deviations. Structural reorganization results in overall reduction of the surface area of the dimer interface in variants G16C and G16S.

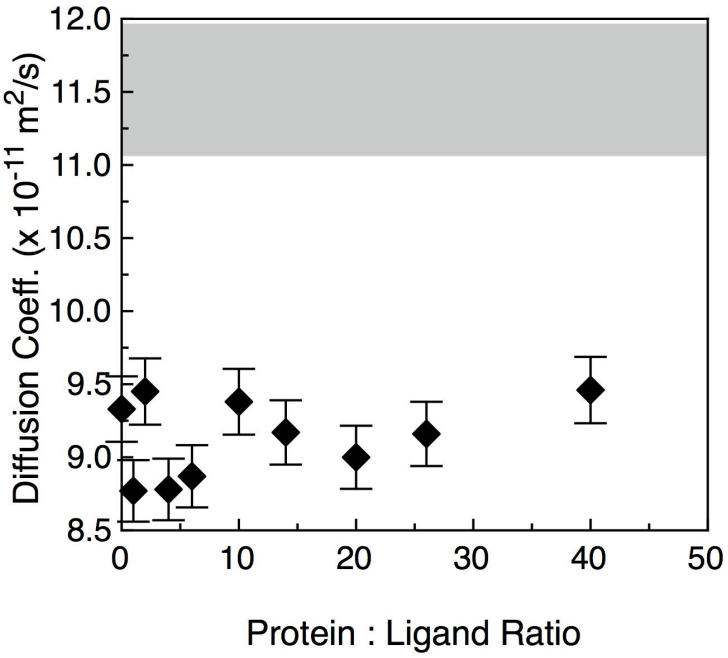

Figure 2.4 NMR extracted diffusion coefficients for WT GAL-7 in absence and presence of increasing concentrations of lactose.

NMR extracted diffusion coefficients for WT GAL-7 in absence and presence of increasing concentrations of lactose. Increasing ligand-to-protein concentrations have a negligible effect on the NMR-extracted diffusion coefficients of GAL-7, suggesting that the protein exists as a homodimer in solution in absence or presence of lactose at the glycan binding site (GBS). Assuming the existence of a homodimeric GAL-7 state with diffusion coefficients roughly ranging between ~8.7 - 9.5 × 10^{-11} m^2/s, the Stokes-Einstein equation would predict a diffusion coefficient ~26 % greater for a monomeric form of GAL-7. As a result, monomeric GAL-7 would appear in the upper shaded region of the graph. Diffusion measurements were conducted using the BPP-LED (bipolar pulse pair – longitudinal-eddy-current delay) sequence (Wu et al., 1995).See methods for details.

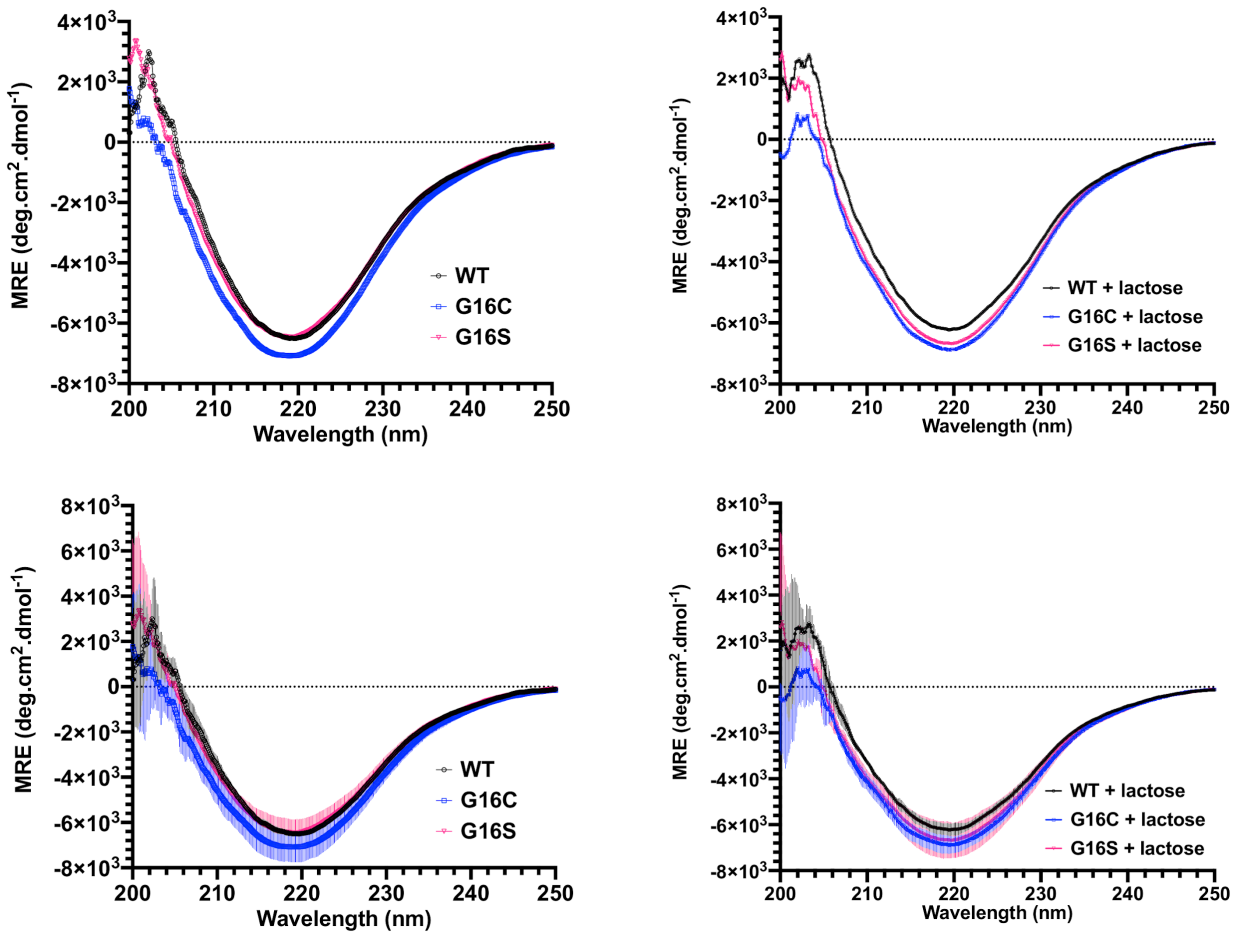

Figure 2.5 UV molar ellipticity spectra of GAL-7 variants obtained by CD spectropolarimetry.

CD spectra are shown for apo proteins WT GAL-7 (black), G16S (pink) and G16C (blue) (left panels) and in presence of 6 mM α-lactose (right panels). Bottom panels show spectra with standard deviation.

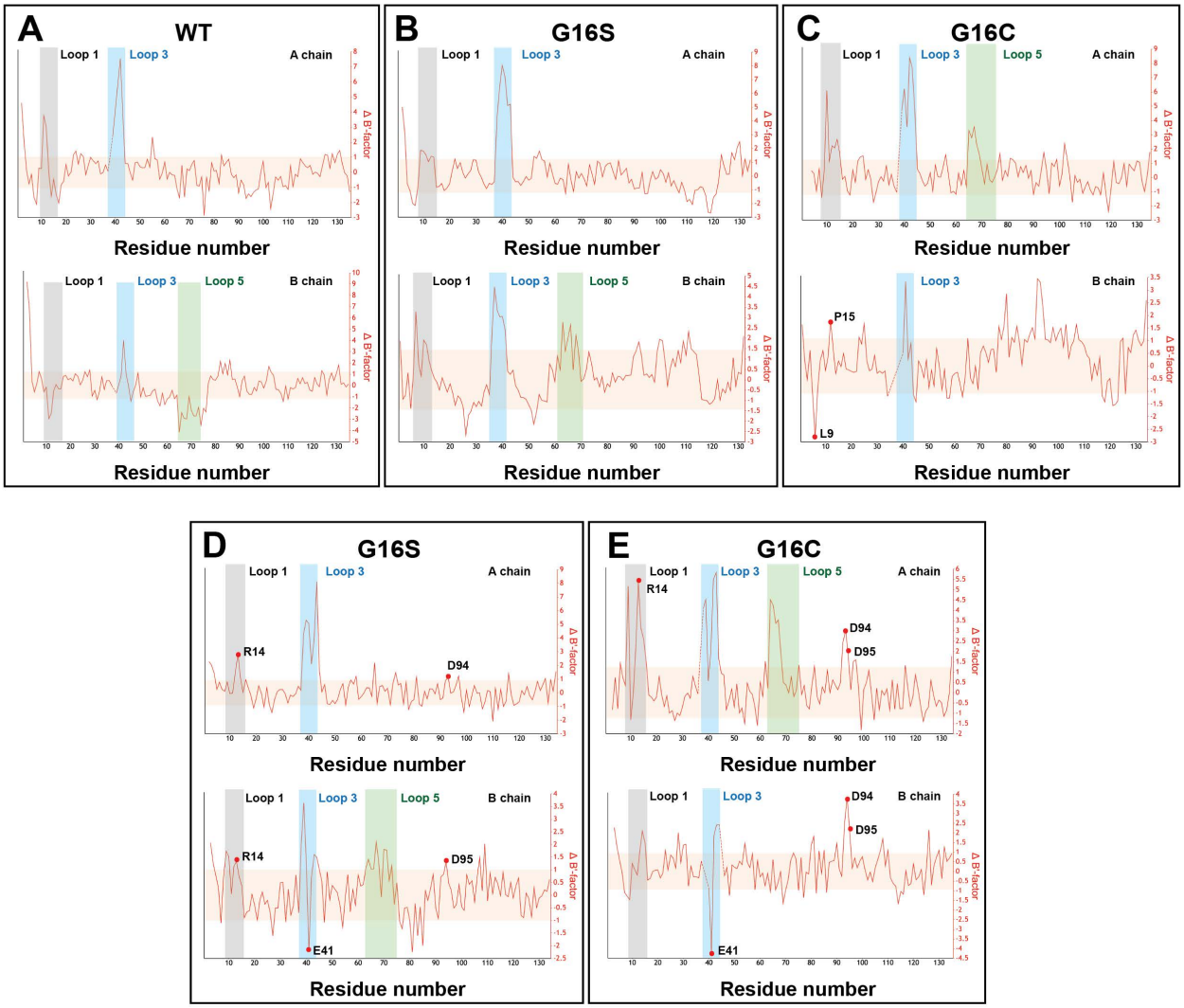

Figure 2.6 Plot of ∆B'-factor analysis between WT, G16S and G16C variants of GAL-7.

Cα B'-factor variations between apo *vs* holo structures for A) WT, B) G16S, and C) G16C. Cα ∆B'-factor values outside the orange box were found to be statistically significant ($p<0.05$). Residues 9-17 (loop 1), residues 39-43 (loop 3) and residues 64-74 (loop 5) are represented by grey, blue and green boxes, respectively. Chains A and B are plotted on top and bottom panels, respectively. Selected residues discussed in the text are labeled in black and shown as red dots on the plots. Cα B'-factor variations are (Barthels et al., 2021).

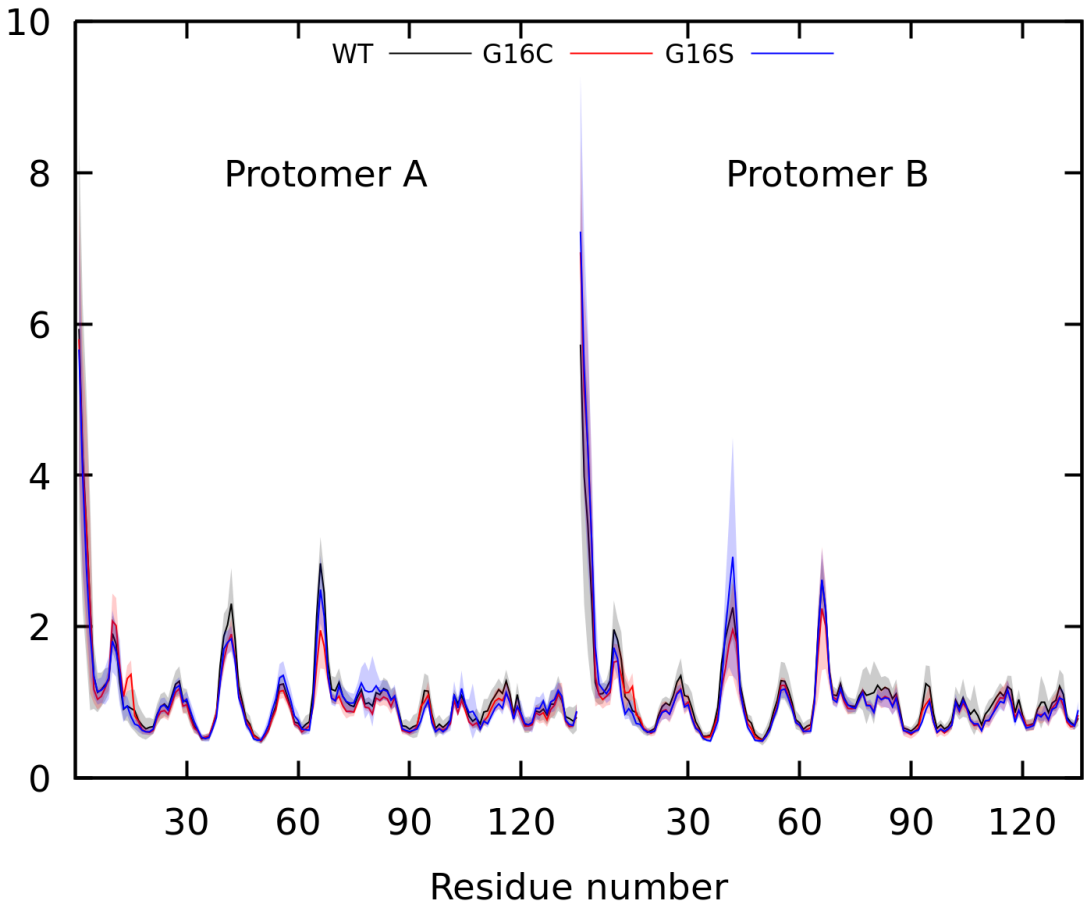

Figure 2.7 Plot of the backbone Cα atoms RMSFs for GAL-7 variants

Plot of the backbone Cα atoms RMSFs for each residue of GAL-7 WT (black), G16C (blue) and G16S (red). The standard deviations calculated from the 10 block trajectories are represented by the shaded area.

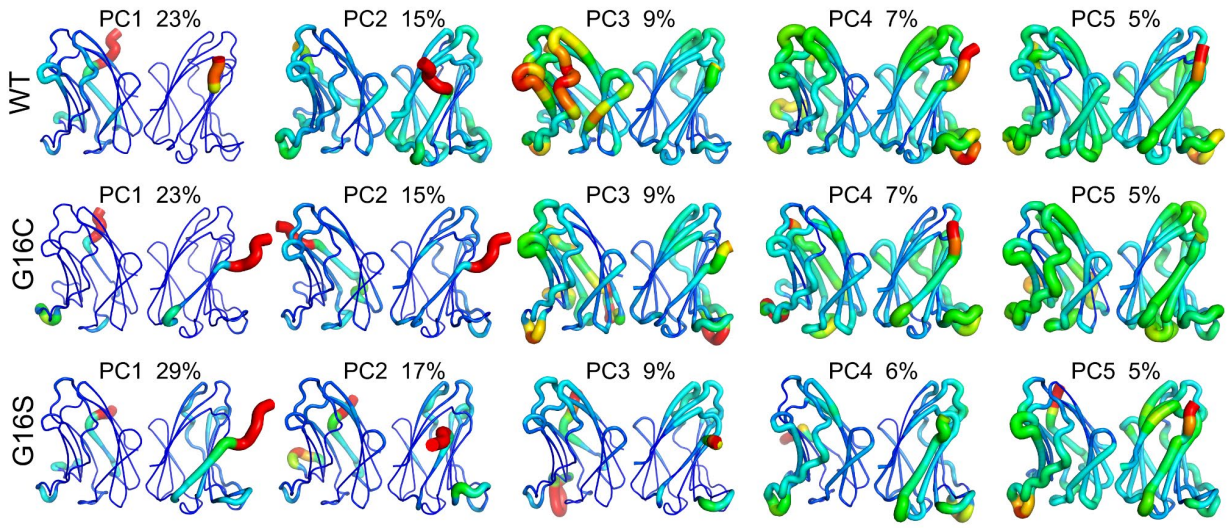

Figure 2.8 Average amplitude of motion for each residue involved in the first five PCA normal modes of GAL-7 variants

Average amplitude of motion for each residue involved in the first five PCA normal modes (PC1 to PC5) of WT (top), G16C (middle), and G16S (bottom). The size of the cartoon and the color spectrum correspond to the average amplitudes of motion within the first ten PCs. Width of putty cartoon representation and red color indicate greater amplitudes of motion. Percentages correspond to contributions to total motions calculated from the respective trajectories. The first ten PCA normal modes are presented in movies provided as supplementary material. All normal modes involve concerted motions between the two protomers. In agreement with the RMSF results for all 3 proteins, the first principal component (PC1, i.e. the greatest amplitude of motion) involves residues from the N-terminus as the primary concerted movement between protomers. The rocking motion observed between protomers as the principal concerted movement involves a pivot at the interface and is characterized by these motion amplitudes for most of the residues in the protein. Such movement appears in PC2 of WT GAL-7, and is also present for the remaining first five principal components. For G16C and G16S, rocking between the two protomers appears only in the third and fourth principal components, respectively. This movement is also present for the remaining first five principal components. Rocking movement between the two protomers as the main concerted motions accounts for 36% of the total motions in WT, while representing 21% and 11% in G16C and G16S, respectively. The concerted rocking movement between protomers is altered as a consequence of the single point mutation at the GAL-7 interface.

3 SECOND ARTICLE: "ALLOSTERIC NETWORK ANALYSIS IN GALECTIN-7 UNCOVERS KEY RESIDUES CONTROLLING COMMUNICATION BETWEEN TWO OPPOSITE GLYCAN BINDING SITES"

In the first article, we demonstrated that by altering the integrity of the homodimer interaction via G16X mutations, we can positively or negatively modulate the immunosuppressive activity of GAL-7. Allosteric communication networks across the dimer interface and between opposite protomers established during the first study suggested that residues involved in protomer-protomer communication at the interface are crucial to maintain allosteric communication. Nevertheless, it remained unclear which residues within the dimer interface network could modulate the positive cooperativity between opposite GBSs. Therefore, in this study, we investigate the consequences of disrupting inter-protomer communication on GAL-7 function and uncovered key residues controlling allosteric communication between long-range functional sites within GAL-7. Results pertaining to this objective are detailed in the second article manuscript presented in this chapter.

L'analyse du réseau allostérique de la galectine-7 révèle des résidus clés qui contrôlent la communication entre les deux sites opposés de liaison aux glycans

N. T. Hang Pham[1], Alex Paré[1], Myriam Létourneau[1], Marlène Fortier[1], David Chatenet[1], Yves St-Pierre[1], Patrick Lagüe[2,3], Charles Calmettes[1,3] , and Nicolas Doucet[1,3]

[1]Centre Armand-Frappier Santé Biotechnologie, Institut National de la Recherche Scientifique (INRS), Université du Québec, Laval, Quebec, Canada

[2]Département de Biochimie, de Microbiologie et de Bio-informatique and Institut de Biologie Intégrative et des Systèmes (IBIS)

[3]PROTEO, the Québec Network for Research on Protein Function, Engineering, and Applications, Université Laval, Québec, Quebec, Canada

Author contributions: I am the main author of this article, with help from Myriam Létourneau, Alex Paré, Patrick Lagüe, and Nicolas Doucet for writing. This manuscript was reviewed by all authors. In this study, I performed all protein expression, biophysical characterization, X-ray crystallography experiments, as well as data analysis of all results. Myriam Létourneau was involved in data analysis of biophysical experiments and biological assays. Apoptosis assays were carried out by Marlène Fortier. I also prepared all crystals, acquired, and analyzed all X-ray structural resolution data, with help from Charles Calmettes. Molecular dynamics simulations

were executed by Alex Paré and Patrick Lagüe. Allosteric network analysis was performed by Alex Paré, Patrick Lagüe, and myself. The overall study was supervised by David Chatenet, Yves St-Pierre, Patrick Lagüe, Charles Calmettes, and Nicolas Doucet.

3.1 Résumé

Sur le plan fonctionnel, la modulation allostérique d'une protéine offre une spécificité et une efficacité supérieures à celles de l'inhibition traditionnelle ciblant un site orthostérique. Cependant, le criblage conventionnel à haut débit visant la découverte de modulateurs allostériques spécifiques nécessite beaucoup de temps et d'investissement. À cet effet, la conception rationnelle de modulateurs à l'aide d'approches computationnelles s'est avérée efficace pour l'amélioration des techniques de prédiction de sites allostériques. Dans la présente étude, nous avons utilisé l'analyse de réseau pour prédire les positions à l'interface du dimère de la galectine-7 (GAL-7) humaine qui modulent allostériquement son activité pro-apoptotique aux sites de liaison des glycanes (GBS). En utilisant l'ingénierie des protéines, nous avons conçu quatre variants (R20A, R22A, D103A et R20A-R22A), qui ont subséquemment été soumis à une caractérisation biophysique, structurale et biologique afin de confirmer nos prédictions fonctionnelles. Tous les variants ont réduit la capacité de GAL-7 à induire l'apoptose des cellules T humaines. Les résultats de nos analyses de réseau ont également démontré que le nombre de contacts impliqués dans la communication inter-protomères a été diminuée chez presque tous les variants. En particulier, 70% des contacts inter-protomères sont perdus chez le variant D103A, conduisant à une baisse de la communication globale entre deux GBS opposés. De plus, nous avons observé la déstabilisation de l'interaction homodimère et de l'intégrité de la structure chez tous les variants. En général, notre étude illustre que l'utilisation de l'analyse de réseau et de la technique de « shortest pathway » permet d'évaluer la communication du flux global pour révéler R20, R22 et D103 comme des résidus clés qui contrôlent la fonction de GAL-7 via la communication entre ses deux GBSs opposés. Cette étude met en évidence de potentiels sites allostériques prédictifs permettant l'amélioration de la conception de modulateurs fonctionnels ciblant GAL-7.

3.2 Abstract

Functional allosteric modulation of a protein offers greater fine-tuning specificity than traditional orthosteric site inhibition. However, applying conventional high-throughput screening to the discovery of specific allosteric modulators remains an expensive and time-consuming

endeavor. To this end, the rational design of small-molecule modulators using computational approaches has proven to be effective for improving allosteric site predictions. In the present study, we used computational network analysis and the shortest pathway method to predict residue positions at the homodimeric interface of human galectin-7 (GAL-7) that allosterically modulate the pro-apoptotic activity mediated by its glycan binding sites (GBSs). Based on our predictions, we designed four mutational variants (R20A, R22A, D103A, and R20A-R22A) that were subjected to biophysical, structural, and biological characterization to confirm our functional hypotheses. As predicted, all variants were found to reduce the ability of GAL-7 to induce apoptosis in human T cells. The network analysis also demonstrated that the number of contacts involved in inter-protomeric communication was significantly decreased in almost all variants. In particular, we found that 70% of inter-protomer contacts were lost in variant D103A, leading to a decrease in overall communication between the two opposing GBSs. In addition, we observed destabilization of homodimer interactions and structural integrity perturbations in all variants. Overall, our study illustrates that the combined use of network analysis and shortest pathway techniques allow for predictive assessments of global flow communication in GAL-7. They also reveal Arg20, Arg22, and Asp103 as key residue modulators that control GAL-7 function via GBS communication. This study highlights potential predictive allosteric sites for improved design of functional modulators targeting GAL-7, in addition to illustrating the power of predictive dynamic residue network fingerprinting in protein engineering approaches.

3.3 Introduction

Human galectins (hGALs) are multifunctional proteins playing a critical role in the development of high fatality cancers (HFCs) (Dubé-Delarosbil et al., 2018). For decades, many studies have focused on biological, structural, and functional characterization of galectins in an attempt to design inhibitors for the treatment of HFCs. hGALs belong to a subfamily of animal lectins characterized by their conserved β-galactoside glycan binding site (GBS) within a carbohydrate recognition domain (CRD) of ~130-140 amino acid residues. 13 hGALs have been identified to date, subdivided into three groups according to their quaternary structure: tandem repeat (galectin-4, -8, -9, -12), chimera (galectin-3), and prototype (galectin-1, -2, -7, -10, -13, -14, -16, -17) (Varki et al., 2015). Tandem repeat galectins are formed by two different carbohydrate recognition domains (CRDs) covalently joined by a short peptide chain linker. Chimera-type galectin-3 exists in monomeric/oligomeric state and has a CRD covalently attached to a collagen-like N-terminus. In contrast, prototype galectins are structured by two identical CRDs

forming a non-covalent homodimer, except for GAL-13, whose protomers are stabilized by two disulfide bridges (Su et al., 2018).

Among prototype galectin, galectin-7 (GAL-7) plays dual roles as a pro-tumorigenic (breast, cervix, esophagus, gastric, lymph, oral skin, ovaries, and thyroid) (Campion et al., 2013; Demers et al., 2007, 2009, 2010; Grosset et al., 2016; Guo et al., 2017; Higareda-Almaraz et al., 2016; Kim et al., 2013; Labrie et al., 2014; Moisan et al., 2003; Park et al., 2009; Rorive et al., 2002; Schulz et al., 2017; Wang et al., 2020; Zhu et al., 2013; Zhu et al., 2010) and anti-tumorigenic (colon, prostate) protein (Kuwabara et al., 2002; Labrie et al., 2015; Ueda et al., 2004). It promotes or inhibits the progression of different types of cancers by regulating multiple cellular functions such as apoptosis, cell adhesion and migration, cell differentiation, and proliferation (Chen et al., 2018; Guo et al., 2017; Kuwabara et al., 2002; Labrie et al., 2014, 2015; Park et al., 2009; Truong et al., 2007; Villeneuve et al., 2011). These cellular functions are linked to GBS-dependent or -independent interactions with other protein partners. Indeed, expression of the cell migration factor MMP-9 can be induced by activating p38 MAPK, ERK1/2 pathways through interaction between extracellular GAL-7 and glycol-receptors, or through GBS independent interactions between intracellular GAL-7 and TCF-3 in the nucleus, leading to cancer aggressiveness (Chen et al., 2018; Guo et al., 2017; Park et al., 2009). Extracellular GAL-7 produced by cancer cells can induce apoptosis of activated Jurkat T cells through formation of a glycoprotein-galectin lattice at the surface of T cells via its GBS, facilitating cancer cell immune escape (Labrie et al., 2014). Conversely, intracellular GAL-7 can trigger the apoptosis of cervical cancer HeLa cells, of colorectal adenocarcinoma DLD-1 cells, and of prostate cancer DU-145 cells via the JNK pathway in a GBS-independent fashion (Kuwabara et al., 2002; Labrie et al., 2015). In addition, intracellular GAL-7 has GBS independent interactions with the anti-apoptotic BCL-2 regulator (Villeneuve et al., 2011). Besides, intracellular GAL-7 was demonstrated to upregulate keratinocyte proliferation and differentiation via direct interaction with JNK1, but it is unknow whether the GBS is involved in such interaction (Truong et al., 2007).

In recent years, the development of inhibitors and activity modulators targeting GAL-7 have almost exclusively focused on glycan-based molecules targeting GBS-dependent functions (Cumpstey et al., 2005; Masuyer et al., 2012; Salameh et al., 2006). However, carbohydrate-based small molecules that specifically target GAL-7 are difficult to synthesize due to the high degree of similarity between GBSs among galectin subfamily members. Moreover, GBS modulators cannot inhibit GBS-independent activities of GAL-7 (Kuwabara et al., 2002; Labrie et al., 2015). Therefore, the development of new approaches to design novel modulators targeting

both glycan-dependent and glycan-independent GAL-7 functions with high selectivity, low cytotoxicity, and good solubility will help the development of new HFC treatments.

In regards to selectivity and efficiency, allosteric modulation has shown significant advantages over traditional orthosteric modulation (Wenthur et al., 2014). In 2012, an allosteric inhibitor targeting the non GBS (F-face) of GAL-1 was shown to reduce lactose binding affinity at the GBS located on the opposite S-face (Dings et al., 2012). This perturbation prevented GAL-1 from binding to cell surface glycans, attenuating tumor angiogenesis in melanoma mouse models (Dings et al., 2013). Based on this successful study, we hypothesized that the same strategy could be applied to GAL-7 functional modulator design. This is also supported by previous observations suggesting the existence of long-range positive cooperativity of ligand binding in GAL-7 (Ermakova et al., 2013). Communication between the two distant GBSs is expected to be maintained by selected electrostatic interactions involving dimer interface residues within opposite protomers. These observations suggest the existence of allosteric communication between the two GAL-7 protomers, potentially controlled by homodimer interactions (Ermakova et al., 2013). As a result, targeting the dimer interface could be used as an efficient strategy to specifically alter the biological activities promoted by GAL-7 in the cell. In addition, perturbing homodimer interactions would also prevent galectin-glycoprotein cross-linking at the cell surface, further impeding signal transduction pathways (Boscher et al., 2011; Brewer, 2002; Sacchettini et al., 2001).

Although the conventional development of allosteric modulators typically proceeds by high-throughput screening (HTS), rational predictions using computational approaches have been concomitantly applied to improve allosteric site predictions (Chatzigoulas et al., 2021). We postulate that characterizing GAL-7 allosteric pathways that govern positive cooperativity across the GAL-7 dimer interface would significantly help identify potentially essential dynamic nodes amenable to functional modulation. In support of this hypothesis, we recently used a protein engineering approach to confirm that the GBS-dependent proapoptotic activity of GAL-7 on Jurkat T cells can be modulated by controlling homodimer strength (Pham et al., 2021). We designed a structurally predicted disulfide bridge at interface position Gly16 and efficiently used G16C and G16S variants as functional switches to control GAL-7 homodimer integrity and proapoptotic activity (Pham et al., 2021). We showed that perturbation of the hydrophobic core at the dimer interface can irreversibly alter the structure of GAL-7, and that interprotomer edges are involved in communication pathways between opposite GBSs. We also uncovered the first model of allosteric communication network across the dimer interface of GAL-7 and between opposite

protomers (Pham et al., 2021), further suggesting that the R20-D103 contact is essential to maintain long-range communication between the two GBSs. However, the molecular details governing these putative interprotomer allosteric contacts remain elusive, especially with respect to the importance of physicochemical requirements.

In the present work, we characterize perturbations induced in the network of electrostatic interactions that maintain the integrity of the R20-D103 interprotomer contact in GAL-7. We individually mutated electrostatic interactions for neighboring residues Asp103, Arg20, and Arg22, in addition to building the Arg20-Arg22 double mutant. Our results show that the R20A, R22A, D103A, and R20A-R22A variants negatively modulate the pro-apoptotic activity of GAL-7. Biophysical, structural and network analyses illustrate that these functional alterations could be due to the loss and reorganization of important interprotomer communication within variant residue networks, destabilization of homodimer interactions, perturbation of structural integrity, and reduction of global flow communication between the two distant GBSs. Overall, our results demonstrate that interface residues Arg20, Arg22, and especially Asp103 maintain key electrostatic interactions that modulate the pro-apoptotic activity of GAL-7.

3.4 Results and discussion

3.4.1 Asp103 acts as a key electrostatic node for maintaining interprotomer communication in GAL-7

In our previous GAL-7 study (Pham et al., 2021), we used a combination of predictive dynamical network analysis and shortest path methodology to uncover seven critical contacts (or critical edges) encompassing six residues involved in long-range allosteric interprotomer communication between the two glycan-binding sites (GBS): Val18, Arg20, Ile91, Val100, Asp103, and Phe135 (Figure 3.1A-C). Intercommunication between these interface residues is presumed to be essential for maintaining positive cooperativity between the two distant GBSs and to preserve optimal GAL-7 function (Ermakova et al., 2013). Our dynamical network analysis suggests that electrostatic residues Arg20 and Asp103 act as the two most important interface residues in GAL-7 interprotomer communication, linking the two distant GBSs through the following shortest path [i.e., residue (protomer unit)]: N62(A)-F61(A)-Y106(A)-A104(A)-D103(A)-R20(B)-V88(B)-F50(B)-H49(B) (Figure 3.1A). Since the physicochemical importance of residues governing this interprotomer communication remains elusive, the present work focuses on the role of electrostatic interactions governing the GAL-7 dimer interface (Figure 3.1C).

To investigate the effect of interprotomer perturbations at this critical R20-D103 node, we first performed a predictive computational dynamical network analysis of designed electrostatic single variants R20A, D103A, R22A, and double mutant R20A-R22A (Figure 3.2). Mutations to alanine abrogate WT electrostatic interactions between residues Arg20 and Asp103 (Figure 3.1C), significantly affecting the weight of the critical edge between these residues (Figure 3.3A). Arg22 is also in direct contact with Asp103 (Figure 3.1C), so the R22A mutation is also expected to alter the WT R20-D103 connection (Figure 3.3A). To compensate for the loss of a critical edge between residues Arg20 and Asp103, all variants increase connectivity between hydrophobic residues at the dimer interface core, primarily favoring the Val18-Ile91 critical edge (Figure 3.3A). In addition, the dynamical network of variant R20A establishes three new critical edges between protomers A and B to maintain the integrity of interprotomer communication: D103(A)-R22(B), K98(A)-T17(B), and G16(A)-I91(B) (Figure 3.3A). In contrast, no new critical edge is formed in the R22A variant, whereas the D103A network loses 70% of its critical edges between both protomers, i.e. D103(A)-R20(B), R20(A)-D103(B), F135(A)-V100(B), V100(A)-F135(B), and V18(A)-V18(B) (Figure 3.3A). Interestingly, the double mutant R20A-R22A mirrors the critical edges of the D103A variant network but gains two additional critical edges between protomers A and B: T17(A)-K98(B) and F135(A)-A104(B). Overall, these observations suggest that Asp103 is a crucial connector of interprotomer communication in GAL-7.

3.4.2 Perturbing electrostatic interactions at the dimer interface reduces the proapoptotic activity of GAL-7

GAL-7 is well known to induce apoptosis of human T cells by binding to their glycosylated receptors (Grosset et al., 2014; Labrie et al., 2014; López de los Santos et al., 2020; Pham et al., 2021; Vladoiu et al., 2015). To investigate the impact of dimer interface electrostatic interactions on GAL-7 function, Jurkat T cell apoptosis was carried out with WT GAL-7, single variants R20A, R22A, D103A, and double mutant R20A-R22A. Our results show that WT GAL-7 induces Jurkat T cell apoptosis with an EC50 of 7.2 μM (95% confidence interval [CI95%] between 6.5–8.2 μM) (Figure 3.1B). Albeit subtle, all electrostatic mutations decrease the proapoptotic activity of WT GAL-7, yielding an EC50 of 8.7 μM for R20A (CI95% 8.1 and 9.4 μM), 10.9 μM for R22A (CI95% 10.0–11.9 μM), and 11.6 μM for D103A (CI95% 10.0–13.3 μM) (Figure 3.1B). In contrast, the activity of the R20A-R22A double mutant is drastically reduced, dropping its relative pro-apoptotic function almost 4-fold relative to WT at 50 μM (Figure 3.5). This functional perturbation is likely attributed to reduced protein stability induced by the loss of two critical electrostatic interactions at the dimer interface. Indeed, R20A-R22A is the only variant that was found to exhibit clear

aggregation behavior during apoptosis assays, which likely reduces the concentration of properly folded and accessible R20A-R22A binding targets to glycosylated receptors. Accordingly, our circular dichroism experiments also showed decreased concentration of folded R20A-R22A in solution (Figure 3.7). Since only R20A-R22A undergoes observable changes in structural integrity, these results suggest that the decrease in proapoptotic activity for other variants (R20A, R22A, D103A) is likely caused by perturbations in interprotomer communication.

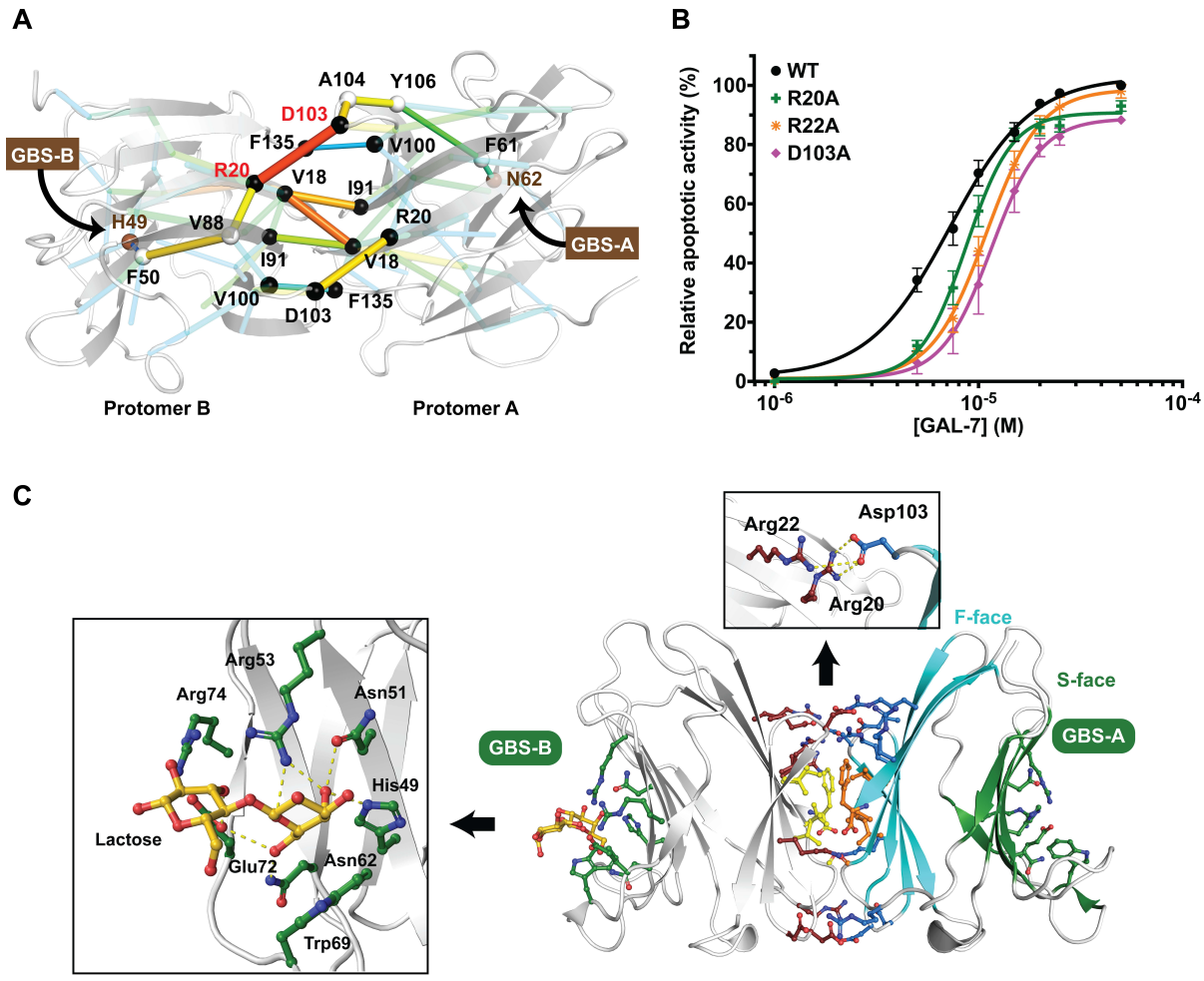

Figure 3.1 Perturbing interprotomer contacts negatively modulates the pro-apoptotic activity of GAL-7.

A, the residue network of WT GAL-7 highlights the shortest pathway between two opposite GBSs (N62-H49) and residues involved in interprotomer communication at the dimer interface (black spheres). GBS residues are represented by brown spheres. B, apoptotic activity of human Jurkat T cells induced by WT GAL-7 (black circles), R20A (green plus signs), R22A (orange asterisks), and D103A (violet diamonds) were assessed by positive Annexin V staining using flow cytometry analysis. C, overall structure of GAL-7. GAL-7 folds as jelly roll-type β-sheet fold composed of a S-face (green) and F-face (cyan). The back-to-back homodimer quaternary structure is stabilized by electrostatic interactions shielding a central hydrophobic core. Residues at the interface between protomer A (right) and B (left) are shown as ball-and-sticks representation using marine (protomer A) and brown (protomer B) coloring for electrostatic residues, and orange (protomer A) and yellow (protomer B) for hydrophobic residues. Top inset shows salt bridges between Arg20, Arg22, and Asp103 as yellow dashed lines (4 Å distance cut-off). GBS residues are shown as green ball-and-sticks representation in protomers A and B. Left inset shows molecular interactions between GBS residues and lactose (gold).

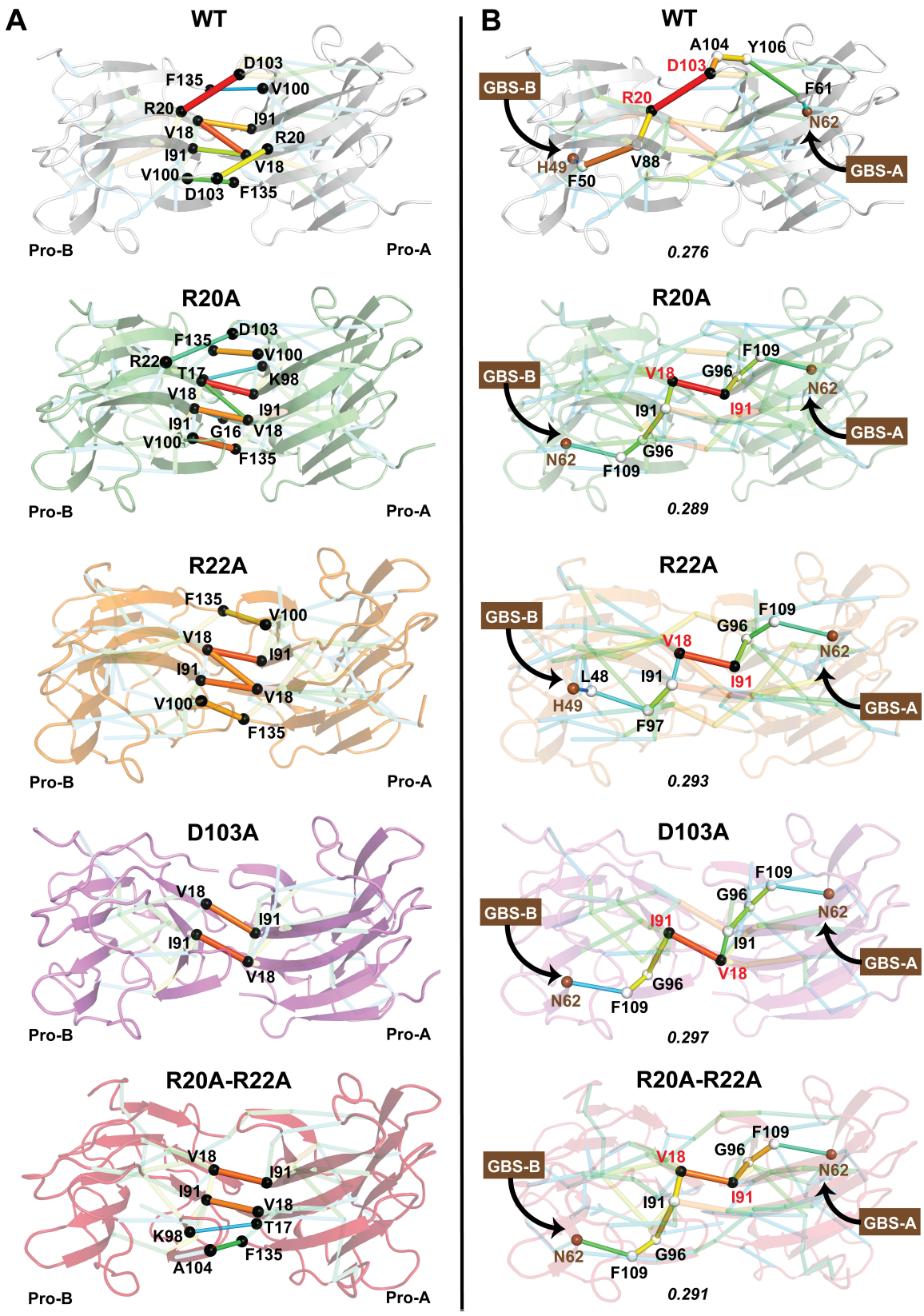

Figure 3.2 Dynamical network analysis of WT GAL-7 and variants R20A, R22A, D103A, and R20A-R22A.

A, critical interprotomer residue contacts at the dimer interface of WT GAL-7 (white, top), R20A (green, 2nd row), R22A (orange, 3rd row), D103A (violet, 4th row), and R20A-R22A (firebrick, bottom row), as defined by dynamical network analysis. Dimer interface residues are represented by black spheres and critical edges are represented by sticks. The importance of the critical edge is scaled by thickness and colored-ramped from blue to red. B, the shortest pathway between two opposite GBSs is highlighted for WT (connecting N62-A and H49-B), and variants R20A (connecting N62-A and N62-B), R22A (connecting N62-A and H49-B), D103A (connecting N62-A and N62-B), and R20A-R22B (connecting N62-A and N62-B). GBS residues are represented by brown spheres. Residues mutated in this study are shown as cyan spheres on structures in (A). Stars represent sites of mutations for each individual structure.

3.4.3 R20A, R22A, D103A, and R20A-R22A mutations perturb homodimer interactions and protein stability

Since Arg20, Arg22, and Asp103 are located at the dimer interface, we investigated the strength of dimer association and equilibrium induced by their replacement to alanine using microscale thermophoresis (MST). Our MST results indicate that all mutants induce homodimer destabilization in GAL-7, yielding a dimer equilibrium dissociation constant (K_D) of 1.1 μM for R20A (CI95% 0.6–2.4 μM) and 1.2 μM for R22A (CI95% 0.8–1.9 μM), relative to 0.06 μM (CI95% 0.03–0.11 μM) for WT GAL-7 (Figure 3.3 and Table 3.4). We were unable to reach binding saturation with variants D103A and R20A-R22A due to limitations in protein stability at higher concentrations, further demonstrating significant perturbations of homodimer interactions. Their respective K_D are therefore estimated to be higher than 10 μM for D103A and 100 μM for R20A-R22A (Figure 3.6 and Table 3.4). Altogether, these results illustrate that dimer association strength is weakened in all variants, especially for D103A and R20A-R22A.

We also monitored the overall fold of the GAL-7 variants in the presence and absence of lactose using CD spectropolarimetry. The far UV molar ellipticity spectra (200-250 nm) of all proteins is similar between WT GAL-7, R20A, and R22A, indicating minimal structural perturbations in these variants (Figure 3.7). In contrast, ellipticity is slightly perturbed for D103A and significantly affected in R20A-R22A (Figure 3.7A). Moreover, we observe high UV molar ellipticity variation between R20A-R22A measurements in presence of lactose (Figure 3.7B). These results suggest high heterogeneity of folded and partially unfolded R20A-R22A population in the stock sample. Since lactose was previously shown to stabilize GAL-7 structure (Ermakova et al., 2013; Pham et al., 2021), lactose binding may induce proper folding and/or further stabilize structural integrity of the folded R20A-R22A population, yielding a better ellipticity signal. In contrast, predominantly unfolded R20A-R22A might lose the ability to bind lactose, negatively affecting ellipticity. Since spectral measurements were carried out at the same concentration for all GAL-7 variants, these results suggest mild structural perturbation of the D103A variant and significant changes in structural integrity and dimer stability for variant R20A-R22A.

The effects of mutations on GAL-7 stability was further assessed by thermal denaturation experiments. CD melting curves show that all mutations weaken GAL-7 stability. Indeed, T_m values of variants R20A (T_m = 60.9 ± 0.1 °C), R22A (T_m = 59.4 ± 0.1 °C), D103A (T_m = 55.8 ± 0.1 °C), and R20A-R22A (T_m = 54.4 ± 0.6 °C) are respectively 6.9 °C, 8.4 °C, 12 °C, and 13.4 °C lower than that of WT (T_m = 67.8 ± 0.2 °C). In the presence of lactose, we observe an overall thermal stability increase of 2.7 °C for WT (T_m = 70.5 ± 0.1 °C), 3 °C for R20A (T_m = 63.9 ± 0.7 °C), 3.3 °C for R22A (T_m = 62.7 ± 0.2 °C), 3 °C for D103A (T_m = 58.8 ± 0.1 C), and 2.4 °C for R20A-R22A (T_m = 56.8 ± 0.5 °C) (Figure 3.3A and Table 3.3). These results illustrate that lactose binding is preserved in all electrostatic dimer interface variants, although this effect is less pronounced in R20A-R22A. This is also in agreement with our previous observation suggesting sample heterogeneity of R20A-R22A folded/unfolded populations in solution.

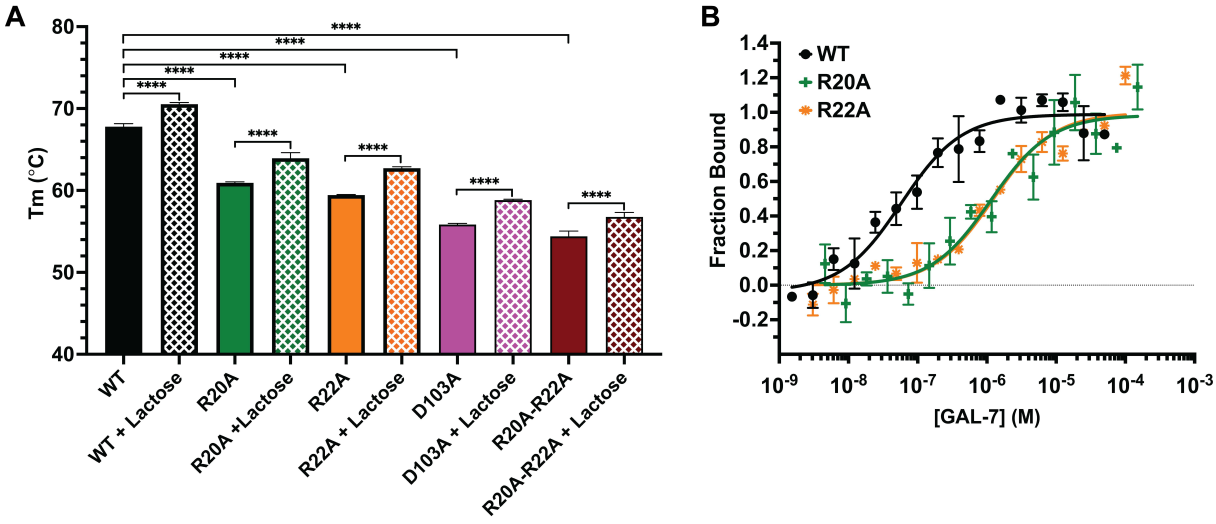

Figure 3.3 Perturbing R20, R22, and D103 electrostatic interactions destabilizes GAL-7 homodimer integrity.

A, thermal stability of WT GAL-7 (black) and variants R20A (green), R22A (orange), D103A (violet), and double mutant R20A-R22A (firebrick) in the absence (filled bars) and presence of lactose (pattern bars), as measured by CD-induced thermal denaturation. These values are statistically significant, with *p-value* ≤0.0001 (illustrated by four asterisks) evaluated by one-way ANOVA with Tukey post-hoc tests. B, homodimer equilibrium affinity of WT GAL-7 (black circles), variants R20A (green plus signs), and R22A (orange asterisks), as measured by MST.

3.4.4 R20A, R22A, D103A and R20A-R22A variants maintain GAL-7 dimer architecture in free and lactose-bound states

To investigate whether changes in proapoptotic activity is caused by significant molecular changes in GAL-7 variants, crystal structures of single variants R20A, R22A, D103 were solved in their apo and holo states (in complex with lactose), in addition to the apo structure of double mutant R20A-R22A (Supplementary data

Table 3.1). All mutants were solved at resolutions ranging from 1.95 to 3 Å and were found to maintain GAL-7 dimer architecture in their bound and free forms. Except for the apo structure of D103A (PDB 7N96), which crystallized in the $P12_11$ space group, apo structures of R20A (PDB 7N4O), R22A (PDB 7N6C), R20A-R22A (PDB 7N8G) and holo structures of R20A (PDB 7N57), R22A (PDB 7N8D), and D103A (PDB 7RDG) all crystallized in the $P2_12_12_1$ space group. Cα structural alignments between apo WT GAL-7 (PDB 3ZXF) and variants R20A (RMSD 7N4O vs 3ZXF = 0.486 Å), R22A (RMSD 7N6C vs 3ZXF = 0.470 Å), D103A (RMSD 7N96 vs 3ZXF = 0.637 Å), R20A-R22A (RMSD 7N8G vs 3ZXF = 0.472 Å), or between holo WT GAL-7 (PDB 6VTO) and variants R20A (RMSD 7N57 vs 6VTO = 0.295 Å), R22A (RMSD 7N8D vs 6VTO = 0.272 Å), D103A (RMSD 7RDG (A and B chain) vs 6VTO = 0.437 Å) all indicate minimal structural perturbation of the overall GAL-7 dimer architecture.

Since the proapoptotic activity of GAL-7 is directly linked to its ability to bind glycoreceptors at the GBS, we performed detailed structural comparison of the dimer interface and local GBS environment between holo WT GAL-7 and mutational variants. We observed significant changes in side chain orientations for residues located near and away from the site of mutation, inducing the reorganization of salt bridge interactions between the two opposite protomers in all variants (Figure 3.9, Figure 3.10, Figure 3.11 and Figure 3.12). Relative to holo WT, holo R20A, R22A, and D103A structures experience side chain reorientation of dimer interface residues Arg14, Asp94, or Asp95, which triggers formation of new interprotomer salt bridges between Arg14 and Asp94 (or Asp95) in point mutants R20A and R22A (Figure 3.9 and Figure 3.10). These new interactions may compensate for the loss of a dimer interface salt bridge induced by an alanine replacement, further contributing to the integrity of homodimer interactions in the variants. Moreover, we observe side chain reorganization of residues Glu87, Arg133, Asp103 in the R20A structure, Arg20, Glu87, Arg133, D103 in the R22A structure, and Arg20, Glu87, Arg133 in the D103A structure. While these changes induce formation of a new salt bridge between D103(A)-R133(B) in the R20A structure, no additional salt bridge interactions are observed at the dimer interface for R22A and D103A structures (Figure 3.9, Figure 3.11 and Figure 3.12). Since we were unable to crystalize a lactose-bound structure for double mutant R20A-R22A, we instead compared its apo structure to apo WT GAL-7. Similarly to other variants, this structural comparison shows side chain reorientation for Asp103, Arg133, and Glu87. As expected from alanine replacements, the WT salt-bridge network involving these residues is almost completely abrogated in apo R20A-R22A GAL-7, with only the R133(A)-D103(B) interaction remaining (Figure 3.12). Overall, these results support the weakening of homodimer affinity observed by MST, especially for variants D103A and R20A-R22A, as described above. Despite significant

electrostatic perturbations at the dimer interface, the R20A-R22A structure still maintains the prototypical GAL-7 dimer architecture, suggesting that the unperturbed hydrophobic core at the dimer interface plays a crucial role in dimer fold stability. However, variants experience greater exposure of their hydrophobic core to solvent due to weakening of the observed 'electrostatic shield' provided by top and bottom polar interactions at the dimer interface in WT (Figure 3.9, Figure 3.10, Figure 3.11 and Figure 3.12). This may certainly contribute to the aggregation behavior observed in all variants, especially for D103A and R20A-R22A, as illustrated above.

3.4.5 Perturbing interprotomer electrostatic interactions alters efficiency of global communication but does not affect lactose-binding affinity of point mutants

Consistent with the overall structural similarity between WT and variants, GBS residue orientation and lactose positioning also remain largely unperturbed between WT and single point mutants (Figure 3.13). Except for Arg71, the side chain conformation of all GBS residues is similar in all structures. Since Arg71 is positioned at the crystal contact interface, the high positional variability of its side chain could be caused by crystal packing artifacts. In accordance with this observation, lactose binding affinities (K_D) calculated for WT GAL-7 and point mutants using isothermal titration calorimetry (ITC) and MST are largely unaffected (Figure 3.8, Table 3.2 and Table 3.5). In contrast, we observed low binding to the lactose affinity column during purification of double mutant R20A-R22A. This is coupled to our inability to determine a robust lactose binding affinity with this variant due to protein aggregation at high concentrations required for ITC, in addition to high MST signal variability caused by heterogeneity of folded/unfolded equilibrium in the sample. Moreover, crystallization of 0.5 mM R20A-R22A saturated with 150 mM lactose did not show the presence of lactose in the GBS. These results illustrate that lactose binding affinity is significantly perturbed in variant R20A-R22A.

We further investigated whether perturbing interprotomer communication has an impact on communication between the two distant GBSs. Using the solved apo state crystal structures of variants R20A, R22A, D103A, and R20A-R22A, we performed a combination of dynamical network and shortest path analysis, as described previously (Barbeau et al., 2017; Pham et al., 2021). The shortest pathways connecting both opposite GBSs in apo structures is N62(A)-F61(A)-Y106(A)-A104(A)-D103(A)-R20(B)-V88(B)-F50(B)-H49(B) in WT, N62(A)-F109(A)-G96(A)-I91(A)-V18(B)-I91(B)-F97(B)-L48(B)-H49(B) in R22A, N62(A)-F109(A)-G96(A)-I91(A)-V18(A)-I91(B)-G96(B)-F109(B)-N62(B) in D103A, and N62(A)-F109(A)-G96(A)-I91(A)-V18(B)-I91(B)-G96(B)-F109(B)-N62(B) in both R20A and R20A-R22A variants (Figure 3.2B). As expected, the

shortest pathway is altered in all GAL-7 variants due to the loss of the Arg20-Asp103 interprotomer critical edge found in WT. However, terminal GBS residues Asn62 and His49 are conserved in all shortest pathways, suggesting that they play an important role in positive cooperativity. In addition, the shortest pathway weight scores are slightly increased in all variants, with values of 0.289 for R20A, 0.293 for R22A, 0.297 for D103, and 0.291 for R20A-R22A, relative to 0.276 in WT. Since lower weight values describe higher allosteric communication efficiency, these results suggest that altering the shortest path residue identity connecting both GBSs also reduces allosteric communication efficiency in GAL-7 variants.

The GBS pocket of GAL-7 is formed by a complex array of hydrogen bonding network and electrostatic interactions involving residues Arg31, His33, His49, Asn51, Arg53, Glu58, Val60, Arg62, Ser63, Lys64, Trp69, Arg71, Glu72, Glu73, and Arg74. To investigate how the perturbation of electrostatic interactions between Arg20, Arg22, and Asp103 at the dimer interface influences the global flow of communication between the two GBSs, we extracted all pathways connecting GBS residues on opposite protomers and calculated their respective weight score. From these values, we established a pathway score matrix of 225 couplings (15 GBSs residues in protomer A x 15 GBSs residues in protomer B), allowing visualization of the global communication network between the two opposite GBSs (Figure 3.4A). The lower the weight score, the higher the efficiency of communication between two coupling residues. To evaluate the effect of mutation on global communication, the value of each GBS residue pair coupling in a variant network was subtracted to the value of the same residue pair in the WT network to generate a difference matrix. Positive or negative results respectively indicate a decrease or increase in communication efficiency between two opposite GBSs in the variant relative to WT (Figure 3.4B). Our results show both increases and decreases in weight scores for different residue couplings, illustrating that GBS communication shifts from one coupling to another in response to dimer interface mutation. For instance, we observe that GBS communication generally increases relative to WT (red rows and columns in Figure 3.4B) for couplings involving terminal residues (A)-33, (A)-49, (A)-64, (B)-62, (B)-71 in R20A; (A)-33, (A)-49, (A)-64, (B)-62, (B)-63, (B)-71 in R22A; (B)-62, (B)-63, (B)-71 in D103A; and (A)-33, (A)-49, (A)-63, (A)-64, (B)-62, (B)-71 in R20A and R20A-R22A. However, most mutant network couplings exhibit higher weight scores (particularly in D103A) than in WT networks (blue rows and columns in Figure 3.4B). Accordingly, statistical analysis indicates that the average score of all 225 couplings in all mutant networks is significantly higher than in WT, suggesting an overall decrease in GBS global communication efficiency in all variants. Moreover, among 49 couplings between GBS residues forming direct interactions with lactose, few couplings show decreases in their weight score (i.e. increased efficiency). These include

seven residue pairs in R20A ((A)-49-(B)-62, (A)-49-(B)-72, (A)-49-(B)-74, (A)-62-(B)-49, (A)-62-(B)-62, (A)-69-(B)-62, (A)-69-(B)-72), 5 in R22A ((A)-49-(B)-62, (A)-49-(B)-72, (A)-49-(B)-74, (A)-62-(B)-62, (A)-69-(B)-62), 3 in D103A ((A)-51-(B)-62, (A)-53-(B)-62, (A)-62-(B)-62), and 7 in R20A-R22A ((A)-49-(B)-62, (A)-49-(B)-69, (A)-49-(B)-72, (A)-49-(B)-74, (A)-62-(B)-62, (A)-62-(B)-62, (A)-69-(B)-62) (Figure 3.4B). Within these last couplings, almost all involve residues Asn62 or His49, confirming their importance as key GBS positions to maintain allosteric communication between the two opposite binding sites. Overall, these results suggest that the perturbation of interprotomer communication alters the global communication between the two opposite GBSs in GAL-7.

3.5 Conclusion

We previously uncovered and characterized an allosteric network that may be essential for modulating the biological function of GAL-7 in the cell (Pham et al., 2021), further suggesting that the Arg20-Asp103 contact is crucial to maintain allosteric communication between protomers. In the present work, we demonstrated that altering electrostatic interactions between Asp103 and its neighbors Arg20 or Arg22 at the dimer interface negatively modulate the pro-apoptotic activity of GAL-7. Functional GAL-7 activity perturbation caused by mutations R20A, R22A, D103A, and R20A-R22A are caused by weakening of protomer-protomer interactions and lower protein stability, in addition to reorganization of interprotomer communication. Except for variant R20A, which shows reorganization in different communication contacts at the interface, other variants exhibit loss of at least two critical contacts between A(B)-20 and B(A)-103. Remarkably, point mutation D103A alone induces a loss of 70% interprotomer contacts at the dimer interface, suggesting that D103A could be the most important residue to maintain allosteric communication between the two GAL-7 protomers.

Our ligand binding experiments and crystallization of holo structures show no significant change in lactose binding affinity and ligand positioning in single mutants, while double mutant R20A-R22A might reduce lactose binding affinity. However, it remains unclear whether this effect is caused by heterogeneity of unfolded vs. folded R20A-R22A population in solution and/or intrinsic physicochemical properties of this mutant. Since lactose is a simplified *in vitro* model ligand of GAL-7, it is not surprising that these binding results do not reflect the negative modulation observed in pro-apoptotic assays with the same variants. Further investigation is required to evaluate the binding affinity of GAL-7 to biologically relevant partners and the downstream effects of this interaction to the pro-apoptotic activity. Shortest path analyses connecting GBS residues

between two opposite protomers nevertheless suggest a decrease in the efficiency of global communication between the two GBSs in all variants, supporting the observed decline in pro-apoptotic activity. Our global communication results also suggest that Asn62 and His49 are the most important GBS residues preserving the integrity of GBS communication in GAL-7.

Overall, we identified dimer interface residues Arg20, Arg22, and Asp103 as potential sites for modulating positive ligand cooperativity and pro-apoptotic activity in GAL-7. Our proof-of-concept demonstrates that a comprehensive network analysis and shortest pathway analysis provides relevant measures to predict potential sites of communication breakdown between two protomers, resulting in perturbation of protein function. Cross-linking glycoreceptors by galectins on the cell surface is known to regulate multiple cellular processes (cell adhesion, migration, apoptosis, proliferation, and differentiation) that favor the formation of a tumor micro-environment (Boscher et al., 2011; Brewer, 2002; Sacchettini et al., 2001). As a result, these computational analyses represent a promising approach to predict residue positions that may be essential for non-covalent dimer association within galectins, which may help prevent the cross-linking of galectin-glycoprotein matrices in cancer treatment. Given that galectins can also form heterodimers exerting a synergistic effect on cellular functions (Dings et al., 2021; Miller et al., 2018), this approach may not be limited to the perturbation of protypical galectin homodimers but also be applicable to heterodimer formation. However, the success of this approach will clearly rely on identification of dimer interface between heteroprotomers using structural methodologies and predictions.

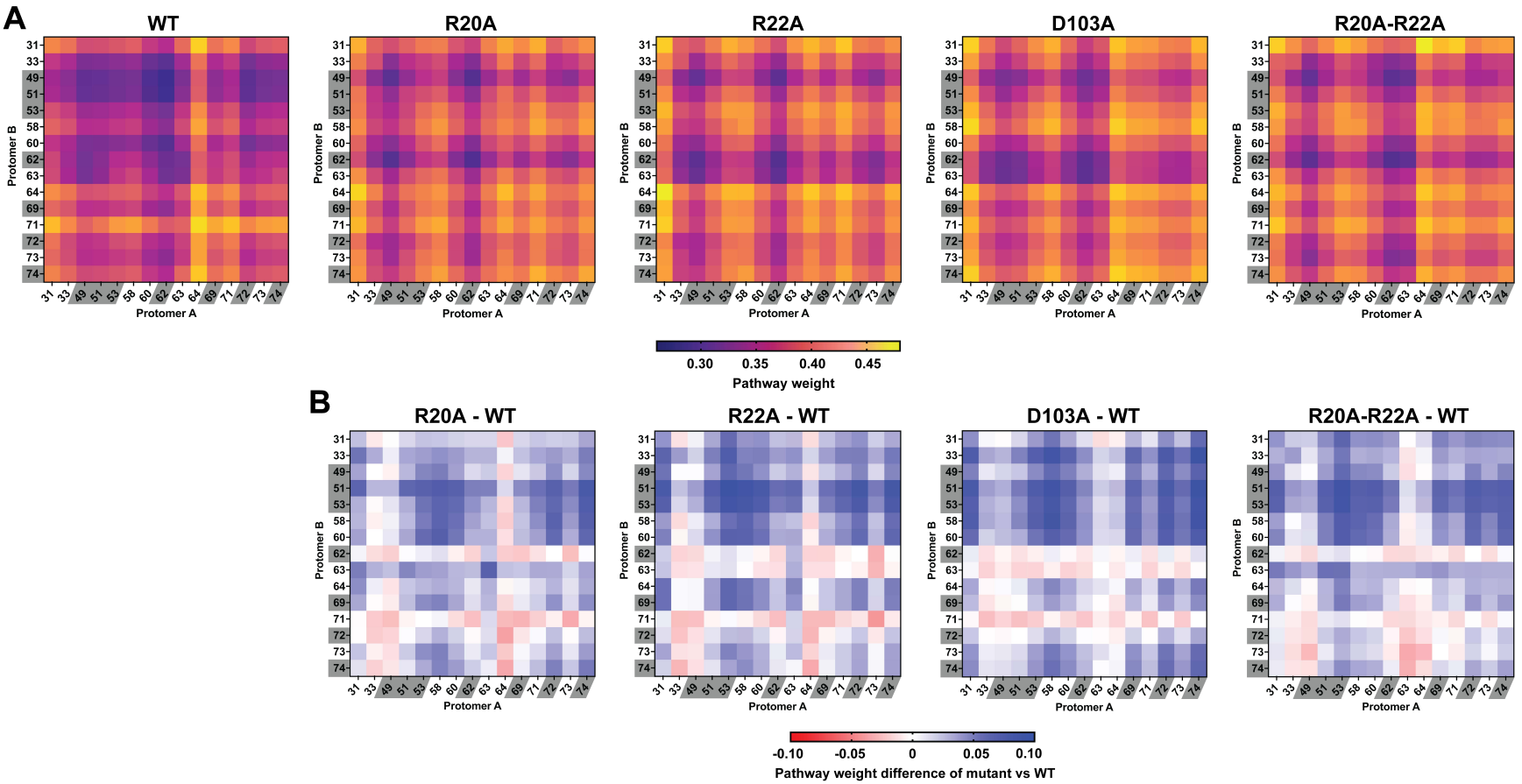

Figure 3.4 GBS global flow analysis of WT GAL-7 and variants R20A, R22A, D103A, and R20A-R22A.

A. Matrix representation of the shortest pathway value connecting all GBS residues between two protomers in WT and variants R20A, R22A, D103A, and R20A-R22A. Pathway weight values are scaled by color from purple to yellow. The lower the weight (purple), the higher the efficiency of communication between GBS pair residues. B. Weight differences between mutant and WT matrices. Pathway weight difference values are scaled by color from red to blue. Positive (blue) or negative (red) results respectively indicate a decrease or increase in communication efficiency between two opposite GBS in the mutant relative to WT. Residues involved in direct interactions with lactose are highlighted in gray boxes.

3.6 Experimental procedures

3.6.1 Site-directed mutagenesis and protein expression

The pET-22b(+) vector encoding for recombinant human galectin-7 (WT GAL-7) was described in a previous study (Pham et al., 2021). R22A and D103A mutants were generated with the Q5® Site-Directed Mutagenesis Kit (NEB) using the forward (R22Af: 5'-gctgagaattgccggcttggttc-3'; D103Af: 5'-gtggttggggccgcccagtacc-3') and reverse (R22Ar: 5'-accgtgccagggcggatg-3'; D103Ar: 5'-ggccttgaagccgtcgtctgacg-3') primers. R20A and R20A-R22A mutants were generated by the QuikChange site-directed mutagenesis method with iProof High-Fidelity DNA Polymerase kit (BioRad) using the forward (R20Af: 5'-cctggcacggtgctggcaattcgcggcttgg-3'; R20A-R22Af: 5'-cacggtgctggcaattgccggcttggttcctcccaatg-3') and reverse (R20Ar: 5'-cattgggaggaaccaagccggcaattctcagcaccgtg-3'; R20A-R22Ar: 5'-cattgggaggaaccaagccggcaattgccagcaccgtg-3') primers. All plasmid constructs were confirmed by DNA sequencing prior to protein expression. Recombinant WT GAL-7 and variants were expressed in *Escherichia coli* BL21(DE3) and purified by lactose affinity gravity-flow purification at 4°C, as previously described (Pham et al., 2021).

3.6.2 Apoptosis assays with Annexin V/PI staining.

Purified proteins were prepared in PBS solution (0.144 g/L KH_2PO_4, 0.795 g/L NaH_2PO_4, 9 g/L NaCl, pH 7.4) for WT GAL-7, R20A, R22A, and D103A or in buffer A (50 mM Tris pH 8.0, 150 mM NaCl) for WT GAL-7 and R20A-R22A. All apoptosis assays were performed as previously described (Pham et al., 2021).

3.6.3 Biophysical characterisation.

Isothermal Titration Calorimetry (ITC), Circular Dichroism (CD), and thermal unfolding experiments were performed as previously described (Pham et al., 2021). Homodimer K_D determination was performed by microscale thermophoresis (MST), as follows. WT GAL-7, R20A, R22A, D103A, and R20A-R22A were labeled with Cy5 or AlexaFluo647 in accordance with the protocols, as previously described (Pham et al., 2021). Each binding assay experiment consisted of 16 2-fold serial dilutions of 50 µM, 150 µM, 100 µM, 326.5 µM, and 189.5 µM (starting concentration) of unlabeled WT GAL-7, R20A, R22A, D103A, or R20A-R22A. Unlabeled samples were then prepared in 5 nM labeled GAL-7. Depending on the protein stability of each GAL-7 variant, each sample was incubated at a specific time and temperature to avoid aggregation and

adsorption during experiments. WT and R20A samples were incubated at 40°C in a water bath for 45 min while R22A samples were incubated at room temperature for 30 min. No incubation was performed for D103A and R20A-R22A. After incubation, all samples were loaded into a NT.115 MST standard coated capillary and thermophoresis was measured using the Monolith NT.115 Pico instrument (NanoTemper Technologies GmbH). MST was induced by a 21s infrared laser (IR-laser) activation at room temperature. All experiments were performed in triplicate. Data analysis and K_D calculation were processed as previously described (Pham et al., 2021). Lactose binding assays were also performed by MST using 16 2-fold serial dilutions of 50 µM and 100 µM of lactose (starting concentrations) prepared in 5 nM labeled WT GAL-7 and 10 nM labeled D103A, respectively. MST measurements and analysis was carried out as described above.

3.6.4 Statistical analysis.

All experiments were carried out in triplicate. The mean and standard error of the mean (SEM) of all measured results were plotted using GraphPad Prism 9.0 (GraphPad Software, San Diego, CA). Statistical significance was evaluated with F-test (cell assays, ITC, and MST experiments), one-way ANOVA with Tukey post-hoc tests (CD experiments), or one-tailed paired Student's *t*-test (comparison of GBS coupling between WT and variants). The difference between two data sets was considered statistically significant if the *p-value* ≤ 0.05.

3.6.5 Protein crystallization.

- *Apo GAL-7 (R20A)*

1 µl of 7.5 mg/ml GAL-7 (R20A) solution of 20 mM Tris pH 8.0, 150 mM NaCl (buffer A) was mixed at 1:1 ratio with a solution of 0.1 M NaCl, 0.1 M Tris pH 8.0, 20 % w/v PEG 6000, 20 % v/v glycerol. Crystals were obtained by the sitting-drop vapor diffusion technique at room temperature after one week.

- *Apo GAL-7 (R22A)*

1 µl of 7.5 mg/ml GAL-7 (R22A) solution (in buffer A) was mixed at 1:1 ratio with 0.1 M NaCl, 0.1 M Tris pH 8.0, 20 % w/v PEG 6000, 17.5 % v/v glycerol. Crystals were obtained by the sitting-drop vapor diffusion technique at room temperature after one week.

- *Apo GAL-7 (D103A)*

1 µl of 7.5 mg/ml GAL-7 (D103A) solution (in buffer A) was mixed at 1:1 ratio with 0.1 M NaCl, 0.1 M Tris pH 8.0, 20 % w/v PEG 6000, 15 % v/v glycerol. Crystals were obtained by the sitting-drop vapor diffusion technique at room temperature after one week. Crystals were cryo-protected by soaking in a solution of 0.1 M NaCl, 0.1 M Tris pH 8.0, 20 % w/v PEG 6000, 30 % v/v glycerol.

- *Apo GAL-7 (R20A-R22A)*

1 µl of 7.5 mg/ml GAL-7 (R20A-R22A) solution in buffer of 20 mM Tris pH 8.0, 150 mM NaCl, 150 mM lactose was mixed at 1:1 ratio with 0.1 M NaCl, 0.1 M Tris pH 8.0, 20 % w/v PEG 6000, 17.5 % v/v glycerol. Crystals were obtained by the sitting-drop vapor diffusion technique at room temperature after one week. Crystals were cryo-protected by soaking in a solution of 0.1 M NaCl, 0.1 M Tris pH 8.0, 20 % w/v PEG 6000, 30 % v/v glycerol. Since lactose did not bind and crystallize to this variant, we considered it an apo structure.

- *Lactose-bound GAL-7 (R20A)*

Co-crystallization of GAL-7 (R20A) with α-lactose was performed using the sitting-drop vapor diffusion technique. Crystals were obtained by incubating a drop consisting of a 1:1 mixture of 1 µl of 7.5 mg/ml GAL-7 (R20A) solution (50 mM Tris pH 8.0, 150 mM NaCl, 7.5 mM α-lactose) with 0.2 M NaCl, 0.1 M Tris pH 8.0, 20 % w/v PEG 6000, 17.5 % v/v glycerol at room temperature after one week. Crystals were cryo-protected by soaking in paratone.

- *Lactose-bound GAL-7 (R22A)*

Co-crystallization of GAL-7 (R22A) with α-lactose was performed using the sitting-drop vapor diffusion technique. Crystals were obtained by incubating a drop consisting of a 1:1 mixture of 1 µl of 7.5 mg/ml GAL-7 (R22A) solution (50 mM Tris pH 8.0, 150 mM NaCl, 7.5 mM α-lactose) with 0.1 M NaCl, 0.1 M Tris pH 8.0, 20 % w/v PEG 6000, 17.5 % v/v glycerol at room temperature after one week.

- *Lactose-bound GAL-7 (D103A)*

Co-crystallization of GAL-7 (D103A) with α-lactose was performed using the hanging-drop vapor diffusion technique. Crystals were obtained by incubating a drop consisting of a 1:1 mixture of 1 µl of 7.5 mg/ml GAL-7 (D103A) solution (50 mM Tris pH 8.0, 150 mM NaCl, 150 mM α-

lactose) with 0.1 M NaCl, 0.1 M Tris pH 7.3, 0.1 M NaCl, 18% v/v P400, 26% w/v PEG 3350 at room temperature after two weeks.

3.6.6 Data collection, structure resolution, and refinement

All diffraction data of crystals was collected at the Canadian Macromolecular Crystallography Facility Beamline CMCF-BM of the Canadian Light Source Synchrotron (Fodje et al., 2014; Grochulski et al., 2011). Raw data was immediately processed on the MxLive platform after collection. Phase calculation was determined by a molecular replacement method using 1BKZ and 4GAL PDB structures as models for apo and holo structures, respectively. Structure resolution and refinement were carried out using the PHENIX software suite, version 1.19.2. All structural comparisons and visualizations were performed with the Open-Source PyMOL Molecular Graphics System, Version 2.4 (Schrödinger, LLC).

3.6.7 Molecular dynamics simulations

Molecular dynamics (MD) simulations were performed for the apo structures of WT GAL-7, variants R20A, R22A, D103A, and R20A-R22A, as previously described (Pham et al., 2021). Briefly, systems were built using CHARMM-GUI (Jo et al., 2008; Lee et al., 2016) and structural coordinates from PDB 4GAL (Leonidas et al., 1998). Mutations were introduced using the CHARMM-GUI tools. MD simulations were performed with NAMD 2.14 (Phillips et al., 2020) using the CHARMM36m force field parameters for proteins (Huang et al., 2017) and TIP3P waters (Price et al., 2004). Simulations were carried out at 303.15 K under isothermal-isobaric (NPT) ensemble conditions with a 2-fs time step and periodic boundary conditions. Langevin damping with a coefficient of 1 ps^{-1} was used to maintain constant temperature, while pressure was controlled by a Nosé–Hoover Langevin piston at 1 atm. Bond length between hydrogen and heavy atoms was constrained using SETTLE (Miyamoto et al., 1992) for water molecules and SHAKE (Ryckaert et al., 1977) for all other molecules. Cutoffs for the short-range electrostatics and the Lennard–Jones interactions were set at 12 Å, with the latter smoothed via a switching function over the range of 10-12 Å. Long-range electrostatic interactions were calculated with the Particle Mesh Ewald (PME) method (Darden et al., 1993; Essmann et al., 1995) using a sixth order interpolation and a grid spacing of ≈1 Å at every integration step. Nonbonded pair lists were updated at every ten steps, and coordinates were saved every 10 ps for analysis. For each system, three 1500-ns trajectories were recorded.

3.6.8 Trajectory analysis

The analysis of the trajectories was performed as described in a previous study (Pham et al., 2021). To summarize, for each system, the last 1000 ns of each of the three trajectories was concatenated into a single trajectory, at a rate of five frames every ns, for a total of 15,000 frames per trajectory. In these concatenated trajectories, proteins were aligned on the initial structure. The interface binding energies of the respective dimers were evaluated using the AnalyseComplex command from FoldX (Schymkowitz et al., 2005). This analysis was conducted on 1500 frames from the respective concatenated trajectories. For surface areas, final values were calculated using ten block averages over the trajectories and errors were calculated as standard deviations.

3.6.9 Allosteric analysis

The detailed methodology for the protein dynamical network analysis is presented in previous works (Barbeau et al., 2017; Pham et al., 2021). In short, for each system, the nodes of the network were represented by the residue heavy atom center of mass. The edges that transfer allosteric information between the nodes were drawn between the neighboring residues that maintained any of its heavy atoms within a distance of 4.5 Å for at least 75% of the time in the trajectories. The weight of the edges between the nodes was defined as the coefficient of variation of the distance between the nodes. NetworkX (Hagberg et al., 2008) was used to calculate the edge betweenness centralities using the Ulrik-Brandes algorithm (Brandes, 2001). All edges were ranked based on their betweenness centrality, the critical edges identified as edges with a prevalence of being part of an optimal path between any two nodes of at least three standard deviations (3σ) from the edge prevalence distribution.

3.7 Data availability

X-ray coordinates for apo GAL-7 variants R20A, R22A, D103A, R20A-R22A, and holo GAL-7 variants R20A, R22A, D103A in complex with lactose were deposited in the RCSB PDB under accession codes 7N4O, 7N6C, 7N96, 7N8G, 7N57, 7N8D, and 7RDG, respectively.

3.8 Acknowledgements

The authors thank Pr. Philippe Constant (INRS), Philippe Egesborg (INRS), Jacinthe Gagnon (INRS) and CMCF staff for technical assistance. Part of this research was also performed using beamlines CMCF-ID and CMCF-BM at the Canadian Light Source, a national research

facility of the University of Saskatchewan, which is supported by NSERC, the Canada Foundation for Innovation (CFI), the National Research Council (NRC), the Canadian Institutes of Health Research (CIHR), the Government of Saskatchewan, and the University of Saskatchewan. All computations were performed on the Helios supercomputer at Université Laval, which is managed by Calcul Québec and Compute Canada. Operation of this supercomputer is funded by the CFI, the ministère de l ’Économie et de l’Innovation du Québec (MEI), and the Fonds de recherche du Québec–Nature et technologies (FRQNT).

3.9 Author contributions

Conceptualization and design, N.T.H.P., M.L., P.L., and N.D.; cloning, expression, purification, and biophysical characterization (CD, MST, ITC), N.T.H.P. and M.L.; apoptosis assays, M.F. and Y.S.P.; X-ray crystallization and structural analysis, N.T.H.P., C.C., P.L. and N.D.; MD simulations and analysis, A.P. and P.L.; allosteric analysis, N.T.H.P., A.P., and P.L.; formal analysis, N.T.H.P., M.L., A.P., P.L., and N.D.; writing-original draft, N.T.H.P., M.L., A.P, P.L. and N.D.; writing-review and edit, all authors; supervision and funding acquisition, C.C., Y.S.P., P.L., D.C., N.D.

3.10 Funding

This work was supported in part by the National Institute of General Medical Sciences (NIGMS) of the NIH (under Award R01GM105978, to N. D.) and the Natural Sciences and Engineering Research Council of Canada (NSERC) (Discovery Grants RGPIN 2016-05557 to N. D. and RGPIN-2017-06091 to C. C.). N. T. H. P. was the recipient of a Doctoral Training scholarship from the Fonds de Recherche du Québec–Santé (FRQS) (287239) and a graduate student scholarship from PROTEO. A.P. was the recipient of a summer undergraduate summer studentship from PROTEO and a master’s scholarship awards from the Fondation Armand-Frappier. C. C. holds a FRQS Research Scholar Junior 1 Career Award (251848), and N.D. holds a FRQS Research Scholar Senior Career Award (281993). The content is solely the responsibility of the authors and does not necessarily represent the official views of the National Institutes of Health. Conflict of interest—The authors declare that they have no conflicts of interest with the contents of this article.

3.11 Abbreviations

The abbreviations used are: CRD, carbohydrate recognition domain; GAL-7, galectin-7; GBS, glycan-binding site.

3.12 Supplementary data

Table 3.1 Data collection and refinement statistics of R20A, R22A, D103A, and R20A-R22A crystal structures

	Apo GAL-7 R20A	*GAL-7 R20A - Lactose*	*Apo GAL-7 R22A*	*GAL-7 R22A - Lactose*	*Apo GAL-7 D103A*	*GAL-7 D103A - Lactose*	*Apo GAL-7 R20A-R22A*
PDB ID	**7N40**	**7N57**	**7N6C**	**7N8D**	**7N96**	**7RDG**	**7N8G**
Data collection[a]							
Space group	$P\ 2_12_12_1$	$P\ 2_12_12_1$	$P\ 2_12_12_1$	$P\ 2_12_12_1$	$P\ 2_12_12_1$	$P\ 12_11$	$P\ 2_12_12_1$
Cell dimensions							
a, b, c (Å)	53.43 64.64 71.81	30.22 76.19 111.19	53.35 64.89 71.9	30.53 77.62 111.95	53.51 67.11 68.01	30.33 112.28 77.04	53.24 64.96 72.16
α, β, γ (°)	90, 90, 90	90, 90, 90	90, 90, 90	90, 90, 90	90, 90, 90	90 91.085 90	90, 90, 90
Resolution (Å)	41.19 - 2.05 (2.12 - 2.05)	44.91 - 1.83 (1.90 - 1.83)	48.17 - 2.1 (2.18 - 2.1)	31.89 - 2.49 (2.58 - 2.49)	47.77 - 2.38 (2.47 - 2.38)	38.51 - 3.0 (3.11 - 3.0)	48.28 - 1.95 (2.02 - 1.95)
R_{merge}	0.11 (1.18)	0.15 (0.38)	0.12 (1.07)	0.07 (0.19)	0.15 (1.52)	0.07 (0.16)	0.07 (0.23)
$I/\sigma I$	16.1 (1.9)	8.1 (4.5)	13.58 (2.31)	22.2 (11.4)	13.74 (1.89)	12.81 (7.31)	22.58 (9.98)
$CC_{1/2}$	0.999 (0.636)	0.984 (0.936)	0.998 (0.758)	0.998 (0.99)	0.998 (0.719)	0.993 (0.978)	0.998 (0.986)
*CC**	1 (0.882)	0.996 (0.983)	1 (0.929)	1 (0.998)	0.999 (0.914)	0.998 (0.994)	0.999 (0.997)
Completeness (%)	100 (100.00)	99.9 (99.9)	100 (99.9)	99.6 (100)	99.8 (99.8)	98.7 (98.2)	99.4 (98.7)
Redundancy	7.2 (7.3)	6.9 (7.2)	10.1 (10.2)	8.9 (9.6)	9.6 (9.8)	3.2 (3.2)	9.7 (9.9)
Refinement							
Resolution (Å)	2.05	1.83	2.1	2.49	2.38	3	1.95
No. reflections	16151 (1573)	23497 (2324)	15102 (1459)	9850 (966)	10282 (1003)	10242 (1022)	18712 (1790)
R_{work} / R_{free}	0.185/0.252	0.171/0.208	0.197/0.235	0.242/0.281	0.218/0.259	0.204/0.268	0.167/0.204
No. of (non-hydrogen) atoms	2333	2382	2303	2321	2190	4372	2458
Protein	2162	2131	2133	2099	2108	4178	2153
Ligand/ion	66	133	129	98	42	210	120
Water	143	187	117	172	64	90	255
B factors	38.65	26.12	43.82	25.35	47.64	37.17	28.03
Protein	38.17	24.77	43.45	24.98	47.71	37.28	26.52
Ligand/ion	51.02	44.28	61.27	27.12	54.25	35.92	47.48
Water	43.40	35.30	42.69	29.38	43.45	33.59	36.94
r.m.s. deviations							
Bond lengths (Å)	0.006	0.012	0.005	0.011	0.006	0.016	0.008
Bond angles (°)	1.16	1.51	1.08	1.34	1.21	1.89	1.35

(a) Statistics for the highest-resolution shell are shown in parentheses

Table 3.2 Thermodynamic properties of α-lactose binding to WT GAL-7 and R20A, R22A variants.

	α-lactose		
	WT	**R20A**	**R22A**
K_D (μM)	135.3 ± 1.2	162.7 ± 10.7	145.7 ± 3.2
N	0.93 ± 0.03	0.81 ± 0.01	0.76 ± 0.07
Δ*H* (kJ/mol)	-22.8 ± 0.1	-20.8 ± 0.4	-21.6 ± 2.9
Δ*S* (J/mol·K)	-0.7 ± 3.2	2.6 ± 0.8	0.9 ± 10

Table 3.3 Melting temperature of GAL-7 variants in presence and absence of α-lactose

	Without Lactose (°C)	With Lactose (°C)
WT	67.8 ± 0.2	70.5 ± 0.1
R20A	60.9 ± 0.01	63.9 ± 0.4
R22A	59.4 ± 0.1	62.7 ± 0.1
D103A	55.8 ± 0.1	58.8 ± 0.1
R20A-R22A	54.4 ± 0.4	56.8 ± 0.3

Table 3.4 Homodimer dissociation constants (K_D)

	Dissociation Constant (μM)	95% Confidence Interval
WT	0.06	0.03-0.12
R20A	1.14	0.55–2.35
R22A	1.20	0.79–1.94
D103A	> 10	N.A
R20A-R22A	> 100	N.A

Table 3.5 Binding affinity of α-lactose to WT GAL-7 and variant D103A, as measured by MST

	K_D (μM)	95% Confidence Interval
WT	540	358 - 806
D103A	748	516 - 1079

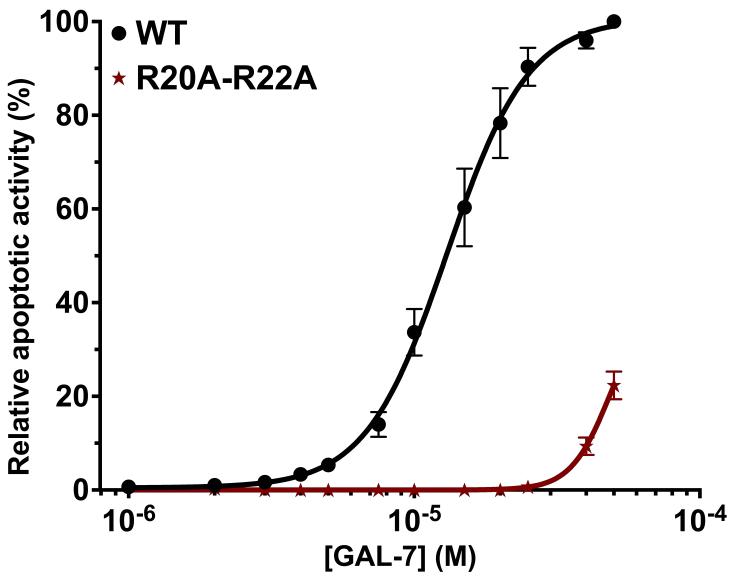

Figure 3.5 Pro-apoptotic activity of human Jurkat T cells induced by GAL-7 double mutant R20A-R22A

Activity of WT GAL-7 (black circles) and double mutant R20A-R22A (firebrick stars) was assessed by positive Annexin V staining using flow cytometry analysis (see Materials & Methods for details).

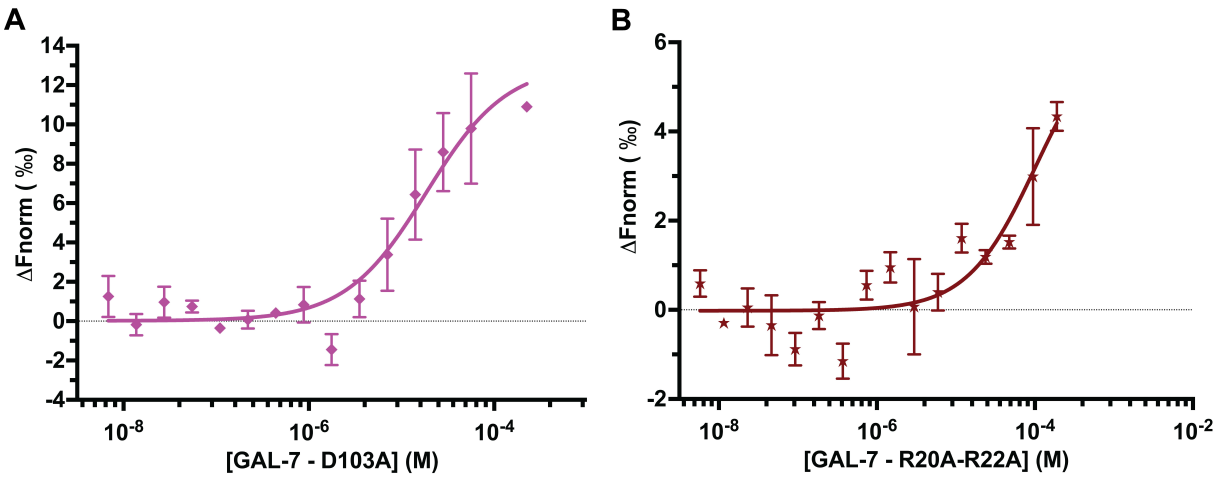

Figure 3.6 Unsaturated homodimer equilibrium curves for GAL-7 variants, as measured by MST.

D103A (A, violet) and R20A-R22A (B, firebrick).

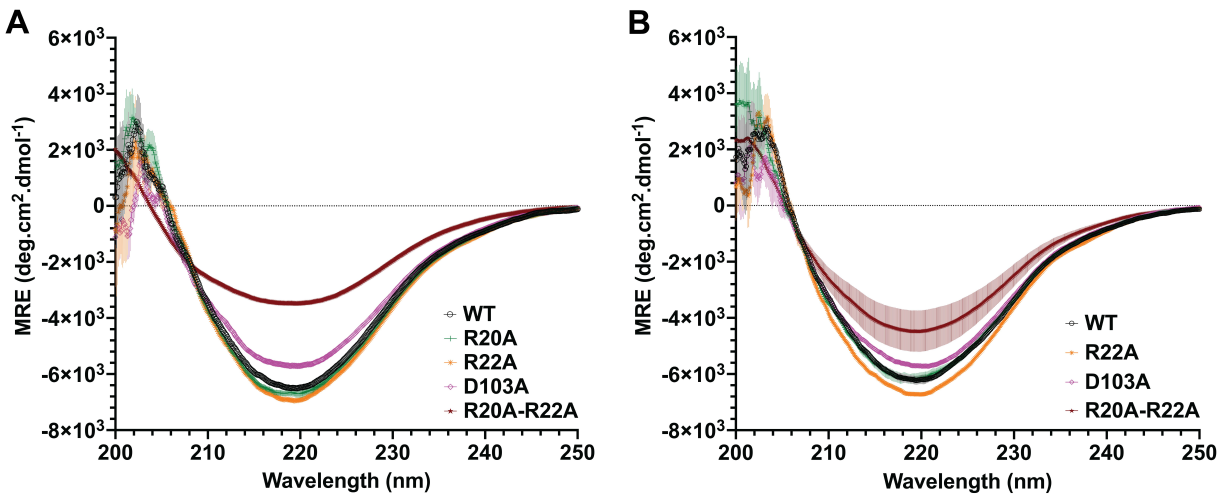

Figure 3.7 UV molar ellipticity spectra of GAL-7 variants

WT GAL-7 (black), R20A (green), R22A (orange), D103A (violet) and R20A-R22A (firebrick) spectra are measured by CD spectropolarimetry. CD spectra are shown for (A) apo proteins and (B) in presence of 6 mM α-lactose. Standard deviation is shown as pale colored line thickness.

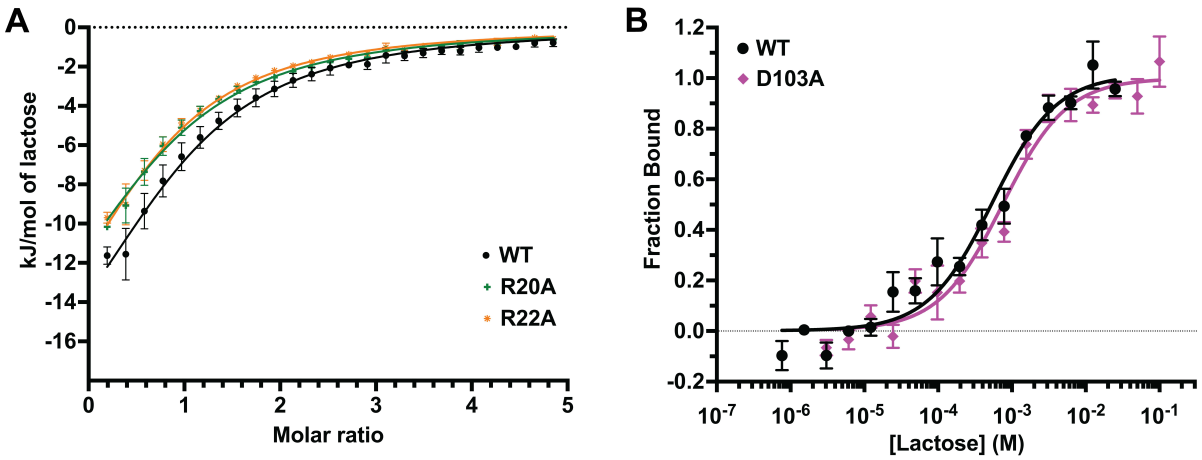

Figure 3.8 Lactose binding affinity for WT GAL-7 and variants R20A, R22A, and D103A

Lactose binding to WT GAL-7 (black spheres), R20A (green crosses), R22A (orange stars), and D103A (violet diamonds), as measured by (A) ITC or (B) MST.

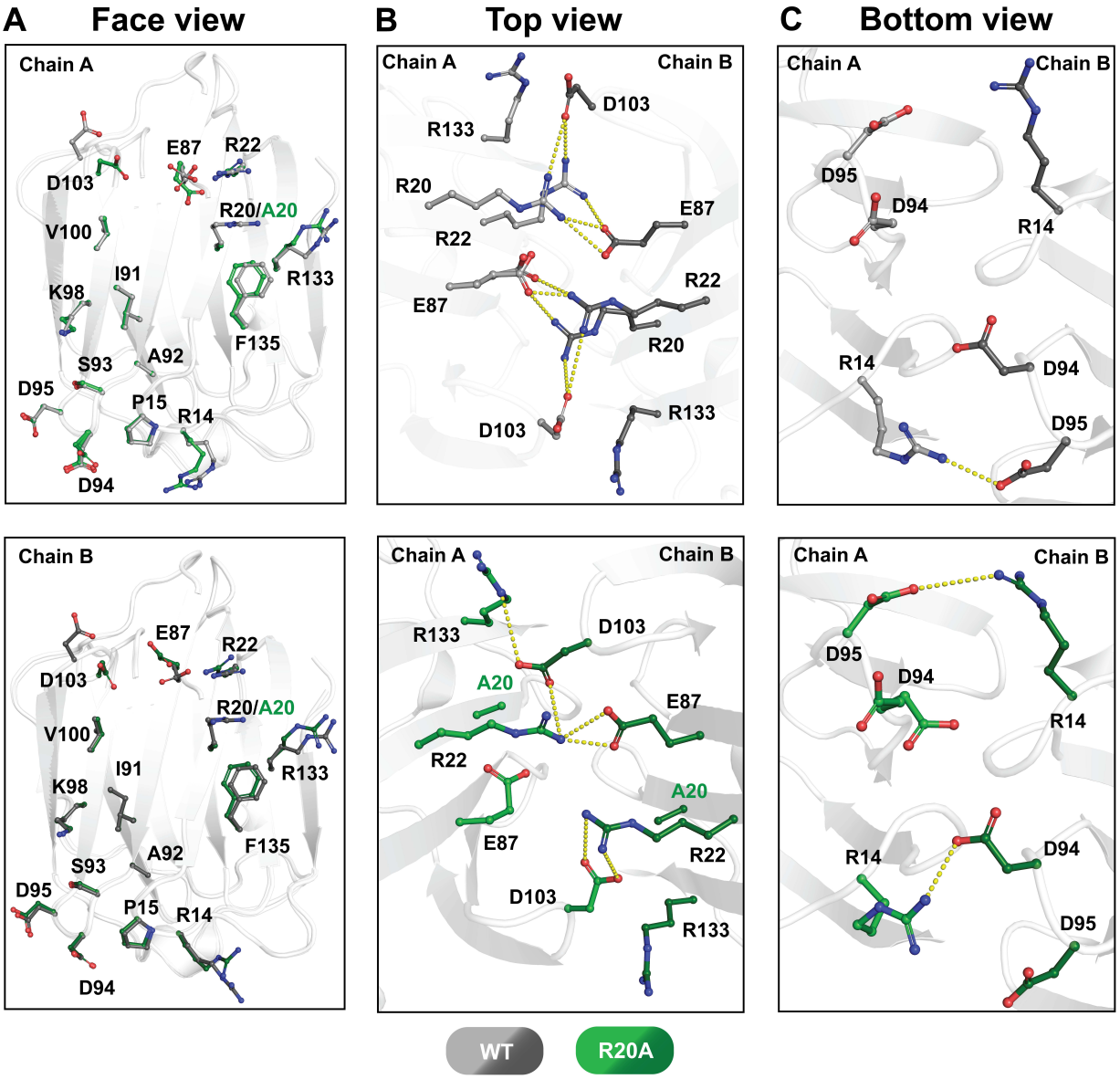

Figure 3.9 Structural comparison between holo WT GAL-7 and holo R20A

A, structural alignment of residues involved in homodimer interactions between WT and R20A at the dimer interface of protomer A (top) and protomer B (bottom). Residues are shown in grey (WT) and green (R20A) ball-and-sticks representation. B, salt bridge interactions (yellow dashed lines) between dimer interface residues A/R20, R22, E87, D103, and R133 in WT (top) and R20A (bottom). C, salt bridge interactions between dimer interface residues R14, D94, and D95 in WT (top) and R20A (bottom). (PDB 6VTO and 7N57).

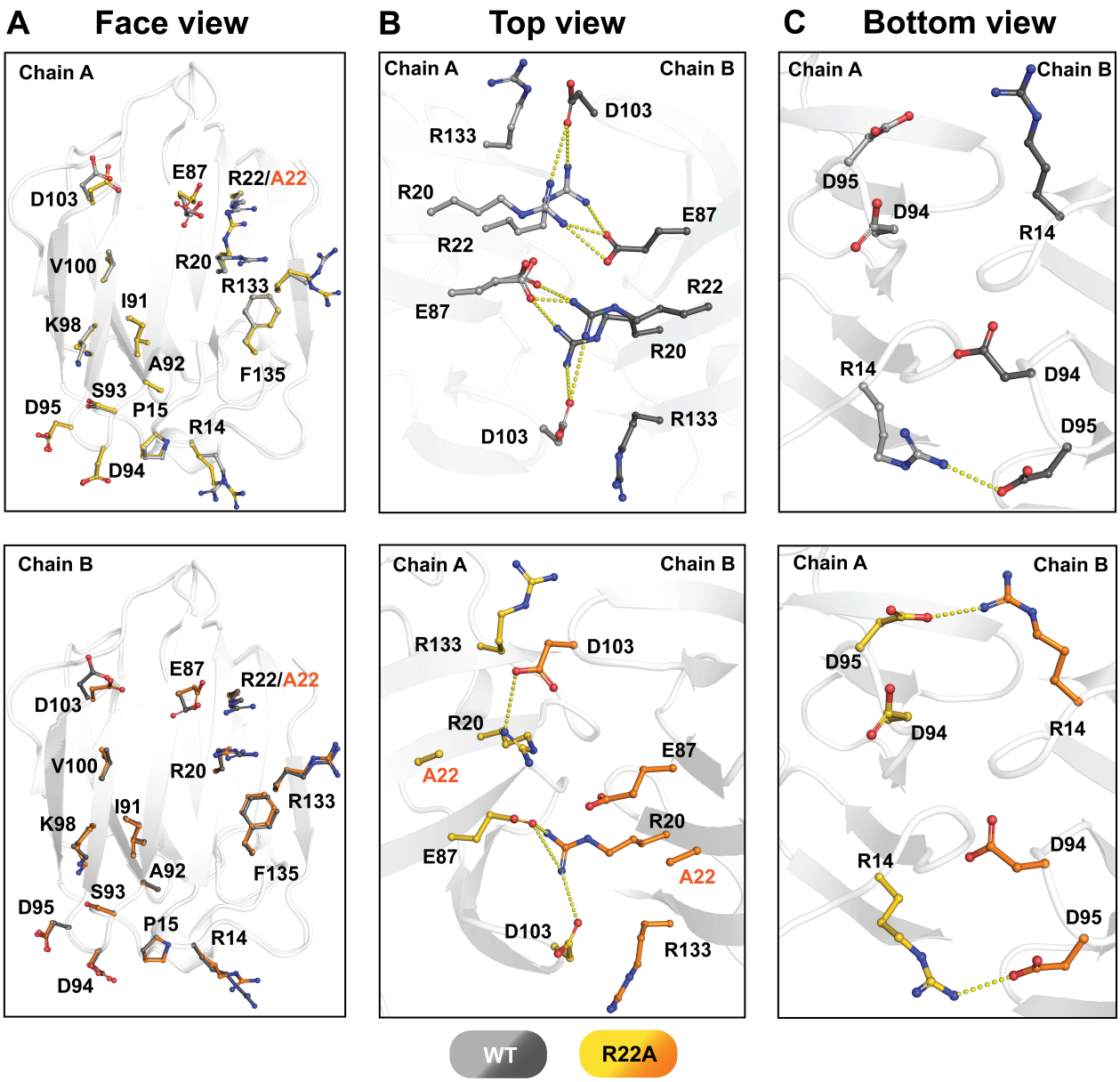

Figure 3.10 Structural comparison between holo WT GAL-7 and holo R22A

A, structural alignment of residues involved in homodimer interactions between WT and R22A at the dimer interface of protomer A (top) and protomer B (bottom). Residues are shown in grey (WT) and yellow-orange (R22A) ball-and-sticks representation. B, salt bridge interactions (yellow dashed lines) between dimer interface residues R20, A/R22, E87, D103, and R133 in WT (top) and R22A (bottom). C, salt bridge interactions between dimer interface residues R14, D94, and D95 in WT (top) and R22A (bottom). (PDB 6VTO and 7N8D).

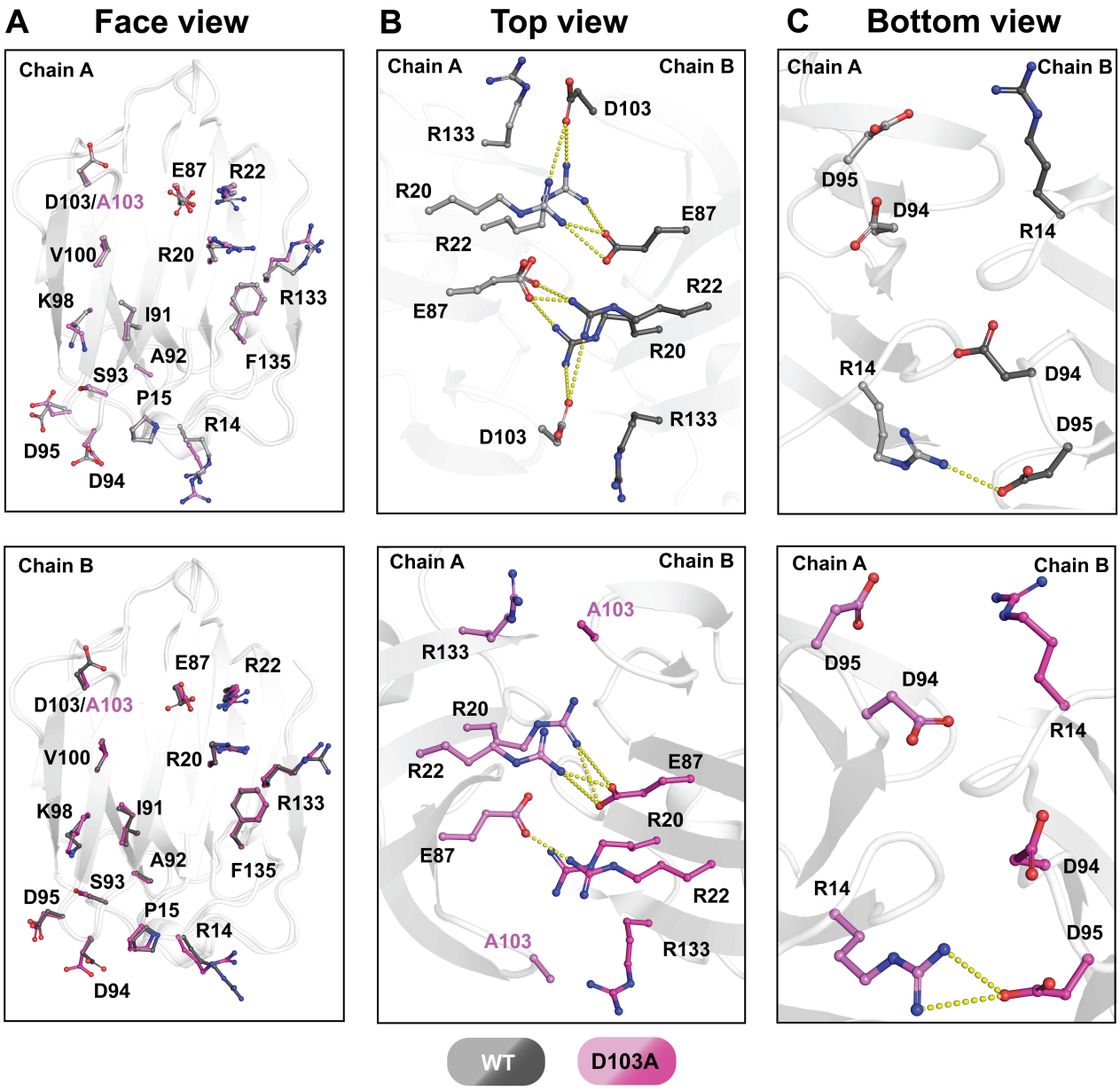

Figure 3.11 Structural comparison between holo WT GAL-7 and holo D103A

A, structural alignment of residues involved in homodimer interactions between WT and D103A at the dimer interface of protomer A (top) and protomer B (bottom). Residues are shown in grey (WT) and pink (D103A) ball-and-sticks representation. B, salt bridge interactions (yellow dashed lines) between dimer interface residues R20, R22, E87, A/D103, and R133 in WT (top) and D103A (bottom). C, salt bridge interactions between dimer interface residues R14, D94, and D95 in WT (top) and D103A (bottom). (PDB 6VTO and 7RDG).

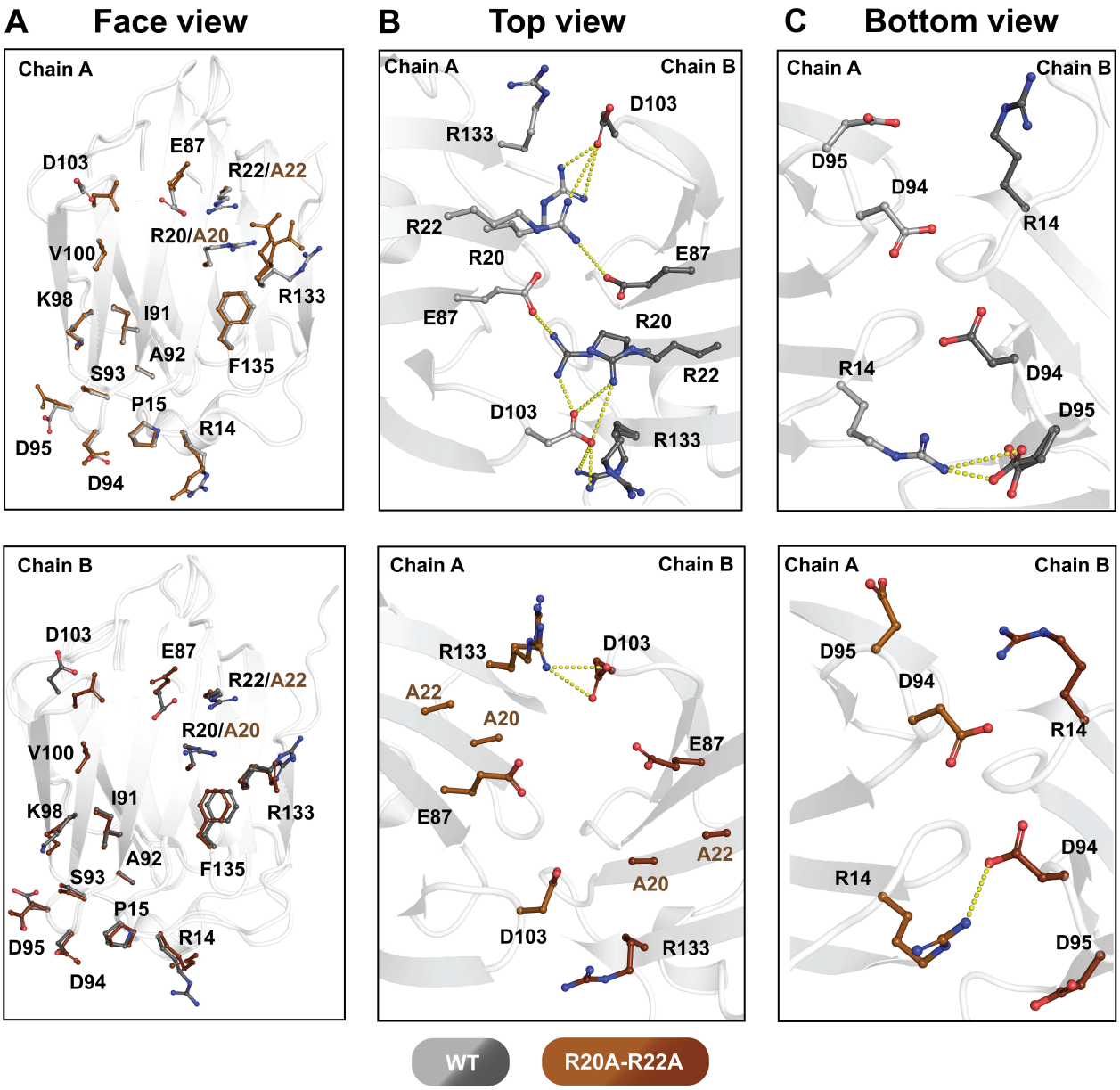

Figure 3.12 Structural comparison between apo GAL-7 WT and apo R20A-R22A

A, structural alignment of residues involved in homodimer interactions between WT and R20A-R22A at the dimer interface of protomer A (top) and protomer B (bottom). Residues are shown in grey (WT) and brown (R20A-R22A) ball-and-sticks representation. B, salt bridge interactions (yellow dashed lines) between dimer interface residues A/R20, A/R22, E87, D103, and R133 in WT (top) and R20A-R22A (bottom). C, salt bridge interactions between dimer interface residues R14, D94, and D95 in WT (top) and R20A-R22A (bottom). (PDB 3ZXF and 7N8G).

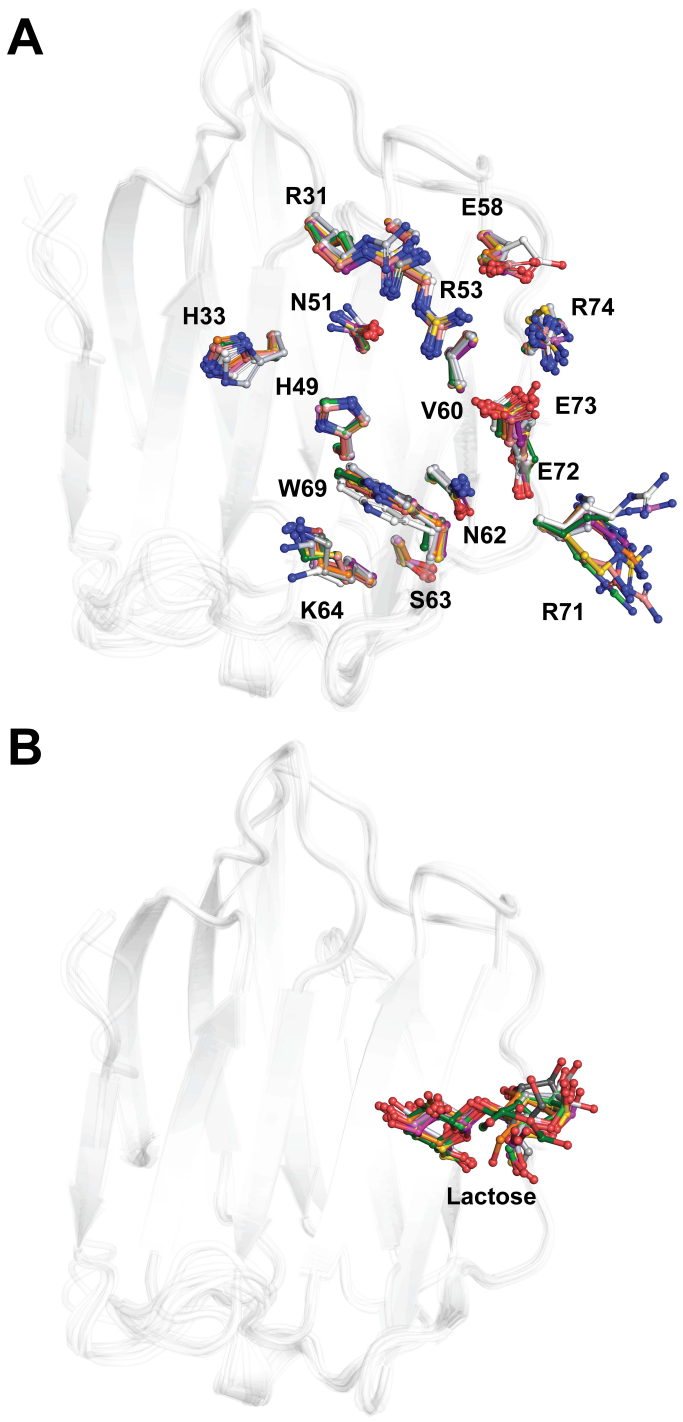

Figure 3.13 Glycan binding site (GBS) superposition between holo WT GAL-7 and single variants R20A, R22A, and D103A

A. Structural alignment of residues involved in GBS. Residues are shown as ball-and-sticks representation with white-grey, green, yellow-orange, and violet-purple colors for WT, R20A, R22A, and D103A, respectively. B. Structural alignment of lactose ligands bound to the GBS of all holo GAL-7 structures. (PDB 6VTO, 7N57, 7N8D and 7RDG.

4 EFFECTS OF PERTURBING R14, D94, AND D95 ELECTROSTATIC INTERACTIONS ON THE PROAPOPTOTIC ACTIVITY OF GAL-7

In the first article, we demonstrated that the proapoptotic activity of GAL-7 can be positively and negatively modulated by altering the integrity of the homodimer interactions via G16X mutations (central section of the dimer interface). In the second article, we demonstrated that the perturbation of protomer-protomer interactions, in combination with the disruption of inter-protomer communication via Arg20, Arg22, and Asp103 mutations (top section of the dimer interface) decreases the proapoptotic activity of GAL-7. To achieve a complete overview of the involvement of homodimer interactions in GAL-7 function, here we focus on the bottom section of the dimer interface, primarily consisting of Arg14, Asp94, and Asp95 residues. Moreover, Arg14 was previously outlined as a potential residue involved in dynamical communication transitioning between the GBS and the dimer interface (Ermakova et al., 2013). To verify this hypothesis, we investigated the proapoptotic effects of perturbing electrostatic interactions at these positions in GAL-7.

4.1 Results and discussion

4.1.1 Perturbing the D94-R14 electrostatic interaction can positively and negatively modulate the proapoptotic activity of GAL-7

To investigate the effect of the R14-D94 electrostatic interaction on GAL-7 activity, we carried out Jurkat T cell apoptosis experiments on variants R14A and D94A. Although located in opposite sections of the dimer interface, we also investigated the effects of double mutants R14A-R20A and R14A-R22A. Our results show no significant change in the proapoptotic activity of the R14A variant, yielding an EC50 of 6.5 μM (CI95% between 6.1 and 7.0 μM) relative to 6.6 μM (CI95% 6.4-6.8 μM) for WT GAL-7 (Figure 4.1). Accordingly, the R14A-R20A double mutant and R20A single mutant exhibit comparable cellular activity, yielding an EC50 of 10.9 μM (CI95% 8.6-13.7 μM) and 8.7 μM (CI95% 8.1-9.4 μM), respectively. However, the R14A-R22A double mutant shows a more pronounced effect on the proapoptotic activity of GAL-7, yielding an EC50 of 16.5 μM (CI95% 15.1-18.2 μM) relative to 10.9 μM (CI95% 10.0–11.9 μM) for R22A. This suggests that the combination of single mutations R22A and R14A has a synergistic effect on the inhibition of GAL-7 function. Additionally, contrary to R14A, variant D94A promotes the ability of GAL-7 to induce Jurkat T cell apoptosis, yielding an EC50 of 4.6 μM (CI95% 4.0-5.2 μM) (Figure 4.1). These

results suggest that pertrubing the R14A-D94A contact could negatively or positively modulate the proapoptotic activity of GAL-7 regardless of interprotomer communication perturbation.

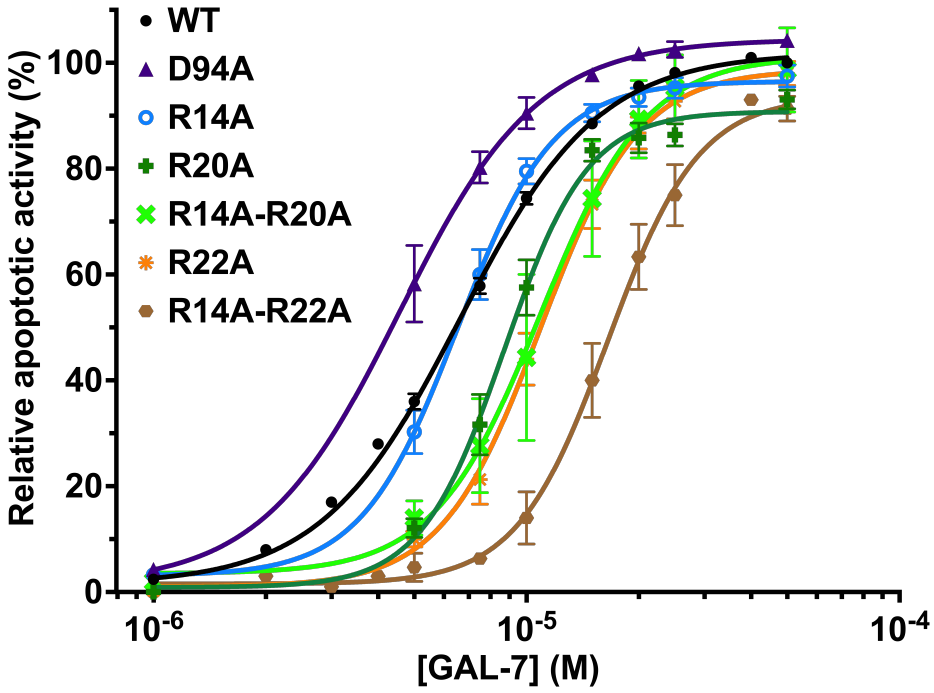

Figure 4.1 Apoptosis of human Jurkat T cells induced by GAL-7 variants.

WT (black circles), D94A (purple triangles), R14A (blue circle), R20A (green plus signs), R14A-R20A (lime crosses), R22A (orange asterisks), R14A-R22A (brown hexagons).

4.1.2 R14A, D94A, R14A-R20A, and R14A-R22A variants perturb homodimer interactions and protein stability

Given that D94A, R14A, R14A-R20A, and R14A-R22A are homodimer interface residues, we investigated the strength of dimer association/equilibrium and protein stability using MST and CD, respectively. As previously mentioned on other interface variants (chapters 2-3), R14A, D94A, R14A-R20A, and R14-R22A exhibit destabilization of the homodimer interface in GAL-7. While the R14A mutation minimally perturbs dimer stability relative to WT, variants D94A, R14A-R20A, and R14A-R22A share a similar K_D range as variants R20A and R22A, which are 19-fold and 20-fold less stable than WT, respectively (Table 4.1).

Our CD results show that all mutations reduce protein stability but still preserve stability enhancements induced by lactose binding. Indeed, the T_m value of D94A (T_m = 64.5 ± 0.3°C), R14A (T_m = 64.1 ± 0.1 °C), R20A (T_m = 60.9 ± 0.1 °C), R14A-R20A (T_m = 56.9 ± 0.1 °C), R22A (T_m = 59.4 ± 0.1 °C), R14A-R22A (T_m = 54.8 ± 0.1 °C), are respectively 3.3 °C, 3.7 °C, 6.9 °C, 10.9 °C, 8.4°C, and 13 °C lower than WT (T_m = 67.8 ± 0.2 °C) (Figure 4.2). In presence of lactose,

thermal stability is increased by 2.7 °C for WT (T_m = 70.5 ± 0.1 °C), 2.5 °C for D94A (T_m = 67.0 ± 0.2 °C), 1.9 °C for R14A (T_m = 66.0 ± 0.2 °C), 3 °C for R20A (T_m = 63.9 ± 0.7 °C), 2.6 °C for R14A-R20A (T_m = 59.5 ± 0.1 C), 3.3 °C for R22A (T_m = 62.7 ± 0.2 °C), and 5.2 °C for R14A-R22A (T_m = 60.0 ± 0.5 °C) (Figure 4.2).

Table 4.1 Homodimer dissociation constants (K_D)

	K_D (μM)	95% Confidence Interval
WT	0.06	0.03-0.12
R14A	0.16	0.08-0.32
R20A	1.14	0.55–2.35
R22A	1.2	0.79–1.94
D94A	0.97	0.46-1.81
R14A-R20A	0.79	0.33-1.82
R14A-R22A	0.41	0.18-0.98

Overall, these results suggest that destabilization of homodimer interactions at positions Arg14 or Asp94, along with the reduction in protein stability did not decrease the proapoptotic activity of GAL-7. Conversely, the fact that the D94A mutation increases the ability of GAL-7 to induce apoptosis of T cells on its own is puzzling. This result suggests that the biological activity of GAL-7 is not exclusively controlled by homodimer strength but may also be governed by another unknown mechanism. Considering that R14A and D94A are both located in loop regions while R20A and R22A are beta strand residues, this unknown mechanism controlling the proapoptotic activity might relate to other dynamical effects experienced by GAL-7 and/or involve other GAL-7 protein binders, as previously described for other GBS-independent biological interactions (Advedissian et al., 2017b; Villeneuve et al., 2011).

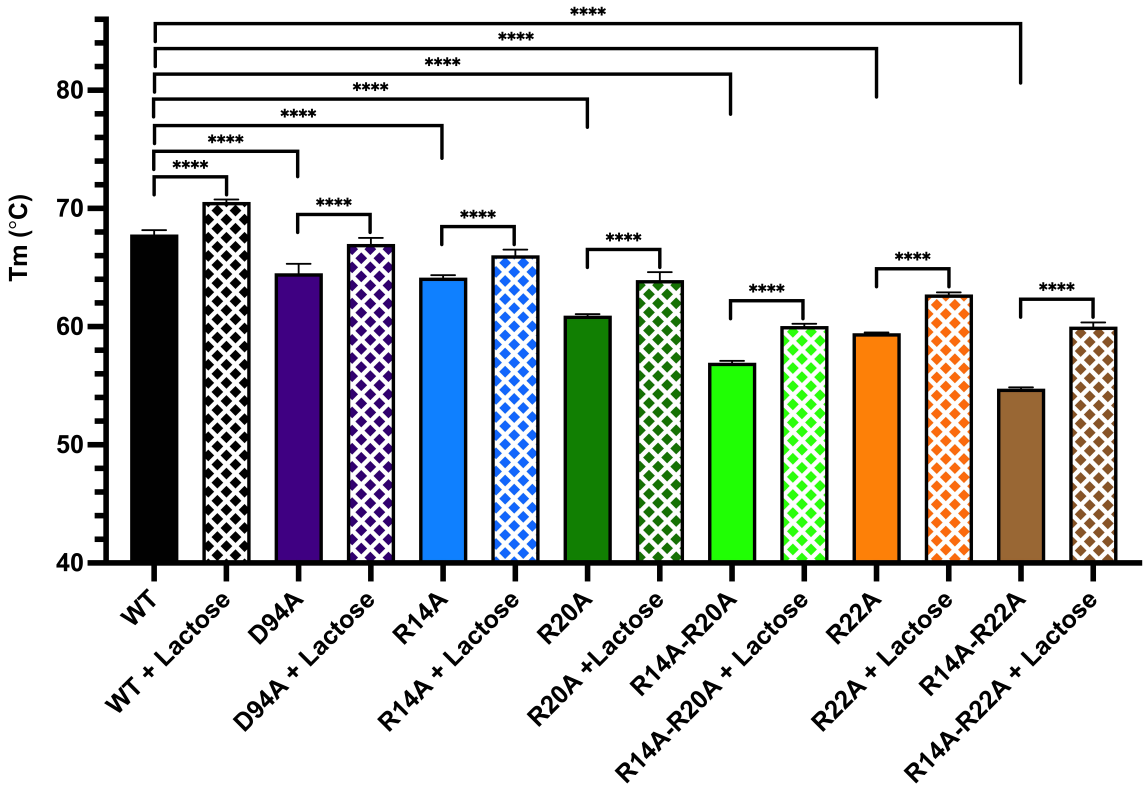

Figure 4.2 Thermal stability of GAL-7 variants in presence and absence of lactose.

WT (black) and mutants D94A (purple), R14A (aquamarine), R20A (green), R14A-R20A (lime), R22A (orange), and R14A-R22A (brown) in the absence (filled bar) and presence of lactose (pattern bar), as measured by CD-induced thermal denaturation. These values are statistically significant, with *p-value* ≤0.0001 (illustrated by four asterisks) evaluated by one-way ANOVA with Tukey post-hoc tests.

4.1.3 R14A, D94A, R14A-R20A, and R14A-R22A variants maintain GAL-7 dimer architecture in free and lactose-bound states

The X-ray structures of R14A, D94A, and R14A-R20A variants in their apo and holo states (in complex with lactose) were solved (Table 7.1) to investigate the relationship between structural changes and the proapoptotic activity of GAL-7 mutants. The resolutions of all solved X-ray structures range from 1.8 to 2.53 Å. Except for the apo structure of R14A-R20A (PDB 7TRN), which crystallized in the *P*1 group, all other apo structures of R14A (PDB 7TKW), D94A (PDB 7TKY), and holo structures of R14A (PDB 7TKX), D94A (PDB 7TKZ), and R14A-R20A (PDB 7TRO) crystallized in the $P2_12_12_1$ group. The GAL-7 dimer architecture in the free and lactose bound states was maintained for all mutants. Except for the apo R14A-R20A structure, all other variants show the dimer complex in a single asymmetric group. Indeed, the asymmetric unit of apo R14A-R20A consists of four monomers that form a dimer complex with the monomer from four different asymmetric units (Figure 7.1). Cα structural alignments of dimer structures between apo WT GAL-7 (PDB 3ZXF) and variants R14A (PDB 7TKW), D94A (PDB 7TKY), and four dimeric

complexes of R14A-R20A (PDB 7TRN) show no significant change in the overall GAL-7 dimer architecture (Table 7.4). This is also the case between holo WT GAL-7 (PDB 6VTO) and variants R14A (PDB 7TKX) and D94A (PDB 7TKZ).

To investigate the link between homodimer interactions and the GBS-dependent proapoptotic activity of GAL-7, the side chain conformation of dimer interface residues was compared between holo WT GAL-7 and R14A, D94A, and R14A-R20A structures. As expected, the R14A mutation abrogates the electrostatic interaction between residues Arg14 and Asp95 in variants R14A and R14A-R20A (Figure 7.2 and Figure 7.4). Similar to the R20A single mutant, the salt bridge interaction between residue Ala20 and opposite residues Asp103 and Asp87 are missing in the R14A-R20A variant (Figure 3.9 and Figure 7.4). No change of side chain conformation was observed for interface residues in the D94A structure, while R14A and R14A-R20A variants induced conformational changes in residues Asp94 and Asp103, and Arg133, respectively (Figure 7.2, Figure 7.3, and Figure 7.4). However, only one Arg133 conformation in variant R14A-R20A was shown to form a new salt bridge with Asp103, as previously observed in the R20A variant (Figure 3.9 and Figure 7.4). Overall, the loss of the Arg14-Asp95 salt bridge did not cause significant impact on the position of other neighboring interface residues, explaining the unaltered proapoptotic activity in variant R14A, and similar activity observed between variants R20A and R14-R20A. Although no structural perturbation was observed at the dimer interface in variant D94A, protein stability and homodimer affinity was reduced. This observation may be explained by different structural behaviors observed between immobilized protein in crystal forms and in solution. Even though no electrostatic interaction was observed between Arg14 and Asp94 in holo WT GAL-7 (Figure 7.3), it is possible that this interaction still occurs in solution. Indeed, since Arg14, Asp94, and Asp95 are all located in loop regions, the movement of these loops may continuously form and break the Arg14-Asp94 and Arg14-Asp95 salt bridges as the protein experiences conformational exchange in solution. The D94A mutation inevitably causes a loss in the stabilizing Arg14-Asp94 salt bridge in solution, resulting in overall destabilization of the protein and homodimer affinity. In contrast, the increase in apoptotic activity observed with the D94A remains unexplained.

4.1.4 Double mutants R14A-R20A and R14A-R22A affect lactose binding affinity in GAL-7

Since the proapoptotic activity of GAL-7 is known to be GBS dependent, we investigated the effects of mutations on lactose binding affinity using X-ray crystallography, ITC, and MST. The overall GBS organization and lactose positioning are similar between WT (PDB 6VTO) and

variants R14A (PDB 7TKX), D94A (PDB 7TKZ), and R14A-R20A (7TRO) (Figure 7.5). Only the side chain conformation of Arg71 is positioned differently among these structures. As previously outlined, since Arg71 is located at the crystal contact surface, this dissimilarity could easily be an artifact of crystal packing. However, while a lactose molecule is observed in the GBS of each protomer (A and B) in WT, R14A, and D94A X-ray structures, it is only present in a single GBS of double mutant R14A-R20A (Figure 4.3D). Accordingly, our MST results show significantly lower lactose binding affinity for double mutant R14A-R20A, yielding a K_D value of 790 μM relative to 116 μM for WT (Figure 4.3A and Table 7.3). Moreover, we were unable to achieve saturation of lactose binding with the R14A-R22A mutant (Figure 4.3B and Table 7.3). In contrast, our ITC results indicate no significant change in lactose binding affinity between WT GAL-7 (K_D = 135.3 ± 1.2) and variants R14A (K_D = 163.7 ± 17.0) or D94A (K_D = 157.3 ± 6.4) (Figure 4.3C and Table 7.2). This is consistent with the pro-apoptotic activity observed with all variants exhibiting a mutation at position Arg14. Indeed, the proapoptotic activity of the R14A variant is comparable to WT GAL-7, while that of the R14A-R20A and R14A-R22A double mutants is lower than WT. Since no lactose binding affinity change was observed in variant D94A, the increase in its proapoptotic activity remains unexplained.

4.2 Conclusion

Our studies showed that perturbing the Arg14-Asp94 electrostatic interaction alters the pro-apoptotic activity of GAL-7. Mutations R14A and R22A act synergistically to negatively modulate the function of GAL-7. In contrast to other mutations reported in this vicinity, the D94A replacement improves the ability of GAL-7 to induce the apoptosis of Jurkat T cells. However, our characterization of protein stability, homodimer interaction, lactose binding affinity, and solving of the X-ray structure cannot adequately explain this increase in biological function. Since Asp94 is located in a loop region of GAL-7 (L7-β8) that was proposed to be involved in correlating motions between the GBS and the dimer interface in presence of lactose (Ermakova et al., 2013), conformational changes induced by the D94A mutation might be involved in positive modulation of GAL-7 activity. Further dynamical investigation and biophysical characterization would be warranted to clarify this hypothesis.

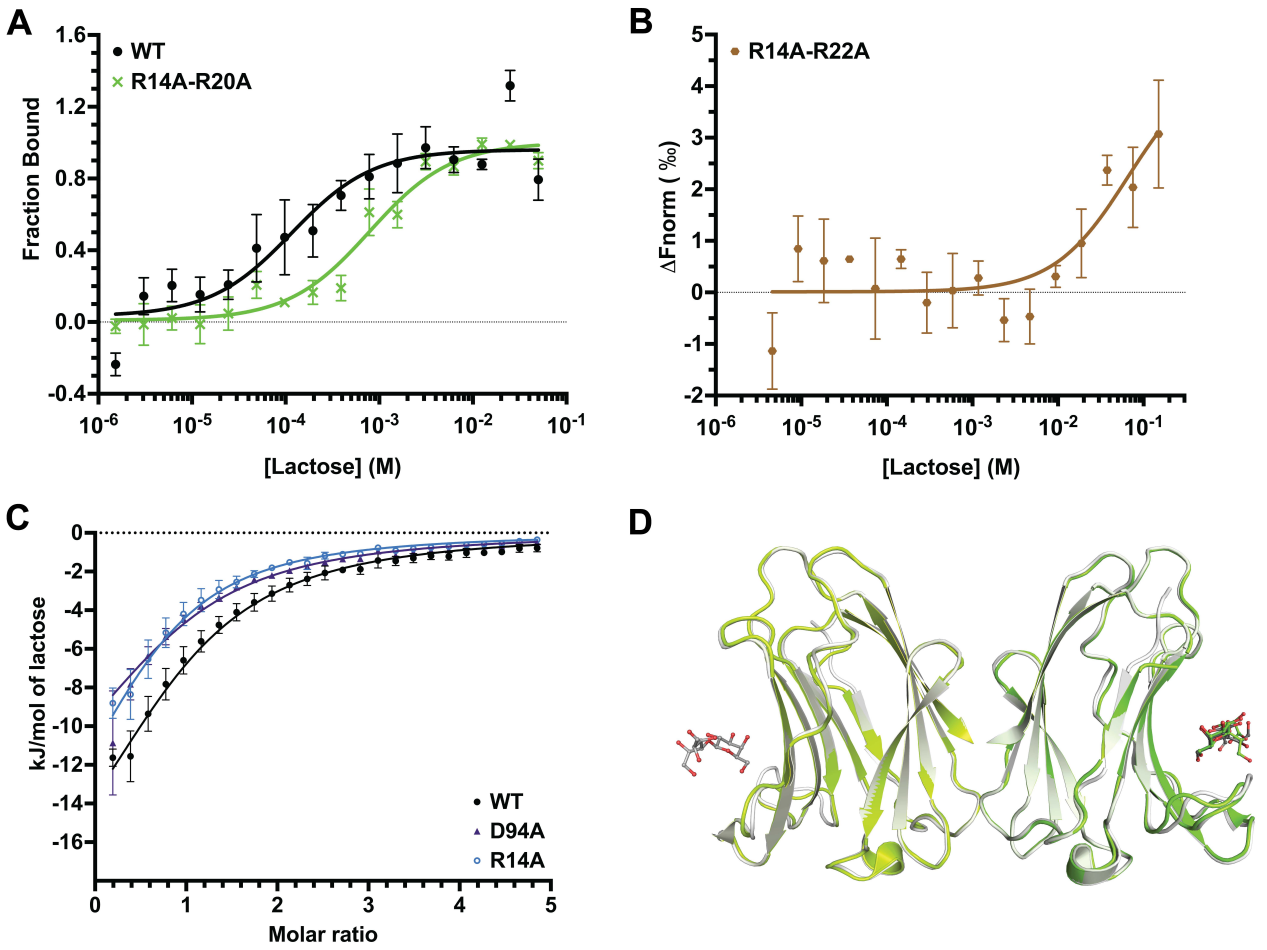

Figure 4.3 Lactose binding affinity for WT GAL-7, R14A, D94A, and R14A-R20A variants

Lactose binding affinity for (A) WT and R14A-R20A, (B) R14A-R22A, as measured by MST, and for (C) WT, D94A, and R14A, as measured by ITC. (D) A lactose molecule is only observed in one GBS in the X-ray structure of variant R14A-R20A. The WT and R14A-R20A cartoon structures are superimposed and colored in white and green, respectively. Lactose molecules are shown as balls and sticks.

4.3 Experimental procedures

4.3.1 Site-directed mutagenesis and protein expression

The pET-22b(+) vector encoding for recombinant human galectin-7 (WT GAL-7) was reused from the previous study (Pham et al., 2021). R14A and D94A mutants were generated by the QuikChange site-directed mutagenesis method with iProof High-Fidelity DNA Polymerase kit (BioRad) using the forward (R14Af: 5'-cccgagggcatcgcccctggcacggtg-3'; D94Af: 5'-catcatcgcgtcagccgacggcttcaagg-3') and reverse (R14Ar: 5'-caccgtgccaggggcgatgccctcggg-3'; D94Ar: 5'-ccttgaagccgtcggctgacgcgatgatg-3') primers. R14A-R20A and R14A-R22A mutants were generated by introducing the R14A mutation in the R20A and R22A mutants constructs from the previous study using the Q5® Site-Directed Mutagenesis Kit (NEB) and the forward (R14Af:

5’-cgagggcatcgcccctggcacgg-3’) and reverse (R14Ar: 5’-ggcagtgaggacttgtgggggacg-3’) primers. All plasmid constructs were confirmed by DNA sequencing before being used for protein expression. Recombinant WT GAL-7 and variants were expressed in *E.coli* BL21(DE3) and purified by lactose affinity gravity-flow purification at 4°C, as previously described (Pham et al., 2021).

4.3.2 Apoptosis assays with Annexin V/PI staining

Purified proteins were prepared in PBS solution (0.144 g/L KH_2PO_4, 0.795 g/L NaH_2PO_4, 9 g/L NaCl, pH 7.4) All apoptosis assays were performed as previously described (Pham et al., 2021).

4.3.3 Biophysical characterisation

ITC, CD, and Tm calculation experiments were performed and processed as previously described (Pham et al., 2021). MST experiments were carried out as detailed (Pham et al., 2021), with the following modifications:

- *Dimer K_D determination*

WT GAL-7, R14A, D94A, R14A-R20A, and R14A-R22A were labeled with Cy5 or AlexaFluo647 in accordance with the manufacturer’s protocols, as previously described (Pham et al., 2021). Each binding assay experiment consisted of 16 2-fold serial dilutions of 50 μM (starting concentration) of unlabeled WT GAL-7, R14A, D94A, R14A-R20A, or R14A-R22A. Unlabeled samples were then prepared in 5 nM labeled GAL-7 for WT, R14A-R20A, and R14A-R22A, or in 20 nM labeled sample for R14A and D94A. Depending on protein stability of each GAL-7 variant, each sample was incubated at a specific time and temperature to avoid aggregation and adsorption during experiment. WT, R14A, and D94A samples were incubated at 40°C in a water bath for 45 min, while R14A-R20A and R14A-R22A variants required no incubation. MST acquisition, data, and K_D calculation were processed as previously described (Pham et al., 2021).

- *Lactose binding assay*

Each binding assay experiment consisted of 16 2-fold serial dilutions of 50 μM (WT), 50 μM (R14A-R20A), and 150 μM (R14A-R22A) (starting concentration) of lactose prepared in 5 nM

labeled WT GAL-7, R14A-R20A, and R14A-R22A, respectively. The MST measurement and analysis was carried out as described above.

4.3.4 Statistical analysis

All experiments were carried out at least in triplicate. The mean and standard error of the mean (SEM) of all measured results are plotted using GraphPad Prism 9.0 (GraphPad Software, San Diego, CA). Statistical significance was evaluated with or one-way ANOVA with Tukey post-hoc tests (CD experiments) or F-test (cell assays, ITC, and MST experiments). *p-value* cut off was set 0.05 to confirm the statistical difference between two data sets.

4.3.5 Protein crystallization.

- *Apo GAL-7 (R14A)*

1 µl of 2 mg/ml GAL-7 (R14A) solution (in buffer A) was mixed at 1:1 ratio with 0.1 M NaCl, 0.1 M Tris pH 8.0, 20 % w/v PEG 6000, 20 % v/v glycerol. Crystals were obtained by the sitting-drop vapor diffusion technique at room temperature after one week. Crystals were cryo-protected by soaking in paratone.

- *Apo GAL-7 (D94A)*

1 µl of 7.5 mg/ml GAL-7 (D94A) solution (in buffer A) was mixed at 1:1 ratio with 0.1 M NaCl, 0.1 M Tris pH 8.0, 20 % w/v PEG 6000, 15 % v/v glycerol. Crystals were obtained by the sitting-drop vapor diffusion technique at room temperature after one week. Crystals were cryo-protected by soaking in a solution of 0.1 M NaCl, 0.1 M Tris pH 8.0, 20 % w/v PEG 6000, 30 % v/v glycerol.

- *Apo GAL-7 (R14A-R20A)*

1 µl of 7.5 mg/ml GAL-7 (*R14A-R20A*) solution (in buffer A) was mixed at 1:1 ratio with 0.1 M NaCl, 0.1 M Tris pH 8.0, 20 % w/v PEG 6000, 17.5 % v/v glycerol. Crystals were obtained by the sitting-drop vapor diffusion technique at room temperature after one week.

- *Lactose-bound GAL-7 (R14A)*

Co-crystallization of GAL-7 (R14A) with α-lactose was performed using the sitting-drop vapor diffusion technique. Crystals were obtained by incubating a drop consisting of a 1:1 mixture

of 1 µl of 7.5 mg WT GAL-7 solution (50 mM Tris pH 8.0, 150 mM NaCl, 7.5 mM α-lactose) with 0.1 M NaCl, 0.1 M Tris pH 8.0, 20 % PEG 6000, 10% glycerol at room temperature after one week. Crystals were cryo-protected by soaking in paratone.

- *Lactose-bound GAL-7 (D94A)*

Co-crystallization of GAL-7 (D94A) with α-lactose was performed using the sitting-drop vapor diffusion technique. Crystals were obtained by incubating a drop consisting of a 1:1 mixture of 1 µl of 7.5 mg WT GAL-7 solution (50 mM Tris pH 8.0, 150 mM NaCl, 7.5 mM α-Lactose) with 0.1 M NaCl, 0.1 M Tris pH 8.0, 20 % PEG 6000, 15% glycerol at room temperature after one week. Crystals were cryo-protected by soaking in a solution of 0.1 M NaCl, 0.1 M Tris pH 8.0, 20 % PEG 6000, 30% glycerol.

- *Lactose-bound GAL-7 (R14A-R20A)*

Co-crystallization of GAL-7 (R14A) with α-lactose was performed using the sitting-drop vapor diffusion technique. Crystals were obtained by incubating a drop consisting of a 1:1 mixture of 1 µl of 7.5 mg WT GAL-7 solution (50 mM Tris pH 8.0, 150 mM NaCl, 7.5 mM α-Lactose) with 0.1 M NaCl, 0.1 M Tris pH 8.0, 20 % PEG 6000, 5% glycerol at room temperature after one week. Crystals were cryo-protected by soaking in paratone.

4.3.6 Data collection, structure resolution, and refinement

All diffraction data of crystals was collected at the Canadian Macromolecular Crystallography Facility Beamline CMCF-BM or CMCF-OD of the Canadian Light Source Synchrotron (Fodje et al., 2014; Grochulski et al., 2011). Raw data processing, structures resolution and refinement was processed as previously described in chapter 3. All structural comparisons and visualizations were performed with the Open-Source PyMOL Molecular Graphics System, Version 2.4 (Schrödinger, LLC).

4.4 Data availability

X-ray coordinates for apo GAL-7 variants R14A, D94A, R14A-R20A, and holo GAL-7 variants R14A, D94A, R14A-R20A in complex with lactose have been deposited in the RCSB PDB under accession codes 7TKW, 7TKY, 7TRN, 7TKX, 7TKZ, and 7TRO, respectively.

5 GENERAL DISCUSSION AND CONCLUSION

5.1 Summary

Given that galectins play critical roles in cancer (Chou et al., 2018; Dubé-Delarosbil et al., 2018; Girotti et al., 2019; Liu et al., 2005; Vladoiu et al., 2014; Wdowiak et al., 2018), many studies have focused on the synthesis of galectin inhibitors as cancer therapeutics (Chou et al., 2018; Girard et al., 2018; Sörme et al., 2003). Despite more than two decades dedicated to this field, progress is slow, with only six submitted compounds currently in clinical trial with a narrow target span comprising GAL-1, -3, and -9 (Chou et al., 2018; Girard et al., 2018). This significantly limits the number of cancer types that could be treated using this therapeutic approach. Therefore, it is essential to extend available inhibition tools to other galectins. In this research, we focused on GAL-7 since it represents a new potential target for the treatment of TNBC, which is hard to eradicate due to the absence of the usual breast cancer receptor markers (ER-, PR-, HER2-) (Demers et al., 2010; Grosset et al., 2014, 2016; Wu et al., 2021). GAL-7 is a prototypic galectin characterized by a β-galactoside glycan binding site (GBS) and a homodimeric quaternary structure (Leonidas et al., 1998). Overexpression of GAL-7 in breast cancer cells helps them acquire resistance to apoptosis, which can be induced by immune cells, but also induces apoptosis of activated T cells by making galectin-glycoprotein lattices at the T cell membrane (Demers et al., 2010; Grosset et al., 2014, 2016; St-Pierre, 2012). Since the first attempt 16 years ago, development of GAL-7 inhibitors has focused on sugar-based, small-molecule compounds aimed at perturbing glycoreceptor interactions (Cumpstey et al., 2005; Masuyer et al., 2012; Salameh et al., 2006). To this day, this approach has yet to reach a turning point. This GAL-7 GBS inhibitor design has encountered many challenges due to the high GBS structural similarity among different galectins, which likely causes unwanted off-target effects through binding to other highly homologous and often beneficial, anti-tumorigenic galectin members (Morishita et al., 2021; Satelli et al., 2011; Tadokoro et al., 2016). Moreover, this strategy will most likely fail to target other GBS-independent activities promoted by GAL-7 (Advedissian et al., 2017b; Kuwabara et al., 2002; Labrie et al., 2015; Villeneuve et al., 2011). As a result, the development of a new approach to inhibit GAL-7 is required.

As a case study, allosteric modulators were previously demonstrated to be more selective and effective than inhibitors that target the active site (Wenthur et al., 2014). Thus, targeting non-GBS regions of GAL-7 could allow specific modulation of the GBS-dependent and -independent GAL-7 activities. In support of this idea, one goal would be to exploit the quaternary oligomeric

architecture of human galectins, which differs among family members despite an overall similar tertiary structure (Kamitori, 2018). For instance, targeting the homodimeric interface would significantly improve the specificity of GAL-7 inhibitors. Moreover, quaternary oligomeric architecture is important for galectins to form galectin-glycoprotein lattices, a scaffold involved in multiple cellular processes associated with cancer progression (Boscher et al., 2011; Brewer, 2002; Sacchettini et al., 2001). In addition, Ermakova et al. showed that lactose binding induces long-range positive cooperativity that crosses the dimer interface between the two GBSs on opposite GAL-7 protomers (Ermakova et al., 2013). Hence, GAL-7 dimer interfering peptides (DIPs) were recently developed to alter dimer stability and biological function (Vladoiu et al., 2015). Among designed DIPs, peptide hGAL-7(129–135) was shown to successfully decrease the GBS-dependent proapoptotic activity of GAL-7 on Jurkat T cells by disrupting the monomer-monomer interaction equilibrium in solution. However, designed DIPs have relatively low affinity for GAL-7 ($K_D \geq$ 1mM) and low solubility in physiological condition buffers, restricting their use as therapeutics. Improving DIP design requires a better understanding of the role played by each residue along the homodimer interface in relation with the regulation of GAL-7 activity. Are all residues involved in controlling GAL-7 activity? How are they involved in controlling the GBS-dependent activity of GAL-7? Are they important for allosteric communication between the two long-range GBSs? Which residue position needs to be targeted (or avoided) to negatively or positively modulate GAL-7 activity? To answer all these questions, we characterized the molecular mechanisms governing homodimer interactions and modulating the GBS-dependent proapoptotic activity of GAL-7.

Starting with the hypothesis that the dimer interaction strength could modulate GAL-7 proapoptotic activity, the Chapter 2 article **"Perturbing dimer interactions and allosteric communication modulates the immunosuppressive activity of human galectin-7"** (Pham et al., 2021) described *in silico* analyses using the PoPMuSiC and BeAtMuSiC algorithms to predict covalent disulfide bridge (G16C) and destabilizing mutation (G16S) to control homodimer strength. To assess the impact of these mutations on GAL-7 activity and on biophysical properties, apoptosis assays on Jurkat T cells, X-ray crystallography, biophysical, and computational characterizations were performed. We also established the first allosteric network analysis of GAL-7, which allowed us to identify potential allosteric pathways that interconnect the GBS within each protomer, partly explaining the positive binding cooperativity behavior of GAL-7 (Ermakova et al., 2013). Our results demonstrated that despite the conservation of overall GAL-7 structure, lactose binding affinity, and allosteric pathways connecting the two GBSs, the

proapoptotic activity of GAL-7 could be positively or negatively modulated via strengthening or weakening homodimer interface interactions, respectively.

With the Chapter 3 manuscript "**Allosteric network analysis in galectin-7 uncovers key residues controlling communication between two opposite glycan binding sites**", we further investigated the impact of perturbing interprotomer communication previously highlighted in our network analysis study (Pham et al., 2021). The analysis of GAL-7 allosteric networks suggested that R20, R22, and D103 were important to maintain communication between the two protomers of GAL-7 (Ermakova et al., 2013). Therefore, we used similar approaches from the previous study to characterize the consequences of three important interface point mutants (R20A, R22A, D103A) and one double mutant (R20A-R22A) on GAL-7 activity, along with evaluation of their biophysical and structural properties. Our results showed that despite the preservation of the overall GAL-7 structure, these mutations induced differences in lactose binding affinity, reduction of inter-protomer communication, alteration of allosteric pathways, and perturbation of homodimer interactions/stability that prevented GAL-7 from inducing apoptosis of Jurkat T cells. This study also contributed to the development of a new approach to assess global flow communication between the two distant GBSs, demonstrating a decrease in overall communication between GBSs in all protein variants.

To complete our study, which already investigated the impact of perturbing homodimer interactions at the top (R20, R22, D103) and the middle (F135, G16) regions (Pham et al., 2021) on GAL-7 proapoptotic activity, we investigated the effects of perturbing R14 and D94/D95 electrostatic interaction (bottom region of dimer interface) on apoptosis of Jurkat T cells, X-ray crystal structure and biophysical properties of such GAL-7 mutants. Our results indicated that D94A mutation increased the ability of GAL-7 to induce Jurkat T cell apoptosis while there was no alteration caused by the single R14A mutation. However, we observed a synergetic effect of R14A-R22A mutations on negative modulation of GAL-7 proapoptotic activity. This effect could be explained by a destabilization of the homodimer interaction and protein stability and perhaps the reduction of ligand binding affinity for the R14A-R22A GAL-7 mutant. Nevertheless, the increase of proapoptotic activity caused by the D94A mutation remains enigmatic since no correlation were defined between this activity and ligand binding affinity, protomer-protomer affinity, or protein stability. Since residues D94 and R14 are located on loop regions of the protein, their modulation mechanism might be through interfering with molecular dynamics between the GBS and the dimer interface (Ermakova et al., 2013). To confirm this, dynamical experiments

including biophysical techniques and *in silico* molecular dynamics need to be carried out in the future.

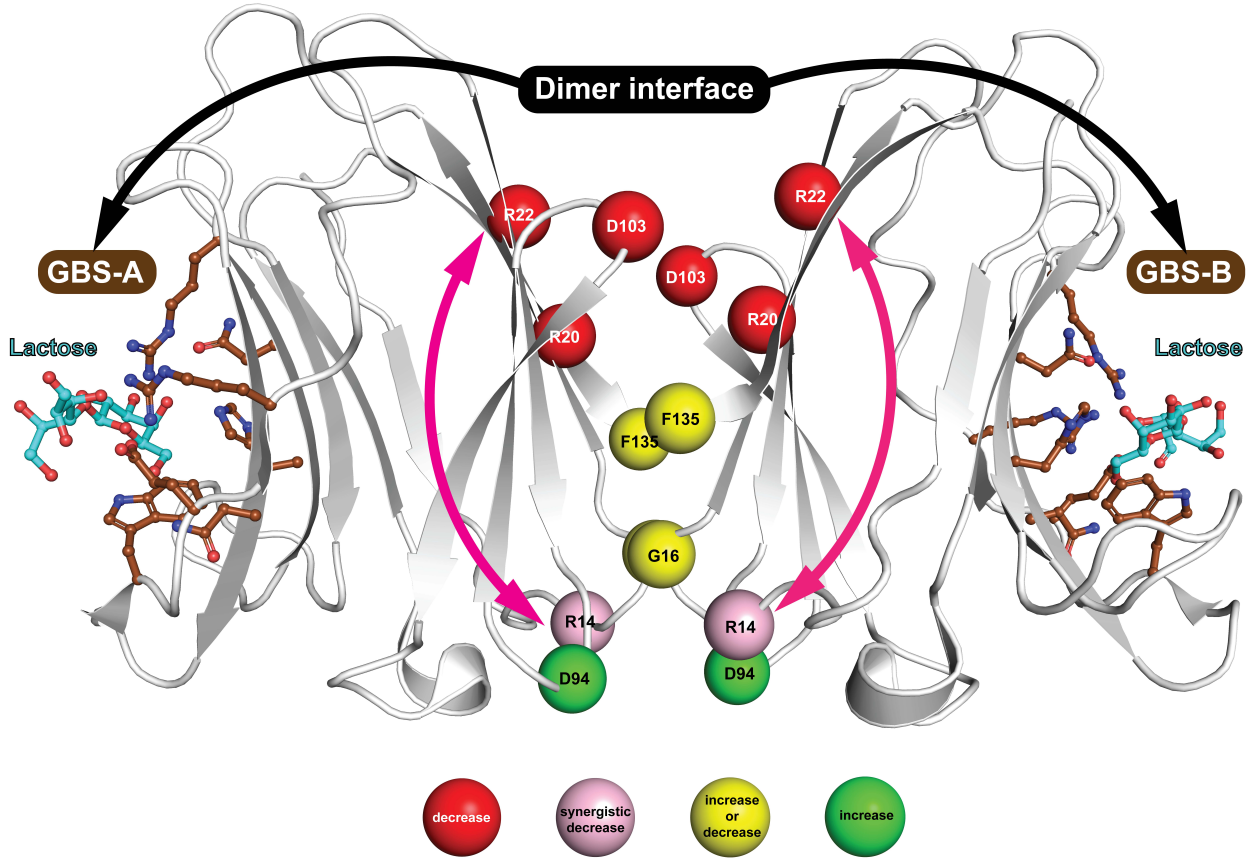

Figure 5.1 Effect of dimer perturbation on the GBS dependent proapoptotic activity of GAL-7

Dimer interface residues investigated in this study are shown in spheres. The GBS residues (brown) and lactose (cyan) are represented as balls-and-sticks. Perturbation of electrostatic interactions between top residues (R22, D103, R20) at the dimer interface decreases the proapoptotic activity of GAL-7 on Jurkat T cells (red). The perturbation of the hydrophobic core allows to modulate positively or negatively this proapoptotic activity (yellow). At the bottom region of the dimer interface, the substitution to alanine of D94 increases the proapoptotic activity of GAL-7 (green) while R14A mutation contributes to a negative synergistic effect with R22A mutation on this Jurkat T cell activity (pink). However, R14A single mutation has no effect on GAL-7 induced T cell apoptosis. (PDB 6VTO)

5.2 Discussion, conclusion and perspectives

In these studies, we demonstrated that interactions involving residues at the dimer interface play a critical role in modulation of GAL-7 proapoptotic activity (Figure 5.1). Interestingly, depending on the residue pair interaction targeted, this proapoptotic activity can be negatively or positively regulated through different molecular mechanisms. Indeed, mutations within the middle region of the dimer interface allows to increase or decrease the GAL-7 proapoptotic activity via controlling the interaction strength between protomers (Pham et al., 2021). Electrostatic alteration

of the top region of the dimer interface only enabled to negatively modulate GAL-7 proapoptotic activity by interrupting protomer-protomer allosteric communication as well as destabilizing homodimer interactions. The substitution of Asp by Ala at position 94 of the bottom region of the dimer interface can enhance or prevent the GAL-7 proapoptotic effect through probably a molecular dynamic regulation of GAL-7 (Ermakova et al., 2013). However, we cannot conclude that targeting the above mentioned positions would specifically increase or decrease the proapoptotic effect of GAL-7 since only few substitutions were tested. For example, we did not evaluate the effect of introducing a covalent bridge, or a substitution of hydrophobic residues to favor hydrophobic interactions at the top or bottom regions of the dimer interface. It is plausible that various type of perturbations at the same position would generate different outcomes on the proapoptotic activity of GAL-7. Overall, targeting positions 20, 22, 103, 16, 94, 14 could allow to modulate the GAL-7 proapoptotic activity with different perturbation trends. The perturbation type favoring destabilization of protomer-protomer interaction would probably reduce the proapoptotic activity of GAL-7.

In a previous study, four DIPs were designed to mimick S β-strands of GAL-7 in order to disrupt GAL-7 homodimerization (Figure 5.2A) (Vladoiu et al., 2015). These peptides encompass residues 13–25 (β-strand S4, IRPGTVLRIRGLV, Figure 5.2A), 86–102 (β-strands S2–S3,FEVLIIASDDGFKAVVG Figure 5.2A), 95–108 (β-strands S1–S2, DGFKAVVGDAQYHH, Figure 5.2A), and 129–135 (β-strand S5, LDSVRIF, Figure 5.2A). However, they are composed of more than 50% hydrophobic residues, and not surprisingly, these peptides encounter low solubility problems that could affect their functional binding to the GAL-7 dimer interface and minimize their effect on GAL-7 activity. Among these DIPs, only $DIP_{129\text{-}135}$ could slightly reduce GAL-7 proapoptotic activity by disrupting GAL-7 homodimerization. In support with this result, the F135S mutation results in protein expression within inclusion bodies most probably due to loss of essential hydrophobic interactions involved in preserving monomer–dimer stability in GAL-7. Nevertheless, an approach to perturb GAL-7 dimerization through DIPs could benefit of results gathered in this study. Since residues R20, R22, G16 and R14, identified as key players of GAL-7, are all located on the S4 β-strand, and D103 is positioned on the loop between β-strands S1–S2 (Figure 5.2A), a new DIP could be designed to comprise these features (β-strands S1–S2 and S4) along with β-strand S5 ($DIP_{129\text{-}135}$) to improve the inhibitory effect on proapoptotic activity of GAL-7. To this end, various peptide chemistry techniques, cyclization reactions or backbone modifications, can allow construction of different peptide scaffolds without altering the critical residues (R20, R22, G16, R14, D103) with the objective to improve effectiveness against protein-protein interaction as well as pharmacological properties (Wang et al., 2021) (Figure 5.2A). For

example, interaction between the two proteins p53 and MDM2 was successfully inhibited by using peptidomimetics termed γ-AA peptides because they are oligomers of γ-substituted amino acids (Sang et al., 2020a, 2020b; Shi et al., 2020). Moreover, starting from a peptide sequence showing desirable binding and pharmacological properties, side chain optimization can be achieved through generation of a small targeted peptide library as it was shown with a peptide-based inhibitor of the APC-Asef interaction to improve its disrupting effectiveness (Yang et al., 2018). Beside optimization of existing peptides, different tools have been developed to support the design of peptide-based drugs such as dTERMen, a computational protein design method using tertiary structural motif energies to identify sequence features that can stabilize a given structural motif, SORTCERY, a high-throughput method for ranking peptide protein affinity, and studies of the data-parameterized protein interaction landscape to generate peptide libraries targeting new regions encompassing critical residues (Frappier et al., 2019; Jenson et al., 2018; Dutta et al., 2015). These tools were part of the approaches used successfully to design high-affinity peptide binders (K_D in nm range) of the anti-apoptotic proteins Bfl-1 and Mcl-1 (Frappier et al., 2019; Jenson et al., 2018; Dutta et al., 2015). Applied to the GAL-7 context of this study, a peptide binding the interface surface that encompasses residues R20, R22, D103 (Figure 5.2B) or R20, R22, D103, G16 and F135 (Figure 5.2C) could be designed to block the interaction between the two protomers.

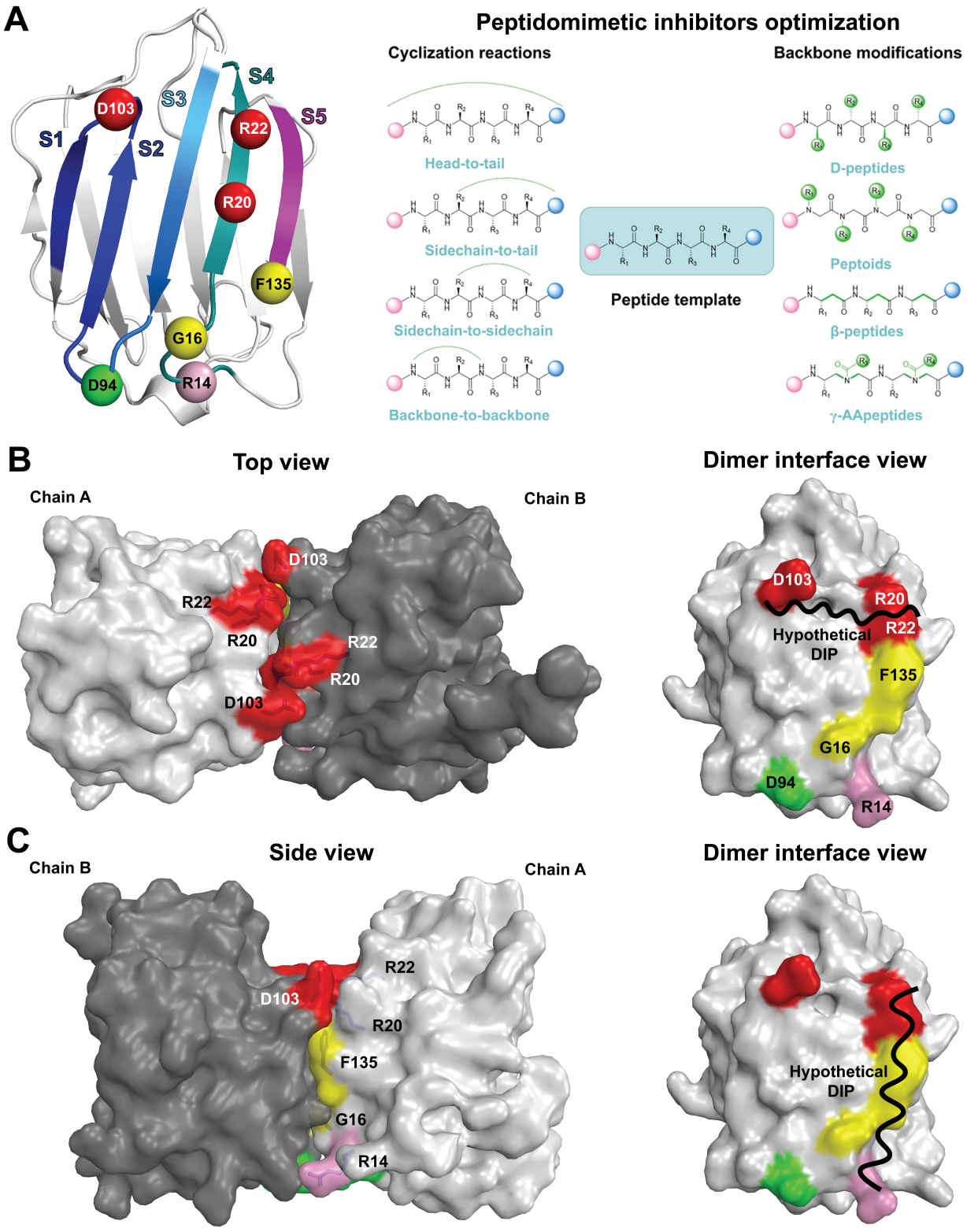

Figure 5.2 Avenues for optimization of DIPs for GAL-7

A. (left side) Localization of previous GAL-7 DIPs sequences on the protein structure highlighted in blue (β-strands S1–S2), marine (β-strands S2–S3), deepteal (β-strands S4), purple (β-strands S5)). Due to sequence overlap between

designed peptides from β-strands S1–S2 and S2-S3, only β-strand S3 of peptide 86–102 is colored marine on the structure. Destabilization of the protomer-protomer interaction at critical residues (spheres) allows to modulate negatively (red, pink, yellow) or positively (green, yellow) the pro-apoptotic activity of GAL-7. (right side) Different methods allow to improve pharmacological properties of peptide targeting protein-protein interactions (adapted from (Wang et al., 2021)). B. Top view of GAL-7 (left side) shows the surface contact between residues R22, R20, and D103 of protomer A (white) and B (grey). Right, dimer interface view indicates hypothetical targeted region to design a novel DIP to disrupt protomer-protomer interaction of GAL-7 by blocking interactions between residues R22, R20, D103 of opposite protomers. C. Face view of GAL-7 (left side) shows the surface contact between residues R22, R20, D103, F135, G16 and R14 of protomer A (white) with protomer B (grey). Right, hypothetical targeted region to design a novel DIP to disrupt protomer-protomer interaction of GAL-7 by blocking contact of R22, R20, D103, F135, G16 and R14 with the surface of the opposite protomer.

Even if we were not able to establish a correlation between lactose binding affinity and a GAL-7 molecular dynamic regulation, it is still possible that a relationship exists between effective GAL-7 binding partners at the T cell membrane surface and molecular dynamics taking place within the protein homodimer. Indeed, lactose is only a subunit of the glycan structures binding on GAL-7 (Noll et al., 2016). Glycan microarrays of GAL-7 showed that GAL-7 binds different glycan motifs (Noll et al., 2016). Results from this study did not highlight differences in lactose binding affinity but it is possible that GAL-7 glycan binding profile was affected by dimer interface mutations, inducing a change of GAL-7 glycosylated-protein lattice organization. Therefore, introduced mutations could affect the proapoptotic activity of GAL-7. Results from a glycan array using the GAL-7 mutants described herein would allow to verify the effect of dimer interface mutations on the binding of GAL-7 to a large variety of sugar moieties. In addition, it is important to acknowledge the fact that the proapoptotic activity of galectins on activated T cells can be induced by binding on different glycosylated cell membrane proteins. For example, GAL-1 induces apoptosis of T cells by binding on CD3, CD7, CD34 and CD45 receptors, while the proapoptotic activity of GAL-3 on T cells is related to interaction with CD7, CD29, CD45 and CD71 receptors (Fukumori et al., 2003; Grigorian et al., 2009; Motran et al., 2008; Pace et al., 1999; Perillo et al., 1995; Rabinovich et al., 2009; Stillman et al., 2006; Toscano et al., 2007). Furthermore, GAL-9 activates apoptosis of T cells by binding to Tim-3 (Zhu et al., 2005).Therefore, it would be valuable to identify the partner(s) of GAL-7 involved in Jurkat T cells apoptosis induction and evaluate the impact of all mutations presented in our studies on the binding affinity with these putative cell membrane protein partners.

Given that we revealed different spots that can modulate positively or negatively activity of GAL-7, the knowledge obtained through this study is not only limited to guide the development of GAL-7 inhibitor for TNBC, but can also applied for all other cancer associated with GAL-7 which can be a pro-tumorigenic (oral skin, thyroid, esophagus, breast, gastric, ovaries, cervix, lymphs) or an anti-tumorigenic (colon, prostate) (Campion et al., 2013; Demers et al., 2007, 2009, 2010; Grosset et al., 2016; Guo et al., 2017; Higareda-Almaraz et al., 2016; Kim et al., 2013; Kuwabara

et al., 2002; Labrie et al., 2014; Moisan et al., 2003; Park et al., 2009; Rorive et al., 2002; Schulz et al., 2017; Wang et al., 2020; Zhu et al., 2013; Zhu et al., 2010). However, in this study, we only tested the ability of GAL-7 to induce apoptosis in Jurkat T cells, one of the mechanisms contributing to the progression TNBC. The behavior of our tested mutants on cancer cells, TBNC or other cancer types, has not been yet evaluated. Such a study would complete our understanding of the impact of homodimer strength, interprotomer communication, protein stability on cellular response. For instance, and in the context of TNBC, it is important to determine if a negative modulation of T-cell apoptosis is associated with a reduced resistance to apoptosis of cancer cells. Proper position targeting to generate galectin inhibitors should induce the desired effect on cancer cells as well as other cell types involved in the pathological state.

For a while, cross-linking of cell surface glycoproteins was demonstrated to be important to regulate multiple cellular processes (cell proliferation, cell differentiation, adhesion, migration, and apoptosis) promoting cancer progression (Boscher et al., 2011; Brewer, 2002; Sacchettini et al., 2001). Our study evidences that by altering the homodimer interaction of GAL-7, the galectin glycoprotein lattice organization at the cell membrane surface might be affected, resulting in changes in GAL-7 proapoptotic activity on Jurkat T cells. Therefore, our results can serve as a proof of concept that modulating protomer-protomer interactions can be the basis for the design of galectin activity inhibitors. A combination of computational analyses, X-ray crystallography, biophysical and biological characterization for identication of critical residues involved in maintaining the homodimeric structure of galectins could offer means to design specific inhibitors of the galectin-glycoprotein interactions at the cell surface. Hence, these approaches could be applied for all prototypic galectins to identify their potential target positions at the dimer interface that control the formation of galectin lattices in the context of cancer regulation. The application might not only be limited to homodimer interactions but could also be extended to non-covalent heterodimer interactions between galectin monomers (Dings et al., 2021a; Miller et al., 2018) as long as prior knowledge of the interacting region was obtained by other structural techniques (X-ray crystallography, NMR, cryo-EM, cross-linking mass spectrometry, etc.).

6 REFERENCES

1. Aboulhagag, N. A., El-Deek, H. E. M., & Sherif, M. F. (2018). Expression of galectin-1 and galectin-3 in renal cell carcinoma; immunohistochemical study. *Annals of Diagnostic Pathology*, *36*, 31–37. https://doi.org/10.1016/j.anndiagpath.2018.06.005
2. Advedissian, T., Deshayes, F., & Viguier, M. (2017a). Galectin-7 in Epithelial Homeostasis and Carcinomas. *International Journal of Molecular Sciences*, *18*(12), 2760. https://doi.org/10.3390/ijms18122760
3. Advedissian, T., Proux-Gillardeaux, V., Nkosi, R., Peyret, G., Nguyen, T., Poirier, F., Viguier, M., & Deshayes, F. (2017b). E-cadherin dynamics is regulated by galectin-7 at epithelial cell surface. *Scientific Reports*, *7*(1), 17086. https://doi.org/10.1038/s41598-017-17332-y
4. Ahmad, N., Gabius, H.-J., André, S., Kaltner, H., Sabesan, S., Roy, R., Liu, B., Macaluso, F., & Brewer, C. F. (2004). Galectin-3 Precipitates as a Pentamer with Synthetic Multivalent Carbohydrates and Forms Heterogeneous Cross-linked Complexes*. *Journal of Biological Chemistry*, *279*(12), 10841–10847. https://doi.org/10.1074/jbc.M312834200
5. Ahmed, H., Du, S.-J., & Vasta, G. R. (2009). Knockdown of a galectin-1-like protein in zebrafish (Danio rerio) causes defects in skeletal muscle development. *Glycoconjugate Journal*, *26*(3), 277–283. https://doi.org/10.1007/s10719-008-9178-9
6. Akahani, S., Nangia-Makker, P., Inohara, H., Kim, H.-R. C., & Raz, A. (1997). Galectin-3: A Novel Antiapoptotic Molecule with A Functional BH1 (NWGR) Domain of Bcl-2 Family. Cancer Research, 57(23), 5272–5276.
7. Ajarrag, S., & St-Pierre, Y. (2021). Galectins in Glioma: Current Roles in Cancer Progression and Future Directions for Improving Treatment. Cancers, 13(21), 5533
8. Almkvist, J., Dahlgren, C., Leffler, H., & Karlsson, A. (2002). Activation of the Neutrophil Nicotinamide Adenine Dinucleotide Phosphate Oxidase by Galectin-1. *The Journal of Immunology*, *168*(8), 4034–4041. https://doi.org/10.4049/jimmunol.168.8.4034
9. Almkvist, J., Fäldt, J., Dahlgren, C., Leffler, H., & Karlsson, A. (2001). Lipopolysaccharide-Induced Gelatinase Granule Mobilization Primes Neutrophils for Activation by Galectin-3 and Formylmethionyl-Leu-Phe. *Infection and Immunity*, *69*(2), 832–837. https://doi.org/10.1128/IAI.69.2.832-837.2001
10. Altman, E., Harrison, B. A., Latta, R. K., Lee, K. K., Kelly, J. F., & Thibault, P. (2001). Galectin-3-mediated adherence of Proteus mirabilis to Madin-Darby canine kidney cells. *Biochemistry and Cell Biology*, *79*(6), 783–788. https://doi.org/10.1139/o01-135

11. Aretz, J., Anumala, U. R., Fuchsberger, F. F., Molavi, N., Ziebart, N., Zhang, H., Nazaré, M., & Rademacher, C. (2018). Allosteric Inhibition of a Mammalian Lectin. *Journal of the American Chemical Society*, *140*(44), 14915–14925. https://doi.org/10.1021/jacs.8b08644
12. Arthur, C. M., Baruffi, M. D., Cummings, R. D., & Stowell, S. R. (2015). Evolving mechanistic insights into galectin functions. *Methods in Molecular Biology (Clifton, N.J.)*, *1207*, 1–35. https://doi.org/10.1007/978-1-4939-1396-1_1
13. Ayona, D., Fournier, P.-E., Henrissat, B., & Desnues, B. (2020). Utilization of Galectins by Pathogens for Infection. *Frontiers in Immunology*, *11*, 1877. https://doi.org/10.3389/fimmu.2020.01877
14. Bacigalupo, M. L., Manzi, M., Espelt, M. V., Gentilini, L. D., Compagno, D., Laderach, D. J., Wolfenstein-Todel, C., Rabinovich, G. A., & Troncoso, M. F. (2015). Galectin-1 Triggers Epithelial-Mesenchymal Transition in Human Hepatocellular Carcinoma Cells. *Journal of Cellular Physiology*, *230*(6), 1298–1309. https://doi.org/10.1002/jcp.24865
15. Baker, G. J., Chockley, P., Yadav, V. N., Doherty, R., Ritt, M., Sivaramakrishnan, S., Castro, M. G., & Lowenstein, P. R. (2014). Natural Killer Cells Eradicate Galectin-1–Deficient Glioma in the Absence of Adaptive Immunity. *Cancer Research*, *74*(18), 5079–5090. https://doi.org/10.1158/0008-5472.CAN-14-1203
16. Barondes, S. H., Castronovo, V., Cooper, D. N., Cummings, R. D., Drickamer, K., Feizi, T., ... & Kasai, K. I. (1994). Galectins: a family of animal beta-galactoside-binding lectins. Cell, 76(4), 597-8
17. Barrionuevo, P., Beigier-Bompadre, M., Ilarregui, J. M., Toscano, M. A., Bianco, G. A., Isturiz, M. A., & Rabinovich, G. A. (2007). A Novel Function for Galectin-1 at the Crossroad of Innate and Adaptive Immunity: Galectin-1 Regulates Monocyte/Macrophage Physiology through a Nonapoptotic ERK-Dependent Pathway. *The Journal of Immunology*, *178*(1), 436–445. https://doi.org/10.4049/jimmunol.178.1.436
18. Barrow, H., Guo, X., Wandall, H. H., Pedersen, J. W., Fu, B., Zhao, Q., Chen, C., Rhodes, J. M., & Yu, L.-G. (2011). Serum Galectin-2, -4, and -8 Are Greatly Increased in Colon and Breast Cancer Patients and Promote Cancer Cell Adhesion to Blood Vascular Endothelium. *Clinical Cancer Research*, *17*(22), 7035–7046. https://doi.org/10.1158/1078-0432.CCR-11-1462
19. Belo, A. I., van der Sar, A. M., Tefsen, B., & van Die, I. (2013). Galectin-4 Reduces Migration and Metastasis Formation of Pancreatic Cancer Cells. *PloS One*, *8*(6), e65957. https://doi.org/10.1371/journal.pone.0065957

20. Bhaumik, P., St-Pierre, G., Milot, V., St-Pierre, C., & Sato, S. (2013). Galectin-3 Facilitates Neutrophil Recruitment as an Innate Immune Response to a Parasitic Protozoa Cutaneous Infection. *The Journal of Immunology*, *190*(2), 630–640. https://doi.org/10.4049/jimmunol.1103197

21. Blaževitš, O., Mideksa, Y. G., Šolman, M., Ligabue, A., Ariotti, N., Nakhaeizadeh, H., Fansa, E. K., Papageorgiou, A. C., Wittinghofer, A., Ahmadian, M. R., & Abankwa, D. (2016). Galectin-1 dimers can scaffold Raf-effectors to increase H-ras nanoclustering. *Scientific Reports*, *6*(1), 24165. https://doi.org/10.1038/srep24165

22. Blois, S. M., Ilarregui, J. M., Tometten, M., Garcia, M., Orsal, A. S., Cordo-Russo, R., Toscano, M. A., Bianco, G. A., Kobelt, P., Handjiski, B., Tirado, I., Markert, U. R., Klapp, B. F., Poirier, F., Szekeres-Bartho, J., Rabinovich, G. A., & Arck, P. C. (2007). A pivotal role for galectin-1 in fetomaternal tolerance. *Nature Medicine*, *13*(12), 1450–1457. https://doi.org/10.1038/nm1680

23. Bojić-Trbojević, Ž., Jovanović Krivokuća, M., Vilotić, A., Kolundžić, N., Stefanoska, I., Zetterberg, F., Nilsson, U. J., Leffler, H., & Vićovac, L. (2019). Human trophoblast requires galectin-3 for cell migration and invasion. *Scientific Reports*, *9*(1), 2136. https://doi.org/10.1038/s41598-018-38374-w

24. Borrok, M. J., & Kiessling, L. L. (2007). Non-carbohydrate Inhibitors of the Lectin DC-SIGN. *Journal of the American Chemical Society*, *129*(42), 12780–12785. https://doi.org/10.1021/ja072944v

25. Boscher, C., Dennis, J. W., & Nabi, I. R. (2011). Glycosylation, galectins and cellular signaling. *Current Opinion in Cell Biology*, *23*(4), 383–392. https://doi.org/10.1016/j.ceb.2011.05.001

26. Brinda, K. V., Surolia, A., & Vishveshwara, S. (2005). Insights into the quaternary association of proteins through structure graphs: A case study of lectins. *Biochemical Journal*, *391*(1), 1–15. Scopus. https://doi.org/10.1042/BJ20050434

27. Cai, Z., Zeng, Y., Xu, B., Gao, Y., Wang, S., Zeng, J., Chen, L., Huang, A., Liu, X., & Liu, J. (2014). Galectin-4 serves as a prognostic biomarker for the early recurrence / metastasis of hepatocellular carcinoma. *Cancer Science*, *105*(11), 1510–1517. https://doi.org/10.1111/cas.12536

28. Campion, C. G., Labrie, M., Grosset, A.-A., & St-Pierre, Y. (2014). The CCAAT/Enhancer-Binding Protein Beta-2 Isoform (CEBPβ-2) Upregulates Galectin-7 Expression in Human Breast Cancer Cells. *PLOS ONE*, *9*(5), e95087. https://doi.org/10.1371/journal.pone.0095087

29. Campion, C. G., Labrie, M., Lavoie, G., & St-Pierre, Y. (2013). Expression of Galectin-7 Is Induced in Breast Cancer Cells by Mutant p53. *PLOS ONE*, *8*(8), e72468. https://doi.org/10.1371/journal.pone.0072468

30. Cao, A., Alluqmani, N., Buhari, F. H. M., Wasim, L., Smith, L. K., Quaile, A. T., Shannon, M., Hakim, Z., Furmli, H., Owen, D. M., Savchenko, A., & Treanor, B. (2018). Galectin-9 binds IgM-BCR to regulate B cell signaling. *Nature Communications*, *9*(1), 3288. https://doi.org/10.1038/s41467-018-05771-8

31. Cao, Z., Said, N., Amin, S., Wu, H. K., Bruce, A., Garate, M., Hsu, D. K., Kuwabara, I., Liu, F.-T., & Panjwani, N. (2002). Galectins-3 and -7, but not Galectin-1, Play a Role in Re-epithelialization of Wounds *. *Journal of Biological Chemistry*, *277*(44), 42299–42305. https://doi.org/10.1074/jbc.M200981200

32. Cao, Z., Said, N., Wu, H. K., Kuwabara, I., Liu, F.-T., & Panjwani, N. (2003). Galectin-7 as a Potential Mediator of Corneal Epithelial Cell Migration. *Archives of Ophthalmology*, *121*(1), 82–86. https://doi.org/10.1001/archopht.121.1.82

33. Cedeno-Laurent, F., Opperman, M. J., Barthel, S. R., Hays, D., Schatton, T., Zhan, Q., He, X., Matta, K. L., Supko, J. G., Frank, M. H., Murphy, G. F., & Dimitroff, C. J. (2012). Metabolic Inhibition of Galectin-1-Binding Carbohydrates Accentuates Antitumor Immunity. *Journal of Investigative Dermatology*, *132*(2), 410–420. https://doi.org/10.1038/jid.2011.335

34. Charroux, B., Pellizzoni, L., Perkinson, R. A., Yong, J., Shevchenko, A., Mann, M., & Dreyfuss, G. (2000). Gemin4: A Novel Component of the Smn Complex That Is Found in Both Gems and Nucleoli. *Journal of Cell Biology*, *148*(6), 1177–1186. https://doi.org/10.1083/jcb.148.6.1177

35. Chauhan, S., Kumar, S., Jain, A., Ponpuak, M., Mudd, M. H., Kimura, T., Choi, S. W., Peters, R., Mandell, M., Bruun, J.-A., Johansen, T., & Deretic, V. (2016). TRIMs and Galectins Globally Cooperate and TRIM16 and Galectin-3 Co-direct Autophagy in Endomembrane Damage Homeostasis. *Developmental Cell*, *39*(1), 13–27. https://doi.org/10.1016/j.devcel.2016.08.003

36. Chen, H.-L., Chiang, P.-C., Lo, C.-H., Lo, Y.-H., Hsu, D. K., Chen, H.-Y., & Liu, F.-T. (2016). Galectin-7 Regulates Keratinocyte Proliferation and Differentiation through JNK-miR-203-p63 Signaling. *Journal of Investigative Dermatology*, *136*(1), 182–191. https://doi.org/10.1038/JID.2015.366

37. Chen, H.-Y., Fermin, A., Vardhana, S., Weng, I.-C., Lo, K. F. R., Chang, E.-Y., Maverakis, E., Yang, R.-Y., Hsu, D. K., Dustin, M. L., & Liu, F.-T. (2009). Galectin-3 negatively

regulates TCR-mediated CD4+ T-cell activation at the immunological synapse. *Proceedings of the National Academy of Sciences*, *106*(34), 14496–14501. https://doi.org/10.1073/pnas.0903497106

38. Chen, L., Deng, H., Cui, H., Fang, J., Zuo, Z., Deng, J., Li, Y., Wang, X., & Zhao, L. (2017). Inflammatory responses and inflammation-associated diseases in organs. *Oncotarget*, *9*(6), 7204–7218. https://doi.org/10.18632/oncotarget.23208
39. Chen, Y., Zhou, J., Cheng, Z., Yang, S., Chu, H., Fan, Y., Li, C., Wong, B. H.-Y., Zheng, S., Zhu, Y., Yu, F., Wang, Y., Liu, X., Gao, H., Yu, L., Tang, L., Cui, D., Hao, K., Bossé, Y., … Li, L. (2015). Functional variants regulating LGALS1 (Galectin 1) expression affect human susceptibility to influenza A(H7N9). *Scientific Reports*, *5*(1), 8517. https://doi.org/10.1038/srep08517
40. Chen, Y.-S., Chang, C.-W., Tsay, Y.-G., Huang, L.-Y., Wu, Y.-C., Cheng, L.-H., Yang, C.-C., Wu, C.-H., Teo, W.-H., Hung, K.-F., Huang, C.-Y., Lee, T.-C., & Lo, J.-F. (2018). HSP40 co-chaperone protein Tid1 suppresses metastasis of head and neck cancer by inhibiting Galectin-7-TCF3-MMP9 axis signaling. *Theranostics*, *8*(14), 3841–3855. https://doi.org/10.7150/thno.25784
41. Chernyy, E. S., Rapoport, E. M., Andre, S., Kaltner, H., Gabius, H.-J., & Bovin, N. V. (2011). Galectins promote the interaction of influenza virus with its target cell. *Biochemistry (Moscow)*, *76*(8), 958. https://doi.org/10.1134/S0006297911080128
42. Chou, F.-C., Chen, H.-Y., Kuo, C.-C., & Sytwu, H.-K. (2018). Role of Galectins in Tumors and in Clinical Immunotherapy. *International Journal of Molecular Sciences*, *19*(2), 430. https://doi.org/10.3390/ijms19020430
43. Chun, S.-J. K. & K.-H. (2020). Non-classical role of Galectin-3 in cancer progression: Translocation to nucleus by carbohydrate-recognition independent manner. *BMB Reports*, *53*(4), 173–180. https://doi.org/10.5483/BMBRep.2020.53.4.020
44. Clark, M. C., Pang, M., Hsu, D. K., Liu, F.-T., de Vos, S., Gascoyne, R. D., Said, J., & Baum, L. G. (2012). Galectin-3 binds to CD45 on diffuse large B-cell lymphoma cells to regulate susceptibility to cell death. *Blood*, *120*(23), 4635–4644. https://doi.org/10.1182/blood-2012-06-438234
45. Compagno, D., Tiraboschi, C., Garcia, J. D., Rondón, Y., Corapi, E., Velazquez, C., & Laderach, D. J. (2020). Galectins as checkpoints of the immune system in cancers, their clinical relevance, and implication in clinical trials. Biomolecules, 10(5), 750

46. Cooper, D. N. W. (2002). Galectinomics: Finding themes in complexity. *Biochimica et Biophysica Acta (BBA) - General Subjects*, *1572*(2), 209–231. https://doi.org/10.1016/S0304-4165(02)00310-0

47. Cooper, D., Norling, L. V., & Perretti, M. (2008). Novel insights into the inhibitory effects of Galectin-1 on neutrophil recruitment under flow. *Journal of Leukocyte Biology*, *83*(6), 1459–1466. https://doi.org/10.1189/jlb.1207831

48. Cortegano, I., Pozo, V. del, Cárdaba, B., Andrés, B. de, Gallardo, S., Amo, A. del, Arrieta, I., Jurado, A., Palomino, P., Liu, F.-T., & Lahoz, C. (1998). Galectin-3 Down-Regulates IL-5 Gene Expression on Different Cell Types. *The Journal of Immunology*, *161*(1), 385–389.

49. Cummings, R. D., Liu, F.-T., & Vasta, G. R. (2015). Galectins. In A. Varki, R. D. Cummings, J. D. Esko, P. Stanley, G. W. Hart, M. Aebi, A. G. Darvill, T. Kinoshita, N. H. Packer, J. H. Prestegard, R. L. Schnaar, & P. H. Seeberger (Eds.), *Essentials of Glycobiology* (3rd ed.). Cold Spring Harbor Laboratory Press. http://www.ncbi.nlm.nih.gov/books/NBK453091/

50. Cumpstey, I., Carlsson, S., Leffler, H., & Nilsson, U. J. (2005). Synthesis of a phenyl thio-β-D-galactopyranoside library from 1,5-difluoro-2,4-dinitrobenzene: Discovery of efficient and selective monosaccharide inhibitors of galectin-7. *Organic & Biomolecular Chemistry*, *3*(10), 1922–1932. https://doi.org/10.1039/B502354H

51. Dagher, S. F., Wang, J. L., & Patterson, R. J. (1995). Identification of galectin-3 as a factor in pre-mRNA splicing. *Proceedings of the National Academy of Sciences*, *92*(4), 1213–1217. https://doi.org/10.1073/pnas.92.4.1213

52. Dai, S.-Y., Nakagawa, R., Itoh, A., Murakami, H., Kashio, Y., Abe, H., Katoh, S., Kontani, K., Kihara, M., Zhang, S.-L., Hata, T., Nakamura, T., Yamauchi, A., & Hirashima, M. (2005). Galectin-9 Induces Maturation of Human Monocyte-Derived Dendritic Cells. *The Journal of Immunology*, *175*(5), 2974–2981. https://doi.org/10.4049/jimmunol.175.5.2974

53. Debierre-Grockiego, F., Niehus, S., Coddeville, B., Elass, E., Poirier, F., Weingart, R., Schmidt, R. R., Mazurier, J., Guérardel, Y., & Schwarz, R. T. (2010). Binding of Toxoplasma gondii Glycosylphosphatidylinositols to Galectin-3 Is Required for Their Recognition by Macrophages *. *Journal of Biological Chemistry*, *285*(43), 32744–32750. https://doi.org/10.1074/jbc.M110.137588

54. Delacour, D., Gouyer, V., Zanetta, J.-P., Drobecq, H., Leteurtre, E., Grard, G., Moreau-Hannedouche, O., Maes, E., Pons, A., André, S., Le Bivic, A., Gabius, H. J., Manninen, A., Simons, K., & Huet, G. (2005). Galectin-4 and sulfatides in apical membrane trafficking in enterocyte-like cells. *Journal of Cell Biology*, *169*(3), 491–501. https://doi.org/10.1083/jcb.200407073

55. Delgado, V. M. C., Nugnes, L. G., Colombo, L. L., Troncoso, M. F., Fernández, M. M., Malchiodi, E. L., Frahm, I., Croci, D. O., Compagno, D., Rabinovich, G. A., Wolfenstein-Todel, C., & Elola, M. T. (2011). Modulation of endothelial cell migration and angiogenesis: A novel function for the “tandem-repeat” lectin galectin-8. *The FASEB Journal*, *25*(1), 242–254. https://doi.org/10.1096/fj.09-144907

56. Demers, M., Biron-Pain, K., Hébert, J., Lamarre, A., Magnaldo, T., & St-Pierre, Y. (2007). Galectin-7 in Lymphoma: Elevated Expression in Human Lymphoid Malignancies and Decreased Lymphoma Dissemination by Antisense Strategies in Experimental Model. *Cancer Research*, *67*(6), 2824–2829. https://doi.org/10.1158/0008-5472.CAN-06-3891

57. Demers, M., Couillard, J., Giglia-Mari, G., Magnaldo, T., & St-Pierre, Y. (2009). Increased galectin-7 gene expression in lymphoma cells is under the control of DNA methylation. *Biochemical and Biophysical Research Communications*, *387*(3), 425–429. https://doi.org/10.1016/j.bbrc.2009.07.015

58. Demers, M., Magnaldo, T., & St-Pierre, Y. (2005). A Novel Function for Galectin-7: Promoting Tumorigenesis by Up-regulating MMP-9 Gene Expression. *Cancer Research*, *65*(12), 5205–5210. https://doi.org/10.1158/0008-5472.CAN-05-0134

59. Demers, M., Rose, A. A. N., Grosset, A.-A., Biron-Pain, K., Gaboury, L., Siegel, P. M., & St-Pierre, Y. (2010). Overexpression of Galectin-7, A Myoepithelial Cell Marker, Enhances Spontaneous Metastasis of Breast Cancer Cells. *The American Journal of Pathology*, *176*(6), 3023–3031. https://doi.org/10.2353/ajpath.2010.090876

60. Demetriou, M., Granovsky, M., Quaggin, S., & Dennis, J. W. (2001). Negative regulation of T-cell activation and autoimmunity by Mgat5 N-glycosylation. *Nature*, *409*(6821), 733–739. https://doi.org/10.1038/35055582

61. Denavit, V., Lainé, D., Tremblay, T., St-Gelais, J., & Giguère, D. (2018). Synthetic Inhibitors of Galectins: Structures and Syntheses. *Trends in Glycoscience and Glycotechnology*, *30*(172), SE21–SE40. https://doi.org/10.4052/tigg.1729.1SE

62. D’Haene, N., Sauvage, S., Maris, C., Adanja, I., Mercier, M. L., Decaestecker, C., Baum, L., & Salmon, I. (2013). VEGFR1 and VEGFR2 Involvement in Extracellular Galectin-1- and Galectin-3-Induced Angiogenesis. *PLOS ONE*, *8*(6), e67029. https://doi.org/10.1371/journal.pone.0067029

63. Diehl, R. C. (2021). *CH-[pi] interactions play a central role in protein recognition of carbohydrates/* [Thesis, Massachusetts Institute of Technology]. https://dspace.mit.edu/handle/1721.1/130817

64. Dings, R. P. M., Miller, M. C., Nesmelova, I., Astorgues-Xerri, L., Kumar, N., Serova, M., Chen, X., Raymond, E., Hoye, T. R., & Mayo, K. H. (2012). Antitumor Agent Calixarene 0118 Targets Human Galectin-1 as an Allosteric Inhibitor of Carbohydrate Binding. *Journal of Medicinal Chemistry*, *55*(11), 5121–5129. https://doi.org/10.1021/jm300014q

65. Dings, R. P., Kumar, N., Mikkelson, S., Gabius, H. J., & Mayo, K. H. (2021). Simulating cellular galectin networks by mixing galectins in vitro reveals synergistic activity. Biochemistry and Biophysics Reports, 28, 101116

66. Domogalla, M. P., Rostan, P. V., Raker, V. K., & Steinbrink, K. (2017). Tolerance through Education: How Tolerogenic Dendritic Cells Shape Immunity. *Frontiers in Immunology*, *8*, 1764. https://doi.org/10.3389/fimmu.2017.01764

67. Dubé-Delarosbil, C., & St-Pierre, Y. (2018). The emerging role of galectins in high-fatality cancers. *Cellular and Molecular Life Sciences*, *75*(7), 1215–1226. https://doi.org/10.1007/s00018-017-2708-5

68. Dutta, S., & Keating, A. E. (2015). SORTCERY—a high–throughput method to affinity rank peptide ligands. Journal of molecular biology, 427(11), 2135-2150

69. Elad-Sfadia, G., Haklai, R., Balan, E., & Kloog, Y. (2004). Galectin-3 Augments K-Ras Activation and Triggers a Ras Signal That Attenuates ERK but Not Phosphoinositide 3-Kinase Activity *. *Journal of Biological Chemistry*, *279*(33), 34922–34930. https://doi.org/10.1074/jbc.M312697200

70. Elantak, L., Espeli, M., Boned, A., Bornet, O., Bonzi, J., Gauthier, L., Feracci, M., Roche, P., Guerlesquin, F., & Schiff, C. (2012). Structural Basis for Galectin-1-dependent Pre-B Cell Receptor (Pre-BCR) Activation *. *Journal of Biological Chemistry*, *287*(53), 44703–44713. https://doi.org/10.1074/jbc.M112.395152

71. Ermakova, E., Miller, M. C., Nesmelova, I. V., López-Merino, L., Berbís, M. A., Nesmelov, Y., Tkachev, Y. V., Lagartera, L., Daragan, V. A., André, S., Cañada, F. J., Jiménez-Barbero, J., Solís, D., Gabius, H.-J., & Mayo, K. H. (2013). Lactose binding to human galectin-7 (p53-induced gene 1) induces long-range effects through the protein resulting in increased dimer stability and evidence for positive cooperativity. *Glycobiology*, *23*(5), 508–523. https://doi.org/10.1093/glycob/cwt005

72. Espeli, M., Mancini, S. J. C., Breton, C., Poirier, F., & Schiff, C. (2009). Impaired B-cell development at the pre-BII-cell stage in galectin-1–deficient mice due to inefficient pre-BII/stromal cell interactions. *Blood*, *113*(23), 5878–5886. https://doi.org/10.1182/blood-2009-01-198465

73. Fang, Q., Ni, R., Xiao, M., Jiang, F., & Lu, C. (2011). [Serum and tissue expressions of galectin-3 in hepatocellular carcinoma and the clinical significances]. *Zhonghua Gan Zang Bing Za Zhi = Zhonghua Ganzangbing Zazhi = Chinese Journal of Hepatology*, *19*(7), 527–531. https://doi.org/10.3760/cma.j.issn.1007-3418.2011.07.014

74. Farnworth, S. L., Henderson, N. C., MacKinnon, A. C., Atkinson, K. M., Wilkinson, T., Dhaliwal, K., Hayashi, K., Simpson, A. J., Rossi, A. G., Haslett, C., & Sethi, T. (2008). Galectin-3 Reduces the Severity of Pneumococcal Pneumonia by Augmenting Neutrophil Function. *The American Journal of Pathology*, *172*(2), 395–405. https://doi.org/10.2353/ajpath.2008.070870

75. Feeley, E. M., Pilla-Moffett, D. M., Zwack, E. E., Piro, A. S., Finethy, R., Kolb, J. P., Martinez, J., Brodsky, I. E., & Coers, J. (2017). Galectin-3 directs antimicrobial guanylate binding proteins to vacuoles furnished with bacterial secretion systems. *Proceedings of the National Academy of Sciences*, *114*(9), E1698–E1706. https://doi.org/10.1073/pnas.1615771114

76. Forrest, M. P., Hill, M. J., Quantock, A. J., Martin-Rendon, E., & Blake, D. J. (2014). The emerging roles of TCF4 in disease and development. *Trends in Molecular Medicine*, *20*(6), 322–331. https://doi.org/10.1016/j.molmed.2014.01.010

77. Fouillit, M., Joubert-Caron, R., Poirier, F., Bourin, P., Monostori, E., Levi-Strauss, M., Raphael, M., Bladier, D., & Caron, M. (2000). Regulation of CD45-induced signaling by galectin-1 in Burkitt lymphoma B cells. *Glycobiology*, *10*(4), 413–419. https://doi.org/10.1093/glycob/10.4.413

78. Fowler, M., Thomas, R. J., Atherton, J., Roberts, I. S., & High, N. J. (2006). Galectin-3 binds to Helicobacter pylori O-antigen: It is upregulated and rapidly secreted by gastric epithelial cells in response to H. pylori adhesion. *Cellular Microbiology*, *8*(1), 44–54. https://doi.org/10.1111/j.1462-5822.2005.00599.x

79. Frappier, V., Jenson, J. M., Zhou, J., Grigoryan, G., & Keating, A. E. (2019). Tertiary structural motif sequence statistics enable facile prediction and design of peptides that bind anti-apoptotic Bfl-1 and Mcl-1. Structure, 27(4), 606-617.

80. Fred Brewer, C. (2002). Binding and cross-linking properties of galectins. *Biochimica et Biophysica Acta (BBA) - General Subjects*, *1572*(2), 255–262. https://doi.org/10.1016/S0304-4165(02)00312-4

81. Fukumori, T., Takenaka, Y., Yoshii, T., Kim, H. R. C., Hogan, V., Inohara, H., ... & Raz, A. (2003). CD29 and CD7 mediate galectin-3-induced type II T-cell apoptosis. Cancer research, 63(23), 8302-8311

82. Fukumori, T., Takenaka, Y., Oka, N., Yoshii, T., Hogan, V., Inohara, H., Kanayama, H., Kim, H.-R. C., & Raz, A. (2004). Endogenous Galectin-3 Determines the Routing of CD95 Apoptotic Signaling Pathways. *Cancer Research*, *64*(10), 3376–3379. https://doi.org/10.1158/0008-5472.CAN-04-0336

83. Fukushi, J., Makagiansar, I. T., & Stallcup, W. B. (2004). NG2 Proteoglycan Promotes Endothelial Cell Motility and Angiogenesis via Engagement of Galectin-3 and α3β1 Integrin. *Molecular Biology of the Cell*, *15*(8), 3580–3590. https://doi.org/10.1091/mbc.e04-03-0236

84. Garner, O. B., Yun, T., Pernet, O., Aguilar, H. C., Park, A., Bowden, T. A., Freiberg, A. N., Lee, B., & Baum, L. G. (2014). Timing of Galectin-1 Exposure Differentially Modulates Nipah Virus Entry and Syncytium Formation in Endothelial Cells. *Journal of Virology*. https://journals.asm.org/doi/abs/10.1128/JVI.02435-14

85. Gauthier, S., Pelletier, I., Ouellet, M., Vargas, A., Tremblay, M. J., Sato, S., & Barbeau, B. (2008). Induction of galectin-1 expression by HTLV-I Tax and its impact on HTLV-I infectivity. *Retrovirology*, *5*(1), 105. https://doi.org/10.1186/1742-4690-5-105

86. Gauthier, L., Rossi, B., Roux, F., Termine, E., & Schiff, C. (2002). Galectin-1 is a stromal cell ligand of the pre-B cell receptor (BCR) implicated in synapse formation between pre-B and stromal cells and in pre-BCR triggering. Proceedings of the National Academy of Sciences, 99(20), 13014-13019

87. Gendronneau, G., Sanii, S., Dang, T., Deshayes, F., Delacour, D., Pichard, E., Advedissian, T., Sidhu, S. S., Viguier, M., Magnaldo, T., & Poirier, F. (2015). Overexpression of Galectin-7 in Mouse Epidermis Leads to Loss of Cell Junctions and Defective Skin Repair. *PLOS ONE*, *10*(3), e0119031. https://doi.org/10.1371/journal.pone.0119031

88. Gendronneau, G., Sidhu, S. S., Delacour, D., Dang, T., Calonne, C., Houzelstein, D., Magnaldo, T., & Poirier, F. (2008). Galectin-7 in the Control of Epidermal Homeostasis after Injury. *Molecular Biology of the Cell*, *19*(12), 5541–5549. https://doi.org/10.1091/mbc.e08-02-0166

89. Georgiadis, V., Stewart, H. J. S., Pollard, H. J., Tavsanoglu, Y., Prasad, R., Horwood, J., Deltour, L., Goldring, K., Poirier, F., & Lawrence-Watt, D. J. (2007). Lack of galectin-1 results in defects in myoblast fusion and muscle regeneration. *Developmental Dynamics*, *236*(4), 1014–1024. https://doi.org/10.1002/dvdy.21123

90. Gheysen, L., Soumoy, L., Trelcat, A., Verset, L., Journe, F., & Saussez, S. (2021). New Treatment Strategy Targeting Galectin-1 against Thyroid Cancer. *Cells*, *10*(5), 1112. https://doi.org/10.3390/cells10051112

91. Giovannone, N., Liang, J., Antonopoulos, A., Geddes Sweeney, J., King, S. L., Pochebit, S. M., Bhattacharyya, N., Lee, G. S., Dell, A., Widlund, H. R., Haslam, S. M., & Dimitroff, C. J. (2018a). Galectin-9 suppresses B cell receptor signaling and is regulated by I-branching of N-glycans. *Nature Communications*, *9*(1), 3287. https://doi.org/10.1038/s41467-018-05770-9

92. Giovannone, N., Smith, L. K., Treanor, B., & Dimitroff, C. J. (2018b). Galectin-Glycan Interactions as Regulators of B Cell Immunity. *Frontiers in Immunology*, *9*, 2839. https://doi.org/10.3389/fimbmu.2018.02839

93. Girard, A., & Magnani, J. L. (2018). Clinical Trials and Applications of Galectin Antagonists. *Trends in Glycoscience and Glycotechnology*, *30*(172), SE211–SE220. https://doi.org/10.4052/tigg.1744.1SE

94. Girotti, M. R., Salatino, M., Dalotto-Moreno, T., & Rabinovich, G. A. (2019). Sweetening the hallmarks of cancer: Galectins as multifunctional mediators of tumor progression. *Journal of Experimental Medicine*, *217*(2). https://doi.org/10.1084/jem.20182041

95. Gonzalez, M. I., Rubinstein, N., Ilarregui, J. M., Toscano, M. A., Sanjuan, N. A., & Rabinovich, G. A. (2005). Regulated Expression of Galectin-1 after In Vitro Productive Infection with Herpes Simplex Virus Type I: Implications for T Cell Apoptosis. *International Journal of Immunopathology and Pharmacology*, *18*(4), 615–623. https://doi.org/10.1177/039463200501800402

96. Gordon-Alonso, M., Hirsch, T., Wildmann, C., & van der Bruggen, P. (2017). Galectin-3 captures interferon-gamma in the tumor matrix reducing chemokine gradient production and T-cell tumor infiltration. *Nature Communications*, *8*(1), 793. https://doi.org/10.1038/s41467-017-00925-6

97. Gordon-Weeks, A., & Yuzhalin, A. E. (2020). Cancer extracellular matrix proteins regulate tumour immunity. Cancers, 12(11), 3331

98. Grigorian, A., Torossian, S., & Demetriou, M. (2009). T-cell growth, cell surface organization, and the galectin–glycoprotein lattice. Immunological reviews, 230(1), 232-246

99. Grosset, A.-A., Labrie, M., Gagné, D., Vladoiu, M.-C., Gaboury, L., Doucet, N., & St-Pierre, Y. (2014). Cytosolic galectin-7 impairs p53 functions and induces chemoresistance in breast cancer cells. *BMC Cancer*, *14*(1), 801. https://doi.org/10.1186/1471-2407-14-801

100. Grosset, A.-A., Labrie, M., Vladoiu, M. C., Yousef, E. M., Gaboury, L., & St-Pierre, Y. (2016). Galectin signatures contribute to the heterogeneity of breast cancer and provide new prognostic information and therapeutic targets. *Oncotarget*, *7*(14), 18183–18203. https://doi.org/10.18632/oncotarget.7784

101. Guo, J., & Zhou, H.-X. (2016). Protein Allostery and Conformational Dynamics. *Chemical Reviews*, *116*(11), 6503–6515. https://doi.org/10.1021/acs.chemrev.5b00590

102. Guo, J.-P., & Li, X.-G. (2017). Galectin-7 promotes the invasiveness of human oral squamous cell carcinoma cells via activation of ERK and JNK signaling. *Oncology Letters*, *13*(3), 1919–1924. https://doi.org/10.3892/ol.2017.5649

103. Gupta, S. K., Masinick, S., Garrett, M., & Hazlett, L. D. (1997). Pseudomonas aeruginosa lipopolysaccharide binds galectin-3 and other human corneal epithelial proteins. *Infection and Immunity*, *65*(7), 2747–2753. https://doi.org/10.1128/iai.65.7.2747-2753.1997

104. Hadari, Y. R., Arbel-Goren, R., Levy, Y., Amsterdam, A., Alon, R., Zakut, R., & Zick, Y. (2000). Galectin-8 binding to integrins inhibits cell adhesion and induces apoptosis. *Journal of Cell Science*, *113*(13), 2385–2397. https://doi.org/10.1242/jcs.113.13.2385

105. Harazono, Y., Kho, D. H., Balan, V., Nakajima, K., Zhang, T., Hogan, V., & Raz, A. (2014). Galectin-3 leads to attenuation of apoptosis through Bax heterodimerization in human thyroid carcinoma cells. *Oncotarget*, *5*(20), 9992–10001. https://doi.org/10.18632/oncotarget.2486

106. Haudek, K. C., Spronk, K. J., Voss, P. G., Patterson, R. J., Wang, J. L., & Arnoys, E. J. (2010). Dynamics of galectin-3 in the nucleus and cytoplasm. *Biochimica et Biophysica Acta (BBA) - General Subjects*, *1800*(2), 181–189. https://doi.org/10.1016/j.bbagen.2009.07.005

107. Hayashi, T., Saito, T., Fujimura, T., Hara, K., Takamochi, K., Mitani, K., Mineki, R., Kazuno, S., Oh, S., Ueno, T., Suzuki, K., & Yao, T. (2013). Galectin-4, a Novel Predictor for Lymph Node Metastasis in Lung Adenocarcinoma. *PLOS ONE*, *8*(12), e81883. https://doi.org/10.1371/journal.pone.0081883

108. Higareda-Almaraz, J. C., Ruiz-Moreno, J. S., Klimentova, J., Barbieri, D., Salvador-Gallego, R., Ly, R., Valtierra-Gutierrez, I. A., Dinsart, C., Rabinovich, G. A., Stulik, J., Rösl, F., & Rincon-Orozco, B. (2016). Systems-level effects of ectopic galectin-7 reconstitution in cervical cancer and its microenvironment. *BMC Cancer*, *16*(1), 680. https://doi.org/10.1186/s12885-016-2700-8

109. Hokama, A., Mizoguchi, E., Sugimoto, K., Shimomura, Y., Tanaka, Y., Yoshida, M., Rietdijk, S. T., de Jong, Y. P., Snapper, S. B., Terhorst, C., Blumberg, R. S., & Mizoguchi,

A. (2004). Induced Reactivity of Intestinal CD4+ T Cells with an Epithelial Cell Lectin, Galectin-4, Contributes to Exacerbation of Intestinal Inflammation. *Immunity*, *20*(6), 681–693. https://doi.org/10.1016/j.immuni.2004.05.009

110. Hong, M.-H., Lin, W.-H., Weng, I.-C., Hung, Y.-H., Chen, H.-L., Chen, H.-Y., Chen, P., Lin, C.-H., Yang, W. Y., & Liu, F.-T. (2019). Intracellular galectins control cellular responses commensurate with cell surface carbohydrate composition. *Glycobiology*, *30*(1), 49–57. https://doi.org/10.1093/glycob/cwz075
111. Hong, M.-H., Weng, I.-C., Li, F.-Y., Lin, W.-H., & Liu, F.-T. (2021). Intracellular galectins sense cytosolically exposed glycans as danger and mediate cellular responses. *Journal of Biomedical Science*, *28*(1), 16. https://doi.org/10.1186/s12929-021-00713-x
112. Huang, Z., Mou, L., Shen, Q., Lu, S., Li, C., Liu, X., Wang, G., Li, S., Geng, L., Liu, Y., Wu, J., Chen, G., & Zhang, J. (2014). ASD v2.0: Updated content and novel features focusing on allosteric regulation. *Nucleic Acids Research*, *42*(D1), D510–D516. https://doi.org/10.1093/nar/gkt1247
113. Huang, Z., Zhu, L., Cao, Y., Wu, G., Liu, X., Chen, Y., Wang, Q., Shi, T., Zhao, Y., Wang, Y., Li, W., Li, Y., Chen, H., Chen, G., & Zhang, J. (2011). ASD: A comprehensive database of allosteric proteins and modulators. *Nucleic Acids Research*, *39*(suppl_1), D663–D669. https://doi.org/10.1093/nar/gkq1022
114. Huang, Y., Wang, H. C., Zhao, J., Wu, M. H., & Shih, T. C. (2021). Immunosuppressive roles of galectin-1 in the tumor microenvironment. Biomolecules, 11(10), 1398
115. Inagaki, Y., Higashi, K., Kushida, M., Hong, Y. Y., Nakao, S., Higashiyama, R., Moro, T., Itoh, J., Mikami, T., Kimura, T., Shiota, G., Kuwabara, I., & Okazaki, I. (2008). Hepatocyte Growth Factor Suppresses Profibrogenic Signal Transduction via Nuclear Export of Smad3 With Galectin-7. *Gastroenterology*, *134*(4), 1180–1190. https://doi.org/10.1053/j.gastro.2008.01.014
116. Inufusa, H., Nakamura, M., Adachi, T., Aga, M., Kurimoto, M., Nakatani, Y., Wakano, T., Miyake, M., Okuno, K., Shiozaki, H., & Yasutomi, M. (2001). Role of galectin-3 in adenocarcinoma liver metastasis. *International Journal of Oncology*, *19*(5), 913–919. https://doi.org/10.3892/ijo.19.5.913
117. Jenson, J. M., Xue, V., Stretz, L., Mandal, T., Reich, L. L., & Keating, A. E. (2018). Peptide design by optimization on a data-parameterized protein interaction landscape. *Proceedings of the National Academy of Sciences*, *115*(44), E10342-E10351
118. Jia, J., Abudu, Y. P., Claude-Taupin, A., Gu, Y., Kumar, S., Choi, S. W., Peters, R., Mudd, M. H., Allers, L., Salemi, M., Phinney, B., Johansen, T., & Deretic, V. (2018). Galectins

Control mTOR in Response to Endomembrane Damage. *Molecular Cell*, *70*(1), 120-135.e8. https://doi.org/10.1016/j.molcel.2018.03.009

119. Johannes, L., & Billet, A. (2020). Glycosylation and raft endocytosis in cancer. *Cancer and Metastasis Reviews*, *39*(2), 375–396. https://doi.org/10.1007/s10555-020-09880-z

120. Johannes, L., Jacob, R., & Leffler, H. (2018). Galectins at a glance. *Journal of Cell Science*, *131*(9). https://doi.org/10.1242/jcs.208884

121. Kamili, N. A., Arthur, C. M., Gerner-Smidt, C., Tafesse, E., Blenda, A., Dias-Baruffi, M., & Stowell, S. R. (2016). Key regulators of galectin–glycan interactions. *PROTEOMICS*, *16*(24), 3111–3125. https://doi.org/10.1002/pmic.201600116

122. Kamitori, S. (2018). Three-Dimensional Structures of Galectins. *Trends in Glycoscience and Glycotechnology*, *30*(172), SE41–SE50. https://doi.org/10.4052/tigg.1731.1SE

123. Karlsson, A., Follin, P., Leffler, H., & Dahlgren, C. (1998). Galectin-3 Activates the NADPH-Oxidase in Exudated but not Peripheral Blood Neutrophils. *Blood*, *91*(9), 3430–3438. https://doi.org/10.1182/blood.V91.9.3430

124. Katzenmaier, E. M., Fuchs, V., Warnken, U., Schnölzer, M., Gebert, J., & Kopitz, J. (2019). Deciphering the galectin-12 protein interactome reveals a major impact of galectin-12 on glutamine anaplerosis in colon cancer cells. Experimental cell research, 379(2), 129-139

125. Kiessling, L. L., & Diehl, R. C. (2021). CH−π Interactions in Glycan Recognition. *ACS Chemical Biology*, *16*(10), 1884–1893. https://doi.org/10.1021/acschembio.1c00413

126. Kim, B.-W., Beom Hong, S., Hoe Kim, J., Hoon Kwon, D., & Kyu Song, H. (2013). Structural basis for recognition of autophagic receptor NDP52 by the sugar receptor galectin-8. *Nature Communications*, *4*(1), 1613. https://doi.org/10.1038/ncomms2606

127. Kim, D.-W., Kim, K. H., Yoo, B. C., Hong, S.-H., Lim, Y. C., Shin, Y.-K., & Park, J.-G. (2008). Identification of mitochondrial F1F0-ATP synthase interacting with galectin-3 in colon cancer cells. *Cancer Science*, *99*(10), 1884–1891. https://doi.org/10.1111/j.1349-7006.2008.00901.x

128. Kim, H.-J., Jeon, H.-K., Lee, J.-K., Sung, C. O., Do, I.-G., Choi, C. H., Kim, T.-J., Kim, B.-G., Bae, D.-S., & Lee, J.-W. (2013). Clinical Significance of Galectin-7 in Epithelial Ovarian Cancer. *Anticancer Research*, *33*(4), 1555–1561.

129. Kim, H.-R. C., Lin, H.-M., Biliran, H., & Raz, A. (1999). Cell Cycle Arrest and Inhibition of Anoikis by Galectin-3 in Human Breast Epithelial Cells. *Cancer Research*, *59*(16), 4148–4154.

130. Kleshchenko, Y. Y., Moody, T. N., Furtak, V. A., Ochieng, J., Lima, M. F., & Villalta, F. (2004). Human Galectin-3 Promotes Trypanosoma cruzi Adhesion to Human Coronary

Artery Smooth Muscle Cells. *Infection and Immunity*. https://doi.org/10.1128/IAI.72.11.6717-6721.2004

131. Klibi, J., Niki, T., Riedel, A., Pioche-Durieu, C., Souquere, S., Rubinstein, E., Le Moulec, S., Guigay, J., Hirashima, M., Guemira, F., Adhikary, D., Mautner, J., & Busson, P. (2009). Blood diffusion and Th1-suppressive effects of galectin-9–containing exosomes released by Epstein-Barr virus–infected nasopharyngeal carcinoma cells. *Blood*, *113*(9), 1957–1966. https://doi.org/10.1182/blood-2008-02-142596

132. Kohatsu, L., Hsu, D. K., Jegalian, A. G., Liu, F.-T., & Baum, L. G. (2006). Galectin-3 Induces Death of Candida Species Expressing Specific β-1,2-Linked Mannans. *The Journal of Immunology*, *177*(7), 4718–4726. https://doi.org/10.4049/jimmunol.177.7.4718

133. Komath, S. S., Kavitha, M., & Swamy, M. J. (2006). Beyond carbohydrate binding: New directions in plant lectin research. *Organic & Biomolecular Chemistry*, *4*(6), 973–988. https://doi.org/10.1039/B515446D

134. Konno, A., Kitagawa, A., Watanabe, M., Ogawa, T., & Shirai, T. (2011). Tracing Protein Evolution through Ancestral Structures of Fish Galectin. *Structure*, *19*(5), 711–721. https://doi.org/10.1016/j.str.2011.02.014

135. Kovács-Sólyom, F., Blaskó, A., Fajka-Boja, R., Katona, R. L., Végh, L., Novák, J., Szebeni, G. J., Krenács, L., Uher, F., Tubak, V., Kiss, R., & Monostori, É. (2010). Mechanism of tumor cell-induced T-cell apoptosis mediated by galectin-1. *Immunology Letters*, *127*(2), 108–118. https://doi.org/10.1016/j.imlet.2009.10.003

136. Kuwabara, I., Kuwabara, Y., Yang, R.-Y., Schuler, M., Green, D. R., Zuraw, B. L., Hsu, D. K., & Liu, F.-T. (2002). Galectin-7 (PIG1) Exhibits Pro-apoptotic Function through JNK Activation and Mitochondrial Cytochrome cRelease * 210. *Journal of Biological Chemistry*, *277*(5), 3487–3497. https://doi.org/10.1074/jbc.M109360200

137. Kuwabara, I., & Liu, F. T. (1996). Galectin-3 promotes adhesion of human neutrophils to laminin. *The Journal of Immunology*, *156*(10), 3939–3944.

138. La, M., Cao, T. V., Cerchiaro, G., Chilton, K., Hirabayashi, J., Kasai, K., Oliani, S. M., Chernajovsky, Y., & Perretti, M. (2003). A Novel Biological Activity for Galectin-1: Inhibition of Leukocyte-Endothelial Cell Interactions in Experimental Inflammation. *The American Journal of Pathology*, *163*(4), 1505–1515. https://doi.org/10.1016/S0002-9440(10)63507-9

139. Labrie, M., Vladoiu, M. C., Grosset, A.-A., Gaboury, L., & St-Pierre, Y. (2014). Expression and functions of galectin-7 in ovarian cancer. *Oncotarget*, *5*(17), 7705–7721. https://doi.org/10.18632/oncotarget.2299

140. Labrie, M., Vladoiu, M., Leclerc, B. G., Grosset, A.-A., Gaboury, L., Stagg, J., & St-Pierre, Y. (2015). A Mutation in the Carbohydrate Recognition Domain Drives a Phenotypic Switch in the Role of Galectin-7 in Prostate Cancer. *PLOS ONE*, *10*(7), e0131307. https://doi.org/10.1371/journal.pone.0131307

141. Lakshminarayan, R., Wunder, C., Becken, U., Howes, M. T., Benzing, C., Arumugam, S., Sales, S., Ariotti, N., Chambon, V., Lamaze, C., Loew, D., Shevchenko, A., Gaus, K., Parton, R. G., & Johannes, L. (2014). Galectin-3 drives glycosphingolipid-dependent biogenesis of clathrin-independent carriers. *Nature Cell Biology*, *16*(6), 592–603. https://doi.org/10.1038/ncb2970

142. Lee, P.-H., Liu, C.-M., Ho, T.-S., Tsai, Y.-C., Lin, C.-C., Wang, Y.-F., Chen, Y.-L., Yu, C.-K., Wang, S.-M., Liu, C.-C., Shiau, A.-L., Lei, H.-Y., & Chang, C.-P. (2015). Enterovirus 71 Virion-Associated Galectin-1 Facilitates Viral Replication and Stability. *PLOS ONE*, *10*(2), e0116278. https://doi.org/10.1371/journal.pone.0116278

143. Leonidas, D. D., Vatzaki, E. H., Vorum, H., Celis, J. E., Madsen, P., & Acharya, K. R. (1998). Structural Basis for the Recognition of Carbohydrates by Human Galectin-7,. *Biochemistry*, *37*(40), 13930–13940. https://doi.org/10.1021/bi981056x

144. Lhuillier, C., Barjon, C., Niki, T., Gelin, A., Praz, F., Morales, O., Souquere, S., Hirashima, M., Wei, M., Dellis, O., & Busson, P. (2015). Impact of Exogenous Galectin-9 on Human T Cells: CONTRIBUTION OF THE T CELL RECEPTOR COMPLEX TO ANTIGEN-INDEPENDENT ACTIVATION BUT NOT TO APOPTOSIS INDUCTION*. *Journal of Biological Chemistry*, *290*(27), 16797–16811. https://doi.org/10.1074/jbc.M115.661272

145. Li, F.-Y., Weng, I.-C., Lin, C.-H., Kao, M.-C., Wu, M.-S., Chen, H.-Y., & Liu, F.-T. (2019). Helicobacter pylori induces intracellular galectin-8 aggregation around damaged lysosomes within gastric epithelial cells in a host O-glycan-dependent manner. *Glycobiology*, *29*(2), 151–162. https://doi.org/10.1093/glycob/cwy095

146. Li, H., Wu, K., Tao, K., Chen, L., Zheng, Q., Lu, X., Liu, J., Shi, L., Liu, C., Wang, G., & Zou, W. (2012). Tim-3/galectin-9 signaling pathway mediates T-cell dysfunction and predicts poor prognosis in patients with hepatitis B virus-associated hepatocellular carcinoma. *Hepatology*, *56*(4), 1342–1351. https://doi.org/10.1002/hep.25777

147. Li, Y., Komai-Koma, M., Gilchrist, D. S., Hsu, D. K., Liu, F.-T., Springall, T., & Xu, D. (2008). Galectin-3 Is a Negative Regulator of Lipopolysaccharide-Mediated Inflammation. *The Journal of Immunology*, *181*(4), 2781–2789. https://doi.org/10.4049/jimmunol.181.4.2781

148. Liang, Y., Chen, J., Zhang, Y., & Zhang, W. (2015). Expression of galectin-9 mRNA in hepatocellular carcinoma. *International Journal of Clinical and Experimental Pathology*, *8*(11), 15100–15105.

149. Liu, F. T., Hsu, D. K., Zuberi, R. I., Kuwabara, I., Chi, E. Y., & Henderson, W. R. (1995). Expression and function of galectin-3, a beta-galactoside-binding lectin, in human monocytes and macrophages. *The American Journal of Pathology*, *147*(4), 1016–1028.

150. Liu, F.-T., & Rabinovich, G. A. (2005). Galectins as modulators of tumour progression. *Nature Reviews Cancer*, *5*(1), 29–41. https://doi.org/10.1038/nrc1527

151. Liu, F.-T., & Rabinovich, G. A. (2010). Galectins: Regulators of acute and chronic inflammation. *Annals of the New York Academy of Sciences*, *1183*(1), 158–182. https://doi.org/10.1111/j.1749-6632.2009.05131.x

152. Liu, W., Hsu, D. K., Chen, H.-Y., Yang, R.-Y., Carraway, K. L., Isseroff, R. R., & Liu, F.-T. (2012). Galectin-3 Regulates Intracellular Trafficking of EGFR through Alix and Promotes Keratinocyte Migration. *Journal of Investigative Dermatology*, *132*(12), 2828–2837. https://doi.org/10.1038/jid.2012.211

153. Liu, X., Lu, S., Song, K., Shen, Q., Ni, D., Li, Q., He, X., Zhang, H., Wang, Q., Chen, Y., Li, X., Wu, J., Sheng, C., Chen, G., Liu, Y., Lu, X., & Zhang, J. (2020). Unraveling allosteric landscapes of allosterome with ASD. *Nucleic Acids Research*, *48*(D1), D394–D401. https://doi.org/10.1093/nar/gkz958

154. Lu, S., & Zhang, J. (2017). Designed covalent allosteric modulators: An emerging paradigm in drug discovery. *Drug Discovery Today*, *22*(2), 447–453. https://doi.org/10.1016/j.drudis.2016.11.013

155. Ludwig, A.-K., Kaltner, H., Kopitz, J., & Gabius, H.-J. (2019a). Lectinology 4.0: Altering modular (ga)lectin display for functional analysis and biomedical applications. *Biochimica et Biophysica Acta (BBA) - General Subjects*, *1863*(5), 935–940. https://doi.org/10.1016/j.bbagen.2019.03.005

156. Ludwig, A.-K., Michalak, M., Gabba, A., Kutzner, T. J., Beckwith, D. M., FitzGerald, F. G., García Caballero, G., Manning, J. C., Kriegsmann, M., Kaltner, H., Murphy, P. V., Cudic, M., Kopitz, J., & Gabius, H.-J. (2021). Imitating evolution's tinkering by protein engineering reveals extension of human galectin-7 activity. *Histochemistry and Cell Biology*, *156*(3), 253–272. https://doi.org/10.1007/s00418-021-02004-w

157. Ludwig, A.-K., Michalak, M., Xiao, Q., Gilles, U., Medrano, F. J., Ma, H., FitzGerald, F. G., Hasley, W. D., Melendez-Davila, A., Liu, M., Rahimi, K., Kostina, N. Y., Rodriguez-Emmenegger, C., Möller, M., Lindner, I., Kaltner, H., Cudic, M., Reusch, D., Kopitz, J., …

Percec, V. (2019b). Design–functionality relationships for adhesion/growth-regulatory galectins. *Proceedings of the National Academy of Sciences*, *116*(8), 2837–2842. https://doi.org/10.1073/pnas.1813515116

158. MacKinnon, A. C., Farnworth, S. L., Hodkinson, P. S., Henderson, N. C., Atkinson, K. M., Leffler, H., Nilsson, U. J., Haslett, C., Forbes, S. J., & Sethi, T. (2008). Regulation of Alternative Macrophage Activation by Galectin-3. *The Journal of Immunology*, *180*(4), 2650–2658. https://doi.org/10.4049/jimmunol.180.4.2650

159. Madsen, P., Rasmussen, H. H., Flint, T., Gromov, P., Kruse, T. A., Honoré, B., Vorum, H., & Celis, J. E. (1995). Cloning, Expression, and Chromosome Mapping of Human Galectin-7 (∗). *Journal of Biological Chemistry*, *270*(11), 5823–5829. https://doi.org/10.1074/jbc.270.11.5823

160. Maftouh, M., Belo, A. I., Avan, A., Funel, N., Peters, G. J., Giovannetti, E., & Die, I. van. (2014). Galectin-4 expression is associated with reduced lymph node metastasis and modulation of Wnt/β-catenin signalling in pancreatic adenocarcinoma. *Oncotarget*, *5*(14), 5335–5349. https://doi.org/10.18632/oncotarget.2104

161. Magnaldo, T., Bernerd, F., & Darmon, M. (1995). Galectin-7, a human 14-kDa S-lectin, specifically expressed in keratinocytes and sensitive to retinoic acid. Developmental biology, 168(2), 259-271

162. Magnaldo, T., Fowlis, D., & Darmon, M. (1998). Galectin-7, a marker of all types of stratified epithelia. *Differentiation*, *63*(3), 159–168. https://doi.org/10.1046/j.1432-0436.1998.6330159.x

163. Mandal, D. K., & Brewer, C. F. (1993). Differences in the binding affinities of dimeric concanavalin A (including acetyl and succinyl derivatives) and tetrameric concanavalin A with large oligomannose-type glycopeptides. *Biochemistry*, *32*(19), 5116–5120. https://doi.org/10.1021/bi00070a020

164. Manzi, M., Bacigalupo, M. L., Carabias, P., Elola, M. T., Wolfenstein-Todel, C., Rabinovich, G. A., Espelt, M. V., & Troncoso, M. F. (2016). Galectin-1 Controls the Proliferation and Migration of Liver Sinusoidal Endothelial Cells and Their Interaction With Hepatocarcinoma Cells. *Journal of Cellular Physiology*, *231*(7), 1522–1533. https://doi.org/10.1002/jcp.25244

165. Martínez-Bosch, N., Rodriguez-Vida, A., Juanpere, N., Lloreta, J., Rovira, A., Albanell, J., Bellmunt, J., & Navarro, P. (2019). Galectins in prostate and bladder cancer: Tumorigenic roles and clinical opportunities. *Nature Reviews Urology*, *16*(7), 433–445. https://doi.org/10.1038/s41585-019-0183-5

166. Martínez-Bosch, N., & Navarro, P. (2020). Galectins in the tumor microenvironment: Focus on galectin-1. Tumor Microenvironment, 17-38.

167. Masuyer, G., Jabeen, T., Öberg, C. T., Leffler, H., Nilsson, U. J., & Acharya, K. R. (2012). Inhibition mechanism of human galectin-7 by a novel galactose-benzylphosphate inhibitor. *The FEBS Journal*, *279*(2), 193–202. https://doi.org/10.1111/j.1742-4658.2011.08414.x

168. Mathew, M. P., & Donaldson, J. G. (2018). Distinct cargo-specific response landscapes underpin the complex and nuanced role of galectin–glycan interactions in clathrin-independent endocytosis. *Journal of Biological Chemistry*, *293*(19), 7222–7237. https://doi.org/10.1074/jbc.RA118.001802

169. Matsumoto, R., Hirashima, M., Kita, H., & Gleich, G. J. (2002). Biological Activities of Ecalectin: A Novel Eosinophil-Activating Factor. *The Journal of Immunology*, *168*(4), 1961–1967. https://doi.org/10.4049/jimmunol.168.4.1961

170. Matsumoto, R., Matsumoto, H., Seki, M., Hata, M., Asano, Y., Kanegasaki, S., Stevens, R. L., & Hirashima, M. (1998). Human Ecalectin, a Variant of Human Galectin-9, Is a Novel Eosinophil Chemoattractant Produced by T Lymphocytes*. *Journal of Biological Chemistry*, *273*(27), 16976–16984. https://doi.org/10.1074/jbc.273.27.16976

171. Meinohl, C., Barnard, S. J., Fritz-Wolf, K., Unger, M., Porr, A., Heipel, M., Wirth, S., Madlung, J., Nordheim, A., Menke, A., Becker, K., & Giehl, K. (2020). Galectin-8 binds to the Farnesylated C-terminus of K-Ras4B and Modifies Ras/ERK Signaling and Migration in Pancreatic and Lung Carcinoma Cells. *Cancers*, *12*(1), 30. https://doi.org/10.3390/cancers12010030

172. Menkhorst, E., Griffiths, M., Van Sinderen, M., Rainczuk, K., Niven, K., & Dimitriadis, E. (2018). Galectin-7 is elevated in endometrioid (type I) endometrial cancer and promotes cell migration. *Oncology Letters*, *16*(4), 4721–4728. https://doi.org/10.3892/ol.2018.9193

173. Menkhorst, E. M., Gamage, T., Cuman, C., Kaitu'u-Lino, T. J., Tong, S., & Dimitriadis, E. (2014). Galectin-7 acts as an adhesion molecule during implantation and increased expression is associated with miscarriage. *Placenta*, *35*(3), 195–201. https://doi.org/10.1016/j.placenta.2014.01.004

174. Menkhorst, E., Zhou, W., Santos, L. L., Delforce, S., So, T., Rainczuk, K., Loke, H., Syngelaki, A., Varshney, S., Williamson, N., Pringle, K., Young, M. J., Nicolaides, K. H., St-Pierre, Y., & Dimitriadis, E. (2020). Galectin-7 Impairs Placentation and Causes Preeclampsia Features in Mice. *Hypertension*, *76*(4), 1185–1194. https://doi.org/10.1161/HYPERTENSIONAHA.120.15313

175. Mercier, S., St-Pierre, C., Pelletier, I., Ouellet, M., Tremblay, M. J., & Sato, S. (2008). Galectin-1 promotes HIV-1 infectivity in macrophages through stabilization of viral adsorption. *Virology*, *371*(1), 121–129. https://doi.org/10.1016/j.virol.2007.09.034

176. Metz, C., Döger, R., Riquelme, E., Cortés, P., Holmes, C., Shaughnessy, R., Oyanadel, C., Grabowski, C., González, A., & Soza, A. (2016). Galectin-8 promotes migration and proliferation and prevents apoptosis in U87 glioblastoma cells. *Biological Research*, *49*(1), 33. https://doi.org/10.1186/s40659-016-0091-6

177. Miller, M. C., Ludwig, A.-K., Wichapong, K., Kaltner, H., Kopitz, J., Gabius, H.-J., & Mayo, K. H. (2018). Adhesion/growth-regulatory galectins tested in combination: Evidence for formation of hybrids as heterodimers. *Biochemical Journal*, *475*(5), 1003–1018. https://doi.org/10.1042/BCJ20170658

178. Mk, K. (2020). EFFECT OF DROTAVERINE, A PHOSPHODIESTERASE 4 INHIBITOR IN SCOPOLAMINE-INDUCED COGNITIVE IMPAIRMENT IN RATS. *Asian Journal of Pharmaceutical and Clinical Research*, 99–102. https://doi.org/10.22159/ajpcr.2020.v13i12.39589

179. Modenutti, C. P., Capurro, J. I. B., Di Lella, S., & Martí, M. A. (2019). The Structural Biology of Galectin-Ligand Recognition: Current Advances in Modeling Tools, Protein Engineering, and Inhibitor Design. *Frontiers in Chemistry*, *7*, 823. https://doi.org/10.3389/fchem.2019.00823

180. Moisan, S., Demers, M., Mercier, J., Magnaldo, T., Potworowski, E. F., & St-Pierre, Y. (2003). Upregulation of galectin-7 in murine lymphoma cells is associated with progression toward an aggressive phenotype. *Leukemia*, *17*(4), 751–759. https://doi.org/10.1038/sj.leu.2402870

181. Monod, J., Wyman, J., & Changeux, J.-P. (1965). On the nature of allosteric transitions: A plausible model. *Journal of Molecular Biology*, *12*(1), 88–118. https://doi.org/10.1016/S0022-2836(65)80285-6

182. Morishita, A., Nomura, K., Tani, J., Fujita, K., Iwama, H., Takuma, K., Nakahara, M., Tadokoro, T., Oura, K., Chiyo, T., Fujihara, S., Niki, T., Hirashima, M., Nishiyama, A., Himoto, T., & Masaki, T. (2021). Galectin-9 suppresses the tumor growth of colon cancer in vitro and in vivo. *Oncology Reports*, *45*(6), 1–11. https://doi.org/10.3892/or.2021.8056

183. Motlagh, H. N., Wrabl, J. O., Li, J., & Hilser, V. J. (2014). The ensemble nature of allostery. *Nature*, *508*(7496), 331–339. https://doi.org/10.1038/nature13001

184. Motran, C. C., Molinder, K. M., Liu, S. D., Poirier, F., & Miceli, M. C. (2008). Galectin-1 functions as a Th2 cytokine that selectively induces Th1 apoptosis and promotes Th2 function. European journal of immunology, 38(11), 3015-3027

185. Nabi, I. R., Shankar, J., & Dennis, J. W. (2015). The galectin lattice at a glance. *Journal of Cell Science*, *128*(13), 2213–2219. https://doi.org/10.1242/jcs.151159

186. Nangia-Makker, P., Honjo, Y., Sarvis, R., Akahani, S., Hogan, V., Pienta, K. J., & Raz, A. (2000). Galectin-3 Induces Endothelial Cell Morphogenesis and Angiogenesis. *The American Journal of Pathology*, *156*(3), 899–909. https://doi.org/10.1016/S0002-9440(10)64959-0

187. Nishi, N., Shoji, H., Seki, M., Itoh, A., Miyanaka, H., Yuube, K., Hirashima, M., & Nakamura, T. (2003). Galectin-8 modulates neutrophil function via interaction with integrin αM. *Glycobiology*, *13*(11), 755–763. https://doi.org/10.1093/glycob/cwg102

188. Noll, A. J., Gourdine, J. P., Yu, Y., Lasanajak, Y., Smith, D. F., & Cummings, R. D. (2016). Galectins are human milk glycan receptors. Glycobiology, 26(6), 655-669

189. Norambuena, A., Metz, C., Vicuña, L., Silva, A., Pardo, E., Oyanadel, C., Massardo, L., González, A., & Soza, A. (2009). Galectin-8 Induces Apoptosis in Jurkat T Cells by Phosphatidic Acid-mediated ERK1/2 Activation Supported by Protein Kinase A Down-regulation*. *Journal of Biological Chemistry*, *284*(19), 12670–12679. https://doi.org/10.1074/jbc.M808949200

190. Nussinov, R., & Tsai, C.-J. (2012). The Different Ways through Which Specificity Works in Orthosteric and Allosteric Drugs. *Current Pharmaceutical Design*, *18*(9), 1311–1316.

191. Nussinov, R., & Tsai, C.-J. (2015). Allostery without a conformational change? Revisiting the paradigm. *Current Opinion in Structural Biology*, *30*, 17–24. https://doi.org/10.1016/j.sbi.2014.11.005

192. Nussinov, R., Tsai, C.-J., & Csermely, P. (2011). Allo-network drugs: Harnessing allostery in cellular networks. *Trends in Pharmacological Sciences*, *32*(12), 686–693. https://doi.org/10.1016/j.tips.2011.08.004

193. Ose, R., Oharaa, O., & Nagase, T. (2012). Galectin-1 and Galectin-3 Mediate Protocadherin-24-Dependent Membrane Localization of β-catenin in Colon Cancer Cell Line HCT116. *Current Chemical Genomics*, *6*(1). https://doi.org/10.2174/1875397301206010018

194. Ouyang, J., Juszczynski, P., Rodig, S. J., Green, M. R., O'Donnell, E., Currie, T., Armant, M., Takeyama, K., Monti, S., Rabinovich, G. A., Ritz, J., Kutok, J. L., & Shipp, M. A. (2011). Viral induction and targeted inhibition of galectin-1 in EBV+ posttransplant

lymphoproliferative disorders. *Blood*, *117*(16), 4315–4322. https://doi.org/10.1182/blood-2010-11-320481

195. Pace, K. E., Lee, C., Stewart, P. L., & Baum, L. G. (1999). Restricted receptor segregation into membrane microdomains occurs on human T cells during apoptosis induced by galectin-1. The Journal of Immunology, 163(7), 3801-3811

196. Pace, K. E., Hahn, H. P., Pang, M., Nguyen, J. T., & Baum, L. G. (2000). Cutting Edge: CD7 Delivers a Pro-Apoptotic Signal During Galectin-1-Induced T Cell Death. *The Journal of Immunology*, *165*(5), 2331–2334. https://doi.org/10.4049/jimmunol.165.5.2331

197. Paces-Fessy, M., BOUCHER, D., PETIT, E., PAUTE-BRIAND, S., & BLANCHET-TOURNIER, M.-F. (2004). The negative regulator of Gli, Suppressor of fused (Sufu), interacts with SAP18, Galectin3 and other nuclear proteins. *Biochemical Journal*, *378*(2), 353–362. https://doi.org/10.1042/bj20030786

198. Pacienza, N., Pozner, R. G., Bianco, G. A., D'Atri, L. P., Croci, D. O., Negrotto, S., Malaver, E., Gómez, R. M., Rabinovich, G. A., & Schattner, M. (2008). The immunoregulatory glycan-binding protein galectin-1 triggers human platelet activation. *The FASEB Journal*, *22*(4), 1113–1123. https://doi.org/10.1096/fj.07-9524com

199. Paclik, D., Berndt, U., Guzy, C., Dankof, A., Danese, S., Holzloehner, P., Rosewicz, S., Wiedenmann, B., Wittig, B. M., Dignass, A. U., & Sturm, A. (2008a). Galectin-2 induces apoptosis of lamina propria T lymphocytes and ameliorates acute and chronic experimental colitis in mice. *Journal of Molecular Medicine*, *86*(12), 1395–1406. https://doi.org/10.1007/s00109-007-0290-2

200. Paclik, D., Danese, S., Berndt, U., Wiedenmann, B., Dignass, A., & Sturm, A. (2008b). Galectin-4 Controls Intestinal Inflammation by Selective Regulation of Peripheral and Mucosal T Cell Apoptosis and Cell Cycle. *PLOS ONE*, *3*(7), e2629. https://doi.org/10.1371/journal.pone.0002629

201. Palmer, T., & Bonner, P. L. (2011). 13—Sigmoidal Kinetics and Allosteric Enzymes. In T. Palmer & P. L. Bonner (Eds.), *Enzymes (Second Edition)* (pp. 239–254). Woodhead Publishing. https://doi.org/10.1533/9780857099921.2.239

202. Panjkovich, A., & Daura, X. (2010). Assessing the structural conservation of protein pockets to study functional and allosteric sites: Implications for drug discovery. *BMC Structural Biology*, *10*(1), 9. https://doi.org/10.1186/1472-6807-10-9

203. Park, J. E., Chang, W. Y., & Cho, M. (2009). Induction of matrix metalloproteinase-9 by galectin-7 through p38 MAPK signaling in HeLa human cervical epithelial adenocarcinoma cells. *Oncology Reports*, *22*(6), 1373–1379. https://doi.org/10.3892/or_00000577

204. Park, J. W., Voss, P. G., Grabski, S., Wang, J. L., & Patterson, R. J. (2001). Association of galectin-1 and galectin-3 with Gemin4 in complexes containing the SMN protein. *Nucleic Acids Research*, *29*(17), 3595–3602. https://doi.org/10.1093/nar/29.17.3595

205. Paron, I., Scaloni, A., Pines, A., Bachi, A., Liu, F.-T., Puppin, C., Pandolfi, M., Ledda, L., Di Loreto, C., Damante, G., & Tell, G. (2003). Nuclear localization of Galectin-3 in transformed thyroid cells: A role in transcriptional regulation. *Biochemical and Biophysical Research Communications*, *302*(3), 545–553. https://doi.org/10.1016/S0006-291X(03)00151-7

206. Pellizzoni, L., Kataoka, N., Charroux, B., & Dreyfuss, G. (1998). A Novel Function for SMN, the Spinal Muscular Atrophy Disease Gene Product, in Pre-mRNA Splicing. *Cell*, *95*(5), 615–624. https://doi.org/10.1016/S0092-8674(00)81632-3

207. Pereira, M. S., Alves, I., Vicente, M., Campar, A., Silva, M. C., Padrao, N. A., ... & Pinho, S. S. (2018). Glycans as key checkpoints of T cell activity and function. *Frontiers in immunology*, *9*, 2754.

208. Pergialiotis, V., Papoutsi, E., Androutsou, A., Tzortzis, A.-S., Frountzas, M., Papapanagiotou, A. and Kontzoglou, K. (2021), Galectins-1, -3, -7, -8 and -9 as prognostic markers for survival in epithelial ovarian cancer: A systematic review and meta-analysis. Int. J. Gynecol. Obstet., 152: 299-307.

209. Perillo, N. L., Pace, K. E., Seilhamer, J. J., & Baum, L. G. (1995). Apoptosis of T cells mediated by galectin-1. *Nature*, *378*(6558), 736–739. https://doi.org/10.1038/378736a0

210. Persson, E. K., Verstraete, K., Heyndrickx, I., Gevaert, E., Aegerter, H., Percier, J.-M., Deswarte, K., Verschueren, K. H. G., Dansercoer, A., Gras, D., Chanez, P., Bachert, C., Gonçalves, A., Van Gorp, H., De Haard, H., Blanchetot, C., Saunders, M., Hammad, H., Savvides, S. N., & Lambrecht, B. N. (2019). Protein crystallization promotes type 2 immunity and is reversible by antibody treatment. *Science*, *364*(6442), eaaw4295. https://doi.org/10.1126/science.aaw4295

211. Pham, N. T. H., Létourneau, M., Fortier, M., Bégin, G., Al-Abdul-Wahid, M. S., Pucci, F., Folch, B., Rooman, M., Chatenet, D., St-Pierre, Y., Lagüe, P., Calmettes, C., & Doucet, N. (2021). Perturbing dimer interactions and allosteric communication modulates the immunosuppressive activity of human galectin-7. *Journal of Biological Chemistry*, *297*(5). https://doi.org/10.1016/j.jbc.2021.101308

212. Pineda, M. A., Corvo, L., Soto, M., Fresno, M., & Bonay, P. (2015). Interactions of human galectins with Trypanosoma cruzi: Binding profile correlate with genetic clustering of lineages. *Glycobiology*, *25*(2), 197–210. https://doi.org/10.1093/glycob/cwu103

213. Pudewell, S., Wittich, C., Kazemein Jasemi, N. S., Bazgir, F., & Ahmadian, M. R. (2021). Accessory proteins of the RAS-MAPK pathway: Moving from the side line to the front line. *Communications Biology*, *4*(1), 1–10. https://doi.org/10.1038/s42003-021-02149-3

214. Quattroni, P., Li, Y., Lucchesi, D., Lucas, S., Hood, D. W., Herrmann, M., Gabius, H.-J., Tang, C. M., & Exley, R. M. (2012). Galectin-3 binds Neisseria meningitidis and increases interaction with phagocytic cells. *Cellular Microbiology*, *14*(11), 1657–1675. https://doi.org/10.1111/j.1462-5822.2012.01838.x

215. Rabinovich, G. A., Rubinstein, N., & Toscano, M. A. (2002). Role of galectins in inflammatory and immunomodulatory processes. *Biochimica et Biophysica Acta (BBA) - General Subjects*, *1572*(2), 274–284. https://doi.org/10.1016/S0304-4165(02)00314-8

216. Rabinovich, G. A., Sotomayor, C. E., Riera, C. M., Bianco, I., & Correa, S. G. (2000). Evidence of a role for galectin-1 in acute inflammation. *European Journal of Immunology*, *30*(5), 1331–1339. https://doi.org/10.1002/(SICI)1521-4141(200005)30:5<1331::AID-IMMU1331>3.0.CO;2-H

217. Rabinovich, G. A., van Kooyk, Y., & Cobb, B. A. (2012). Glycobiology of immune responses. *Annals of the New York Academy of Sciences*, *1253*(1), 1–15. https://doi.org/10.1111/j.1749-6632.2012.06492.x

218. Rabinovich, G. A., & Toscano, M. A. (2009). Turning'sweet'on immunity: galectin–glycan interactions in immune tolerance and inflammation. Nature Reviews Immunology, 9(5), 338-352.

219. Renard, H.-F., Tyckaert, F., Lo Giudice, C., Hirsch, T., Valades-Cruz, C. A., Lemaigre, C., Shafaq-Zadah, M., Wunder, C., Wattiez, R., Johannes, L., van der Bruggen, P., Alsteens, D., & Morsomme, P. (2020). Endophilin-A3 and Galectin-8 control the clathrin-independent endocytosis of CD166. *Nature Communications*, *11*(1), 1457. https://doi.org/10.1038/s41467-020-15303-y

220. Romaniuk, M. A., Tribulatti, M. V., Cattaneo, V., Lapponi, M. J., Molinas, F. C., Campetella, O., & Schattner, M. (2010). Human platelets express and are activated by galectin-8. *Biochemical Journal*, *432*(3), 535–547. https://doi.org/10.1042/BJ20100538

221. Rorive, S., Eddafali, B., Fernandez, S., Decaestecker, C., André, S., Kaltner, H., Kuwabara, I., Liu, F.-T., Gabius, H.-J., Kiss, R., & Salmon, I. (2002). Changes in Galectin-7 and Cytokeratin-19 Expression during the Progression of Malignancy in Thyroid Tumors: Diagnostic and Biological Implications. *Modern Pathology*, *15*(12), 1294–1301. https://doi.org/10.1097/01.MP.0000037306.19083.28

222. Sacchettini, J. C., Baum, L. G., & Brewer, C. F. (2001). Multivalent Protein−Carbohydrate Interactions. A New Paradigm for Supermolecular Assembly and Signal Transduction. *Biochemistry*, *40*(10), 3009–3015. https://doi.org/10.1021/bi002544j

223. Saint-Lu, N., Oortwijn, B. D., Pegon, J. N., Odouard, S., Christophe, O. D., de Groot, P. G., Denis, C. V., & Lenting, P. J. (2012). Identification of Galectin-1 and Galectin-3 as Novel Partners for Von Willebrand Factor. *Arteriosclerosis, Thrombosis, and Vascular Biology*, *32*(4), 894–901. https://doi.org/10.1161/ATVBAHA.111.240309

224. Salameh, B. A., Sundin, A., Leffler, H., & Nilsson, U. J. (2006). Thioureido N-acetyllactosamine derivatives as potent galectin-7 and 9N inhibitors. *Bioorganic & Medicinal Chemistry*, *14*(4), 1215–1220. https://doi.org/10.1016/j.bmc.2005.09.050

225. Salatino, M., Dalotto-Moreno, T., & Rabinovich, G. A. (2013). Thwarting galectin-induced immunosuppression in breast cancer. *OncoImmunology*, *2*(5), e24077. https://doi.org/10.4161/onci.24077

226. Satelli, A., Rao, P. S., Thirumala, S., & Rao, U. S. (2011). Galectin-4 functions as a tumor suppressor of human colorectal cancer. *International Journal of Cancer*, *129*(4), 799–809. https://doi.org/10.1002/ijc.25750

227. Sato, S., Ouellet, N., Pelletier, I., Simard, M., Rancourt, A., & Bergeron, M. G. (2002). Role of Galectin-3 as an Adhesion Molecule for Neutrophil Extravasation During Streptococcal Pneumonia. *The Journal of Immunology*, *168*(4), 1813–1822. https://doi.org/10.4049/jimmunol.168.4.1813

228. Saussez, S., & Kiss, R. (2006). Galectin-7. *Cellular and Molecular Life Sciences CMLS*, *63*(6), 686–697. https://doi.org/10.1007/s00018-005-5458-8

229. Schulz, H., Schmoeckel, E., Kuhn, C., Hofmann, S., Mayr, D., Mahner, S., & Jeschke, U. (2017). Galectins-1, -3, and -7 Are Prognostic Markers for Survival of Ovarian Cancer Patients. *International Journal of Molecular Sciences*, *18*(6), 1230. https://doi.org/10.3390/ijms18061230

230. Sebban, L. E., Ronen, D., Levartovsky, D., Elkayam, O., Caspi, D., Aamar, S., Amital, H., Rubinow, A., Golan, I., Naor, D., Zick, Y., & Golan, I. (2007). The Involvement of CD44 and Its Novel Ligand Galectin-8 in Apoptotic Regulation of Autoimmune Inflammation. *The Journal of Immunology*, *179*(2), 1225–1235. https://doi.org/10.4049/jimmunol.179.2.1225

231. Seguin, L., Camargo, M. F., Wettersten, H. I., Kato, S., Desgrosellier, J. S., Schalscha, T. von, Elliott, K. C., Cosset, E., Lesperance, J., Weis, S. M., & Cheresh, D. A. (2017). Galectin-3, a Druggable Vulnerability for KRAS-Addicted Cancers. *Cancer Discovery*, *7*(12), 1464–1479. https://doi.org/10.1158/2159-8290.CD-17-0539

232. Seif, F., Khoshmirsafa, M., Aazami, H., Mohsenzadegan, M., Sedighi, G., & Bahar, M. (2017). The role of JAK-STAT signaling pathway and its regulators in the fate of T helper cells. *Cell Communication and Signaling*, *15*(1), 23. https://doi.org/10.1186/s12964-017-0177-y

233. Serizawa, N., Tian, J., Fukada, H., Baghy, K., Scott, F., Chen, X., Kiss, Z., Olson, K., Hsu, D., Liu, F.-T., Török, N. J., Zhao, B., & Jiang, J. X. (2015). Galectin 3 regulates HCC cell invasion by RhoA and MLCK activation. *Laboratory Investigation*, *95*(10), 1145–1156. https://doi.org/10.1038/labinvest.2015.77

234. Sewgobind, N. V., Albers, S., & Pieters, R. J. (2021). Functions and Inhibition of Galectin-7, an Emerging Target in Cellular Pathophysiology. Biomolecules, 11(11), 1720

235. Shalom-Feuerstein, R., Cooks, T., Raz, A., & Kloog, Y. (2005). Galectin-3 Regulates a Molecular Switch from N-Ras to K-Ras Usage in Human Breast Carcinoma Cells. *Cancer Research*, *65*(16), 7292–7300. https://doi.org/10.1158/0008-5472.CAN-05-0775

236. Shalom-Feuerstein, R., Levy, R., Makovski, V., Raz, A., & Kloog, Y. (2008a). Galectin-3 regulates RasGRP4-mediated activation of N-Ras and H-Ras. *Biochimica et Biophysica Acta*, *1783*(6), 985–993. https://doi.org/10.1016/j.bbamcr.2008.03.009

237. Shalom-Feuerstein, R., Plowman, S. J., Rotblat, B., Ariotti, N., Tian, T., Hancock, J. F., & Kloog, Y. (2008b). K-Ras Nanoclustering Is Subverted by Overexpression of the Scaffold Protein Galectin-3. *Cancer Research*, *68*(16), 6608–6616. https://doi.org/10.1158/0008-5472.CAN-08-1117

238. Shen, Q., Wang, G., Li, S., Liu, X., Lu, S., Chen, Z., Song, K., Yan, J., Geng, L., Huang, Z., Huang, W., Chen, G., & Zhang, J. (2016). ASD v3.0: Unraveling allosteric regulation with structural mechanisms and biological networks. *Nucleic Acids Research*, *44*(D1), D527–D535. https://doi.org/10.1093/nar/gkv902

239. Shimura, T., Takenaka, Y., Fukumori, T., Tsutsumi, S., Okada, K., Hogan, V., Kikuchi, A., Kuwano, H., & Raz, A. (2005). Implication of Galectin-3 in Wnt Signaling. *Cancer Research*, *65*(9), 3535–3537. https://doi.org/10.1158/0008-5472.CAN-05-0104

240. Shimura, T., Takenaka, Y., Tsutsumi, S., Hogan, V., Kikuchi, A., & Raz, A. (2004). Galectin-3, a Novel Binding Partner of β-Catenin. *Cancer Research*, *64*(18), 6363–6367. https://doi.org/10.1158/0008-5472.CAN-04-1816

241. Si, Y., Li, Y., Yang, T., Li, X., Ayala, G. J., Mayo, K. H., Tai, G., Su, J., & Zhou, Y. (2021). Structure–function studies of galectin-14, an important effector molecule in embryology. *The FEBS Journal*, *288*(3), 1041–1055. https://doi.org/10.1111/febs.15441

242. Sörme, P., Kahl-Knutsson, B., Wellmar, U., Magnusson, B.-G., Leffler, H., & Nilsson, U. J. (2003). Design and Synthesis of Galectin Inhibitors. In *Methods in Enzymology* (Vol. 363, pp. 157–169). Academic Press. https://doi.org/10.1016/S0076-6879(03)01050-4

243. Spano, D., Russo, R., Di Maso, V., Rosso, N., Terracciano, L. M., Roncalli, M., Tornillo, L., Capasso, M., Tiribelli, C., & Iolascon, A. (2010). Galectin-1 and Its Involvement in Hepatocellular Carcinoma Aggressiveness. *Molecular Medicine*, *16*(3), 102–115. https://doi.org/10.2119/molmed.2009.00119

244. Stefan, M. I., & Novère, N. L. (2013). Cooperative Binding. *PLOS Computational Biology*, *9*(6), e1003106. https://doi.org/10.1371/journal.pcbi.1003106

245. Stein, E. M., DiNardo, C. D., Pollyea, D. A., Fathi, A. T., Roboz, G. J., Altman, J. K., Stone, R. M., DeAngelo, D. J., Levine, R. L., Flinn, I. W., Kantarjian, H. M., Collins, R., Patel, M. R., Frankel, A. E., Stein, A., Sekeres, M. A., Swords, R. T., Medeiros, B. C., Willekens, C., … Tallman, M. S. (2017). Enasidenib in mutant IDH2 relapsed or refractory acute myeloid leukemia. *Blood*, *130*(6), 722–731. https://doi.org/10.1182/blood-2017-04-779405

246. Stillman, B. N., Hsu, D. K., Pang, M., Brewer, C. F., Johnson, P., Liu, F.-T., & Baum, L. G. (2006). Galectin-3 and Galectin-1 Bind Distinct Cell Surface Glycoprotein Receptors to Induce T Cell Death. *The Journal of Immunology*, *176*(2), 778–789. https://doi.org/10.4049/jimmunol.176.2.778

247. Stowell, S. R., Arthur, C. M., Dias-Baruffi, M., Rodrigues, L. C., Gourdine, J.-P., Heimburg-Molinaro, J., Ju, T., Molinaro, R. J., Rivera-Marrero, C., Xia, B., Smith, D. F., & Cummings, R. D. (2010). Innate immune lectins kill bacteria expressing blood group antigen. *Nature Medicine*, *16*(3), 295–301. https://doi.org/10.1038/nm.2103

248. Stowell, S. R., Karmakar, S., Arthur, C. M., Ju, T., Rodrigues, L. C., Riul, T. B., Dias-Baruffi, M., Miner, J., McEver, R. P., & Cummings, R. D. (2009). Galectin-1 Induces Reversible Phosphatidylserine Exposure at the Plasma Membrane. *Molecular Biology of the Cell*, *20*(5), 1408–1418. https://doi.org/10.1091/mbc.e08-07-0786

249. Stowell, S. R., Karmakar, S., Stowell, C. J., Dias-Baruffi, M., McEver, R. P., & Cummings, R. D. (2006). Human galectin-1, -2, and -4 induce surface exposure of phosphatidylserine in activated human neutrophils but not in activated T cells. *Blood*, *109*(1), 219–227. https://doi.org/10.1182/blood-2006-03-007153

250. Stowell, S. R., Qian, Y., Karmakar, S., Koyama, N. S., Dias-Baruffi, M., Leffler, H., McEver, R. P., & Cummings, R. D. (2008). Differential roles of galectin-1 and galectin-3 in regulating leukocyte viability and cytokine secretion. *Journal of Immunology (Baltimore, Md.: 1950)*, *180*(5), 3091–3102. https://doi.org/10.4049/jimmunol.180.5.3091

251. St-Pierre, Y. (2012). A distinctive role for galectin-7 in cancer ? *Frontiers in Bioscience*, *17*(1), 438. https://doi.org/10.2741/3937

252. St-Pierre, Y. (2021). Towards a Better Understanding of the Relationships between Galectin-7, p53 and MMP-9 during Cancer Progression. *Biomolecules*, *11*(6), 879. https://doi.org/10.3390/biom11060879

253. St-Pierre, Y., Doucet, N., & Chatenet, D. (2018). A New Approach to Inhibit Prototypic Galectins. *Trends in Glycoscience and Glycotechnology*, *30*(172), SE155–SE165. https://doi.org/10.4052/tigg.1730.1SE

254. Sturm, A., Lensch, M., André, S., Kaltner, H., Wiedenmann, B., Rosewicz, S., Dignass, A. U., & Gabius, H.-J. (2004). Human Galectin-2: Novel Inducer of T Cell Apoptosis with Distinct Profile of Caspase Activation. *The Journal of Immunology*, *173*(6), 3825–3837. https://doi.org/10.4049/jimmunol.173.6.3825

255. Su, J., Wang, Y., Si, Y., Gao, J., Song, C., Cui, L., Wu, R., Tai, G., & Zhou, Y. (2018). Galectin-13, a different prototype galectin, does not bind β-galacto-sides and forms dimers via intermolecular disulfide bridges between Cys-136 and Cys-138. *Scientific Reports*, *8*(1), 980. https://doi.org/10.1038/s41598-018-19465-0

256. Sun, R., Kim, A. M. J., & Lim, S. O. (2021). Glycosylation of Immune Receptors in Cancer. Cells, 10(5), 1100

257. Sung, H., Ferlay, J., Siegel, R. L., Laversanne, M., Soerjomataram, I., Jemal, A., & Bray, F. (2021). Global Cancer Statistics 2020: GLOBOCAN Estimates of Incidence and Mortality Worldwide for 36 Cancers in 185 Countries. *CA: A Cancer Journal for Clinicians*, *71*(3), 209–249. https://doi.org/10.3322/caac.21660

258. Suzuki, Y., Inoue, T., Yoshimaru, T., & Ra, C. (2008). Galectin-3 but not galectin-1 induces mast cell death by oxidative stress and mitochondrial permeability transition. *Biochimica et Biophysica Acta (BBA) - Molecular Cell Research*, *1783*(5), 924–934. https://doi.org/10.1016/j.bbamcr.2008.01.025

259. Swarte, V. V. R., Mebius, R. E., Joziasse, D. H., Van den Eijnden, D. H., & Kraal, G. (1998). Lymphocyte triggering via L-selectin leads to enhanced galectin-3-mediated binding to dendritic cells. *European Journal of Immunology*, *28*(9), 2864–2871. https://doi.org/10.1002/(SICI)1521-4141(199809)28:09<2864::AID-IMMU2864>3.0.CO;2-U

260. Tadokoro, T., Morishita, A., Fujihara, S., Iwama, H., Niki, T., Fujita, K., Akashi, E., Mimura, S., Oura, K., Sakamoto, T., Nomura, T., Tani, J., Miyoshi, H., Yoneyama, H., Himoto, T., Hirashima, M., & Masaki, T. (2016). Galectin-9: An anticancer molecule for gallbladder

carcinoma. *International Journal of Oncology*, *48*(3), 1165–1174. https://doi.org/10.3892/ijo.2016.3347

261. Tang, Z.-H., Liang, S., Potter, J., Jiang, X., Mao, H.-Q., & Li, Z. (2013). Tim-3/Galectin-9 Regulate the Homeostasis of Hepatic NKT Cells in a Murine Model of Nonalcoholic Fatty Liver Disease. *The Journal of Immunology*, *190*(4), 1788–1796. https://doi.org/10.4049/jimmunol.1202814
262. Teichberg, V. I., Silman, I., Beitsch, D. D., & Resheff, G. (1975). A beta-D-galactoside binding protein from electric organ tissue of Electrophorus electricus. *Proceedings of the National Academy of Sciences*, *72*(4), 1383–1387. https://doi.org/10.1073/pnas.72.4.1383
263. Thijssen, V. L. J. L., Postel, R., Brandwijk, R. J. M. G. E., Dings, R. P. M., Nesmelova, I., Satijn, S., Verhofstad, N., Nakabeppu, Y., Baum, L. G., Bakkers, J., Mayo, K. H., Poirier, F., & Griffioen, A. W. (2006). Galectin-1 is essential in tumor angiogenesis and is a target for antiangiogenesis therapy. *Proceedings of the National Academy of Sciences*, *103*(43), 15975–15980. https://doi.org/10.1073/pnas.0603883103
264. Thurston, T. L. M., Wandel, M. P., von Muhlinen, N., Foeglein, Á., & Randow, F. (2012). Galectin 8 targets damaged vesicles for autophagy to defend cells against bacterial invasion. *Nature*, *482*(7385), 414–418. https://doi.org/10.1038/nature10744
265. Toledo, K. A., Fermino, M. L., Andrade, C. del C., Riul, T. B., Alves, R. T., Muller, V. D. M., Russo, R. R., Stowell, S. R., Cummings, R. D., Aquino, V. H., & Dias-Baruffi, M. (2014). Galectin-1 Exerts Inhibitory Effects during DENV-1 Infection. *PLOS ONE*, *9*(11), e112474. https://doi.org/10.1371/journal.pone.0112474
266. Toscano, M. A., Bianco, G. A., Ilarregui, J. M., Croci, D. O., Correale, J., Hernandez, J. D., ... & Rabinovich, G. A. (2007). Differential glycosylation of TH1, TH2 and TH-17 effector cells selectively regulates susceptibility to cell death. Nature immunology, 8(8), 825-834
267. Toscano, M. A., Tongren, J. E., De SOUZA, J. B., Liu, F.-T., Riley, E. M., & Rabinovich, G. A. (2012). Endogenous galectin-3 controls experimental malaria in a species-specific manner. *Parasite Immunology*, *34*(7), 383–387. https://doi.org/10.1111/j.1365-3024.2012.01366.x
268. Tribulatti, M. V., Figini, M. G., Carabelli, J., Cattaneo, V., & Campetella, O. (2012). Redundant and Antagonistic Functions of Galectin-1, -3, and -8 in the Elicitation of T Cell Responses. *The Journal of Immunology*, *188*(7), 2991–2999. https://doi.org/10.4049/jimmunol.1102182

269. Truong, A. B., & Khavari, P. A. (2007). Control of Keratinocyte Proliferation and Differentiation by p63. *Cell Cycle*, *6*(3), 295–299. https://doi.org/10.4161/cc.6.3.3753

270. Tsai, C.-M., Guan, C.-H., Hsieh, H.-W., Hsu, T.-L., Tu, Z., Wu, K.-J., Lin, C.-H., & Lin, K.-I. (2011). Galectin-1 and Galectin-8 Have Redundant Roles in Promoting Plasma Cell Formation. *The Journal of Immunology*, *187*(4), 1643–1652. https://doi.org/10.4049/jimmunol.1100297

271. Tsai, C.-M., Wu, H.-Y., Su, T.-H., Kuo, C.-W., Huang, H.-W., Chung, C.-H., Chen, C.-S., Khoo, K.-H., Chen, Y.-J., & Lin, K.-I. (2014). Phosphoproteomic analyses reveal that galectin-1 augments the dynamics of B-cell receptor signaling. *Journal of Proteomics*, *103*, 241–253. https://doi.org/10.1016/j.jprot.2014.03.031

272. Ueda, S., Kuwabara, I., & Liu, F.-T. (2004). Suppression of Tumor Growth by Galectin-7 Gene Transfer. *Cancer Research*, *64*(16), 5672–5676. https://doi.org/10.1158/0008-5472.CAN-04-0985

273. Varki, A., Cummings, R. D., Esko, J. D., Stanley, P., Hart, G. W., Aebi, M., Darvill, A. G., Kinoshita, T., Packer, N. H., Prestegard, J. H., Schnaar, R. L., & Seeberger, P. H. (Eds.). (2015). *Essentials of Glycobiology* (3rd ed.). Cold Spring Harbor Laboratory Press. http://www.ncbi.nlm.nih.gov/books/NBK310274/

274. Vasta, G. R. (2016). Chapter 8 - Lectins as Innate Immune Recognition Factors: Structural, Functional, and Evolutionary Aspects. In D. Malagoli (Ed.), *The Evolution of the Immune System* (pp. 205–224). Academic Press. https://doi.org/10.1016/B978-0-12-801975-7.00008-6

275. Vecchio, M. D., Bajetta, E., Canova, S., Lotze, M. T., Wesa, A., Parmiani, G., & Anichini, A. (2007). Interleukin-12: Biological Properties and Clinical Application. *Clinical Cancer Research*, *13*(16), 4677–4685. https://doi.org/10.1158/1078-0432.CCR-07-0776

276. Villeneuve, C., Baricault, L., Canelle, L., Barboule, N., Racca, C., Monsarrat, B., Magnaldo, T., & Larminat, F. (2011). Mitochondrial proteomic approach reveals galectin-7 as a novel BCL-2 binding protein in human cells. *Molecular Biology of the Cell*, *22*(7), 999–1013. https://doi.org/10.1091/mbc.e10-06-0534

277. Vladoiu, M. C., Labrie, M., Létourneau, M., Egesborg, P., Gagné, D., Billard, É., Grosset, A.-A., Doucet, N., Chatenet, D., & St-Pierre, Y. (2015). Design of a peptidic inhibitor that targets the dimer interface of a prototypic galectin. *Oncotarget*, *6*(38), 40970–40980. https://doi.org/10.18632/oncotarget.5403

278. Vladoiu, M. C., Labrie, M., & St-Pierre, Y. (2014). Intracellular galectins in cancer cells: Potential new targets for therapy (Review). *International Journal of Oncology*, *44*(4), 1001–1014. https://doi.org/10.3892/ijo.2014.2267

279. Vyakarnam, A., Dagher, S. F., Wang, J. L., & Patterson, R. J. (1997). Evidence for a role for galectin-1 in pre-mRNA splicing. *Molecular and Cellular Biology*. https://doi.org/10.1128/MCB.17.8.4730

280. Wan, L., Yang, R.-Y., & Liu, F.-T. (2018). Galectin-12 in Cellular Differentiation, Apoptosis and Polarization. *International Journal of Molecular Sciences*, *19*(1), 176. https://doi.org/10.3390/ijms19010176

281. Wang, F., Xu, J., Liao, Y., Wang, Y., Liu, C., Zhu, X., Chen, Z. K., & Sun, Z. (2011). Tim-3 ligand galectin-9 reduces IL-17 level and accelerates Klebsiella pneumoniae infection. *Cellular Immunology*, *269*(1), 22–28. https://doi.org/10.1016/j.cellimm.2011.03.005

282. Wang, S.-F., Huang, K.-H., Tseng, W.-C., Lo, J.-F., Li, A. F.-Y., Fang, W.-L., Chen, C.-F., Yeh, T.-S., Chang, Y.-L., Chou, Y.-C., Hung, H.-H., & Lee, H.-C. (2020). DNAJA3/Tid1 Is Required for Mitochondrial DNA Maintenance and Regulates Migration and Invasion of Human Gastric Cancer Cells. *Cancers*, *12*(11), 3463. https://doi.org/10.3390/cancers12113463

283. Wang, W., Guo, H., Geng, J., Zheng, X., Wei, H., Sun, R., & Tian, Z. (2014). Tumor-released Galectin-3, a Soluble Inhibitory Ligand of Human NKp30, Plays an Important Role in Tumor Escape from NK Cell Attack. *Journal of Biological Chemistry*, *289*(48), 33311–33319. https://doi.org/10.1074/jbc.M114.603464

284. Wang, Y., Yu, H., Shi, X., Luo, Z., Lin, D., & Huang, M. (2013). Structural Mechanism of Ring-opening Reaction of Glucose by Human Serum Albumin*. *Journal of Biological Chemistry*, *288*(22), 15980–15987. https://doi.org/10.1074/jbc.M113.467027

285. Wdowiak, K., Francuz, T., Gallego-Colon, E., Ruiz-Agamez, N., Kubeczko, M., Grochoła, I., & Wojnar, J. (2018). Galectin Targeted Therapy in Oncology: Current Knowledge and Perspectives. *International Journal of Molecular Sciences*, *19*(1), 210. https://doi.org/10.3390/ijms19010210

286. Wei, G., Xi, W., Nussinov, R., & Ma, B. (2016). Protein Ensembles: How Does Nature Harness Thermodynamic Fluctuations for Life? The Diverse Functional Roles of Conformational Ensembles in the Cell. *Chemical Reviews*, *116*(11), 6516–6551. https://doi.org/10.1021/acs.chemrev.5b00562

287. Weng, I.-C., Hsu, D. K., & Liu, F.-T. (2009). Role of galectin-3 in macrophage response to Listeria monocytogenes infection (133.34). *The Journal of Immunology*, *182*(1 Supplement), 133.34-133.34.

288. Wenthur, C. J., Gentry, P. R., Mathews, T. P., & Lindsley, C. W. (2014). Drugs for Allosteric Sites on Receptors. *Annual Review of Pharmacology and Toxicology*, *54*, 165–184. https://doi.org/10.1146/annurev-pharmtox-010611-134525

289. Wishart, D. S., Knox, C., Guo, A. C., Shrivastava, S., Hassanali, M., Stothard, P., Chang, Z., & Woolsey, J. (2006). DrugBank: A comprehensive resource for in silico drug discovery and exploration. *Nucleic Acids Research*, *34*(Database issue), D668-672. https://doi.org/10.1093/nar/gkj067

290. Wodak, S. J., Paci, E., Dokholyan, N. V., Berezovsky, I. N., Horovitz, A., Li, J., Hilser, V. J., Bahar, I., Karanicolas, J., Stock, G., Hamm, P., Stote, R. H., Eberhardt, J., Chebaro, Y., Dejaegere, A., Cecchini, M., Changeux, J.-P., Bolhuis, P. G., Vreede, J., … McLeish, T. (2019). Allostery in Its Many Disguises: From Theory to Applications. *Structure*, *27*(4), 566–578. https://doi.org/10.1016/j.str.2019.01.003

291. Wootten, D., Christopoulos, A., & Sexton, P. M. (2013). Emerging paradigms in GPCR allostery: Implications for drug discovery. *Nature Reviews Drug Discovery*, *12*(8), 630–644. https://doi.org/10.1038/nrd4052

292. Wu, D. H., Chen, A. D., & Johnson, C. S. (1995). An Improved Diffusion-Ordered Spectroscopy Experiment Incorporating Bipolar-Gradient Pulses. *Journal of Magnetic Resonance, Series A*, *115*(2), 260–264. https://doi.org/10.1006/jmra.1995.1176

293. Wu, Q., Siddharth, S., & Sharma, D. (2021). Triple Negative Breast Cancer: A Mountain Yet to Be Scaled Despite the Triumphs. *Cancers*, *13*(15), 3697. https://doi.org/10.3390/cancers13153697

294. Wu, S.-Y., Yu, J.-S., Liu, F.-T., Miaw, S.-C., & Wu-Hsieh, B. A. (2013). Galectin-3 Negatively Regulates Dendritic Cell Production of IL-23/IL-17–Axis Cytokines in Infection by Histoplasma capsulatum. *The Journal of Immunology*, *190*(7), 3427–3437. https://doi.org/10.4049/jimmunol.1202122

295. Xie, J., & Lai, L. (2020). Protein topology and allostery. *Current Opinion in Structural* Biology, 62, 158–165. https://doi.org/10.1016/j.sbi.2020.01.011

296. Xu, W. D., Huang, Q., & Huang, A. F. (2021). Emerging role of galectin family in inflammatory autoimmune diseases. Autoimmunity Reviews, 20(7), 102847

297. Yamaoka, A., Kuwabara, I., Frigeri, L. G., & Liu, F. T. (1995). A human lectin, galectin-3 (epsilon bp/Mac-2), stimulates superoxide production by neutrophils. *The Journal of Immunology*, *154*(7), 3479–3487.

298. Yang, R. Y., Hsu, D. K., & Liu, F. T. (1996). Expression of galectin-3 modulates T-cell growth and apoptosis. *Proceedings of the National Academy of Sciences*, *93*(13), 6737–6742. https://doi.org/10.1073/pnas.93.13.6737

299. Yu, F., Finley, R. L., Raz, A., & Kim, H.-R. C. (2002). Galectin-3 Translocates to the Perinuclear Membranes and Inhibits Cytochrome c Release from the Mitochondria: A ROLE FOR SYNEXIN IN GALECTIN-3 TRANSLOCATION *. *Journal of Biological Chemistry*, *277*(18), 15819–15827. https://doi.org/10.1074/jbc.M200154200

300. Zhang, P.-F., Li, K.-S., Shen, Y. -h, Gao, P.-T., Dong, Z.-R., Cai, J.-B., Zhang, C., Huang, X.-Y., Tian, M.-X., Hu, Z.-Q., Gao, D.-M., Fan, J., Ke, A.-W., & Shi, G.-M. (2016). Galectin-1 induces hepatocellular carcinoma EMT and sorafenib resistance by activating FAK/PI3K/AKT signaling. *Cell Death & Disease*, *7*(4), e2201–e2201. https://doi.org/10.1038/cddis.2015.324

301. Zhang, Z.-Y., Dong, J.-H., Chen, Y.-W., Wang, X.-Q., Li, C.-H., Wang, J., Wang, G.-Q., Li, H.-L., & Wang, X.-D. (2012). Galectin-9 Acts as a Prognostic Factor with Antimetastatic Potential in Hepatocellular Carcinoma. *Asian Pacific Journal of Cancer Prevention*, *13*(6), 2503–2509. https://doi.org/10.7314/APJCP.2012.13.6.2503

302. Zheng, D., Hu, Z., He, F., Gao, C., Xu, L., Zou, H., Wu, Z., Jiang, X., & Wang, J. (2014). Downregulation of galectin-3 causes a decrease in uPAR levels and inhibits the proliferation, migration and invasion of hepatocellular carcinoma cells. *Oncology Reports*, *32*(1), 411–418. https://doi.org/10.3892/or.2014.3170

303. Zhu, H., Wu, T.-C., Chen, W.-Q., Zhou, L.-J., Wu, Y., Zeng, L., & Pei, H.-P. (2013). Roles of galectin-7 and S100A9 in cervical squamous carcinoma: Clinicopathological and in vitro evidence. *International Journal of Cancer*, *132*(5), 1051–1059. https://doi.org/10.1002/ijc.27764

304. Zhu, X., Ding, M., Yu, M.-L., Feng, M.-X., Tan, L.-J., & Zhao, F.-K. (2010). Identification of galectin-7 as a potential biomarker for esophageal squamous cell carcinoma by proteomic analysis. BMC Cancer, 10(1), 290. https://doi.org/10.1186/1471-2407-10-290

7 ANNEXE I - SUPPLEMENTARY DATA OF CHAPTER 4

Table 7.1 Data collection and refinement statistics of R14A, D94A, and R14A-R20A crystal structures

	Apo GAL-7 R14A	*GAL-7 R14A - Lactose*	*Apo GAL-7 D94A*	*GAL-7 D94A - Lactose*	*Apo GAL-7 R14A-R20A*	*GAL-7 R14A-R20A - Lactose*
PDB ID	**7TKW**	**7TKX**	**7TKY**	**7TKZ**	**7TRN**	**7TRO**
Data collection[a]						
Space group	*P* $2_12_12_1$	*P* $2_12_12_1$	*P* $2_12_12_1$	*P* $2_12_12_1$	*P* 1_1	*P* $2_12_12_1$
Cell dimensions						
a, b, c (Å)	53.75 64.95 70.41	30.25 76.38 111.30	53.97 66.83 69.49	30.23 76.4 111.09	36.05 53.64. 69.37	53.97 66.16 70.55
α, β, γ (°)	90, 90, 90	90, 90, 90	90, 90, 90	90, 90, 90	87.46, 79.03, 84.84	90 90 90
Resolution (Å)	42.72 - 1.85 (1.92 - 1.85)	36.12 - 1.83 (1.90 - 1.83)	48.17 - 2.53 (2.62 - 2.53)	44.93 - 1.83 (1.90 - 1.83)	41.46 - 1.95 (2.02 - 1.95)	48.26 - 1.80 (1.86 - 1.80)
R_{merge}	0.69 (0.89)	0.08 (0.75)	0.18 (1.37)	0.07 (0.25)	0.05 (0.29)	0.05 (0.793)
I/σI	142.7 (12.8)	17.5 (3)	11.9 (1.9)	17.7 (6.8)	16.1 (3.6)	24.7 (2.2)
$CC_{1/2}$	0.714 (0.712)	0.998 (0.828)	0.997 (0.623)	0.997 (0.98)	0.997 (0.874)	1 (0.77)
*CC**	0.908 (0.917)	1 (0.952)	0.999 (0.876)	0.999 (0.995)	0.999 (0.966)	1 (0.93)
Completeness (%)	100 (100)	98.6 (95.8)	100 (100)	99.81 (99.91)	99.77 (99.76)	99.8 (99.8)
Redundancy	12.1 (12.1)	7.2 (7.4)	9.6 (9.8)	6.2 (6.3)	2.6 (2.5)	9.3 (6.6)
Refinement						
Resolution (Å)	1.85	1.83	2.53	1.83	1.95	1.8
No. reflections	21589 (2117)	23270 (2241)	8822 (858)	31442 (1659)	21589 (2117)	23989 (2366)
R_{work} / R_{free}	0.193/0.231	0.169/0.214	0.226/0.283	0.166/0.225	0.195/0.224	0.175/0.221
No. of (non-hydrogen) atoms	2357	2407	2149	2484	4754	2379
Protein	2103	2106	2105	2155	4149	2076
Ligand/ion	90	144	28	117	172	75
Water	216	233	32	272	355	268
B factors	29.79	24.95	48.09	23.3	26.11	34.06
Protein	28.73	23.74	48.05	21.73	25.03	33.04
Ligand/ion	55.44	33.08	62.32	33.52	43.45	56.53
Water	35.62	33.59	44.82	33.53	32.12	39.05
r.m.s. deviations						
Bond lengths (Å)	0.008	0.011	0.007	0.012	0.014	0.012
Bond angles (°)	1.36	1.45	1.34	1.44	1.67	1.47

Table 7.2 ITC binding properties of α-lactose to WT GAL-7 and R14A, D94A variants.

	α-lactose		
	WT	**R14A**	**D94A**
K_D (**μM**)	135.3 ± 1.2	163.7 ± 17.0	157.3 ± 6.4
N	0.93 ± 0.03	0.49 ± 0.02	0.87 ± 0.01
Δ*H* (kJ/mol)	-22.8 ± 0.1	-29.1 ± 2.5	-16.8 ± 0.6
Δ*S* (J/mol·K)	-0.7 ± 3.2	-2.5 ± 8	16.2 ± 1.7

Table 7.3 Binding affinity of α-lactose to WT GAL-7 and variant R14A-R20A, R14A-R22A, as measured by MST

	K_D (μM)	95% Confidence Interval
WT	116	42.8 - 301
R14A-R20A	790	511 – 1214
R14A-R22A	> 60000	N/A

Table 7.4 RMSD value calculated from Cα structural alignments of dimer structures between apo and holo WT GAL-7, R14A, D94A, and R14A-R20A

		RMSD
Apo	WT (3ZXF) *vs* R14A (7TKW)	0.196
	WT *vs* D94A (7TKY)	0.625
	WT *vs* R14A-R20A (7TRN) – Dimer complex 1	0.707
	WT *vs* R14A-R20A – Dimer complex 2	0.486
	WT *vs* R14A-R20A – Dimer complex 3	0.707
	WT *vs* R14A-R20A – Dimer complex 4	0.486
Holo	WT (6VTO) *vs* R14A (7TKX)	0.186
	WT *vs* D94A (7TKZ)	0.213
	WT *vs* R14A-R20A (7TRO)	0.407

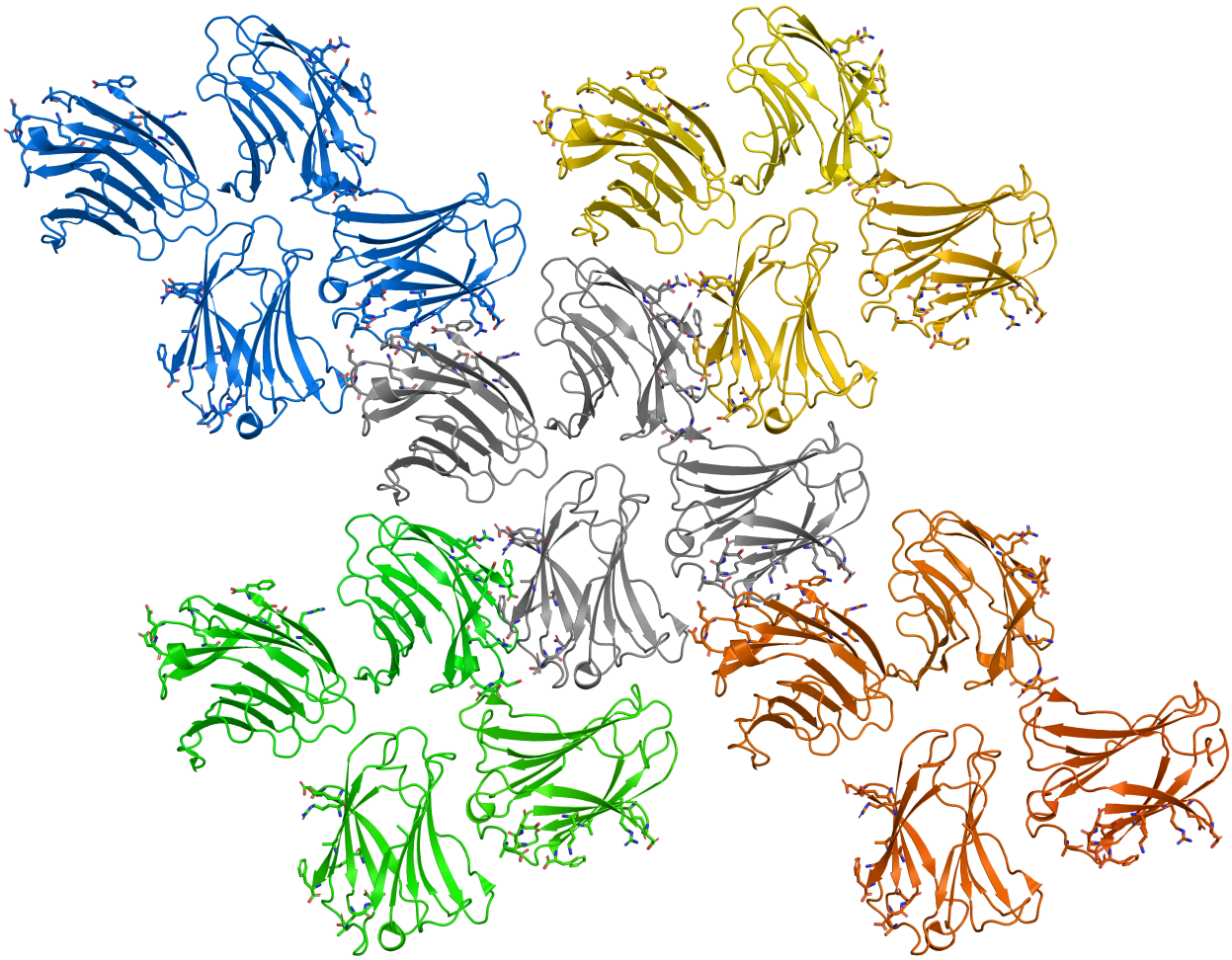

Figure 7.1 Dimer complex formation between monomers belonging to different asymmetric units in apo R14A-R20A structure

Five asymmetric units illustrated by different colors are presented (blue, yellow, orange, green, grey). Each unit consists of four monomers that form dimeric complexes with monomers from the neighboring asymmetric unit. Residues involved in dimer interface interactions are shown as sticks. (PDB 7TRN).

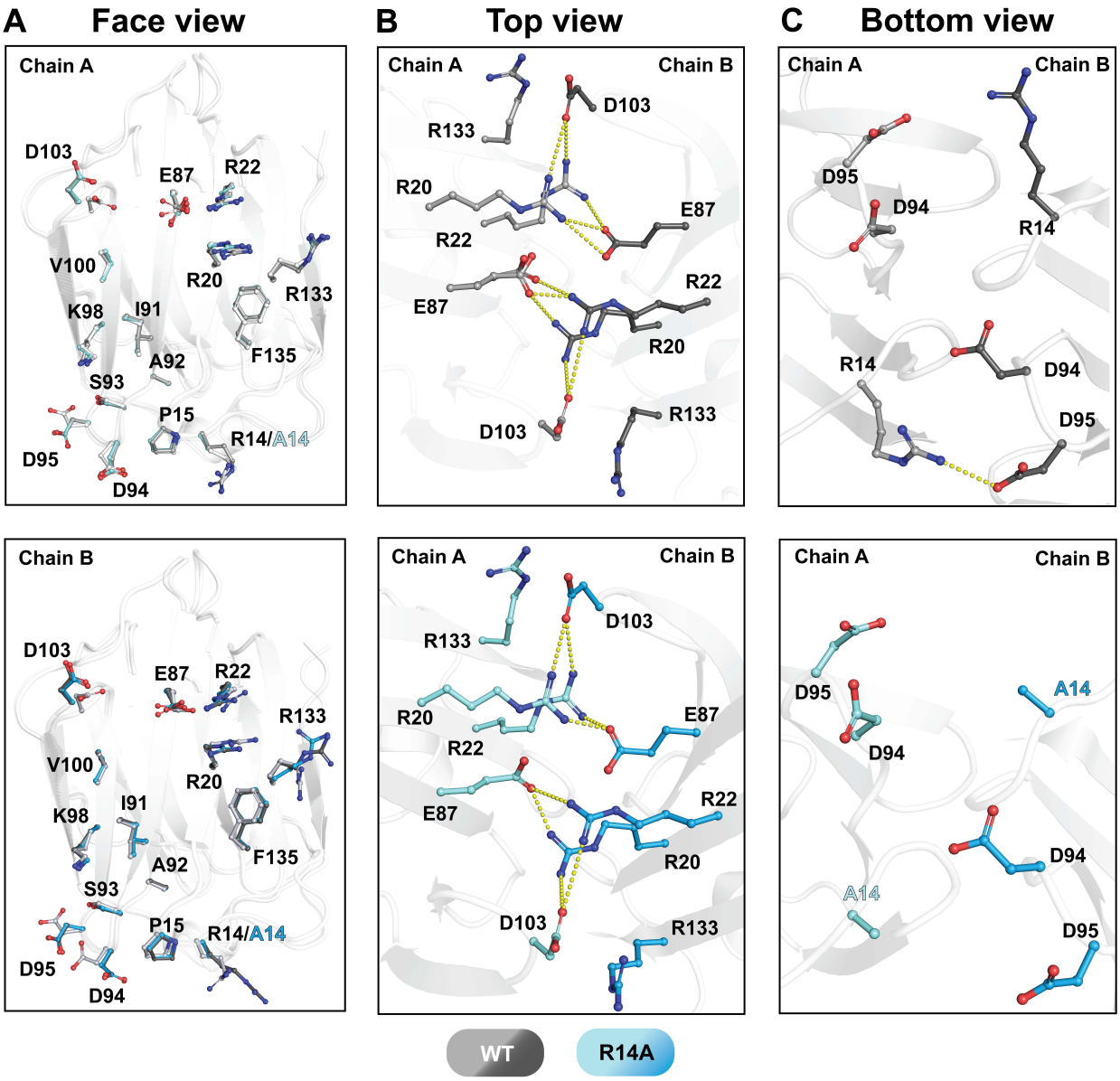

Figure 7.2 Structural comparison between holo GAL-7 WT and R14A

A, superimposition of residues involved in homodimer interaction between WT and R14A at the dimer interface of protomer A (top) and protomer B (bottom). Residues are represented as ball and stick with monochrome grey and aquamarine color for WT and R14A, respectively. B, the salt bridge interaction between dimeric interfacial R20, R22, E87, D103, and R133 residues of WT (top) and R14A (bottom). Salt bridge interactions are represented as yellow dashes. C, the salt bridge interaction between dimeric interfacial A/R14, D94 and D95 residues of WT (top) and R14A (bottom). (PDB 6VTO and 7TKX).

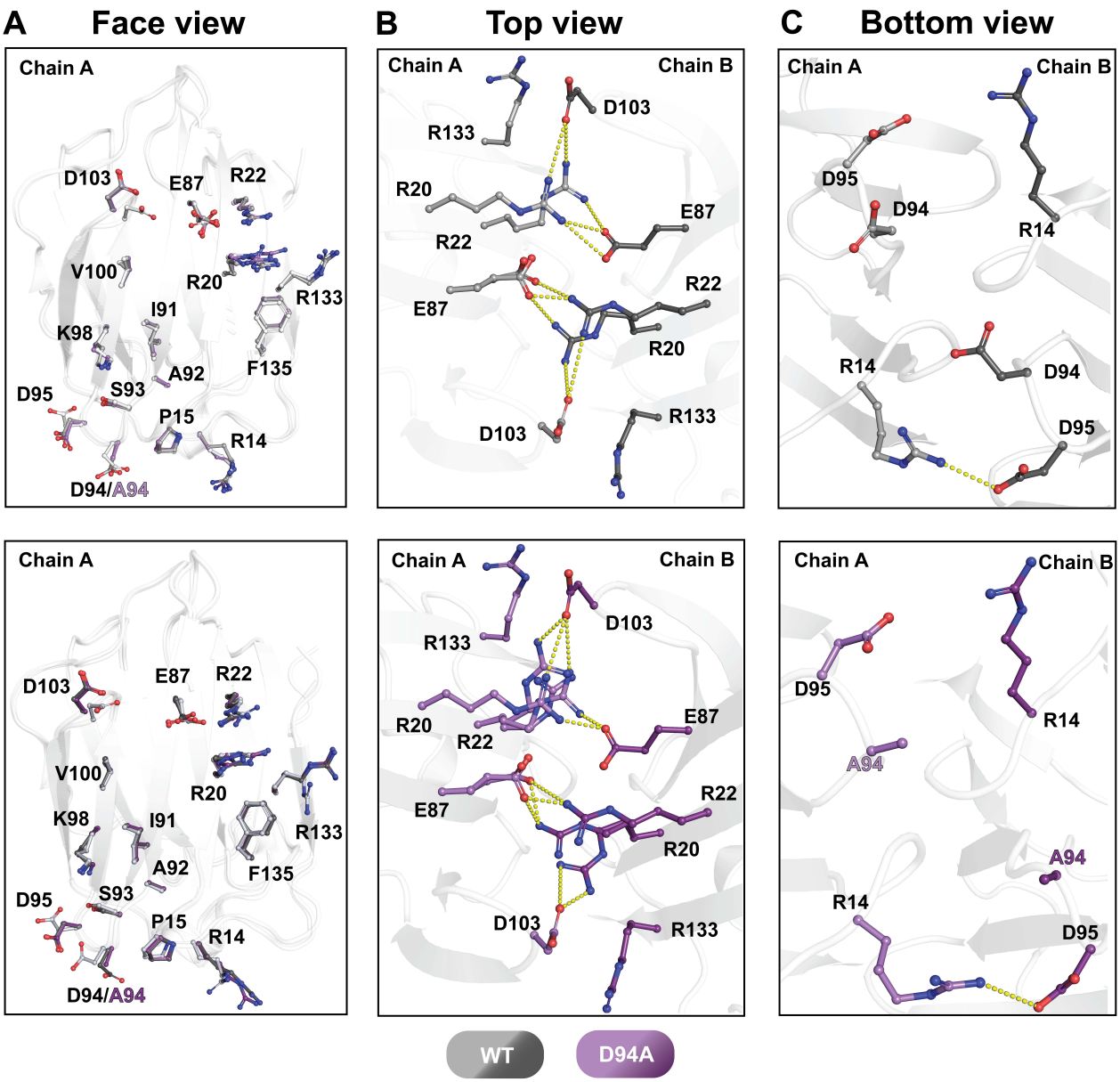

Figure 7.3 Structural comparison between holo GAL-7 WT and D94A

A, superimposition of residues involved in homodimer interaction between WT and D94A at the dimer interface of protomer A (top) and protomer B (bottom). Residues are represented as ball and stick with monochrome grey and purple color for WT and D94A, respectively. B, the salt bridge interaction between dimeric interfacial R20, R22, E87, D103, and R133 residues of WT (top) and D94A (bottom). Salt bridge interactions are represented as yellow dashes. C, the salt bridge interaction between dimeric interfacial R14, A/D94 and D95 residues of WT (top) and D94A (bottom). (PDB 6VTO and 7TKZ).

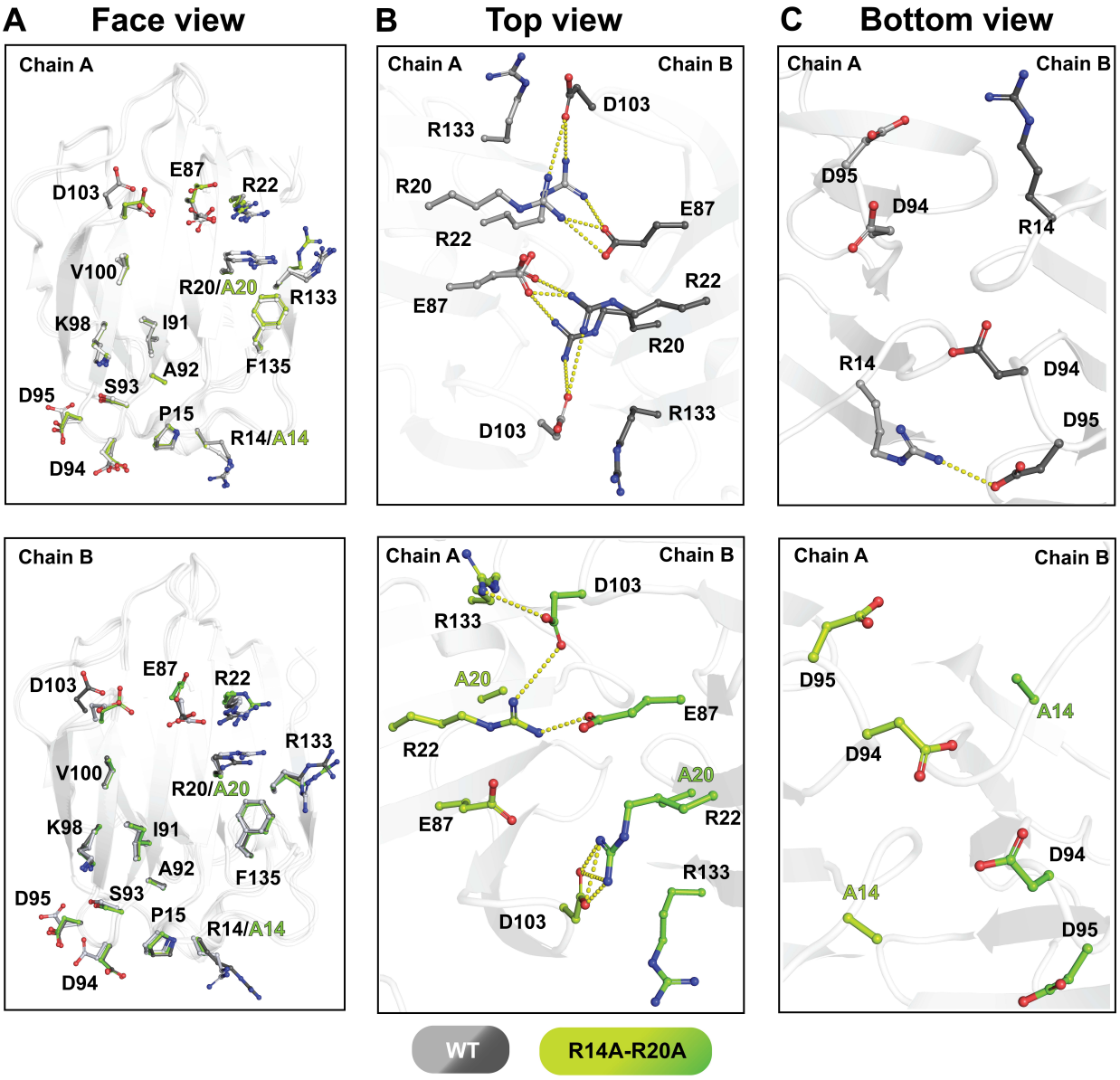

Figure 7.4 Structural comparison between holo GAL-7 WT and R14A-R20A

A, superimposition of residues involved in homodimer interaction between WT and R14A-R20A at the dimer interface of protomer A (top) and protomer B (bottom). Residues are represented as ball and stick with monochrome grey and lime color for WT and R14A-R20A, respectively. B, the salt bridge interaction between dimeric interfacial A/R20, R22, E87, D103, and R133 residues of WT (top) and R14A-R20A (bottom). Salt bridge interactions are represented as yellow dashes. C, the salt bridge interaction between dimeric interfacial A/R14, D94 and D95 residues of WT (top) and R14A-R20A (bottom). (PDB 6VTO and 7TRO).

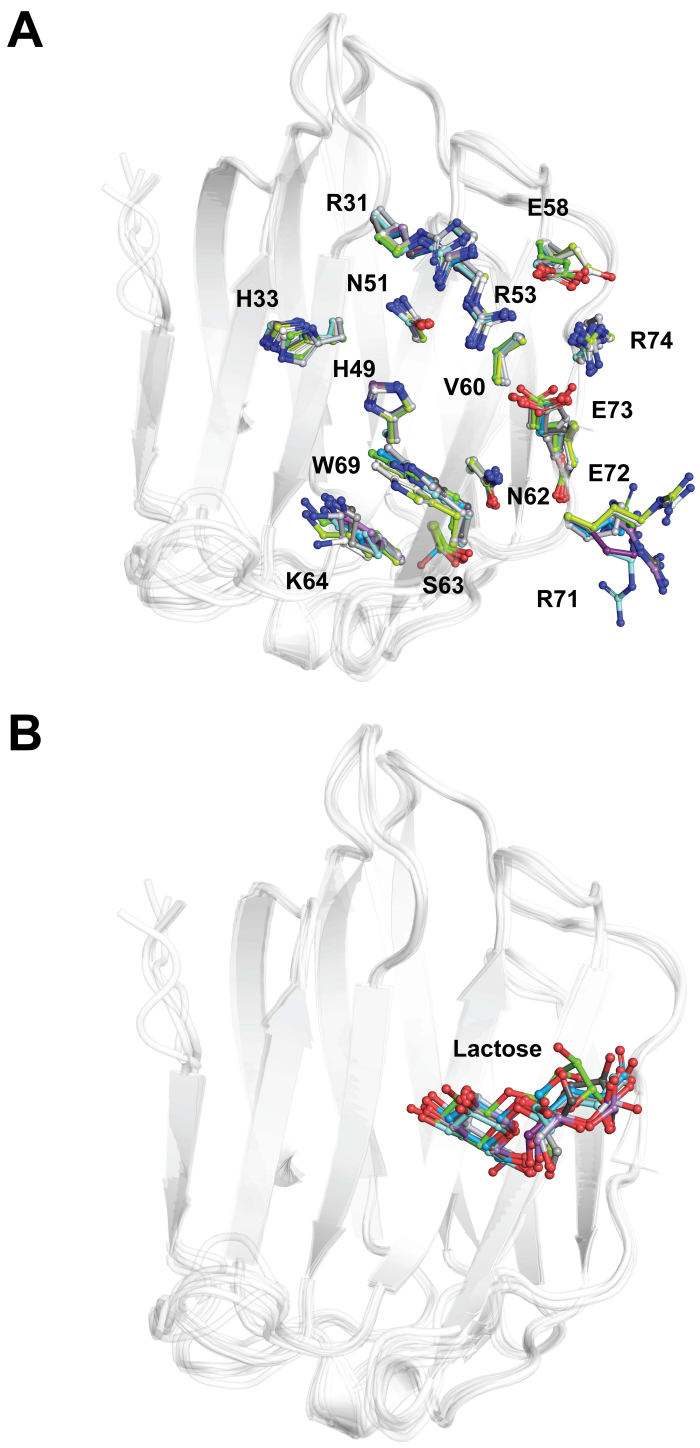

Figure 7.5 Glycan binding site (GBS) superposition between holo WT GAL-7 and variants R14A, D94A, and R14A-R20A

A. Superimposition of residues involved in GBS. Residues are represented as ball and stick with white-grey, blue, green, and violet-purple colors for WT, R14A, D94A and R14A-R20A, respectively. B. Superimposition of lactose position at the GBS. (PDB 6VTO, 7TKX, 7TKZ and 7TRO).